

Nanofiber production from agricultural straw biomass using pressurized fluids and
ultrasound processing for tissue engineering scaffolds

by

Raquel Razzera Huerta

A thesis submitted in partial fulfillment of the requirements for the degree of

Doctor of Philosophy
in
Bioresource and Food Engineering

Department of Agricultural, Food, and Nutritional Science
University of Alberta

© Raquel Razzera Huerta, 2019

Abstract

Agricultural straw is an abundant lignocellulosic biomass mainly composed of cellulose (33-75%), hemicellulose (13-37%) and lignin (3-31%) that offers great potential as a feed material for a biorefinery. Emerging technologies such as pressurized fluid fractionation and high-intensity ultrasound are promising alternatives to be employed for straw biomass refining towards bioactive compounds like phenolic compounds, and nanofiber production. Specifically, cellulose nanofibers have been considered as potential scaffold for tissue engineering applications. Therefore, the objective of this thesis was to employ pressurized fluids such as subcritical water and pressurized aqueous ethanol to fractionate canola straw biomass, and then nanofibrillate the treated fiber via high-intensity ultrasound to produce self-assembled scaffolds, and investigate their cytocompatibility for human gingival fibroblast cells. First, the straw biomass was treated using pressurized fluids at 140-220 °C, 50-200 bar, 0-100% v/v ethanol, with a constant flow rate of 5 mL/min for 40 min. Pressurized aqueous ethanol (20% v/v) at 180 °C and 50 bar, resulted in a hydrolysate with maximum total carbohydrates (443-528 mg GE/g straw) and phenolics (45-53 mg GAE/g straw) contents, and a solid residue mainly composed of 63% cellulose, 9% hemicellulose and 20% lignin. Then, the obtained enriched cellulose fiber was nanofibrillated using high-intensity ultrasound at specific energies of 4-20 kJ/g to obtain lignocellulosic nanofibers with maximum fibrillation yield of 36 wt.%, and an average diameter of 21 nm. Further bleaching of the enriched cellulose fiber (at 75 °C for 2-6 h) removed large amount of lignin and resulted in a bleached cellulose fiber mainly composed of 71-82% cellulose, 4-5% hemicellulose and 8-18% lignin. The nanofibrillation process of bleached fibers using high-intensity ultrasound at specific energies of 4-20 kJ/g

led to nanofibers with maximum fibrillation yield of 46 wt.% and an average diameter of 14 nm, which were self-assembled into a three-dimensional hydrogel structure. Cytocompatibility test performed using the dried hydrogel scaffolds showed no cytotoxicity of the residual lignin of up to 18%, and an increased cell proliferation compared to the control (glass slip) up to day 11. Finally, clove essential oil up to 0.5 wt.%, and cellulose nanofiber hydrogel were used as an emulsion-filled gel system for tissue engineering scaffolds with no cytotoxicity and cell viability of 74-101%. The results suggested that pressurized fluid fractionation followed by high-intensity ultrasound is a promising strategy for biorefining of straw biomass towards nanofiber and tissue engineering scaffold production. Furthermore, the emulsion-filled gel using clove essential oil and cellulose nanofiber hydrogel could provide scaffolds with unique antimicrobial properties, suggesting its potential use in the biomedical field.

Preface

Financial support for this research was granted by Natural Sciences and Engineering Research Council of Canada (Dr. Saldaña's NSERC-Discovery Grant) and my PhD scholarship by the Brazilian Council for Scientific and Technological Development (CNPq). This research project originated with the idea of Dr. Saldaña to provide value-added products from straw biomass for tissue engineering after processing with green technologies. I gathered theoretical information in Chapter 2, and developed a strategic plan to achieve the objectives reported in Chapter 1.

This thesis is an original work by Raquel Razzera Huerta and part of the following chapters have been published or submitted to peer-reviewed journals.

Chapter 3 was published as “Huerta, R.R., and Saldaña, M.D.A. (2018). Pressurized fluid treatment of barley and canola straws to obtain carbohydrates and phenolics. *The Journal of Supercritical Fluids*, 141:12-20”. I was responsible for the experimental design, performing experiments, data collection and analysis, and drafting the manuscript. My supervisor Dr. Saldaña provided the topic research area, discussed the experimental design and data obtained, and revised the manuscript.

Chapter 4 was published as “Huerta, R.R., and Saldaña, M.D.A. (2019). Sequential treatment with pressurized fluid processing and ultrasonication for biorefinery of canola straw towards lignocellulosic nanofiber production. *Industrial Crops and Products*, 139:111521”. I was responsible for the experimental design, performing experiments, data collection and analysis, and drafting the manuscript. Dr. Saldaña provided the topic research area, discussed the experimental design and data obtained, and revised the manuscript.

A revised version of Chapter 5 has been submitted to Cellulose as “Huerta, R.R., and Saldaña, M.D.A. (2019). The effect of chemical composition and ultrasound on the production of nanofibers from canola straw.” I was responsible for the experimental design, performing experiments, data collection and analysis, and drafting the manuscript. Dr. Saldaña provided the topic research area, helped with data discussion, and revision of the manuscript.

Chapter 6 was published as “Huerta, R.R., Silva E.K., Ekaette, I., El-Bialy, T., and Saldaña, M.D.A. (2019). High-intensity ultrasound-assisted formation of cellulose nanofiber scaffold with low and high lignin content and their cytocompatibility with gingival fibroblast cells. *Ultrasonics Sonochemistry*. <https://doi.org/10.1016/j.ultsonch.2019.104759>.” I was responsible for the experimental design, performing experiments, data collection and analysis, and drafting the manuscript. I. Ekaette assisted me with the rheological data collection. Dr. Saldaña provided the topic research area, helped with data discussion, and manuscript revisions. Dr. Silva helped with data discussion. Dr. El-Bialy provided the human gingival cells approved by the University of Alberta Human ethics committee (protocol #MS6_Pro00056111). All co-authors revised the manuscript.

Chapter 7 was published as “Huerta, R.R., Silva E.K., El-Bialy, T., and Saldaña, M.D.A. (2019). Clove essential oil emulsion-filled cellulose nanofiber hydrogel produced by high-intensity ultrasound technology for tissue engineering applications. *Ultrasonics Sonochemistry*. <https://doi.org/10.1016/j.ultsonch.2019.104845>.” The experimental design was discussed with Drs. Saldaña and Silva. I was responsible for performing experiments, data collection and analysis, and drafting the manuscript. Dr. Silva helped me with data

discussion. Dr. El-Bialy provided the human gingival cells approved by the University of Alberta Human ethics committee (protocol #MS6_Pro00056111). All co-authors revised the manuscript.

Acknowledgements

I would like to take this opportunity to thank all people, who helped me directly or indirectly with the completion of this thesis and throughout my PhD program. First, I would like to manifest my sincere gratitude to my supervisor Dr. Marleny D.A. Saldaña, for giving me the opportunity to join her research group and provide me support, encouragement and guidance during my PhD research. I would also like to thank my supervisory committee members, Dr. Temelli and Dr. El-Bialy for their time, and support throughout my research. Many thanks to my examining committee members Dr. Ana Rita Duarte and Dr. Wolodko.

I am forever grateful to my lab mates, colleagues and friends, Angelica Chorio, Azadeh Aghashahi, Carla Valdivieso, Eduardo Rodriguez, Eric Keven Silva, Idaresit Ekaette, Srujana Mekala, Yujia Zhao, Yussef Esparza, and Zhengjie Liu for their friendship, help, and support in my experimental work. I am also grateful for the staff in our department, and my special thanks for Mrs. Arlene Oatway, Mrs. Heather Vandertol-Vanier and Mr. Jun Gao, for their technical support.

My sincere thanks to the financial institutions, who funded my PhD study, the Brazilian Council for Scientific and Technological Development (CNPq) and Natural Sciences and Engineering Research Council of Canada (NSERC).

I would like to express my deepest gratitude to my family and lovely friends for their endless support throughout my PhD study and my life in general.

Thanks to God for being my source of happiness and motivation at the most difficult times, and for His endless blessings during my PhD study.

Table of contents

Chapter 1. Introduction and thesis objectives	1
1.1. Introduction	1
1.2. Hypothesis	5
1.3. Thesis objectives	5
Chapter 2. Literature Review	7
2.1. Agricultural straw biomass	7
2.2. Structural features: cellulose, hemicellulose and lignin	10
2.2.1. Cellulose	10
2.2.2. Hemicellulose	12
2.2.3. Lignin	13
2.3. Production of nanofibers from agricultural straw biomass.....	14
2.3.1. Straw biomass fractionation process	17
2.3.1.1. Acid and alkali hydrolysis	20
2.3.1.2. Bleaching	23
2.3.1.3. Organosolv	25
2.3.1.4. Steam and wet explosion	27
2.3.1.5. Ionic liquid and deep eutectic solvent	32
2.3.1.6. Microwave assisted hydrolysis	36
2.3.1.7. Pressurized fluid treatment	38
2.3.1.7.1. Hemicellulose hydrolysis	40
2.3.1.7.2. Lignin hydrolysis	43
2.3.1.7.3. Cellulose-enriched fiber	46
2.3.2. Mechanical nanofibrillation	48
2.3.2.1. High-intensity ultrasound	52
2.3.2.1.1. Other uses of high-intensity ultrasound	56
2.4. Applications of nanofibers from agricultural straw biomass	59
2.4.1. Hydrogel and aerogel	59
2.4.2. CNF scaffold for tissue engineering	63
2.5. Final remarks	67
Chapter 3. Pressurized fluid treatment of barley and canola straws to obtain carbohydrates and phenolics	68
3.1. Introduction	68
3.2. Materials and methods	70
3.2.1. Proximate compositional analysis	70
3.2.2. Pressurized fluid treatment	71
3.2.3. Characterization of liquid extracts	72
3.2.4. Characterization of solid residues	74
3.2.5. Statistical analysis	75

3.3. Results and discussion	75
3.3.1. Subcritical water hydrolysis	76
3.3.2. Pressurized aqueous ethanol treatment	78
3.3.3. Solid residue after pressurized fluid treatment	82
3.4. Conclusions	88
Chapter 4. Sequential treatment with pressurized fluid processing and ultrasonication for biorefinery of canola straw towards lignocellulosic nanofiber production	89
4.1. Introduction	89
4.2. Materials and methods	91
4.2.1. Materials	91
4.2.2. Methods	91
4.2.2.1. Production of lignocellulosic nanofiber	91
4.2.2.2. Characterization of canola straw	93
4.2.2.3. Characterization of lignocellulosic nanofiber	94
4.2.2.4. Statistical analysis	95
4.3. Results and discussion	96
4.3.1. Pressurized fluid treatment of canola straw	96
4.3.2. Production of lignocellulosic nanofibers	110
4.4. Conclusions	117
Chapter 5. The effect of residual lignin and ultrasound on the production of nanofibers from canola straw	118
5.1. Introduction	118
5.2. Materials and methods	120
5.2.1. Materials	120
5.2.2. Cellulose fiber isolation	121
5.2.3. Nanofiber production via high-intensity ultrasound	121
5.2.4. Fibers characterization	122
5.2.5. Nanofiber characterization	122
5.2.6. Statistical analysis	124
5.3. Results and discussion	123
5.3.1. Cellulose fiber isolation	123
5.3.2. Nanofiber production via high-intensity ultrasound	134
5.4. Conclusions	142
Chapter 6. High-intensity ultrasound-assisted formation of cellulose nanofiber scaffold with low and high lignin content and their cytocompatibility with gingival fibroblast cells	143
6.1. Introduction	143
6.2. Materials and methods	145
6.2.1. Cellulose fiber isolation	146

6.2.2. HIUS-assisted production of cellulose nanofiber scaffolds	146
6.2.3. Cell culture and seeding	147
6.2.4. Cellulose nanofiber suspension characterization	148
6.2.5. Cellulose nanofiber scaffolds characterization and cytocompatibility test	148
6.2.6. Statistical analysis	150
6.3. Results and discussion	150
6.3.1. Characterization of cellulose nanofiber suspension	150
6.3.2. Cellulose nanofiber scaffolds characterization and cytocompatibility	163
6.4. Conclusions	169
Chapter 7. Clove essential oil emulsion-filled cellulose nanofiber hydrogel produced by high-intensity ultrasound technology for tissue engineering applications	170
7.1. Introduction	170
7.2. Materials and methods	172
7.2.1. Preparation of cellulose nanofiber and emulsion-filled hydrogels by HIUS technology	173
7.2.2. Cell culture and seeding	174
7.2.3. Characterization	174
7.2.3.1. Emulsion-filled CNF hydrogel	174
7.2.3.1.1. Oil entrapment efficiency	174
7.2.3.1.2. Water retention value	175
7.2.3.1.3. Color	175
7.2.3.1.4. Optical microscopy	176
7.2.3.1.5. Viscoelastic behavior	176
7.2.3.2. Dried emulsion-filled CNF hydrogel	176
7.2.4. Statistical analysis	177
7.3. Results and discussion	177
7.3.1. HIUS processing parameters	177
7.3.2. Characterization of emulsion-filled CNF hydrogels	179
7.3.3. Characterization of freeze-dried emulsion-filled CNF hydrogel and its cytocompatibility.....	190
7.4. Conclusions	193
Chapter 8. Conclusions and recommendations	195
8.1. Conclusions	195
8.2. Recommendations	200
References	203

List of tables

Table 2.1. Common lignocellulosic biomass straws and their cellulose, hemicellulose and lignin contents	8
Table 2.2. Some of the conventional treatments used to fractionate agricultural straw biomass	18
Table 2.3. Green and emerging treatments to fractionate agricultural straw biomass	28
Table 2.4. Mechanical approaches to obtain cellulose nanofibers (CNF) and lignocellulosic nanofibers (LCNF) from straw	49
Table 3.1. Proximate compositional analysis of barley and canola straws	76
Table 3.2. Influence of pressure and ethanol concentration on the removal of total carbohydrates and phenolics from barley and canola straws at 180 °C and 5 mL/min for 40 min	79
Table 3.3. Decomposition characteristics of untreated barley and canola straws, and pressurized fluid treated straws at 180 °C, 50 bar and 5 mL/min for 40 min	87
Table 4.1. Influence of pressure and temperature on the treated fiber after sCW treatment of canola straw	97
Table 4.2. Cellulose, hemicellulose and lignin contents of canola straw treated fiber obtained using PAE at 180 °C, 50 bar and 5 mL/min for 40 min and addition of ethanol as a co-solvent from 0-100% (v/v)	103
Table 4.3. Regression coefficients and evaluation of the mathematical models for cellulose, hemicellulose and lignin contents from PAE treated canola straw	103
Table 4.4. Water retention value, zeta (ζ) potential and nanofibril content of lignocellulosic nanofibers (1 wt.%) obtained using HIUS at theoretical specific energy of 4-20 kJ/g and its corresponded nominal power of 240-1200 W	112
Table 5.1. Chemical composition and total solid content of untreated, PAE treated and bleached PAE treated canola straw at different reaction times	124
Table 5.2. Decomposition characteristics of untreated, PAE treated (180 °C, 50 bar, 20% ethanol, 5 mL/min for 40 min) and bleached (2, 4 and 6 h reaction time) fibers	132

Table 5.3. Water retention value (WRV), nanofibril content and zeta (ζ) potential values of LCNF and CNF (1 wt.%) obtained using ultrasound at theoretical specific energy (TSE) between 4 to 20 kJ/g	135
Table 6.1. Characterization and visual appearance of high lignin (HL) and low lignin (LL) cellulosic fibers obtained after 2 and 6 h of bleaching, respectively .	151
Table 6.2. Nominal and calculated ¹ power, HIUS efficiency ¹ and intensity ¹ , and the initial and final temperature recorded during HIUS processing of CNF (1 wt.%) suspensions	152
Table 6.3. Water retention value (WRV), zeta (ζ) potential, fibrillation yield and visual appearance of LL-CNF and HL-CNF (1 wt.%) suspensions treated using HIUS at different nominal and acoustical powers	154
Table 6.4. Power law parameters for elastic (G') and viscous (G'') modulus	161
Table 6.5. Comparison of LL-CNF and HL-CNF aerogel properties obtained by freeze drying	163
Table 7.1. Clove essential oil emulsion-filled CNF hydrogel composition	173
Table 7.2. Nominal and acoustical power, theoretical and real specific energy, time, temperature, efficiency and intensity of the HIUS process	178
Table 7.3. Clove essential oil emulsion-filled CNF hydrogels (0.1-1.0 wt.% clove essential oil) obtained at ultrasonic SE of 0.10, 0.17 and 0.24 kJ/g	182
Table 7.4. Power law parameters for elastic (G') and viscous (G'') modulus	189
Table 7.5. Diameter, bulk density, porosity and swelling capacity properties of freeze-dried clove essential oil emulsion-filled CNF hydrogels	191

List of figures

Figure 2.1. Main components of straw biomass cell wall	10
Figure 2.2. Cellulose as molecular level (a), and its organization as a fiber (b)	11
Figure 2.3. Number of articles published using the keywords: “cellulose nanofib*” (CNF) and “cellulose nanofib* from straw” (a), and “lignocellulosic nanofiber” (LCNF) and “lignocellulosic nanofiber from straw” (b). Data analysis performed from 2000 to 2019 using the Web of Science database in July 2019.....	16
Figure 2.4. Hemicellulose hydrolysis pathway using sCW	41
Figure 2.5. Scheme of ultrasound acoustic cavitation	53
Figure 2.6. Physical cross-linked CNF hydrogel	60
Figure 3.1. Subcritical water system: P =pressure gauge, and $T1$ & $T2$ =thermocouples	72
Figure 3.2. Main effects diagram for total carbohydrates, TC (a, b) and total phenolics, TP (c, d) removal from barley (- -) and canola (-) straws using sCW at 5 mL/min for 40 min	77
Figure 3.3. Effect of ethanol concentration for total carbohydrate (TC) removal (bars) and A_{420} values (line) of barley straw (- -) and canola straw (-) at 180 °C, 50 bar and 5 mL/min for 40 min	80
Figure 3.4. Influence of pressurized fluid treatment (180 ° C, 50 bar and 5 mL/ min for 40 min) on lignin content of barley and canola straw residues. Means within the same group of straw with different letters are significantly different at $p < 0.05$	83
Figure 3.5. FT-IR spectra of untreated, and sCW and PAE (20%) treated: (a) barley straw, and (b) canola straw	84
Figure 3.6. TG thermograms of barley straw (a) and canola straws (c), and DTG curves for barley straw (b) and canola straw (d)	85
Figure 3.7. Scanning electron microscopy (SEM) images of: (a) untreated barley straw, (b) sCW treated barley straw, (c) PAE (20%) treated barley straw, (d) untreated canola straw, (e) sCW treated canola straw, and (f) PAE (20%) treated canola straw at 180 °C, 50 bar and 5 mL/min for 40 min ..	88

Figure 4.1. Effects of the processing temperature (140-220 °C) and pressure (50-200 bar) on hemicellulose (a), total lignin (b), soluble lignin (c), insoluble lignin (d) and cellulose (e) contents on the sCW treated fiber. Dotted lines represent the mean values	98
Figure 4.2. FT-IR spectra of canola straw before and after PAE (20%) treatment at 180 °C, 50 bar and 5 mL/min for 40 min	105
Figure 4.3. XRD patterns of canola straw before and after PAE (20%) treatment at 180 °C, 50 bar and 5 mL/min for 40 min. Segal CI: Segal crystallinity index	108
Figure 4.4. TG (a) and DTG (b) thermograms of canola straw before and after PAE (20%) treatment at 180 °C, 50 bar and 5 mL/min for 40 min	109
Figure 4.5. Analysis of means for water retention value (WRV) (a), zeta (ζ) potential (b), and nanofibril content (c) of lignocellulosic nanofibers (1 wt. %) obtained using HIUS at theoretical specific energy (TSE) of 4-20 kJ/g ...	111
Figure 4.6. Optical transmittance (%) of lignocellulosic nanofibers (1 wt. %) obtained using HIUS at theoretical specific energy (TSE) of 4-20 kJ/g (a), and correlation between optical transmittance at 800 nm (\times), nanofibril content (Δ), and theoretical specific energy (TSE) (b)	114
Figure 4.7. Scanning electron microscopic analysis of untreated canola straw (a), PAE treated fiber (b). Transmission electron microscopic analysis and diameter distribution of lignocellulosic nanofibers obtained after HIUS at theoretical specific energy (TSE) of 4 kJ/g (c) and 20 kJ/g (d)	116
Figure 5.1. FT-IR spectra of untreated canola straw, PAE treated fiber (180 °C, 50 bar, 20% (v/v) ethanol, 5 mL/min for 40 min) and bleached (2, 4 and 6 h) fibers	126
Figure 5.2. X-ray diffractograms (XRD) of untreated canola straw and PAE treated fiber (180 °C, 50 bar, 20% (v/v) ethanol, 5 mL/min for 40 min) before and after bleaching (B2-6 h). CI: Segal crystallinity index	129
Figure 5.3. TG (a) and DTG (b) thermograms of untreated canola straw and PAE treated fiber before and after bleaching treatments (B2-6 h)	130
Figure 5.4. Solid material, scanning electron microscopy (SEM) images of untreated canola straw fiber and PAE treated fiber (180 °C, 50 bar, 20% (v/v) ethanol, 5 mL/min for 40 min) before and after bleaching (2, 4 and 6 h reaction time) treatment	133

Figure 5.5. Effect of the theoretical ultrasonic specific energy (TSE) and lignin on: (a) water retention value, WRV, (b) nanofibril content, and (c) zeta (ζ) potential, and the effect of interaction between ultrasonic TSE and lignin on: (d) WRV, (e) nanofibril content, and (f) ζ potential. Dotted lines represent the mean values	136
Figure 5.6. Transmission electron microscopy (TEM) images and size distribution of 1 wt.% LCNF and CNF (B6 h) obtained using ultrasound at TSE of 20 kJ/g	140
Figure 6.1. Transmission electron microscopy (TEM) images and diameter size distribution of 1 wt.% LL-CNF and HL-CNF obtained using HIUS at acoustical powers of 53 and 51 W, respectively	157
Figure 6.2. Strain (γ) sweep and angular frequency (ω) sweep of modulus G' and G'' of LL-CNF hydrogels (a, b), and HL-CNF hydrogels (c, d) obtained using HIUS at acoustical powers of 53 and 51 W, respectively, and complex viscosity (η^*) of obtained CNF hydrogels (e)	159
Figure 6.3. Scanning electron microscopy (SEM) images of 1 wt.% LL-CNF aerogel (a) and HL-CNF aerogel (b) obtained using HIUS at acoustical powers of 53 and 51 W, respectively. Blue arrows show the nanofibers aggregation after freezing step.....	164
Figure 6.4. Biocompatibility test of control (glass slip), LL-CNF and HL-CNF aerogels (1-2 wt.%) on gingival fibroblast cells cultured for 11 days. ^{a-f} Different lowercase letters indicate significant differences ($p < 0.05$) ...	167
Figure 6.5. Stained scaffold sections of LL-CNF aerogel (a) and HL-CNF aerogel (b) after incubation for 11 days. The pink arrows and the dark purple stain indicate the cell nuclei	169
Figure 7.1. Optical microscopy of the fresh clove essential oil emulsion-filled CNF hydrogels	180
Figure 7.2. Strain (γ) sweep of modulus G' and G'' and $\tan \delta$ of clove essential oil emulsion-filled CNF hydrogels with 0.1 wt.% (a, b), 0.5 wt.% (c, d), and 1.0 wt.% (e, f) clove essential oil	185
Figure 7.3. Angular frequency (ω) sweep of modulus G' and G'' of clove essential oil emulsion-filled CNF hydrogels with 0.1 wt.% (a), 0.5 wt.% (b), and 1.0 wt.% (c) clove essential oil. Complex viscosity η^* against ω at 1-100 rad/s (d) for all prepared emulsion-filled CNF hydrogels	186
Figure 7.4. Cell viability of the freeze-dried clove essential oil emulsion-filled CNF hydrogels after 24 h	193

List of abbreviations and symbols

ΔE	Total color difference
a	Hunter color index a
ANOM	Analysis of means
ANOVA	Analysis of variance
ASC	Acidified sodium chlorite
b	Hunter color index b
CI	Crystallinity index
CNF	Cellulose nanofibers
3D	Three-dimensional
DES	Deep eutectic solvent
DMEM	Dulbecco's Modified Eagle's Medium
DSC	Differential scanning calorimetry
DTG	Derivative thermos-gravimetric
ECM	Extracellular matrix
EtOH	Ethanol
FBS	Fetal bovine serum
FRAP	Ferric reducing antioxidant power
FT-IR	Fourier transform infrared spectroscopy
G'	Storage modulus
G''	Loss modulus
GAE	Gallic acid equivalent
GE	Glucose equivalent
H ₂ SO ₄	Sulfuric acid
HCl	Hydrochloric acid
HIUS	High-intensity ultrasound
HL	High lignin
HMF	Hydroxymethyl furfural
HPH	High-pressure homogenization
HPLC	High performance liquid chromatography

IL	Ionic liquid
K_w	Ionic product
L	Hunter color index L
LCC	Lignin-carbohydrate complex
LCNF	Lignocellulosic nanofibers
LL	Low lignin
LVR	Linear viscoelastic region
MeOH	Methanol
MW	Microwave
NaOH	Sodium hydroxide
NMR	Nuclear magnetic resonance
NREL	National Renewable Energy Laboratory
OH	Hydroxyl group
P	Pressure
PAE	Pressurized aqueous ethanol
PBS	Phosphate buffer solution
PF	Pressurized fluid
PVA	Poly(vinyl alcohol)
SCCO ₂	Supercritical carbon dioxide
sCW	Subcritical water
SE	Specific energy
SEM	Scanning electron microscopy
T	Temperature
TC	Total carbohydrate
TEM	Transmission electron microscopy
TEMPO	2,2,6,6-Tetramethylpiperidine-1-oxyl radical
TGA	Thermogravimetric analysis
TP	Total phenolics
TSE	Theoretical specific energy
UAE	Ultrasound-assisted extraction
UV-vis	Ultraviolet-visible

WI	Whiteness index
WRV	Water retention value
XRD	X-Ray diffraction
YI	Yellowness index

Chapter 1. Introduction and thesis objectives

1.1. Introduction

In Canada, canola and barley are two important commodities that produces around 4-8 Million Tonnes (MT) of agricultural straw every year. This straw is a lignocellulosic biomass residue that represents about half the total dry weight of the crop (Yuan & Sun, 2010), and it is mainly composed of cellulose (33-75%), hemicellulose (13-37%) and lignin (3-31%). Cellulose and hemicellulose are polymers of sugar monomers linked mainly by β -(1 \rightarrow 4)-glycosidic bonds and found in the primary and secondary walls of the plant biomass. Lignin is a highly cross-linked complex structure formed by aromatic compounds that constitute the middle lamella of the plant cell wall and provides strength and structure to the plant (Meier, 1962). The straw biomass is an enormous underutilized renewable resource, which has great potential as a raw material for paper, chemicals, biomaterials and biofuel applications. Furthermore, in the last decade, the processing and conversion of agricultural straw biomass into useful value-added nanomaterials such as cellulose nanofibers (CNF) and lignocellulosic nanofibers (LCNF) have also gained increased attention (Kaushik et al., 2010; Jonoobi et al., 2011; Costa et al., 2013; Yousefi et al., 2013; Hasanjanzadeh et al., 2014; Soni et al., 2015; Tarrés et al., 2017; Hassan et al., 2018; Martelli-Tosi et al., 2018; Ewulonu et al., 2019). Nanofibers have diameter in the nanoscale range of 1-100 nm and length of several microns, which contribute to their high aspect ratio and high specific surface area, and their arrangement into an entangled network.

For nanofiber production, first the straw biomass is fractionated into its main components, followed by nanofibrillation via mechanical approaches. The most common processes applied to fractionate the biomass are biological treatment using enzymatic

hydrolysis and chemical treatment using acid and alkali hydrolysis, organosolv process and bleaching. Although some of those processes are already implemented at industrial scale, drawbacks including long processing times, extensive amount of energy use, neutralization steps, low-quality by-products, sugar degradation, environmentally hazardous waste production and equipment corrosion, have been the main challenges for their expansion. Therefore, efforts have been made to develop environmentally friendly processes to fractionate lignocellulosic biomass, including agricultural straws.

Among the environmentally friendly processes studied, pressurized fluids such as pressurized hot water or also known as subcritical water (sCW), and pressurized aqueous ethanol (PAE) have received increased attention for lignocellulosic biomass fractionation. They are considered as green techniques because mainly solvents generally recognized as safe (GRAS) are used, at temperatures above their boiling point but below their critical point, and pressures high enough to keep the solvent in its liquid state. Using sCW treatment, the increased ionization constant of water is the main pathway for hemicellulose autohydrolysis (Cocero et al., 2018). On the other hand, the PAE process induces the cleavage of α - and β -aryl ether linkages in the lignin structure, releasing phenolic compounds, including *trans* isomers of *p*-coumaric (4-hydroxy-cinnamic) and ferulic (4-hydroxy-3-methoxycinnamic) acids, vanillin and syringaldehyde, that are present as the main linkages of the lignin-carbohydrate complex of straw biomass (Mueller-Harvey et al., 1986; Sun et al., 2002; Xu et al., 2006; Buranov & Mazza, 2008). However, due to the high reactivity of the dissolved lignin fragments, they can re-condense in the solid material during the treatment, resulting in a treated fiber with mainly cellulose and residual lignin (Buranov & Mazza, 2012; Ciftci & Saldaña, 2015; Giummarella & Lawoko, 2017;

Martinez-Abad et al., 2018). The nanofibrillation of this enriched material towards LCNF production shows an effective way for complete utilization of the agricultural straw biomass. However, since the CNF production relies on high purity cellulose fiber, strategies for bleaching are further needed to oxidize the remaining lignin and isolate the cellulose fiber prior to the nanofibrillation step.

Common mechanical approaches for nanofibrillation includes grinding, high-pressure homogenization, microfluidization and high-intensity ultrasound (HIUS) processing. The HIUS process is a clean and emerging technique that has shown high performance on the nanofibrillation process of cellulosic materials due to the hydrodynamic forces of acoustical waves (Chen et al., 2011a; Ciftci et al., 2017). The HIUS process uses low-frequency of 20-100 kHz and high-power ultrasound in a liquid medium to promote acoustical waves and subsequent production, growth, and collapse of microbubbles in the medium (Ashokkumar, 2011). This phenomenon is known as acoustic cavitation, which induces micro-shearing of solid materials like cellulose fibers, resulting in their disintegration into smaller fibrils.

One of the interests in CNF is its application in biomedical and pharmaceutical areas as well as in regenerative medicine as tissue engineering scaffolds (Ciolacu et al., 2016; Mertaniemi et al., 2016; Laurén et al., 2017; Kim et al., 2018; Petroudy et al., 2018; Sanandiya et al., 2019). Some exclusive characteristics of CNF for biomedical applications are their variable/controllable solubility, superior structural design, 3D morphology and excellent biocompatibility and cytocompatibility (Du et al., 2019). Furthermore, in comparison with semi-synthetic or synthetic polymers, natural polymers like CNF have better performance in mimicking the extracellular matrix and interaction with surrounding

tissues (Turnbull et al., 2018), which is an essential feature for tissue engineering applications. Despite the above mentioned advantages and wide applicability of CNF in the biomedical area, there are challenges in making CNF-based scaffolds for tissue engineering such as high production cost and chemical demand of surface modified CNF (Delgado-Aguilar et al., 2015), and the possibility of microbial spoilage (Jack et al., 2019; Kabirian et al., 2019), which may restrict their future commercialization as tissue engineering scaffolds. In this context, the use of essential oils within the scaffold matrix is a promising strategy to develop novel therapeutic biomaterials with antibacterial properties (Liakos et al., 2015; Ardekani et al., 2019). Due to the high instability, hydrophobicity, thermal sensitivity, and high volatile nature of essential oils, they are generally encapsulated in different systems, such as oil-in-water emulsions, spray-dried microparticles, liposomes, lipidic nanoparticles, biopolymer-based films, emulsion-filled gels, and others (Fernandes et al., 2016; Torres et al., 2016; Feng et al., 2018; Zhao et al., 2018; Cao & Song, 2019; Wu et al., 2019). Emulsion-filled gels are produced by embedding an emulsion into either a gel phase or a pre-gel polymer solution, which is followed by gelation in response to stimuli such as temperature, pH and shear stress (Farjami & Madadlou, 2019). Earlier, cellulose acetate wound dressing scaffold with encapsulated cinnamon, lemongrass and peppermint essential oils showed good compatibility (75-90% viability) with human epidermal cells, while it was able to inhibit the growth of Gram-negative bacteria (Liakos et al., 2015). However, CNF hydrogel has not been yet used as a gelling agent for emulsion-filled gel scaffold. Thus, more studies are needed to process CNF scaffolds with increased antimicrobial properties, and less dependent on chemical treatment or surface modification.

1.2. Hypothesis

It is hypothesized that pressurized fluid technology and high-intensity ultrasound treatment can produce nanofibers from agricultural straw biomass. It is also hypothesized that cellulose nanofiber with different residual lignin content, and as an emulsion-filled gel system can be used as scaffolds for potential tissue engineering applications.

1.3. Thesis objectives

The main objective of this thesis was to develop a process using pressurized fluid fractionation and high-intensity ultrasound nanofibrillation to understand the mechanism of nanofibers formation from agricultural straw, and to investigate their cytocompatibility with human gingival fibroblast cells.

The specific objectives were:

- To understand the effect of different process parameters of pressurized fluids on the hydrolysate and straw residue (Chapter 3).
- To optimize the processing conditions of pressurized aqueous ethanol (PAE) treatment for maximum removal and recovery of non-cellulosic materials, and to investigate the effects of high-intensity ultrasound specific energy on the nanofibrillation of PAE treated canola straw for lignocellulosic nanofiber (LCNF) production (Chapter 4).
- To evaluate the bleaching process time for maximum delignification of the PAE treated canola straw, and to investigate the single and simultaneous effects of residual lignin and high-intensity ultrasound processing to obtain nanofibers with different residual lignin contents (Chapter 5).

- To investigate the production of self-assembled cellulose nanofiber (CNF) scaffolds with low and high residual lignin contents, and to evaluate the cytotoxicity of residual lignin for human gingival fibroblast cells (Chapter 6).

- To study the use the high-intensity ultrasound processing on the production of emulsion-filled CNF hydrogels using clove essential oil as dispersed phase and evaluate its cytocompatibility with human gingival fibroblast cells (Chapter 7).

Chapter 2. Literature Review

2.1. Agricultural straw biomass

Agricultural straw is a lignocellulosic by-product of several crops, such as cereals (e.g. barley, wheat, rice) and oilseeds (e.g. canola, flax, soybean, mustard). The straw is generated after crop harvesting, and comprises about half of the total dry weight of the crop (Yuan & Sun, 2010). The main uses of straw are as fodder, animal bedding and nitrogen fertilizer, but, when unwanted, it is usually burned in the field. However, there are limitations within those practices. For example, flax straw is difficult to be incorporated in the field as nitrogen fertilizer because the fibres wrap themselves around, plugging disks, wheels and seeder-shanks after harvest (Flax Council of Canada, 2016). Also, due to the high silica, lignin, and phenolic contents of some straws, their use as fodder is limited as they exert harmful effects on cattle's digestive system and have poor rumen degradability (Alexander et al., 1987; Hans et al., 2019). Furthermore, several environmental risks are associated with straw burning practice, such as soil nutrient loss and increased carbon dioxide (CO₂) levels due to the smoke (Hans et al., 2019). Thus, new alternatives for straw management are urgently needed and have been recently gaining increased interest.

Straw biomass is mainly composed of cellulose (31-58%), hemicellulose (17-39%) and lignin (13-31%) with different ratios according to the straw source (Table 2.1). Other minor compounds, including protein, waxes, and ash can also be found in the straw in small percentages. All these components are distributed differently at the cellular level. As a botanical tissue, the cell walls of straw are a rigid, multi-layered structure composed of middle lamella, the primary, and the secondary walls (outer, middle, and inner layers) (Fig. 2.1). Cellulose and hemicellulose are mainly located in the primary and secondary walls of

the plant, while lignin is the main component of the middle lamella (Meier, 1962). As observed in Fig. 2.1, the middle lamella has the role of binding the adjacent cells together, providing strength and structure to the straw.

Table 2.1. Common lignocellulosic biomass straws and their cellulose, hemicellulose and lignin contents.

Lignocellulosic biomass straw	Cellulose (%)	Hemicellulose (%)	Lignin (%)	Reference
Barley	34-40	23-28	15-19	Sun & Tomkinson (2000) Pronyk & Mazza (2012) Espinosa et al. (2017)
Canola	32-37	21-27	14-19	Pronyk & Mazza (2012) Wang et al. (2016a) Huerta & Saldaña (2019)
Corn	39-44	27-31	15-18	Sun & Tomkinson (2000) Espinosa et al. (2017) Xu et al. (2018)
Cotton	31-40	20-26	26-31	Akpinar et al. (2009) Soni et al. (2015) Gaur et al. (2017)
Flax	33-34	17-21	24-30	Buranov & Mazza (2010) Fu et al. (2010) Buranov & Mazza (2012)
Hemp	38-48	31-39	19-28	Immonen et al. (2018) Pacaphol & Aht-Ong (2017)
Kenaf	58	22	18	Jonoobi et al. (2011)
Miscanthus	43	27	25	Li et al. (2019)
Mustard	33	20	18	Pronyk & Mazza (2012)

Table 2.1. Continued.

Lignocellulosic biomass straw	Cellulose (%)	Hemicellulose (%)	Lignin (%)	Reference
Oat	38-39	23-38	16-18	Sun & Tomkinson (2000) Pronyk & Mazza (2012) Espinosa et al. (2017)
Reed	31	34	16	Liu et al. (2019)
Rice	37-47	18-28	12-21	Sun & Tomkinson (2000) Hasanzadeh et al. (2014) Sharma et al. (2015)
Rye	38-42	25-37	18-20	Sun & Tomkinson (2000) Sun et al. (2002) Wörmeyer et al. (2011)
Sorghum	35	24	25	Vázquez et al. (2007)
Soybean	40	23	13	Martelli-Tosi et al. (2018)
Sugarcane	34-41	26-27	26-31	Costa et al. (2013) Candido & Gonçalves (2016)
Sunflower	41-42	19-31	20-27	Akpınar et al. (2009) Ewulonu et al. (2019)
Triticale	36-55	23-33	15-16	Pronyk & Mazza (2012) Fu et al. (2010) Tarrés et al. (2017)
Wheat	38-39	23-33	14-18	Sun & Tomkinson (2000) Pronyk & Mazza (2012) Espinosa et al. (2016)

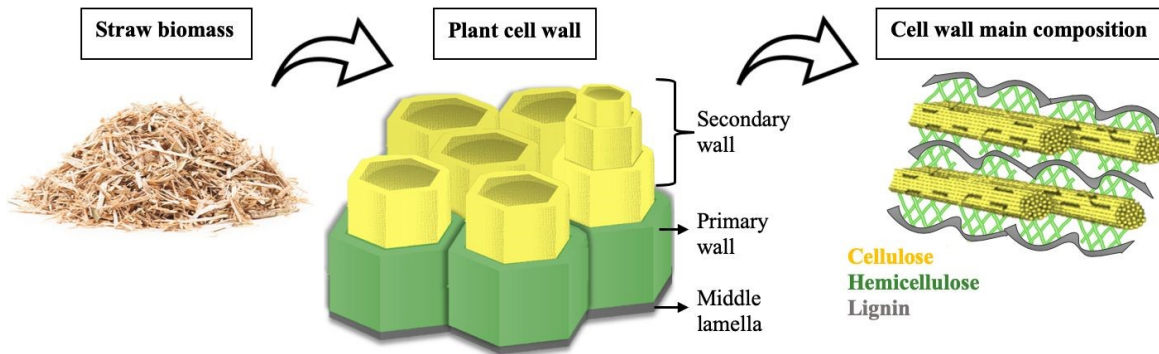


Fig. 2.1. Main components of straw biomass cell wall.

2.1. Structural features: cellulose, hemicellulose and lignin

2.1.1. Cellulose

Cellulose is one of the most abundant natural polymers on earth. It is a linear organic compound of anhydroglucose units ($C_6H_{10}O_5$)_n linked together by β -(1 → 4)-glycosidic bonds, where a dimer of glucose is known as cellobiose (Fig. 2.2a). As shown in Fig. 2.2, each unit of anhydroglucose has six carbon atoms with three hydroxyl groups at C2, C3, and C6 atoms, that form intermolecular hydrogen bonds with adjacent anhydroglucose units. This assembles the cellulose chains into elementary fibrils, which further aggregate into cellulose nanofibers (Meier, 1962). The cellulose nanofibers are then bundled together as larger fibers with diameters of 5-10 μ m and linked to hemicelluloses and lignin in the cell walls of straw (Liu et al., 2006). Within the nanofiber structures, there are regions where the cellulose elementary fibrils are arranged in a highly ordered manner known as the crystalline region, and regions where the elementary nanofibrils are disordered, known as the amorphous region (Fig. 2.2b). Nanocelluloses extracted only from the crystalline region are known as cellulose nanocrystals (CNC), and nanocelluloses extracted from randomised amorphous and crystalline regions are called cellulose nanofibers (CNF).

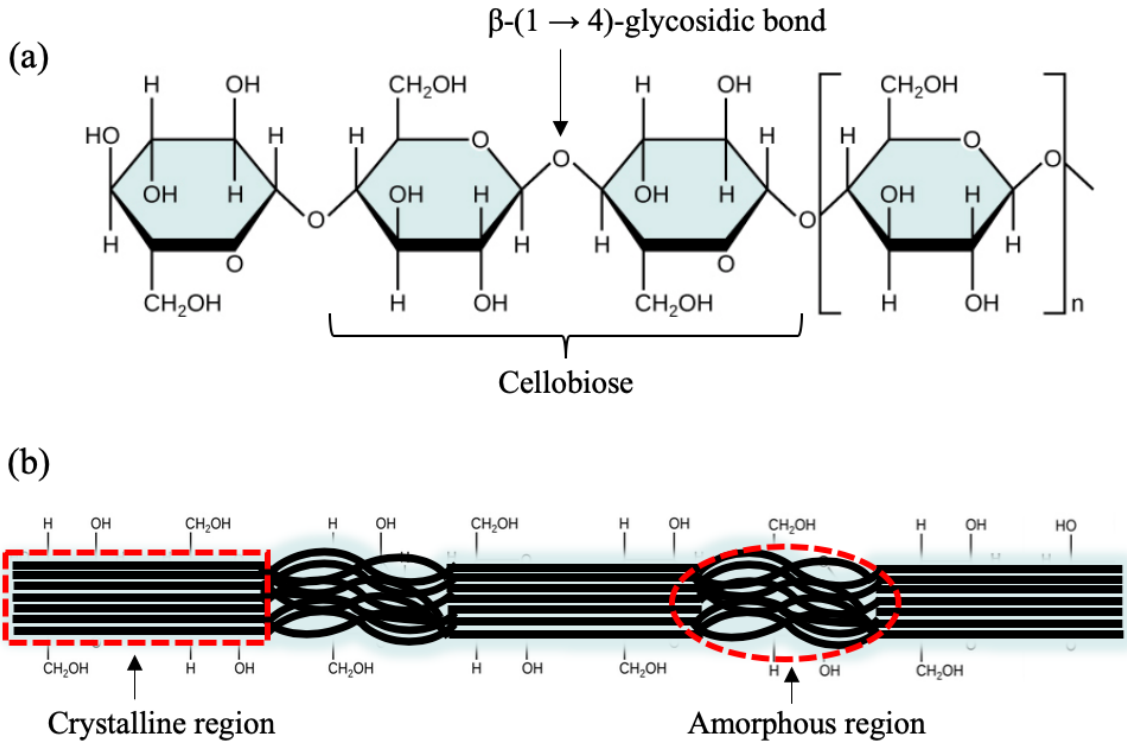


Fig. 2.2. Cellulose at the molecular level (a), and its organization as a fiber (b).

In the crystalline region of cellulose obtained from lignocellulosic biomass, the crystal structure is a metastable cellulose I α and a stable cellulose I β (Nishiyama et al., 2002; Nishiyama et al., 2003). The cellulose from this naturally crystalline state is also known as cellulose I. The ratio or the absence of cellulose I α and/or I β can differ according to the lignocellulosic biomass source. For example, wheat and rice straws are cellulose I allomorph in nature with only I β crystalline structure (Liu et al., 2006; Jiang & Hsieh, 2013). Cellulose I can be irreversibly converted into another crystal form known as cellulose II by successive treatment with strong alkaline solution, a process also known as mercerization (Okano & Sarko, 1985).

Besides the crystal structure change, the hydroxyl groups of cellulose provide great opportunities for surface chemical modifications. Common chemically modified celluloses are cellulose acetate, methylcellulose, ethylcellulose, hydroxyethylcellulose,

hydroxypropylcellulose, sodium carboxymethylcellulose, 2,2,6,6-tetramethylpiperidine-1-oxyl radical (TEMPO)-oxidized cellulose, among others (Rol et al., 2018). The TEMPO-oxidation is well known to be the most common surface functionalization towards nanofiber production. Briefly, the TEMPO is a stable and commercially available organic free radical reagent used to oxidize primary alcohols to aldehydes (Isogai et al., 2011). In the system, catalytic amounts of TEMPO and sodium bromide (NaBr) are dissolved in cellulose solutions at pH 10-11 by the addition of sodium hydroxide (NaOH), and the oxidation is started by the addition of sodium hypochlorite (NaClO) solution as a primary oxidant at room temperature and under constant agitation (Saito et al., 2006). The oxidation process is usually monitored from the pattern of aqueous NaOH consumption, which is continuously added to the reaction mixture to maintain the basic pH during the oxidation (Isogai et al., 2011). The reaction continues until no NaOH consumption is observed, which will mainly depend on the cellulose source, or until the known degree of oxidation is achieved. This process can take from 0.25 up to 72 h, and is stopped by decreasing the pH to 7 by adding HCl (Saito & Isogai, 2004; Saito et al., 2006; 2009). According to Isogai et al. (2011), the C6 primary hydroxyls of cellulose are oxidized to C6 carboxylate groups by the TEMPO/NaBr/NaClO process.

2.1.2. Hemicellulose

In the majority of straw biomass, the hemicellulose is the second most abundant polymer (Table 2.1). The hemicellulose from straw is a branched non-crystalline heteropolymer of pentoses ($C_5H_8O_4$)_n, mainly D-xylose and L-arabinose, hexoses ($C_6H_{10}O_5$)_n, mainly D-mannose, D-glucose, D-galactose, L-rhamnose, and sugar acids, mainly D-glucuronic acid, 4-O-methyl-d-glucuronic acid and D-galacturonic acid (Ren &

Sun, 2010). In contrast to cellulose that has only β -(1 \rightarrow 4)-glycosidic bonds between glucose units, the hemicellulose of straw biomass has multiple types of sugar units with a variety of glycosidic bonds in one molecule. For example, barley and canola straws have the hemicellulosic sugar composition of 66-74% xylose, 3-4% arabinose, 1-8% mannose, 4% galactose, 1-4% rhamnose, and 5-6% sugar acids (Sun & Tomkinson, 2000; Wang et al., 2016a).

The classification of hemicelluloses varies according to the main saccharide in the backbone structure, which depends on the biomass source. From the different classes of hemicelluloses (xylans, mannans, β -glucans, and xyloglucans), xylan is the main hemicellulose backbone structure present in most of the straw biomass (Ebringerová et al., 2005; Ren & Sun, 2010). Xylan consists of a main chain of xylose units linked by β -(1 \rightarrow 4)-glycosidic bonds and branches of small amounts of other saccharides or sugar acids. For instance, hemicelluloses from agricultural straws such as canola, barley, wheat, rye, and corn have essentially a xylan backbone with 4-*O*-methyl- α -D-glucopyranosyluronic acid attached to C2, and L-arabinofuranosyl and D-xylopyranosyl groups attached to C3 (Sun et al., 1998; Xiao et al., 2001; Jin et al., 2009; Wang et al., 2016a).

2.1.3. Lignin

Lignin in straw is a highly cross-linked complex structure formed by the polymerization of three monolignols: *p*-hydroxycinnamyl, coniferyl, and sinapyl alcohols (Xu et al., 2006). These monolignols are the precursors of phenylpropene aromatic units namely *p*-hydroxyphenyl, guaiacyl and syringyl, and their proportion in straw biomass depends on the crop species (Table 2.1). Most straws, including barley and canola straws,

contain lignin with *p*-hydroxyphenyl, guaiacyl, and syringyl units with ratios of 4-15%, 35-49%, and 40-61%, respectively (Buranov & Mazza, 2008). In the cell wall matrix, these aromatic units are linked between their dimers and oligomers via radical coupling with a variety of ether and carbon-carbon bonds, such as β -O-4, α -O-4, β -5, 5-5, 4-O-5, β -1 and β - β linkages (Xu et al., 2006). Although lignin has been studied for centuries, the complexity of the macromolecule and the different lignocellulosic biomass sources still lead to controversies and debate in terms of lignification process at the cellular level, molecular structure and isolation methods (Buranov & Mazza, 2008). At the moment, the association of lignin to carbohydrates in the cell wall is known as the lignin-carbohydrate complex (LCC). In straw biomass, the LCC is mainly linked by phenolic compounds, including *trans* isomers of *p*-coumaric (4-hydroxy-cinnamic) and ferulic (4-hydroxy-3-methoxycinnamic) acids (Mueller-Harvey et al, 1986; Sun et al., 2002; Xu et al., 2006). Another phenolic acid and aldehyde commonly detected in lignin isolated from straws are vanillin and syringaldehyde, which are released when the complex structure of LCC is broken via alkaline oxidation (Sun et al., 2002; Xu et al., 2006). Since the linkage between lignin and carbohydrates involves phenolic compounds, the LCC complex in straw is often referred as lignin/phenolics-carbohydrate complex (Buranov & Mazza, 2008).

2.2. Production of nanofibers from agricultural straw biomass

The lignocellulosic biomass, including agricultural straw, is one of the most economical renewable resources available today. While the biorefinery of lignocellulosic biomass into a spectrum of marketable products such as chemicals and biofuels is a relatively new research area, it is one of the most studied pathways for agricultural straw processing (Yuan & Sun, 2010; Ghaffar et al., 2015; Abrahan et al, 2016; Hans et al., 2019).

The processing and conversion of agricultural straw into useful value-added nanomaterials such as cellulose nanofibers (CNF) and lignocellulosic nanofibers (LCNF) have also gained increased attention due to its wide range of applications mainly in biocomposites and paper making (Chen et al., 2011a; Hassan et al., 2012; Costa et al., 2013; Yousefi et al., 2013; Hasanjanzadeh et al., 2014; Rojo et al., 2015; Soni et al., 2015; Delgado-Aguilar et al., 2016; Espinosa et al., 2017; Tarrés et al., 2017; Martelli-Tosi et al., 2018; Jian et al., 2019; Li et al., 2019; Zhao et al., 2019).

By definition, a nanofiber has a diameter of 100 nm or less, and length of several micrometers (μm) (Khalil et al., 2014). The CNF is known to be obtained from fully bleached cellulose fibers ($> 70\%$ cellulose), while LCNF is mainly obtained from unbleached cellulose fibers and has high amounts of non-cellulosic materials, such as hemicellulose and lignin compared to CNF (Delgado-Aguilar et al., 2016; Espinosa et al., 2017; Hassan et al., 2018; Jiang et al., 2018; 2019). Between the two nanofibers, the production and applications of CNF have been the most studied over the last two decades; whereas, the production and applications of LCNF is more recent, with the first publication in last decade (Fig. 2.3). However, the nomenclature of nanofibers has not been standardized to the chemical composition, which creates some misunderstanding and ambiguities in the literature. In the last few years, the CNF and LCNF obtained from agricultural straw had increased significance in the scientific community due to the shift towards industrialization of nanomaterials and bio-based products. The industrialization of nanofibers from agricultural straw can lead to socioeconomic and environmental benefits by bringing high economic returns to the farmers, generating a cost-effective product chain and minimizing problems associated with improper straw disposal.

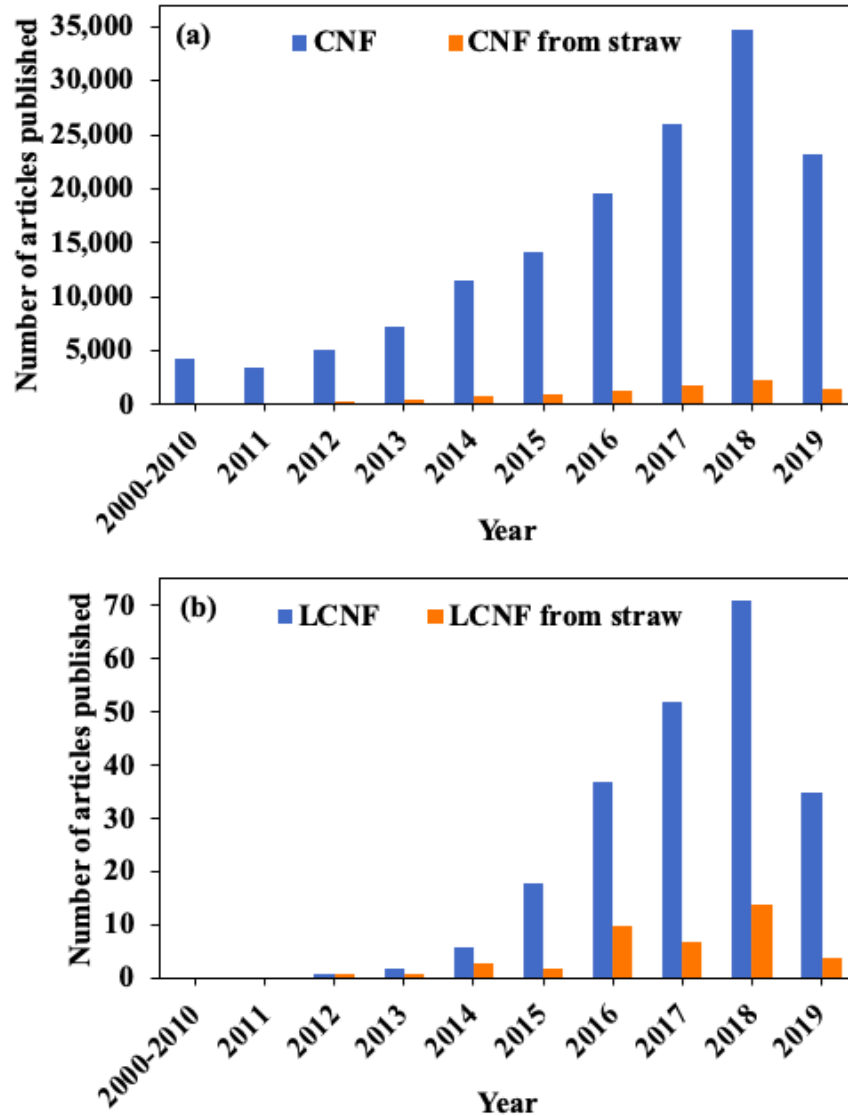


Fig. 2.3. Number of articles published using the keywords: “cellulose nanofib*” (CNF) and “cellulose nanofib* from straw” (a), and “lignocellulosic nanofiber” (LCNF) and “lignocellulosic nanofiber from straw” (b). Data analysis performed from 2000 to 2019 using the Web of Science database in July 2019.

In addition to the high availability and low cost of agricultural straw, the production of nanofibers from this biomass has promising applications in several fields due to its remarkable physical and chemical properties that are well known today, such as high aspect ratio, large specific surface area, unique optical properties, vast number of hydroxyl groups for surface modification, excellent biological properties, high tensile strength, stiffness and

flexibility, and good thermal and viscoelastic properties. These excellent features make it ideal for use as an independent functional material (Yousefi et al., 2013; Hassan & Hassan, 2016; Pacaphol & Aht-Ong, 2017; Li et al., 2019) or as a reinforcement unit for novel hybrid composite materials (Alemdar & Sain, 2008; Kaushik et al., 2010; Hassan et al., 2012; Yousefi et al., 2013; Boufi & Chaker, 2016; Martelli-Tosi et al., 2018; Jiang et al., 2019; Zhao et al., 2019). Furthermore, since the LCNF has higher amounts of lignin compared to the CNF, it has increased hydrophobicity, which is a desirable feature for nanopaper production (Delgado-Aguilar et al., 2016; Espinosa et al., 2016; Tarrés et al., 2017).

Both CNF and LCNF are usually obtained from a pre-treated agricultural straw biomass. The initial treatment aims to fractionate the biomass and isolate the polymers of the cell wall complex. In the case of CNF, fractionation is necessary to isolate the cellulose fiber. But the production of LCNF can be done in pre-treated or not pre-treated straw biomass. However, independent of the fractionation process applied, the production of nanofiber ends generally after the mechanical disintegration.

2.2.1. Straw biomass fractionation process

There are several treatments and techniques commonly applied to fractionate agricultural straw prior to mechanical nanofibrillation. Ideally, for CNF production, the fractionation process should aim for a maximum recovery of cellulose, but also avoid losses of hemicelluloses and lignin during the process. Besides enzymatic treatments, chemical treatments such as acid and alkali hydrolysis, bleaching, and organosolv processing are the most common and well-defined methods for hemicellulose and lignin removal from straw biomass (Table 2.2).

Table 2.2. Some of the conventional treatments used to fractionate agricultural straw biomass.

Straw and its main composition	Treatment conditions	Optimal condition*	Solid recovery	Treated fiber main composition			Reference	
				Cellulose	Hemicellulose	Lignin		
Acid hydrolysis								
Canola straw	36% cellulose	0.3-3% H ₃ PO ₄	3% H ₃ PO ₄	56%	58%	7%	34%	López-Linares et al. (2013)
	23% hemicellulose	145-215 °C	160 °C					
	17% lignin	5-55 min	45 min					
Wheat straw	32% cellulose	50-80% H ₃ PO ₄	80% H ₃ PO ₄	56%	60%	0%	17%	Wang et al. (2016b)
	16% hemicellulose	10-50 °C	50 °C					
	21% lignin	1-5 h	4 h					
Rice straw	42% cellulose	0.2-1% HNO ₃	0.6% HNO ₃	55%	61%	2%	25%	Kim et al. (2014)
	18% hemicellulose	140-180 °C	160 °C					
	17% lignin	1-20 min	11 min					
Alkali hydrolysis								
Canola straw	39% cellulose	5-20% NaOH	15% NaOH	48%	75%	11%	12%	Ciftci et al. (2018)
	24% hemicellulose	25-99 °C	99 °C					
	21% lignin	2-10 h	6 h					
Acid + Alkali hydrolysis								
Wheat straw	43% cellulose	18% NaOH at 25 °C for 2 h		nd	85%	6%	9%	Alemdar & Sain (2008)
	34% hemicellulose	10% HCl at 80 °C for 2 h						
	22% lignin	2% NaOH at 25 °C for 2 h						

*Optimal condition based on the maximum cellulose content of treated straw. H₃PO₄: phosphoric acid; HNO₃: nitric acid; NaOH: sodium hydroxide; HCl: hydrochloric acid; nd: not determined.

Table 2.2. Continued.

Straw and its main composition	Treatment conditions	Optimal condition*	Solid recovery	Treated fiber main composition			Reference
				Cellulose	Hemicellulose	Lignin	
Acid + Alkali + Bleaching treatments							
Sugarcane straw	41% cellulose	10% H ₂ SO ₄ at 100 °C for 1 h	nd	89%	4%	4%	Candido & Gonçalves (2016)
	26% hemicellulose	5% NaOH at 100 °C for 1 h					
	31% lignin	5% H ₂ O ₂ at 70 °C for 1 h					
Organosolv							
Canola straw	33% cellulose	65% EtOH 0.5-1.5% H ₂ SO ₄	65% EtOH 1% H ₂ SO ₄	68%	70%	10%	Brahim et al. (2017)
	20% hemicellulose	160-210 °C	210 °C				
	28% lignin	30-80 min	60 min				

H₂SO₄: sulfuric acid; NaOH: sodium hydroxide; H₂O₂: hydrogen peroxide; EtOH: ethanol; nd: not determined.

2.2.1.1. Acid and alkali hydrolysis

The acid hydrolysis pre-treatment mainly fractionates the lignocellulosic biomass structure through the breakdown of hydronium ions and the inter- and intramolecular bonding between cellulose, hemicellulose, and lignin. The use of acids such as phosphoric acid (H_3PO_4), hydrochloric acid (HCl), nitric acid (HNO_3), and sulphuric acid (H_2SO_4), in concentrated or diluted form are often used in the acid pre-treatment of agricultural straw biomass (Vázquez et al., 2007; Alemdar & Sain, 2008; Kaushik et al., 2010; López-Linares et al., 2013; Kim et al., 2014; Soni et al., 2015; Candido & Gonçalves, 2016; Wang et al., 2016b). The diluted acid pre-treatment is usually done at high temperatures and short processing times (140-200 °C for 1-45 min), while the concentrated acid pre-treatment is usually done at low temperatures and long processing times (10-100 °C for 1-5 h). For a concentrated acid pre-treatment of wheat straw using 80% (v/v) H_3PO_4 at 50 °C for 4 h, the hemicellulose content was completely removed, while the lignin was slightly reduced from 21 to 17%, and the cellulose content increased from 32 to 60% (Wang et al., 2016b). For a diluted H_3PO_4 (3% w/v) treatment at 160 °C for 45 min, the hemicellulose content of canola straw was reduced from 23 to 7%, while the lignin and cellulose contents increased from 17 to 34% and from 36 to 58%, respectively (López-Linares et al., 2013). The use of diluted HNO_3 (0.6% v/v) at 160 °C for 11 min also reduced the hemicellulose content of rice straw from 18 to 2%, while the lignin and cellulose contents were increased from 17 to 25% and from 42 to 61%, respectively (Kim et al., 2014).

Compared to acid hydrolysis, the alkali hydrolysis pre-treatment is commonly employed to solubilize lignin with partial solubilization of hemicellulose. The main mechanism of alkali hydrolysis includes the saponification of intermolecular ester bonds

between hemicellulose and lignin (Sun et al., 1996). The alkali treatment also causes swelling of the cellulose, which leads to an increase in the surface area and a decrease in its degree of crystallinity, depending on time and concentration of the alkali process. The alkaline reagents commonly used are hydroxides of sodium (NaOH) and potassium (KOH) (Alemdar and Sain, 2008; Chen et al., 2011a; Yousefi et al., 2013; Hasanjanzadeh et al., 2014; Espinosa et al., 2017; Ciftci et al., 2018; Xu et al., 2018). Among these chemicals, NaOH is the most common reagent used in agricultural straw biomass pre-treatment, where the process is also known as soda pulping. Ciftci et al. (2018) treated canola straw (39% cellulose, 24% hemicellulose, 21% lignin) using 5-20 wt.% NaOH at 25-99 °C for 2-10 h. At low NaOH concentration of 5 wt.% (at 75 °C for 2 h) a slight reduction of hemicellulose and lignin contents to 18 and 20%, respectively, was obtained. However, increasing the NaOH up to 15 wt.% with an increase in temperature to 99 °C for 6 h, the hemicellulose and lignin contents reduced to 12 and 13%, respectively, with an increase in cellulose content to 75% (Ciftci et al., 2018). Espinosa et al. (2017) recently treated several agricultural straws with NaOH (7 wt.%) solution at 100 °C for 2.5 h to obtain pulped straws with reduced lignin content. Overall, corn (44% cellulose, 31% hemicellulose, 18% lignin), wheat (40% cellulose, 31% hemicellulose and 18% lignin), barley (34% cellulose, 28% hemicellulose, 16% lignin), and oat (38% cellulose, 38% hemicellulose, 13% lignin) straws after treatment had hemicellulose and lignin contents in the range of 16-23% and 9-13%, respectively, while the cellulose content increased to 62-71% (Espinosa et al., 2017).

Although the alkali pre-treatment is mainly used to solubilize lignin, depending on the biomass type, it can also solubilize large amounts of hemicellulose (Hasanjanzadeh et al., 2014; Xu et al., 2018). Xu et al. (2018) reported that after treatment using diluted NaOH

(4 wt.%) at 80 °C for 4 h, the corn straw had the hemicellulose and lignin contents reduced from 28 to 4%, and from 20 to 13%, respectively, with an increase in cellulose content from 44 to 76%. Similarly, rice straw with 47% cellulose, 27% hemicellulose and 21% lignin treated using concentrated NaOH (18 wt.%) solution at 60 °C for 1 h had a higher percentage of hemicellulose removal (80%) compared with that of lignin (30%) (Hasanjanzadeh et al., 2014).

Combination of acid hydrolysis and alkali treatment using NaOH have also been studied for straw fractionation. Alemdar & Sain (2008) first treated the wheat straw with concentrated NaOH (18 wt.%) solution at 25 °C for 2 h, followed by acid hydrolysis with 10% (v/v) HCl at 80 °C for 2 h, and diluted NaOH (2 wt.%) solution at 25 °C for 2 h. After their treatments, the hemicellulose and lignin contents of the straw reduced from 34 to 6%, and from 22 to 9%, respectively, while the cellulose content increased from 43 to 85%.

Another alkaline reagent used for straw pretreatment is sodium sulfite (Na_2S), which is also known as Kraft pulping. Recently, Hassan et al. (2018) compared the pre-treatments of rice straw (43% cellulose, 20% hemicellulose, and 21% lignin) using soda (10 wt.% NaOH) and Kraft (10 wt.% Na_2S) pulping at 160 °C for 2 h. Both pulping pre-treatments reduced the hemicellulose content to 14-15% and lignin content to 15-17%, while increasing the cellulose content to 54-66% (Hassan et al., 2018). Furthermore, for both pulping processes, various catalysts including anthraquinone (AQ) have been used to enhance the results of alkali pre-treatment processes (Costa et al., 2013). Costa et al. (2013) treated sugarcane straw with concentrated Na_2O (16 wt.%) and AQ catalyst (0.15%) at 160 °C for 3.5 h, and reduced the hemicellulose and lignin contents from 27 to 4%, and from 26 to 9%, respectively, while the cellulose content was increased from 34 to 81%.

Overall, the diluted or concentrated acid pre-treatment reduces the hemicellulose content of straw biomass to < 5%, while the alkaline pre-treatment alone is less effective to reduce lignin, but can simultaneously reduce (slightly) the hemicellulose and lignin contents depending on the treatment time and alkali solvent concentration. To isolate cellulose using a combination of acid and alkali hydrolysis, a processing time of around 6 h is needed, but a significant amount of non-cellulosic compounds can still remain on the pre-treated fiber. Besides the long processing time, abundant water is needed to neutralize the pre-treated straw, and chemical streams are generated that need to be properly disposed of to minimize environmental impact. Furthermore, a bleaching step is usually needed to obtain purified cellulose fibers.

2.2.1.2. Bleaching

Since the alkali pulping pre-treatment is usually not enough to remove all lignin content, bleaching is introduced as one more step for the delignification process of agricultural straw biomass. Chemical pulp bleaching is accomplished using various compounds containing chlorine or oxygen, and performed in several stages to increase the efficiency and reduce the concentration of chemicals required. Acidified sodium chlorite (ASC), hydrogen peroxide (H_2O_2), and chlorine dioxide (ClO_2) are the most common bleaching agents in straw biomass processing. Sodium chlorite ($NaClO_2$) in acidified solution decomposes mainly to chlorous acid ($HClO_2$), chlorine dioxide (ClO_2), chloride (Cl^-) and oxygen (O_2). The $HClO_2$ and ClO_2 are strong oxidizing agents, and the main active components during the bleaching process due to the modification of lignin aromatic structure by hydrolytic cleavage, demethylation, quinone formation and electrophilic displacement (Gierer, 1985). Boufi & Chaker (2016) bleached corn straw (38% cellulose,

32% hemicellulose, 19% lignin) with ASC (1 wt.% NaClO with 0.5% acetic acid) at 70 °C for 6 h, where the ASC solvent was freshly added every 1.5 h followed by alkali pulping (5 wt.% NaOH) at 70-80 °C for 6 h. At the end of the process, the treated straw had 69% cellulose, 31% hemicellulose and lignin content of < 1%. Similarly, Ciftci et al. (2018) applied the ASC bleaching (1.7 wt.% ACS at 75°C for 6 h, with fresh ASC added every 2 h) after NaOH treatment to reduce the lignin content of pre-treated canola straw (75% cellulose, 12% hemicellulose, 13% lignin). After ASC bleaching, the treated straw had 81% cellulose, 10% hemicellulose and 8% lignin (Ciftci et al., 2018).

The use of H₂O₂ bleaching agent in combination with alkali pre-treatment and ASC bleaching showed increased solubility of soluble lignin for both sugarcane and soybean straws (Candido & Gonçalves, 2016; Martelli-Tosi et al., 2018). Sugarcane straw (41% cellulose, 26% hemicellulose, 37% total lignin) was first acid hydrolyzed using 10% (v/v) H₂SO₄ at 100 °C for 1 h, followed by alkali treatment using 5% (w/v) NaOH at 100 °C for 1 h and bleaching step using 5% (v/v) H₂O₂ at 70 °C for 1 h. With the acid hydrolysis, the hemicelluloses and insoluble lignin decreased to 13 and 15%, respectively, whereas the soluble lignin slightly increased to 9%. However, after alkali hydrolysis, the insoluble and soluble lignin reduced to 1% and 5%, respectively, with also a reduction in hemicellulose content to 7%. Then, the bleaching step using H₂O₂ mainly reduced the soluble lignin to 3% and hemicellulose to 4%, but with less than 0.2% reduction in insoluble lignin content. In another study, Martelli-Tosi et al. (2018) treated soybean straw (40% cellulose, 23% hemicellulose, 13% lignin) with alkali hydrolysis (18 wt.% NaOH at 30 °C for 15 h) followed by a bleaching step using ASC (3 wt.% NaClO₂ with 1 wt.% acetic acid) at 75 °C for 3 h or diluted H₂O₂ (4 wt.%) at 90 °C for 3 h to isolate cellulose fibers. After both

bleaching treatments, the lignin content reduced to 10%, but the diluted H₂O₂ processing solubilized increased amounts of soluble lignin compared to ASC bleaching.

In general, acid, alkali and bleaching pre-treatments are widely used methods for straw fractionation. However, drawbacks including long processing times (up to 24 h), neutralization steps, low-quality lignin by-product, hemicellulosic sugar degradation (e.g. furans), environmentally hazardous waste and equipment corrosion, have been the main challenges associated with those pre-treatment techniques.

2.2.1.3. Organosolv

Organosolv is applied to dissolve mainly lignin from lignocellulosic biomass using organic solvents (e.g. acetone, ethanol (EtOH) and methanol (MeOH)) with or without catalysts (e.g. NaOH, H₂SO₄, HCl, acetic and formic acids). Delignification using aqueous EtOH is the most common organosolv treatment for agricultural straw biomass. Organosolv processes rely on the cleavage of α - and β -aryl ether linkage bonds of lignin, followed by its dissolution (McDonough, 1993). With the addition of an acid catalyst, the cleavage of α -aryl ether is faster than that of β -aryl ether bonds (Buranov & Mazza, 2008). Due to the extent of delignification using organosolv, large proportions of hemicelluloses are also released and removed during the process, especially when an acid catalyst or high temperatures (> 170 °C) are used. For example, the organosolv treatment of wheat, rice, rye, barley, and corn straws using 60% (v/v) EtOH with 2.0% HCl as a catalyst at 75 °C for 3 h released 52, 51, 47, 44, and 54% of the lignin, respectively, and 44, 50, 31, 36, and 40% of the original hemicelluloses, respectively (Sun et al., 2002). Organosolv treatment of canola straw (33% cellulose, 20% hemicellulose, 28% lignin) with 65% (v/v) EtOH, 1%

H₂SO₄ catalyst at 210 °C for 1 h removed 50 and 54% of hemicellulosic sugars and lignin, respectively (Brahim et al., 2017).

Xu et al. (2006) compared the organosolv treatment of wheat straw using aqueous MeOH (60% v/v) and EtOH (60% v/v) with 0.1% HCl as a catalyst at 85 °C for 4 h. The organosolv using aqueous EtOH removed significantly higher amounts of lignin (22%) compared to organosolv MeOH (14%) treatment. However, comparing organosolv treatment (60% v/v EtOH at 210 °C for 1 h) with soda pulping (7 wt.% NaOH at 100 °C for 2.5 h) and Kraft pulping (16 wt.% NaOH and 25 wt.% nitrous oxide at 170 °C for 0.7 h) of wheat straw (40% cellulose, 31% hemicellulose, 18% lignin) fractionation, the organosolv processing reduced more lignin and hemicellulose contents (reduction to 11 and 8%, respectively) than soda pulping (reduction to 13 and 26%, respectively), but less than Kraft pulping (reduction to 6% and 4%, respectively) (Sánchez et al., 2016). Although the organosolv treatment might not be suitable for complete delignification, the lignin removed with this process is highly purified and can be used for further processing (Wörmeyer et al., 2011). Moreover, the solvent used can be recovered and recycled by evaporation to reduce processing costs.

Although many authors classified the organosolv method as “green” technology due to the quality of lignin extracted, the use of chemical catalysts like mineral acids (e.g. HCl and H₂SO₄) that are corrosive for equipment, and organic acids (e.g. acetic and formic acids) that are expensive and highly volatile, the organosolv process still demands high operation costs and several safety procedures to avoid environmental pollution and explosion. According to Mesa et al. (2016), those major drawbacks have held back the commercial acceptance of organosolv pre-treatment for lignocellulosic biomass

processing. Therefore, new processes based on emerging and green technologies have been studied mainly to meet the growing demand for environmentally friendly methods of modern industry and to overcome many of the disadvantages associated with conventional technologies used for centuries such as long processing times, toxic and hazardous waste, and the need for neutralization steps. Environmentally friendly processing, also called “green” processes, and emerging technologies applied to fractionate agricultural straw biomass are shown in Table 2.3.

2.2.1.4. Steam and wet explosion

The explosion treatments are referred to the processing where the biomass is treated with a high-pressure solvent, and when the pressure is suddenly reduced the materials undergo an explosive decompression that reduces the fiber size, enhancing the fractionation process.

Steam explosion is the most common treatment for agricultural straw biomass fractionation at laboratory scale (Table 2.3). This method uses temperatures of 140-260 °C, and corresponding pressures of 7-44 bar, for seconds to several minutes before decompression to ambient condition (Sun & Cheng, 2002). The principle of steam explosion is that at such pressures the steam condenses and permeates into the biomass, initiating an autohydrolysis reaction mainly on hemicellulose side chains (Duque et al., 2016). With the release of acetic acid from the hemicellulose polymer, the autohydrolysis process is enhanced, inducing cleavage of glycosidic bonds between hemicellulosic sugar units that are solubilized in the pressurized steam.

Table 2.3. Green and emerging treatments to fractionate agricultural straw biomass.

Method	Straw and its main composition	Process parameters	Treated fiber main composition			Reference	
			Cellulose	Hemicellulose	Lignin		
Deep eutectic solvents	Rice straw	34% cellulose 20% hemicellulose 22% lignin	ChCl:oxalic acid dehydrate (molar ratio 1:1) at 120 °C for 1 h	65%	< 1%	14%	Hou et al. (2018)
	Wheat straw	35% cellulose 22% hemicellulose 19% lignin	ChCl:monoethanolamine (molar ratio 1:6) at 130 °C for 12 h	58%	20%	1%	Zhao et al. (2018a)
Ionic liquids	Rice straw	38% cellulose 20% hemicellulose 18% lignin	[Ch]Lys at 90 °C for 24 h	62%	16%	11%	Hou et al. (2012)
	Rice straw	33% cellulose 32% hemicellulose 23% lignin	[C ₄ mim]Cl: K ₂ CO ₃ /H ₂ O (50 wt.%) at 95 °C for 3 h	55%	20%	7%	Gao et al. (2019)
Microwave assisted hydrolysis	Corn straw	33% cellulose 33% hemicellulose 7% lignin	H ₂ O, 800 W for 5 min	38%	33%	6%	Wang et al. (2019)
	Wheat straw	41% cellulose 26% hemicellulose 21% lignin	NaOH (1% w/v), 700 W for 25 min	79%	8%	6%	Zhu et al. (2006)

ChCl: choline chloride; [Ch]Lys: cholinium lysine; [C₄mim]Cl: K₂CO₃/H₂O: 1-butyl-3-methylimidazolium chloride, potassium carbonate and water system; NaOH: sodium hydroxide.

Table 2.3. Continued.

Method	Straw and its main composition	Process parameters	Treated fiber main composition			Reference	
			Cellulose	Hemicellulose	Lignin		
Pressurized fluids	Barley straw	40% cellulose 22% hemicellulose 19% lignin	sCW at 165 °C, 7 bar for 1 h	68%	5%	18%	Pronyk & Mazza (2012)
	Flax straw	34% cellulose 21% hemicellulose 30% lignin	PAE (60% v/v) at 220 °C, 52 bar for 2.5 h	79%	5%	8%	Buranov & Mazza (2012)
Steam explosion	Canola straw	32% cellulose 17% hemicellulose 18% lignin	At 200 °C, 23 bar for 5 min	50%	5%	41%	López-Linares et al. (2015)
	Cotton straw	38% cellulose 21% hemicellulose 29% lignin	At 200 °C, 25 bar for 10 min	53%	12%	34%	Gaur et al. (2017)
Wet explosion	Corn straw	39% cellulose 22% hemicellulose 15% lignin	At 195°C , 12 bar by O ₂ pressure for 15 min	34%	3%	6%	Qiang & Thomsen (2012)
	Rice straw	41% cellulose 21% hemicellulose 12% lignin	At 190°C, 6 bar by air pressure for 20 min	52%	10%	6%	Morone et al. (2017)

sCW: subcritical water; PAE: pressurized aqueous ethanol; O₂: oxygen

For example, rice (40% cellulose, 18% hemicellulose, 21% lignin) and cotton (38% cellulose, 21% hemicellulose, 29% lignin) straws treated using steam explosion at 200-210 °C and 25-100 bar for 10 min had the hemicellulose contents reduced to < 12%, while the lignin and cellulose contents increased to 23-34% and 53-61%, respectively (Sharma et al., 2015; Gaur et al., 2017). Similarly, canola straw (32% cellulose, 17% hemicellulose, 18% lignin) was treated with steam explosion at 220 °C and 23 bar for 5 min, resulting in a significant removal of hemicellulose with a reduction to 6%, and a substantial increase of lignin and cellulose contents to 41 and 50%, respectively (López-Linares et al., 2015). The increase of lignin content on pre-treated straw biomass is due to the re-polymerization of reactive functional groups from lignin fragments such as catechol, phenol, syringols and guaiacols, and the formation of pseudo-lignin during the process (Fang et al. 2008; Sannigrahi et al., 2011).

Steam explosion treatment can also be combined with catalysts such as NaOH and H₂SO₄ for the fractionation of straw towards lignin and hemicellulose removal. For example, wheat straw (46% cellulose, 37% hemicellulose, 17% lignin) treated using alkali (12% NaOH) catalyzed steam explosion at 200 °C and 20 bar for 4 h, had reduced hemicellulose and lignin contents to 22 and 10%, respectively, while the cellulose increased to 65% (Kaushik et al., 2010). However, when wheat straw (34-55% cellulose, 23-40% hemicellulose, 15% lignin) was treated using acid (3% H₂SO₄) catalyzed steam explosion at 145-187 °C and 7 bar for 10-15 min, the hemicellulose was almost completely removed (reduction to < 5%), but the lignin content increased up to 36%, and the cellulose content reduced to 27-35% (Monschein & Nidetzky, 2016; Cornejo et al., 2019), which is not desirable for CNF production purposes.

The wet explosion treatment is similar to the steam explosion, but instead of saturated steam, oxygen (O₂) or air is injected into the reactor with wet biomass. Then, the reaction occurs at temperatures of 140-210 °C and pressures of 4-35 bar for residence times of 5-120 min (Biswas et al., 2015). The hemicellulose side chain depolymerization starts first due to the increase in temperature and water ionization. With a further release of sugar acids, the reactions on the hemicellulose backbone occurs until most of the hemicellulosic oligomers are extracted from the biomass. Also, due to the addition of air or gaseous O₂, the lignin oxidation can occur (Biswas et al., 2015). Furthermore, similar to steam explosion, the wet explosion treatment can be used in combination with a catalyst to enhance the fractionation process.

For example, catalyzed (3.5-9.5% w/v sodium carbonate Na₂CO₃) and uncatalyzed wet explosion treatments at 169 °C and 4 bar air pressure for 18 min was studied for the fractionation of rice straw (41% cellulose, 21% hemicellulose, 12% lignin) (Morone et al., 2018). Uncatalyzed treatment had no effect on hemicellulose content (21%) but had a slight increase on lignin and cellulose contents to 14 and 43%, respectively. However, after increasing the catalyst (Na₂CO₃) concentration up to 9.5%, the wet explosion treatment removed large amounts of hemicellulose (reduction to 5%) and lignin (reduction to 8%), whereas the cellulose content increased up to 64% (Morone et al., 2018).

Similar treatment comparison between uncatalyzed (at 195°C and 12 bar by O₂ pressure for 15 min) and catalyzed (2% Na₂CO₃) wet explosion was studied with corn straw (39% cellulose, 22% hemicellulose, 15% lignin) (Qiang & Thomsen, 2012). However, in this case, the catalyst did not show any significant effect on the composition of treated straw. Instead, both processes slightly reduced the cellulose to 34-35%, and drastically

reduced the hemicellulose and lignin contents to 3-5% and 6-8%, respectively (Qiang & Thomsen, 2012). The concentration of catalyst (0.5-4.0% w/v H₂O₂) on the wet explosion process of rice straw (41% cellulose, 21% hemicellulose, 12% lignin) at 160 and 190 °C and 6 bar air pressure for 20 min, did not show any significant effect on treated fiber composition (Morone et al., 2017). However, by increasing the temperature from 160 to 190 °C, the treated straw fiber cellulose content increased from 48-53 to 62-63%, and hemicellulose content reduced from 18-20 to 10-11%, while the lignin content was reduced to < 6% (Morone et al., 2017).

Steam and wet explosion pre-treatments have some advantages such as reduced hazardous chemicals, and no recycling cost (Duque et al., 2016). On the other side, the risk of cellulose depolymerization and lignin re-polymerization are the main challenges of these technologies for application as a pre-treatment step prior to CNF production.

2.2.1.5. Ionic liquids and deep eutectic solvents

Ionic liquid (IL) treatment uses mainly organic cation and organic/inorganic anion salts with melting point below 100 °C, that are non-flammable, electrochemically stable, with a low vapor pressure and high ionic conductivity and catalytic activity (Zdanowicz et al., 2018). The tunability of the chemistry of IL makes this treatment suitable to dissolve either cellulose or lignin under mild conditions of 25-190 °C for times of up to 24 h (Halder et al., 2019). The use of IL to solubilize lignin is also known as the ionosolv process. The ionosolv approach is mostly determined by the nature of the anion, by which the mechanism of delignification using acidic anions is based on the cleavage of β-aryl ether by initial protonation followed by the dehydration step (Gregorio et al., 2016). However, the ratio of anion-cation and the water content also has notable effects on the fractionation process (Verdia

et al., 2014). The imidazolium cation, and its methylated form methylimidazolium, as well as cholinium cation with amino acid anion ([Ch]AA), have shown remarkable delignification effects of agricultural straw biomass. Also, with aqueous diluted ionic liquid, the viscosity of the solvent is reduced, which increases the solvent diffusion into the straw cell walls and favour hemicellulose hydrolysis, while preventing sulfation reactions with hydroxyl (-OH) groups of the biomass (Brandt, 2017).

A legume straw (38% cellulose, 30% hemicellulose, 24% lignin) was fractionated using diluted 1-butyl-3-methylimidazolium chloride ([C₄mim]Cl) (0-80 wt.%) at 50-170 °C and 1-23 bar for 0.5-4 h (Wei et al., 2012). The IL concentration strongly affected the delignification efficiency, while the pressure and temperature had a positive effect only on the total mass dissolved. Treatment at 150 °C and 1 bar for 2 h using pure [C₄mim]Cl resulted in maximum delignification efficiency of 10%, whereas when 80 wt.% [C₄mim]Cl was used, the delignification efficiency increased to almost three times, resulting in a treated straw mainly composed of 48% cellulose, 27% hemicellulose, and 17% lignin (Wei et al., 2012). Similarly, wheat straw (37% cellulose, 22% hemicellulose, 18% lignin) was treated with 1-ethyl-3-methylimidazolium acetate ([Emim]Ac) at 130-170 °C, with IL concentration of 0-100 wt.% for 0.5-5.5 h (Fu & Mazza, 2011). Although in this case all tested variables had significant effects on the composition of the treated straw fiber, the hydrolysis at 162 °C with 80 wt.% [Emim]Ac for 1.5 h, resulted in a maximum delignification efficiency of 80% and hemicellulose removal up to 75% (Fu & Mazza, 2011). Although ionic liquid treatment is a promising approach for delignification of straw biomass, challenges on process cost and recyclability of the IL are still the main obstacles for scale up.

Ren et al. (2016) utilized seawater instead of fresh water as a dilution media for [Emim]Ac and [Ch]AA treatment of wheat straw. After treatment using 80 wt.% IL/seawater mixtures at 90 °C for 6 h, the maximum delignification of 71% was achieved with cholinium arginine ([Ch]Arg) compared to [Emim]Ac (delignification of 25%) (Ren et al., 2016). Although the use of seawater was a promising option to reduce the cost of ionosolv treatment, the impact of sea salt was not studied. Recently, Gao et al. (2019) studied the change in the composition of rice straw (33% cellulose, 32% hemicellulose, 23% lignin) after treatment with a ternary system of [C₄mim]Cl/inorganic salts (K₃PO₄ and K₂CO₃)/water at 95 °C for 3 h. The system with 50% [C₄mim]Cl, 50% K₂CO₃ and 5% water, resulted in a treated straw fiber with 55% cellulose, 20% hemicellulose, and 7% lignin, with a delignification efficiency of 70%, similar to the seawater treatment obtained by Ren et al. (2016). In another study, Hou et al. (2012) synthesized [Ch]AA with lysine, glycine, alanine, serine, threonine, methionine, proline and phenylalanine for the treatment of rice straw (38% cellulose, 20% hemicellulose, 18% lignin) at 90 °C for 24 h, using fresh and recycled solvents. When rice straw was treated with fresh [Ch]Lys, the lignin and hemicellulose contents were reduced to 11 and 16%, respectively, while the cellulose content increased up to 62%. After [Ch]Lys was used for five times, without purification in between each batch, the delignification efficiency decreased slightly from 59% to 53%. Besides these promising strategies for the reduction of overall processing cost, the applied methods are still limited to few biomass residues, and the economical assessment of those strategies has not been explored.

Mainly due to the economical limitations of IL, deep eutectic solvents (DES) have been attracting attention as a new green solvent for the fractionation process of agricultural

straw biomass. They share many of the promising properties of IL, such as low melting point, low vapor pressure, high solubility and tunability, but are much cheaper and easier to prepare than IL (Vanda et al., 2016). Generally, DES are formed by mixing a hydrogen bond donor, such as organic acids, urea, or glycerol, and a hydrogen bond acceptor like quaternary ammonium salt, which are linked to each other by means of hydrogen bond interactions (Vanda et al., 2018). For lignocellulosic pre-treatment, the most common hydrogen bond acceptor of DES is choline chloride (ChCl). Rice straw (34% cellulose, 20% hemicellulose, 22% lignin) treated with ChCl:oxalic acid dehydrate at a molar ratio of 1:1, and 120 °C for 1 h, had removed almost all hemicellulose (reduction to < 1%) with a good delignification efficiency (lignin content decreased to 14%), while the cellulose content increased up to 65% (Hou et al., 2018). Similarly, when wheat straw (35% cellulose, 22% hemicellulose, 19% lignin) was treated using ChCl:monoethanolamine at a molar ratio of 1:6, and 130 °C for 12 h, the hemicellulose slightly decreased to 20%, while an almost complete delignification was achieved (reduction of lignin to 1%), increasing the cellulose content up to 58% (Zhao et al., 2018a).

In comparison to ionic liquid process, DES are novel solvents, and the research for their application in straw biomass pre-treatment is still limited mostly to biofuel production. However, DES had outstanding advantages compared to IL, mainly due to the lower cost of starting solvent and its ease of recyclability. However, DES solvent had higher density and viscosity with lower stability at temperatures of < 200 °C, compared to IL (Sattlewal et al., 2018). Further studies using DES for different straw biomass are still needed.

2.2.1.6. Microwave assisted hydrolysis

Microwaves (MW) are electromagnetic waves with a frequency band of 300 MHz and 300 GHz (Leonelli & Mason, 2010), between infrared radiation and radio waves in the electromagnetic spectrum, used as a non-conventional heating source, and as a heating source for lignocellulosic biomass fractionation (Liu et al., 2017; Wang et al., 2019). The MW process as a pre-treatment of lignocellulosic biomass relies on the biomass structural disruption by the alignment of its polar molecules that induces internal vibration until the material inside becomes heated by dielectric interaction (Leonelli & Mason, 2010). Compared to the conventional heating process, where heat is transferred to the material by conduction, convection, and radiation, the MW process uses dielectric heating to transfer electromagnetic energy to thermal energy inside the material (Motasemi & Afzal, 2013).

Earlier, Zhu et al. (2006) compared MW-assisted alkali hydrolysis with conventional alkali hydrolysis to treat wheat straw (41% cellulose, 26% hemicellulose, 21% lignin), using diluted NaOH (1% w/v) as a solvent. Conventional treatment was studied at 100 °C for 15-60 min, whereas MW-assisted hydrolysis used powers of 300-700 W, at a constant frequency of 2450 MHz for 15-60 min. During the conventional treatment using NaOH, the hemicellulose and lignin contents were reduced simultaneously with long processing times. At the end of 60 min, the alkali-treated straw had mainly 74% cellulose, 11% hemicellulose, and 7% lignin. Using MW-assisted alkali hydrolysis and increasing the power applied from 300 to 700 W reduced the extraction time of non-cellulosic materials. Using 300 W for 60 min, the treated straw had mainly 80% cellulose, 8% hemicellulose, and 6% lignin, whereas similar results were obtained using MW at 500 W for 35 min, and 700 W for 25 min (Zhu et al., 2006).

Similarly, Liu et al. (2017) treated wheat straw (45% cellulose, 34% hemicellulose, 9% lignin) with a sequential method of steam explosion (100 °C, 30 bar, 2 min) followed by MW-assisted alkali hydrolysis (2% w/v NaOH, 140 °C, 1200 W, 20 min) to isolate cellulose fiber prior to nanofibrillation. After steam explosion, the treated straw had mainly 57% cellulose, 14% hemicellulose, and 9% lignin, and after MW-assisted hydrolysis, the cellulose content increased up to 94%, while hemicellulose and lignin contents decreased to 6 and 2%, respectively. However, a different result was obtained recently by Wang et al. (2019) when only water was used as the solvent during MW treatment (800 W for 5 min) of corn straw (33% cellulose, 33% hemicellulose, 7% lignin). After MW treatment, the corn straw had slightly reduced lignin content to 6%, with no change in hemicellulose content (33%), and a small increase in cellulose content to 38%. Besides, Wang et al. (2019) did not use any chemicals to assist the hydrolysis, the short reaction time of 5 min compared to 15-60 min used by the other authors could be the reason to insignificant delignification results (1%).

Recently, Chen & Wan (2018) used MW-assisted DES hydrolysis to optimize the fractionation of corn straw (32% cellulose, 19% hemicellulose, 17% lignin). The treatment was performed at only one condition using ChCl:lactic acid at a molar ratio of 1:6, and power of 800 W for 45 s, reaching a maximum temperature of 152 °C by the end of the process. Hemicellulose and lignin contents decreased to 5 and 9%, respectively, while the cellulose content of treated straw increased up to 66%. In that study, the MW-assisted DES hydrolysis showed delignification efficiency of 47%, where more than 73% of hemicelluloses were removed within a short period of time of < 1 min (Chen & Wan, 2018). However, further studies should be conducted to optimize this process.

In general, MW is a source of heat for any type of solvent treatment. It has an advantage over conventional heating treatments like water and oil bath due to a short heating period of time. However, common chemical solvents used in MW-assisted hydrolysis are hazardous and the pre-treated biomass needs neutralization steps.

2.2.1.7. Pressurized fluid treatment

Pressurized fluid (PF) treatment is based on the principle of diluted acid hydrolysis technology, but it does not need to use hazardous chemicals, neutralization steps, and minimizes the generation of chemical waste. It is considered as a green technique because it uses mainly solvents generally recognized as safe (GRAS), such as water and ethanol, at temperatures above their boiling point (water at 100 °C and ethanol at 78 °C) but below their critical point (water at 374 °C and ethanol at 240 °C), and pressures high enough (> 1 bar and < 220 bar) to keep the solvent in its subcritical state. When the PF is water, it is also named as subcritical water (sCW) or pressurized hot-water treatment. The PF process can be performed in batch, continuous or semi-continuous modes, where besides temperature and pressure, the flow rate is another important variable. Briefly, the PF system comprises of a high-pressure pump to introduce the solvent into a high pressure vessel, which is maintained at a controlled temperature by an oven, heater band or their combination, and by different valves and restrictors to control the process pressure. In a continuous and semi-continuous system, the hydrolysate is collected throughout the process, whereas in a batch system, the hydrolysate and the solid treated material are separated after the completion of the process.

The PF exhibits unique properties due to the change of dielectric constant, ionic product, density, viscosity, and diffusivity (Cocero et al., 2018). For example, in sCW, as

the process temperature increases the density, viscosity, and dielectric constant of water decrease, while its diffusivity and ionic constant increase, allowing faster mass transfer of the PF into the biomass matrix (Kruse & Dinjus, 2007). The decrease of the dielectric constant of water, which measures polarity, is mainly due to the breakdown of hydrogen bonds under subcritical conditions. Water at 25 °C and 1 bar (ambient conditions) has a high polarity and a dielectric constant close to 80, while when heated at 186 °C and 50 bar, it has a dielectric constant of 39 (same as ethylene glycol, 39), and with a further increase in temperature up to 226 °C and 50 bar, it has a dielectric constant of 27, a value between the dielectric constants of MeOH (33) and EtOH (24) (Akerlof, 1932; Fernández et al., 1997). Under those conditions, sCW is an alternative solvent to extract phenolic compounds mainly present as the linkages of lignin-carbohydrate complex (LCC) in the plant cell wall (Sarkar et al., 2014; Ciftci & Saldaña, 2015).

Ciftci & Saldaña (2015) reported that increasing the treatment temperature of sCW from 160 to 220 °C (200 bar, flow rate of 5 mL/g, 30 min) resulted in an increased extraction of phenolic compounds by ten times from 0.07 to 0.72 mg gallic acid/g lupin hull. Sarkar et al. (2014) hydrolyzed barley hull with sCW at 120-180 °C, 150 bar, flow rates of 2-5 mL/min, and 10-180 min for maximum extraction of phenolic compounds. By increasing the process temperature from 120 to 180 °C after 60 min, the total phenolic content of the hydrolysate increased from 3.23 to 9.47 mg gallic acid/g hull, mainly due to the decrease in the dielectric constant of water. However, a further increase in the extraction of phenolic compounds up to 75.43 mg gallic acid/g hull was obtained when diluted EtOH (12% v/v) was used as the PF at 180 °C, due to a further reduction in dielectric constant of the PF by the addition of EtOH. The main phenolic acids extracted from barley hull were

ferulic acid and coumaric acid, two of the most abundant phenolic acids present in the LCC linkages of lignocellulosic biomass (Buranov & Mazza, 2008). Calculations of dielectric constants of pure water and pure EtOH as a function of temperature can be done using Eqs. (2.1) and (2.2), respectively (Fakhree et al., 2010).

$$\ln D_{H_2O} = 5.769 - 0.00471T \quad (2.1)$$

$$\ln D_{EtOH} = 5.034 - 0.00619T \quad (2.2)$$

where, D (dimensionless) is the dielectric constant, and T is the temperature.

In general, PF treatment using water as a solvent is one of the most promising pre-treatments to extract hemicellulose, whereas the PF processing using aqueous EtOH is recognized as a good fluid for lignin depolymerization. Cellulose is insoluble in sCW at mild temperatures of < 200 °C, mainly due to its crystallinity and high molecular weight, which requires near critical temperature (320-350 °C) to start its decomposition (Sasaki et al., 2000).

2.2.1.7.1. Hemicellulose hydrolysis

The increased ionic product (K_w) of sCW is the main pathway for hemicellulose fractionation. The K_w of water in the subcritical region is some orders of magnitude higher than that at ambient conditions. At ambient conditions (25 °C and 1 bar), the water has K_w of 10^{-14} mol² /L², whereas at temperatures up to 200 °C and 250 bar it has K_w of 10^{-11} mol² /L² (Marshall & Franck, 1981). Overall, the increased production of OH⁻ and H₃O⁺ ions catalyzes the breakdown of hemicellulosic polysaccharides into oligomers of decreasing molecular weight, which continues to reduce in size until they become water-soluble (Cabeza et al., 2016). Then, the hydrolysis of the solubilized oligomers into smaller ones occurs, and in parallel, sugar deacetylation (release of acetyl group from the xylan

backbone) and further acetic acid production occurs, enhancing the autohydrolysis of sugar oligomers into their respective monomers (Cabeza et al., 2016; Garrote et al., 2002). Depending on temperature and residence time, hexoses and pentoses can be dehydrated into hydroxymethyl furfural (HMF) and furfural, respectively, which are unstable at the reaction conditions and further degraded into organic acids (Nabarlatz et al., 2004). The hemicellulosic polymer fractionation pathway using sCW is shown in Fig. 2.4.

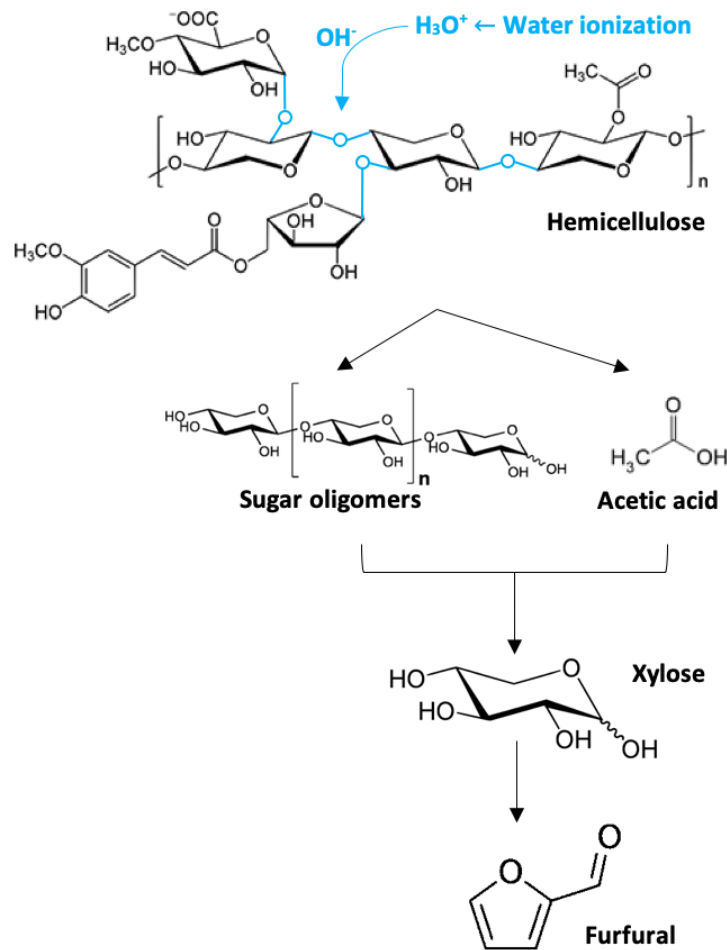


Fig. 2.4. Hemicellulose hydrolysis pathway using sCW.

Specifically for straw biomass fractionation such as barley, canola, mustard, triticale, wheat, sugarcane, oat, and rice straws, sCW at around 160-180 °C has been proven to be an efficient method for hemicellulose hydrolysis into soluble sugars (oligomers and

monomers) with minimal degradation products (Pronyk & Mazza, 2012; Abaide et al., 2019a,b; Batista et al., 2019). Pronyk & Mazza (2012) fractionated some agricultural straws using sCW at only 165 °C, 7 bar, with a flow rate of 115 mL/min, for 60 min. Overall, barley (40% cellulose, 22% hemicellulose, 19% lignin), mustard (33% cellulose, 20% hemicellulose, 18% lignin), oat (40% cellulose, 23% hemicellulose, 18% lignin), triticale (36% cellulose, 25% hemicellulose, 16% lignin), canola (32% cellulose, 21% hemicellulose, 19% lignin) and wheat (40% cellulose, 23% hemicellulose, 18% lignin) straws had low hemicellulose contents of 5-7% after the treatment, with a slight increase in lignin contents to 17-23%, and a significant increase in cellulose contents to 64-71%. The hydrolysate had mainly soluble oligosaccharides (34-43%) and a small amount of sugar monomers (5-8%). The acetyl groups released in the hydrolysate was in the range of 3-6%, whereas furfural, HMF, formic and levulinic acids were detected in trace amounts (< 1%).

As the temperature is the main catalyst for the hemicellulose fractionation process, increasing the temperature of sCW from 170 to 260 °C (12 bar, for 15 min), in a batch system with 10 mL/g, resulted in a decrease in the hemicellulose content of sugarcane straw from 22 to 2%, while the lignin and cellulose contents increased from 27 to 37%, and from 44 to 55%, respectively (Batista et al., 2019). The hydrolysate obtained at 170 °C had mainly sugar monomers (~90%), with low formation of organic acid (< 3%), and trace amounts (< 1%) of degradation products. However, at 260 °C, increased amounts of acetic acid (16%) in the hydrolysate provided acidic protons to catalyze the subsequent hydrolysis of the sugar monomers into formic acid (16%), furfural (25%), and HMF (11%). Same trend was observed by Abaide et al. (2019b) during the treatment of rice straw in sCW

using a semi-continuous reactor system. The dissociation of hemicellulosic sugars into HMF and furfural was not detected after sCW treatment at 180 °C (250 bar, 20 mL/min, 15 min), but when the process temperature was increased up to 260 °C, around 6% of the soluble hemicellulose were converted into HMF and furfural. The difference between sugar degradation products reported by Abaide et al. (2019b) and Batista et al. (2019) are mainly due to the different operational systems used. In the batch system used by Batista et al. (2019), the release of acetyl groups and subsequent formation of acetic acid catalyzes the autohydrolysis reactions and the dehydration of sugar monomers into furfural and HMF. Whereas, in a flow-type system used by Abaide et al. (2019b), the effects of acetic acid accumulation are reduced due to the constant flow of PF, and collection of hydrolysates at ambient conditions.

The production of sugar oligomers and monomers without degradation products is of interest to produce high-value biogas (Joelsson et al., 2016), bioethanol (Yu et al., 2017) and biomethane (Barakat et al., 2012); whereas, the production of furans (HMF and furfural) has potential to be sustainable substitutes for petroleum-based building blocks used in the production of fine chemicals and plastics (Rosatella et al., 2011). However, as reported in the literature, an adverse effect of the sCW pre-treatment, especially at high temperatures of > 170 °C, is that lignin is not removed due to its recalcitrant structure and re-condensation reactions.

2.2.1.7.2. Lignin hydrolysis

Compared to hemicellulose, the hydrolysis of lignin into oligomers or monomers using sCW under mild conditions is still a challenge. During the sCW treatment, the depolymerization and repolymerization of lignin fragments occur almost simultaneously

due to the acidity created during the treatment, resulting in increasing amounts of insoluble residual lignin. Essentially, the depolymerization of β -O-4 linkages and the formation of carbonium ions due to the cleavage of aliphatic side chain carbons, are the main reactive electrophile and nucleophile sites that promote recondensation reactions (Chua & Wayman, 1989). In addition, at high temperature processing (> 200 °C), the sugar degradation products such as furfural, HMF, and their precursors, can also participate extensively in lignin recondensation reactions (Chua & Wayman, 1989). Therefore, the sCW pre-treatment generally led to an insignificant delignification, or to values comparable to or higher than those of the starting material (Huijgen et al., 2012; Ciftci & Saldaña, 2015; Weinwurm et al., 2017; Abaide et al., 2019b; Batista et al., 2019).

At the same time, PF using aqueous alcohols (10-95% v/v) has shown to increase delignification of lignocellulosic biomass. To date, pressurized aqueous ethanol (PAE) is the most widely studied method for delignification of straw biomass (Buranov & Mazza, 2010; 2012; Huijgen et al., 2012; Weinwurm et al., 2017). For example, flax straw (34% cellulose, 21% hemicellulose, 30% lignin) treated using PAE (30% v/v) at 220 °C, 52 bar, 3 mL/min and 45 mL/g, had reduced hemicellulose and lignin contents to 5% and 8%, respectively, while the cellulose content increased to 79% (Buranov & Mazza, 2012). Flax straw (33% cellulose, 17% hemicellulose, 24% lignin) hydrolysis using PAE processing (0 and 30% v/v aqueous EtOH, at 180 °C, 52 bar, 3 mL/min, 27 mL/g for 117 min) was also compared to MW-assisted hydrolysis (0 and 30% v/v aqueous EtOH, at 180 °C, 27 mL/g for 10 min) for maximum extraction of non-cellulosic compounds (Buranov & Mazza, 2010). The PAE processing removed 81-90% of the hemicellulose and 54-78% lignin, while the MW-assisted hydrolysis removed 10-37% of the hemicellulose and 18-39% of

the lignin. The use of aqueous EtOH as a solvent was more efficient than pure water for simultaneous extraction and hydrolysis of hemicellulose and lignin, due to the high solubility of lignin in aqueous EtOH (Buranov & Mazza, 2010). The principle of PAE technology is similar to that of organosolv hydrolysis. However, no acid catalyst is used due to the increased ionic production during the PF processing. The dissolution of lignin in aqueous EtOH is based on the solubility parameter (δ -value). The δ -values of pure water, pure ethanol and commercially available Alcell[®] lignin were calculated as 22.3, 12.1, and 13.7 cal/cm³, respectively (Ni & Hu, 1995). The maximum solubility of the Alcell[®] lignin was obtained at EtOH concentration of about 70% (δ -value of 14 cal/cm³) due to their δ -value similarities (Ni & Hu, 1995).

Sequential hydrolysis and fractionation using sCW followed by PAE has been shown to be a promising strategy to recover sugars and lignin from wheat straw (Huijgen et al., 2012; Weinwurm et al., 2017). Huijgen et al. (2012) first fractionated wheat straw (35% cellulose, 24% hemicellulose, 16% lignin) using sCW at 190 °C and 12 bar for 30 min, followed by PAE (60% v/v) treatment at 200 °C and 17 bar for 60 min. After the first step, the treated straw had its hemicellulose content reduced to 4%, while the lignin and cellulose contents increased to 30 and 54%, respectively. While, after the PAE treatment, the straw had increased cellulose content up to 64%, while the lignin reduced to 18% (Huijgen et al., 2012). Similar processing using sCW (180 °C, 150 bar, 11 mL/g for 60 min) followed by PAE (20% v/v, 200 °C, 150 bar, 11 mL/g for 15 min) was reported by Weinwurm et al. (2017) to fractionate wheat straw (29% cellulose, 24% hemicellulose, 17% lignin). After the first step, the treated straw had 37% cellulose, 18% hemicellulose and 16% lignin, and after the second step, the treated straw had reduced hemicellulose and lignin contents of

6% and 10%, respectively, while the cellulose content reached 52% (Weinwurm et al., 2017).

After the PAE treatment, the lignin and hemicellulose in the hydrolysate can be separated by a two-step process of acid precipitation (H_2SO_4 at pH 3) followed by centrifugation (19,000 g at 10 °C for 20 min) (Buranov & Mazza, 2012). According to Buranov & Mazza (2012), the isolated lignin can reach a purity of > 90%. Then, the isolated lignin can be used as a hybrid material for tissue engineering applications (Quraishi et al., 2015). For example, Quraishi et al. (2015) tested the cytocompatibility of lignin isolated from wheat straw in alginate-based aerogel composite as scaffold for mouse fibroblast cells. Aerogels with 2:1 (w/w) alginate-to-lignin ratio showed no cytotoxicity and promoted satisfactory cells adhesion and viability over 7 days compared to the control (tissue culture polystyrene plate).

2.2.1.7.3. Cellulose-enriched fiber

The treated solid material after PF processing usually has a higher cellulose content than the starting material, mainly due to the large removal of hemicelluloses and partial delignification. To date, this cellulose-enriched fiber has been further processed for bioethanol production (Ahmed et al., 2013), value-added nanomaterials (Ciftci et al., 2017; Zhao et al., 2019), and adsorbant material for wastewater treatment (Abaide et al., 2019a).

Ciftci et al. (2017) first hydrolyzed lupin hull (46% cellulose, 25% hemicellulose, 8% lignin) using sCW at 180 °C, 50 bar, 5 mL/g for 30 min (treated fiber had 79% cellulose, 4% hemicellulose and 15% lignin), followed by ASC bleaching (1.7 wt.% at 75 °C for 4 h) to obtain highly purified cellulose fiber (~97%). Then, high-intensity ultrasound (HIUS) treatment at 560 W for 40 min was used to obtain CNF (average diameter of 15

nm) hydrogel. The hydrogels were further dried to a highly porous (99% porosity) and lightweight (density of 0.009 g/cm³) CNF aerogels via supercritical CO₂ (SCCO₂) drying at 40 °C, 100 bar, and a flow rate of 0.5 L/min (measured at ambient conditions) for 4 h. Although the CNF aerogel had high crystallinity (> 72%) and thermal stability (thermal degradation temperature of 310 °C), no further application was studied. Recently, pre-treated rice straw (36% cellulose, 24% hemicellulose, 12% lignin) after sCW (220 °C, 250 bar, 8 mL/min, 15 min) treatment was used as an adsorbent of 2-nitrophenol for applications in wastewater treatment (Abaide et al., 2019a). Overall, the pre-treated straw with surface area of 7 m²/g had adsorption capacity of 93 mg 2-nitrophenol/g treated straw in neutral pH solution at 25 °C after 24 h, which was almost double the adsorption capacity of untreated rice straw (55 mg 2-nitrophenol/g straw).

Recently, cellulose-enriched fiber (63% cellulose, 9% hemicellulose, 20% lignin) from canola straw obtained after PAE treatment (20% v/v, 180 °C, 50 bar, 5 mL/g for 40 min) was nanofibrillated into lignocellulosic nanofibers (LCNF) (average diameter of 22 nm) using HIUS at 1200 W for 30 min, and used as a reinforced material in starch-based bioactive films for food packaging applications (Zhao et al., 2019). The films were produced in sCW media (100 °C and 85 bar for 10 min) using LCNF to starch ratios of 0.025-0.1 g LCNF/g starch. Overall, the use of 0.1 g LCNF/g starch showed 12.7 times improved tensile strength compared to the film without LCNF. Also, owing to the hydrophobicity of LCNF, the biocomposite films had improved moisture resistance with a reduction of water vapor permeability and film solubility in water (Zhao et al., 2019).

In general, PF treatment is recognized as an environmentally friendly process because it does not use hazardous chemicals or catalysts, no neutralization steps are needed,

and the solvent can be easily recovered. Furthermore, the treated fiber is a potential material for LCNF production. However, a further bleaching step is still needed for CNF production from PF pre-treated straw. Also, further studies should be conducted to expand the applications of the enriched-cellulose fiber co-product.

2.2.2. Mechanical nanofibrillation

Although enzymatic treatment to obtain nanofiber from agricultural straw has been reported (Espinosa et al., 2017), nanofibrillation via mechanical processes is the most common method to obtain CNF and LCNF due to short processing times compared to enzymatic hydrolysis. Table 2.4 presents the main mechanical approaches and their principles used for nanofiber production. These mechanical approaches can be used solely or in combination.

The high-pressure homogenization (HPH) is the most common mechanical approach used for nanofiber production from straw (Table 2.4). Within this process, the cellulose suspension is passed through a small nozzle with diameters of 5-20 μm with the help of a piston pump, under pressures of 300-1500 bar (Kargarzadeh et al., 2017; Blanco et al., 2018). The nanofibrillation occurs due to the high velocity and pressure of the cellulose suspension in the small nozzle, which induces shear forces and turbulences responsible for the cellulose fiber size reduction. In addition, due to the high velocity of the suspension, an increase in the dynamic pressure and a reduction in the static pressure below the vapor pressure of the aqueous phase led to gas bubble formation and implosion (cavitation phenomenon) that enhances the nanofibrillation process (Kargarzadeh et al., 2017).

Table 2.4. Mechanical approaches to obtain cellulose nanofibers (CNF) and lignocellulosic nanofibers (LCNF) from straw.

Method	Principle	Straw	Processing parameters	Fibrillation yield	Nanofiber average diameter size	Reference
Ball milling	Suspension is agitated in a hollow cylindrical container partially filled with balls. Usually requires long milling and cleaning times.	Wheat and kenaf	120 min	CNF: nd	CNF: 21-30 nm	Nuruddin et al. (2016)
Blender	Suspension is blended at a high speed. Usually processing times superior to 20 min are needed.	Rice and corn	30-120 min	CNF: 12% TO-CNF: 80%	CNF: 6 nm TO-CNF: 3 nm	Jiang & Hsieh (2013); Boufi & Chaker (2016)
Cryocrushing	Suspension is frozen with liquid nitrogen and crushed via mortar and pestle. Usually is combined with other mechanical approach to obtain nanofibers.	Wheat	Cryocrushing followed by homogenization at 450 g for 20 passes	CNF: 60%	CNF: 35 nm	Alemdar & Sain (2008)
Grinder	Suspension passed through a rotary and static stones with different gap spaces. Frequent equipment maintenance and disk replacement, as well as long processing times are needed.	Canola, rice and wheat	Gap of -10 to -100 μ m for 140-150 min	CNF: nd LCNF: 36%	CNF: 32 nm LCNF: 13-22 nm	Yousefi et al. (2013); Hassan et al. (2018); Espinosa et al. (2019)

TO: TEMPO-oxidized; nd: not determined.

Table 2.4. Continued.

Method	Principle	Straw	Processing parameters	Fibrillation yield	Nanofiber average diameter size	Reference
High-intensity ultrasound	Suspension is exposed to mechanical vibration of ultrasound waves at different equipment power and processing times. Not suitable for high volumes.	Canola, corn, flax, reed and wheat	420-1200 W for 9 to 120 min	CNF: nd TO-CNF: 90% LCNF: 36-74%	CNF: 60 nm TO-CNF: 3-20 nm LCNF: 5-21 nm	Chen et al. (2011a); Soni et al. (2015); Liu et al. (2019)
Homogenizer	Suspension is passed through a small nozzle of 5 to 20 µm of diameter at high speed by the help of a piston to generate a high-pressure stream. Several passes are needed and the nozzle is easily clogged.	Barley, corn, kenaf, oat and wheat	4-40 passes at 300-1500 bar	CNF: nd TO-CNF: nd LCNF: 14-56% TO-LCNF: 26-95%	CNF: 20-28 nm TO-CNF: 15 nm LCNF: 13-490 nm TO-LCNF: 7-58 nm	Jonoobi et al. (2011); Davoudpour et al. (2015); Espinosa et al. (2017; 2019); Sánchez et al. (2016); Petroudy et al. (2018); Xu et al. (2018)
Microfluidizer	Suspension is pumped through a chamber (Z or Y shape), with an orifice with a diameter of 100-400 µm. The chamber should be changed to achieve nanofiber with small diameter.	Canola, hemp and wheat	120 min or 5-6 passes at 850-1700 bar.	CNF: nd	CNF: 4-35 nm	Liu et al. (2017); Pacaphol & Aht-Ong (2017); Svärd et al. (2019)

TO: TEMPO-oxidized; nd: not determined.

A crucial problem associated with clogging is likely to occur during HPH process due to the small diameter of the nozzle. Therefore, this process is usually applied after a primary mechanical (e.g. blender, refiner or crushing methods) or chemical step (acid hydrolysis), or in dilute cellulose suspension (0.2 wt.%). Davoudpour et al. (2015) implemented an acid hydrolysis step prior to the HPH process (562 bar with 44 passes) to reduce the size of the isolated cellulose fiber from kenaf straw and to avoid clogging problems. However, the authors still reported clogging problems when cellulose suspension at a concentration of 0.2 wt.% was used. Other authors successfully used a pre-mechanical step with a blender, refiner or crushing methods, followed by HPH processing at 300-1500 bar for 4-40 passes to obtain nanofibers from several pre-treated straw biomass (wheat, corn, barley, oat, and kenaf) (Alemdar & Sain, 2008; Jonoobi et al., 2011; Espinosa et al., 2016; Sánchez et al., 2016; Espinosa et al., 2017; Petroudy et al., 2018; Xu et al., 2018).

Similarly, a microfluidizer works by pumping the cellulose suspension at high pressures of up to 2700 bar through a thin chamber with a Z or Y shape, that has an outlet orifice with diameters of 100-400 μm (Kargarzadeh et al., 2017; Blanco et al., 2018). The nanofibrillation is achieved by the shear forces created in the system and the impact of the suspension against the channel walls. However, the chamber should be changed to different geometries to achieve nanofiber with small diameter and a high production yield (Lavoine et al., 2012). For example, CNF from canola straw were obtained using microfluidizer with a chamber of 400/200 μm in diameter at 850-900 bar at one pass, and then five subsequent passes through a chamber of 200/100 μm in diameter at 1600-1700 bar (Svärd et al., 2019).

The extent of nanofibrillation using HPH and microfluidizer methods, depends mainly on the number of passes/cycles (~4 to 40 passes) (Lavoine et al., 2012).

Grinding is another method used to nanofibrillate cellulose fiber from straw biomass. In this case, the cellulose suspension is carried out through a small gap between stator and rotor porous stone discs, where the mechanical shearing and frictional forces result in the size reduction of the fibers (Blanco et al., 2018). This method is similar to double-disk refining; however, a lower gap between the discs is possible with grinders (Nechyporchuk et al., 2016). The effectiveness of grinding process is mainly determined by processing time (140-150 min) and the gap between the stone discs that usually range from -10 to -100 μm (Table 2.4). However, due to the constant friction of the suspension with the disk, the main disadvantages of this process are a frequent maintenance of the equipment and the need for disk replacement (Kargarzadeh et al., 2017). In addition, nanofibrillation using ball milling, blender and cryocrushing has been reported as non-conventional mechanical processes to obtain CNF and LCNF from agricultural straw biomass.

In general, the yield of fibrillation depends on the mechanical approach used, straw biomass source and composition, and the pre-treatment applied (Table 2.4). Independent of the mechanical approach used, TEMPO-oxidized nanofibers are known to have higher number of carboxylate groups on its surface, which facilitates the nanofibrillation process due to the repulsion forces between nanofibers, increasing its fibrillation yield (Table 2.4).

2.2.2.1. High-intensity ultrasound

High-intensity ultrasound (HIUS) processing is an emerging and non-conventional method used to obtain nanofibers from agricultural straw biomass. Usually, a probe-type sonicator at low-frequency of ~20 kHz and high nominal powers of 300-1500 watts (W)

are applied for the nanofibrillation process. The fiber size reduction using HIUS technology highly depends on the acoustic cavitation phenomenon. This phenomenon occurs due to the mechanical vibration of ultrasound (high-frequency pressure wave) in a liquid medium, which creates regions of high (compression) and low (rarefaction) pressure. If the changes in pressure are big enough, microbubbles of gas and vapor are created, which undergo successive compression and rarefaction phases under the influence of the ultrasound waves, until they violently collapse (Fig. 2.5) (Kentish & Ashokkumar, 2011). The high shear forces, shock waves, microjets and turbulence induced by the microbubble collapse are responsible for the breakdown of the dispersed solid (Chemat et al., 2017).

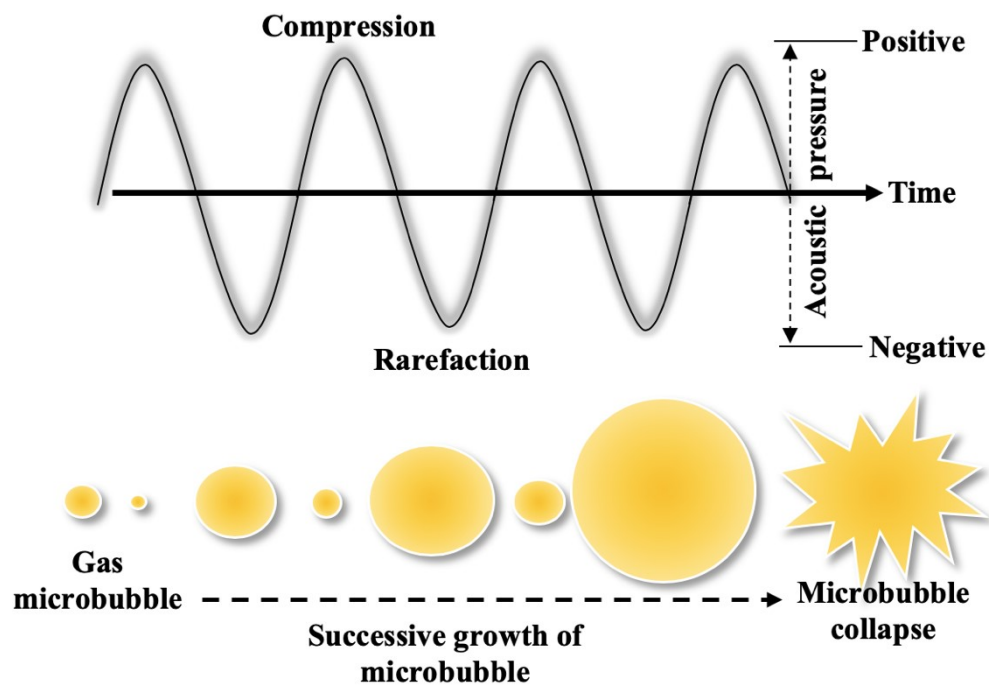


Fig. 2.5. Scheme of ultrasound acoustic cavitation.

In general, nominal power (input power) and time are the main parameters reported and studied during nanofibrillation of cellulosic material. Sometimes the amplitude is reported instead of the power, which means that they did not use the 100% nominal power of the equipment. However, the volume or mass of the system and the probe design can

also influence the process. In a model-type system, Wang & Cheng (2009) evaluated the effects of temperature, fiber concentration and size, nominal power, processing time and distance from the probe tip to the bottom of the flask, on the nanofibrillation process of commercially available cellulose using HIUS. Overall, a higher nanofibrillation was obtained when the power was increased from 600 to 1200 W, the initial fiber size was reduced from 900 to 30 μm , the processing time was increased from 10 to 60 min, and the distance of the probe to the bottom of the flask was increased from 4 to 7 mm. The data acquired from the model-type system of Wang & Cheng (2009) provided a good basis to understand some parameters of the HIUS during the nanofibrillation process for highly purified cellulose. However, when using a complex cellulosic material like pre-treated agricultural straw biomass, the chemical composition as well as the surface chemical modifications have been shown to strongly affect the nanofibrillation results of HIUS processing (Chen et al., 2011a; Soni et al., 2015; Liu et al. 2019).

Chen et al. (2011a) isolated CNF from pre-treated wheat straw (84% cellulose, 14% hemicellulose, 2% lignin) and flax fiber (89% cellulose, 9% hemicellulose, <1% lignin) using HIUS processing at 1000 W for 30 min. Wheat straw CNF were uniformly nanofibrillated to CNF with a diameter range of 15-35 nm; whereas, flax fiber CNF were not uniformly nanofibrillated, with about 20% of the nanofibers with diameter > 100 nm. According to Chen et al. (2011a), this is due to the high cellulose content (75%) of the untreated flax fiber, which led to strong H-bonding between the nanofiber bundles, requiring higher energy to break (Chen et al., 2011a). Soni et al. (2015) also reported different nanofibrillation in cotton straw pre-treated fiber without surface modification compared to TEMPO-oxidized and acid-treated cotton straw fibers after HIUS process at

600 W for 20 min. The CNF from TEMPO-oxidized fiber had needle-shaped structures with diameters ranging from 3 to 15 nm, and lengths from 10 to 100 nm. Also, acid treated CNF had diameters and lengths in the range of 10-50 nm and 200-500 nm, respectively. However, bleached CNF had a broader size distribution with diameters of 50-500 nm and lengths of > 1500 nm. Since the same HIUS process was applied for all cotton straw pre-treated fibers, the difference in nanofibrillation was mainly due to the higher number of carboxylate and sulfonate groups on the surface of TEMPO-oxidized and acid-treated fibers, respectively, which facilitated the nanofibrillation process due to the repulsion forces between the nanofibers.

The use of HIUS technology for nanofibrillation of straw biomass was almost exclusively applied to fully bleached cellulose fiber for CNF production until a few years ago. The production of LCNF from pre-treated reed straw using HIUS processing was recently reported by Liu et al. (2019). The reed straw biomass was pre-treated using ball-milling under mild alkaline conditions (1, 4, 7 wt.% NaOH) at a speed of 10 g and room temperature for 120 min, followed by HIUS treatment at 450 W for 120 min. The LCNF from pre-treated straw with 1 wt.% NaOH (38% cellulose, 25% hemicellulose, 14% lignin) had 74% of nanofibers with diameter of 5 nm, whereas LCNF prepared with 7 wt.% NaOH pre-treated straw biomass (41% cellulose, 24% hemicellulose, 7% lignin) had 60% of nanofibers with diameter over 10 nm. Liu et al. (2019) reported that the high lignin content (14% lignin) of pre-treated straw fiber facilitated the nanofibrillation process, as lignin stabilizes possible recombination reactions between reactive cellulose radicals generated in the alkali ball-milling process. Although the obtained LCNF showed promising

application as nanofilm, the long processing time of HIUS (120 min) applied was definitely a drawback in terms of energy consumption.

Although nanofibrillation using the HIUS approach has been used for more than a decade for CNF, in a recent review, Rol et al. (2019) highlighted the need for further studies using HIUS to improve this method towards biomass nanofibrillation. The HIUS process parameters such as ultrasound intensity and specific energy were well studied for the ultrasound-assisted extraction process, but there is a lack of information on their use for the nanofibrillation process for both CNF and LCNF production.

2.2.2.1.1. Other uses of high-intensity ultrasound

HIUS is commonly used in various unit operations during food processing, considering its physical effects for extraction, homogenization, emulsification, degassing, crystallization, and sterilization.

Ultrasound-assisted extraction (UAE) has been studied as a promising and emerging technique to obtain bioactive compounds from food and biological matrices such as carrots (Encalada et al., 2019a and b), araticum peel (Arruda et al., 2019), mandarin peel (Sun et al., 2011), and spirulina (Vernès et al., 2019). In UAE, process variables such as solvent type, temperature, energy density or specific energy, acoustical power, and ultrasound intensity have been explored. The solvent and control process temperature (with or without a cold bath) in UAE is mainly driven by the solubility and volatility of the target bioactive compounds, whereas the other parameters (energy density or specific energy, acoustical power, and ultrasound intensity) are usually applied as criteria for comparison. Due to the variety of equipment used for generating acoustic cavitation, such as the ultrasonic probe (horn) and ultrasonic bath, with different sizes and specifications, using unified criteria of

specific energy (amount of energy applied per unit mass), or ultrasound intensity (energy transmitted per second and per square meter of emitting surface) is a helpful tool to evaluate the system alone as a chemical reaction medium, and to compare the efficacy with other methods or devices. For example, the measurement of the actual applied acoustical power, which is further used for calculation of ultrasound intensity and efficiency, can be done by physical methods like calorimetric method (Mason et al., 1994), or by chemical methods like the indirect measurement of hydroxyl radicals via spectroscopic approach (Suslick et al., 2011). Within the calorimetric method, it is considered that the actual input power from the ultrasound device is converted to heat, which is dissipated in the medium. Therefore, Eq. (2.3) is usually applied to calculate the acoustical power of the system (Mason et al., 1994):

$$\text{Power (W)} = m C_p \left(\frac{\Delta T}{\Delta t} \right) \quad (2.3)$$

where, m (g) is the mass of the system, C_p (J/g°C) is the heat capacity of the solvent, and $\Delta T/\Delta t$ is the temperature rise of the system per unit time.

HIUS has been also used for the preparation of different lipid-based engineered structures such as oil-water emulsions, Pickering emulsion, nanoemulsion, nanoliposomes, dendrimers, and emulsion-filled gels (Paradiso et al., 2015; Costa et al., 2018; Koshani & Jafari, 2019; Perdi et al., 2019). Ultrasonic emulsification is believed to occur in two stages via different mechanisms. First, the mechanical vibrations from ultrasound waves disrupt the stability of the interface between the oil and water (Rayleigh-Taylor instability), resulting in large oil droplets into the water medium. Secondly, due to the acoustic cavitation effects like shockwaves, the breakup of initial oil droplets into smaller ones are responsible to stabilize the emulsion (Li & Fogler, 1978). Costa et al. (2018) compared

HIUS process (225-675 W) and HPH (100-700 bar) for 2 min, as energy sources to stabilize Pickering emulsion using CNF from banana peel as an emulsifier. The fresh CNF-Pickering emulsion prepared by HIUS had increased viscosity ($2.1-2.3 \times 10^{-3}$ Pa.s) and small oil droplet size (2 μm), compared to the one prepared by HPH processing ($1.8-2.0 \times 10^{-3}$ Pa.s and 5 μm). However, independent of the parameter used, both mechanical systems led to creaming phenomenon of oil droplets (loss of stability) after 6 days. The creaming phenomenon in CNF-Pickering emulsion prepared by HIUS was mainly due to flocculation of the droplets (association of two or more droplets that maintain their individual droplet interface), whereas in CNF-Pickering emulsion prepared by HPH was mainly due to the coalescence phenomenon (droplets unite to form larger droplets) (Costa et al., 2018).

In emulsion-filled gel, HIUS is also used as an energy source to disrupt the oil-gel interface and stabilize the oil droplets into the gel. As definition, emulsion-filled gel is made of a continuous phase (gel/hydrogel) that has dispersed oil droplets (fillers), which can interact or not with the gel phase. Emulsion-filled gel based on inulin and extra virgin olive oil was produced via HIUS or homogenization and used as a base for functional spread to bread sample (Paradiso et al., 2015). In general, HIUS treated emulsion-filled gels had smaller droplets and fine cloudy dispersions than homogenized ones, and showed the highest microbiological quality, given by the absence of Enterobacteriaceae, *Listeria monocytogenes*, molds and yeasts over 30 days of storage period, mainly due to the synergistic effect of HIUS in emulsifying and sterilizing of the product, which inhibited the growth of microorganisms. In another study, HIUS process at low powers of 31-300 W (time not specified) was used to obtain emulsion-filled gel using inulin (11-48%), rice bran oil (up to 38%), and rosemary essential oil (0 or 3000 ppm) (Nourbehesht et al., 2018).

Results showed that inulin, rice bran oil, and HIUS power applied variables significantly affected the stability (calculated by the creaming phenomena) and consistency of the emulsion-filled gel, where the addition of rosemary essential oil reduced the rice bran oxidation during HIUS processing. The maximum stability of 99% and simultaneous maximum consistency of 291 N.s were obtained using 45% inulin, 18% rice bran oil, and 256 W. Furthermore, the addition of rosemary essential oil prior to HIUS process slightly reduced the oxidation of rice bran oil by reducing the peroxides production (peroxides and hydroperoxides) from 6.1 to 5.8 meq O₂/kg, and the thiobarbituric acid production from 0.0413 to 0.0368 (mg malonaldehyde/kg). However, the stability of rosemary essential oil during the HIUS processing was not studied. To date, there is no study using CNF hydrogel as a continuous phase in an emulsion-filled gel.

2.3. Applications of nanofibers from straw biomass

Among the various potential applications of CNF and LCNF, the most promising ones are film, membrane, nanopaper, hydrogel and aerogel formation. In those applications, CNF and LCNF are used alone or as biocomposites for a diverse spectrum of products such as food additives and packaging applications, tissue engineering scaffolds and wound dressing, drug delivery systems, construction materials like insulation, and ink coating applications (Alemdar & Sain, 2008; Kaushik et al., 2010; Yousefi et al., 2013; Espinosa et al., 2016; Hassan & Hassan, 2016; Martelli-Tosi et al., 2018; Petroudy et al., 2018; Li et al., 2019; Zhao et al., 2019).

2.3.1. Hydrogel and aerogel

By definition, hydrogels are three-dimensional (3D) network structures that contain large amounts of water and can be chemically or physically cross-linked (Chang & Zhang, 2011). Physical cross-linked hydrogels are formed by self-assembled interactions such as van der Waals forces, hydrogen bonds, hydrophobic interactions, or ionic associations, which are reversible by application of force or environmental changes (e.g. temperature and pH) (Fig. 2.6). For example, the physical cross-linking can be between cellulosic nanofibers (Pääkkö et al., 2007; Tanaka et al., 2015; Ciolacu et al., 2016; Martoia et al., 2016; Ciftci et al., 2017; Costa et al., 2018; Moberg et al., 2018; Li et al., 2019; Sanandiya et al., 2019), between cellulosic nanofibers and other polymers such as chitosan, alginate and galactoglucomannan (Prokobna et al., 2015; Toivonen et al., 2015; Aarstad et al., 2017; Doench et al., 2019), and between cellulosic nanofibers and salts such as aluminum, calcium, cupric, iron, potassium, sodium and zinc nitrates (Dong et al., 2013; Zander et al., 2014; Suenaga et al., 2018).

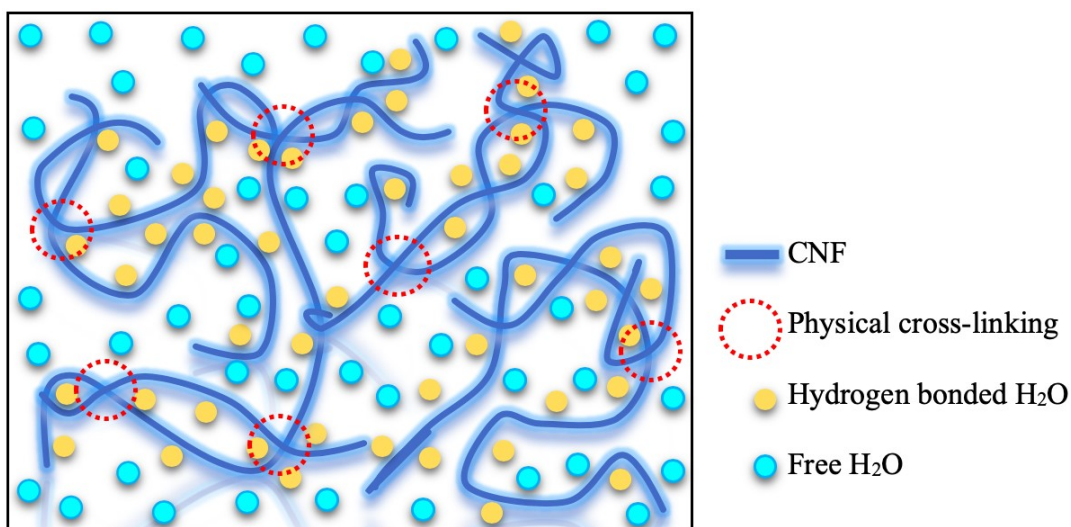


Fig. 2.6. Physical cross-linked CNF hydrogel.

On the other hand, chemically cross-linked hydrogels are irreversible structures mainly obtained based on covalent bonds via radical polymerization, chemical reactions, Schiff base formation or energy irradiation (Chang & Zhang, 2011). Based on the method of preparation, chemical cross-linked hydrogels can be classified as homopolymers, where only cross-linkers such as epichlorohydrin, glutaraldehyde, citric acid and sodium citrate are used within the nanofibers (Ciolacu et al., 2016; Mertaniemi et al., 2016), or copolymers, where the cross-linkers are used between LCNF or CNF and other synthetic or natural polymers such as poly(vinyl alcohol) (PVA), polylactide, poly(ethylene glycol), poly(butylene succinate), alginate, chitosan and gelatin (Markstedt et al., 2015; Naseri et al., 2016; Laurén et al., 2017; Shin et al., 2017; Bian et al., 2018; Immonen et al., 2018; Moberg et al., 2018; Abudula et al., 2019; Cheng et al., 2019; Siqueira et al., 2019).

In general, CNF hydrogels exhibited non-Newtonian properties, such as shear-thinning behaviour, where the viscosity decreases while shear rate increases (nanofibers align along shear direction and lose their entanglements) and thixotropic behavior (time-dependent shear thinning property) (Moberg et al., 2018; Sanandiya et al., 2019). However, the rheological properties of CNF hydrogel depend significantly on the solid concentration, nanofiber dimensions (aspect ratio) and surface-chemical composition, and the type of gel (physical or chemical) created. For example, TEMPO-oxidized CNF hydrogel had the storage modulus varying from ~36 to 301 Pa at 10 rad/s, as the concentration of the hydrogel increased from 0.5 to 1 wt.% (Sanandiya et al., 2019), which was significantly higher than that of hydrogel obtained from CNF without surface modification, where storage modulus varied from ~3 to 10 Pa at 10 rad/s as the concentration of the hydrogel increased from 0.4 to 1 wt.% (Pääkkö et al., 2007). This behavior is due to the electrostatic

repulsion between nanofibers of TEMPO-oxidized CNF hydrogel (due to the carboxylate groups on the surface) which creates a stable structure.

Such CNF and LCNF suspensions/hydrogels promote the structure to form aerogels, a highly porous lightweight material produced by sublimating the liquid component of hydrogels mainly via freeze-drying or SCCO₂ drying. The properties of CNF aerogel depend mainly on the structure of the initial hydrogel. For example, aerogels from CNF only hydrogels had densities of 0.0002-0.6 g/cm³, porosity ≥ 98%, surface areas of 11-284 m²/g and modulus of 35-5700 kPa; whereas, aerogels from CNF hydrogels copolymers (e.g. hydroxyl apatite, soy protein, collagen and PVA) had densities of 0.005-1.47 g/cm³, porosity ≥ 91%, surface areas of 3-246 m²/g and modulus of 4-10440 kPa (France et al., 2017).

Earlier, Martoia et al. (2016) compared aerogels from TEMPO-oxidized and enzymatic processed CNF with different morphology structures. Enzymatic processed CNF hydrogels had polydisperse fibrils with average diameters of 20-100 nm and lengths of 150-300 μm. In contrast, TEMPO-oxidized CNF were more homogeneous nanofibrillated with a diameter and length that ranged between 3 and 5 nm and between 1 and 1.4 μm, respectively. During the freezing step (-80 °C) prior to sublimation (freeze-drying technique), the TEMPO-oxidized CNF were homogeneously redistributed by the moving ice front, leading to an aerogel with a more regular network with small pore sizes of 20-50 μm and a lower density of 0.011 g/cm³, but poor mechanical properties (compression modulus of 80 kPa and yield stress of 7 kPa) compared to the enzymatic processed CNF aerogel (pore sizes of 50-100 μm, density of 0.023 g/cm³, compression modulus of 30 kPa and yield stress of 3 kPa). The difference in the mechanical properties

of the CNF aerogels obtained by Martoia et al. (2016) is due to the “packed” nanofibers walls of enzymatic processed CNF that provided resistance to the aerogel structure.

2.3.2. CNF scaffold for tissue engineering

The CNF hydrogels and aerogels are promising structures to be used in the biomedical area as drug delivery systems and cell culture scaffolds (Ciolacu et al., 2016; Mertaniemi et al., 2016; Laurén et al., 2017; Kim et al., 2018; Sanandiya et al., 2019). Particularly, substrates with nanometer-sized features like CNF are highly desirable for tissue engineering scaffolds due to their similar size-scale and physical morphology as the natural collagen fibrils in the extracellular matrix (ECM) (~10-300 nm diameter, but vary according to the tissue type) (Aamodt & Grainger, 2016). In general, due to the large surface-area-to-volume of the CNF hydrogels and aerogels, these materials have high porosity and swelling capacity, which is critical for cellular infiltration, adequate diffusion of metabolites, vascularization, and avoiding necrotic core due to hypoxia (Hickey et al., 2018; Turnbull et al., 2018). CNF hydrogels have also been attractive materials for bio-inks used in 3D bio-printers towards scaffold manufacture (Markstedt et al., 2015; Shin et al., 2017). A recent comprehensive review on CNF for 3D bio-printing scaffold can be found somewhere else (Dai et al., 2019).

In comparison with other polymer materials, the CNF scaffolds overcome the poor stability and mechanical properties (e.g. tensile modulus, ultimate tensile strength and elongation at break) of natural polymers, such as chitosan and alginate, and overcome the potential of immunogenicity and disease transmission concerns using synthetic and animal-derived polymeric matrices (Aamodt & Grainger, 2016; Turnbull et al., 2018). The biodegradability, non-cytotoxicity and nanomorphology of CNF-based scaffolds have

been proven *in vitro* to be suitable in multiple regenerative tissue engineering applications, such as skin regeneration, periodontal and oral regeneration, neural regeneration, bone regeneration, intervertebral disc regeneration, cartilage regeneration and blood vessels regeneration (Chiaoprakobkij et al., 2011; Naseri et al., 2016; Abudula et al., 2019; Doench et al., 2019; Cheng et al., 2019; Siqueira et al., 2019; Zhang et al., 2019). Also, CNF alone or as a copolymer scaffold with alginate, gelatin and growth factors like morphogenetic protein-2, have shown good biocompatibility *in vivo* in mice, rabbits, rats and dogs (Li et al., 2016; Laurén et al., 2017; Hickey et al., 2018; Rashad et al., 2019; Zhang et al., 2019).

Specifically in oral tissue regenerative medicine, bacterial CNF and alginate scaffolds have been developed for culture of gingival fibroblasts cells (Chiaoprakobkij et al., 2011). Scaffold from alginate alone showed high cytotoxicity (< 15% cell viability) compared to control (tissue culture polystyrene plate) after 6-48 h. The scaffold from CNF alone showed high cell viability of 73% (48 h). However, when 30 wt.% alginate was used with CNF scaffold the cell viability reduced to 40% of the control (tissue culture polystyrene plate) (Chiaoprakobkij et al., 2011). No studies using CNF from straw biomass has been done for periodontal and oral regeneration.

Kim et al. (2018) compared CNF hydrogel scaffold with Matrigel™, a popular commercial ECM-like scaffold for 3D cell cultures. Overall, the CNF hydrogel showed similar porosity (96%) but higher average pore size of 310 µm than Matrigel™ scaffold (porosity of 95%, and average pore sizes of 120-150 µm). Increased pore size of CNF hydrogel led to a ~1.4-fold higher diffusion coefficient ($\sim 3.0 \times 10^{-7} \text{ cm}^2/\text{s}$) of macromolecules like bovine serum albumin than that with Matrigel™ ($< 2.2 \times 10^{-7} \text{ cm}^2/\text{s}$), factor that can interfere on the mass transfer of nutrients and metabolites between the

scaffold and surrounding media. Osteoblast cells (MC3T3-E1) exhibited poor cell spreading morphology in CNF hydrogel compared to those in Matrigel™ 1 h after seeding. However, after the adaptation period (~5 days), the osteoblast cells proliferated exponentially during the 21 days in CNF scaffold (Kin et al., 2018). In case of the Matrigel™, the osteoblast cells were well spread out and rapidly proliferated reaching its maximum at day 7, where the cell viability drastically declined, and after 14 days, no cell proliferation was detected. The cell death in Matrigel™ might occur due to chronic stress conditions and poor diffusion coefficient of the scaffold. *In vivo*, the poor diffusion coefficient of a scaffold can interfere in the vascular network by delivering scarce oxygen, which eventually can lead to necrosis (Hickey et al., 2018).

Although vascular network within scaffold *in vivo* is important, the blood-contacting surface of implanted scaffold is also a site for microbial adhesion, colonization and proliferation, which creates a competitive process between cells and bacteria that can prevent tissue integration (Kabirian et al., 2019). Furthermore, infection in open fractures, burn wounds and surgical procedures where the use of scaffolds is needed, are other routes for adherence and survival of pathogenic bacteria, which considerably increases the threat to human health (Lin & Dufresne, 2014; Khalid et al., 2017; Liu et al., 2018; Pant et al., 2018; Ardekani et al., 2019). It has been reported that by incorporating different antimicrobial agents, such as silver, zinc- and nitric oxide particles/nanoparticles, tetracycline hydrochloride drug, and organic agents, such as porphyrin, lysozyme and sorbic acid, in CNF scaffold can reduce the incidence of microbial contamination (Lin & Dufresne, 2014; Khalid et al., 2017; Liu et al., 2018). Furthermore, the recent use of essential oils (e.g. tyme, cinnamon, lemongrass and peppermint) in the polymeric matrix

seems to be a promising strategy to develop scaffolds with antimicrobial properties for tissue engineering applications (Laikos et al., 2015; Ardekani et al., 2019).

Essential oils have been widely used in Ayurvedic medicine and has advantages over other synthetic antimicrobial agents, because they are widely available natural compounds with a low degree of toxicity. Laikos et al. (2015) prepared wound dressing scaffold using cellulose acetate with encapsulated essential oils (cinnamon, lemongrass and peppermint) via electrospinning process. First, the cellulose acetate suspension (15 wt.%) was mixed with 1 or 5 wt.% essential oil, and then the suspensions were electrospun at 3-5 mL/h and 15-25 kV. The electrospun mats (0.2 mm thickness) inhibited the growth of *Escherichia coli*, and the mats had non-cytotoxicity (75-90% viability) against human keratinocytes cells. However, no studies using essential oils and CNF have been performed targeting scaffold production.

In summary, CNF scaffolds offer a promising alternative for applications in tissue engineering due to their cyto- and biocompatibility *in vitro* and *in vivo*. Understanding the effects of different CNF properties, such as dimension (aspect ratio) and surface-chemical composition can provide scaffolds with different morphology and porosity, parameters that have direct influence on its functionality. However, considerable attention should be given to develop CNF scaffolds with increased antimicrobial properties.

2.4. Final remarks

Agricultural straw is a lignocellulosic biomass co-product with great potential as a feedstock for biorefinery towards value-added materials, such as hemicellulosic sugars, phenolic compounds and nanofibers like cellulose and lignocellulosic nanofibers. The use of pressurized fluid processing shows a promising strategy to reduce the use of hazardous chemicals, neutralization steps and waste disposal in biorefineries. From the emerging and non-conventional methods studied for nanofibrillation of pre-treated straw biomass, the use of high-intensity ultrasound has been shown to be a promising approach to obtain either lignocellulosic nanofiber or cellulose nanofiber. Lignocellulosic nanofiber is a novel material with great potential as nanopaper and as a reinforcement agent for biocomposites like films for food packaging. Further processing of cellulose nanofibers towards hydrogels and aerogels production is a prominent alternative to get functional materials towards tissue engineering applications.

Chapter 3. Pressurized fluid treatment of barley and canola straws to obtain carbohydrates and phenolics*

3.1. Introduction

Every year, Canada produces Million Tonnes (MT) of agricultural crops, such as barley and canola, that after harvest generates large quantities of straw. In 2015, the total estimated production in Canada was 7.8 MT of barley grain, generating 4.1 MT of barley straw, and 15.8 MT of canola seed, generating 7.7 MT of canola straw. Those straws are renewable lignocellulosic biomass that can be used as biorefinery feedstock to obtain bioactive compounds. Barley and canola straws are mainly composed of cellulose (30-40%), hemicellulose (20-25%) and lignin (15-17%) (Pronyk & Mazza, 2012).

The treatment of lignocellulosic biomass can yield valuable compounds, such as carbohydrates and phenolics, which can be used in the chemical, food, and pharmaceutical industries (Nabarlatz et al., 2004). Sugars can be removed from hemicellulose and cellulose, while phenolics can be obtained by the cleavage of lignin-cellulose complex (LCC) (Gorrete et al., 2008). For the treatment of lignocellulosic biomass, acid and alkali hydrolysis, enzymatic hydrolysis and thermochemical processes have commonly been used. Acid hydrolysis has been studied under different operating conditions to hydrolyze a variety of biomass, such as barley straw (Kim et al., 2011), canola straw (Lu et al., 2009; Jeong et al., 2010), rice straw (Karimi et al., 2006), sunflower and tobacco stalk (Akpınar et al., 2009), sugarcane bagasse (Rodrigues et al., 2010) and wheat straw (Sun et al., 1996). Kim et al. (2011) reported that 81% of hemicellulose from barley straw was hydrolyzed using 1.2% H₂SO₄ at optimal conditions of 150 °C and ambient

*A version of this chapter was published as Huerta, R.R. and Saldaña, M.D.A. (2018). Pressurized fluid treatment of barley and canola straws to obtain carbohydrates and phenolics. *The Journal of Supercritical Fluids*, 141, 12-20.

pressure for 17 min. Similarly, Jeong et al. (2010) removed 79% of hemicellulose from canola straw using 1.7% H₂SO₄ at 159 °C and ambient pressure for 21 min. Lu et al. (2009) also removed 75% of hemicellulosic sugars from canola straw using acid hydrolysis (1% H₂SO₄ at 180 °C and ambient pressure for 10 min) followed by enzymatic hydrolysis. However, a drawback of those methods is the use of toxic and corrosive chemicals, such as H₂SO₄ and HCl, and the cost of enzymes which compromises the economic feasibility of enzymatic hydrolysis.

Thermochemical processes for fractionation of lignocellulosic biomass involves steam explosion, wet explosion, organosolv process, ionic liquids and pressurized fluids, such as pressurized aqueous ammonia, pressurized aqueous ethanol (PAE) and subcritical water (sCW) (Kim & Lee, 2006; Buranov & Mazza, 2007; Sarkar et al., 2014) Among pressurized fluids, the benefits of sCW and PAE treatment for the fractionation of lignocellulosic biomass include no generation of waste streams from neutralization of extracts, and the use of a non-toxic processing solvent, as discussed in Chapter 2.

Earlier, PAE treatment showed better results than sCW treatment for removal of phenolics and carbohydrates from barley hull at temperatures in the range of 120-180 °C, static holding times of 2-20 min, a pressure of 150 bar and flow rates of 2-6 mL/min for 180 min (Sarkar et al., 2014). The best condition for the removal of total carbohydrates (450.3 mg glucose equivalent (GE)/g barley hull) and total phenolics (80.3 mg gallic acid equivalent (GAE)/g barley hull) was obtained at 180 °C, 150 bar, 12% ethanol, 5 mL/min and 15 min of static holding time (Sarkar et al., 2014). Previously, canola and barley straws were hydrolyzed using sCW at only one condition of 165 °C with a flow rate of 115 mL/min and a solvent-to-solid ratio of 60 mL/g by Pronyk & Mazza (2012). The

process yielded 83% and 81% of the initial hemicellulose in barley and canola straws, respectively, indicating a promising approach for straw fractionation. Therefore, the main objective of this study was to evaluate the effects of temperature (140-220 °C), pressure (50-200 bar) and ethanol concentration (0-100%) at a constant flow rate of 5 mL/min for maximum removal of total carbohydrates and phenolics. Moreover, chemical, structural and physicochemical properties of the solid residues after pressurized fluid treatment were also characterized by scanning electron microscopy (SEM), Fourier transform infrared (FT-IR) spectroscopy and thermogravimetric (TG and DTG) analysis.

3.2. Materials and methods

Barley and canola straws (a mixture of varieties not specified by the donors) were kindly provided by Alberta Agriculture and Forestry (Lacombe, AB, Canada) and Dr. Barry Irving (University of Alberta, Edmonton, AB, Canada), respectively. Samples were ground in a centrifugal mill (Retsch, Haan, Germany) and sieved to obtain a powder of < 1 mm particle size, then stored in a Ziplock bag and kept at 25 °C until further use.

Sulfuric acid (97%, ACS reagent), ethanol (99.9%, HPLC grade), sodium carbonate anhydrous (99%, ACS reagent), Folin-Ciocalteu's phenol reagent (2 M), gallic acid standard (99.9% purity), 2,4,6-tripyridyl-*s*-triazine (TPTZ) (99% purity) and d-(+)-glucose standard (99% purity) were obtained from Sigma Aldrich (Oakville, ON, Canada). The Type 1 water used was obtained from a Milli-Q water purification system (Millipore, Bedford, MA, USA).

3.2.1. Proximate compositional analysis

Moisture content was determined gravimetrically by drying the straw in an air oven at 105 °C for 3 h and the ash content was determined by incineration of the dried sample at

550 °C overnight. The protein content was determined using a Leco nitrogen analyzer using a conversion factor of 6.25 to convert nitrogen to protein (Model FP-428, Leco instruments Ltd., Mississauga, ON, Canada) and the fat content was determined by Soxhlet extraction using hexane for 6 h. The total carbohydrate content of the straw was calculated by the difference of 100% minus the sum of moisture, ash, protein and fat contents.

3.2.2. Pressurized fluid treatment

A semi-continuous flow type subcritical fluid system previously described by Ciftci & Saldaña (2015) was used (Fig. 3.1). Briefly, the system consisted of an HPLC pump (Gilson 307, Villiers-le-Bel, IDF, France), a pre-heater, a heater band, a stainless steel high-pressure vessel, a digital pressure gauge, a cooling system (Swagelok, Edmonton, AB, Canada), an oven (Binder, Bohemia, NY, USA) and a back pressure regulator (Tescom, Elk River, MN, USA). All hydrolysis was carried out using a high-pressure reaction vessel of 2.54 cm diameter × 10 cm length, which had inlet and outlet filters of 20 µm. The barley or canola straw (3 g) was mixed with 27 g of glass beads (2.3 mm diameter) and then loaded into the reaction vessel. The reactor was heated by the heater band inside the oven and the temperature was monitored throughout the process. Type 1 water was first degassed in an ultrasound bath for 20 min, and then delivered by the HPLC pump at a constant flow rate of 5 mL/min. The pressure of the system was maintained constant using the back pressure regulator. After flowing through the cooler, the extracts were collected in vials every 10 min for 40 min and stored at -18 °C for further analysis. The experiments were conducted at temperatures of 140-220 °C, pressures of 50-200 bar and ethanol concentrations of 0-100% (v/v). All experiments were performed at least in duplicates. The solid residue left in the high-pressure vessel after each experiment was abundantly washed

with Type 1 water to separate the glass beads, dried in an oven at 30 °C, and stored at -18 °C for further analysis.

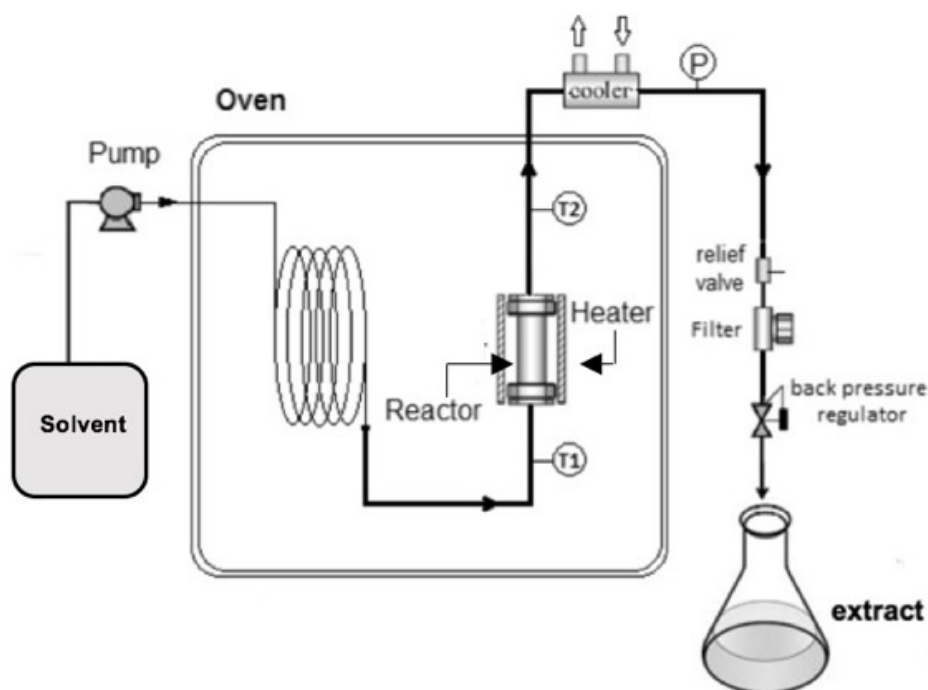


Fig. 3.1. Subcritical water system: *P*=pressure gauge, and *T1* & *T2*=thermocouples.

3.2.3. Characterization of liquid extracts

Analysis of total carbohydrates of liquid extracts was performed following the methodology of Dubois et al. (1956). Dilutions of the extracts were done depending on the concentration of each liquid extract sample. The amount of 0.5 mL phenol and 2.5 mL sulfuric acid (96%) was added to 1 mL of sample and vortexed for 2 min. Then, reaction was stopped using a water bath at 20 °C for 20 min. The calibration curve for total carbohydrates was prepared using glucose solutions ranging from 0.5 to 10 mg glucose/g of water (Fig. A.1a in Appendix A), and the absorbance was measured at 490 nm using a spectrophotometer (Jenway 6320D, Bibby Scientific Ltd., Dunmow, Essex, UK). The final results were expressed as milligram of glucose equivalent (GE) per gram of straw.

Total phenolic content of liquid extracts was determined following the methodology of Singleton & Rossi (1965), with minor modifications. Briefly, 0.04 mL of sample was mixed with 3.16 mL of distilled water and vortexed. Then, 0.2 mL of Folin-Ciocalteu's phenol reagent was added and the mixture was thoroughly vortexed. After 6 min of reaction, 0.6 mL of sodium carbonate solution (20% w/v) was added to the mixture. After stirring, the mixture was incubated for 90 min in a dark place. The absorbance of the samples was measured at 765 nm against the blank using a spectrophotometer and the measurements were compared with the calibration curve of gallic acid solution (Fig. A.1b in Appendix A). The results were expressed as milligrams of gallic acid equivalent (GAE) per gram of sample.

The ferric reducing/antioxidant power (FRAP) was used to estimate the antioxidant activity of the extracts. The FRAP analysis was performed according to the methodology reported by Benzie and Strain (1996), with some modifications. The FRAP solution was prepared by mixing 0.3 M buffer sodium acetate (pH 3.6), 10 mM of 2,4,6-tripyridyl-*s*-triazine solution and 20 mM ferric chloride solution at a ratio of 10:1:1 (v/v/v), respectively. The FRAP solution (3 mL) reacted with 0.1 mL of the extract solution and 0.3 mL of water. Then, solution was incubated at 37 °C in a water bath for 30 min and the absorbance of the colored solution was read at 593 nm. The results were expressed as mM FeSO₄ per gram of sample.

The brown color of the liquid extracts was measured at 420 nm using a UV-vis spectrophotometer (model DU-800, Beckman Coulter Ltd., London, UK), similarly to the method reported by Ajandouz & Puigserver (1999). Results were obtained using the equation provided by Alvarez et al. (2014).

3.2.4. Characterization of solid residues

Raw material and solid residues after pressurized fluid treatment were analyzed for lignin content. Lignin analysis was performed according to the NREL Chemical Analysis and Testing Standard Procedures (Sluiter et al., 2008). The solid samples were hydrolyzed with 72% sulfuric acid for 1 h in a water bath at 30 °C, diluted to 4% sulfuric acid, and autoclaved at 121 °C for 1 h. The hydrolysis solution was vacuum filtered using a porcelain porous-bottom crucible (CoorsTM #60531, Golden, CO, USA) and the insoluble fraction was dried at 30 °C followed by incineration at 575 °C overnight. The acid insoluble lignin was determined from the insoluble fraction mass following the equation provided by Sluiter et al. (2008). Acid soluble lignin in the hydrolysate was determined by the spectrophotometric method at 320 nm (Sluiter et al., 2008).

Infrared spectra of raw and treated samples were performed using a Nicolet iS50 Fourier Transform Infrared Spectrometer (Thermo Fisher Scientific Inc., Waltham, MA, USA) equipped with an Omnic software. The spectra were recorded from 400 to 4000 cm⁻¹ with a resolution of 4 cm⁻¹ and 32 scans to determine the changes in functional groups that may have been caused by the pressurized fluid treatment.

Thermal stability of untreated and treated barley and canola straws was analyzed using a thermogravimetric analyzer TGA Q50 (TA Instrument, New Castle, DE, USA). About 10 mg of sample was placed in a platinum pan and heated from 25 to 600 °C at a heating rate of 10 °C/min under a nitrogen flow of 60 mL/min. Derivative form of thermogravimetric (TG) was obtained using differentials of TG values and referred as DTG. Data were analyzed by the TA Universal analysis software (TA Instruments, New Castle, DE, USA).

The morphology of untreated and treated straw samples were observed using Zeiss Sigma Field Emission SEM (Carl Zeiss AG, Oberkochen, BW, Germany). A thin layer of the straw sample was placed on the SEM specimen stubs with double-size conductive carbon tape and coated with carbon using a Leica EM SCD005 evaporative carbon coater.

3.2.5. Statistical analysis

Data in tables and figures are presented as mean±standard deviation based on at least duplicate experiments and analyses. One-way analysis of variance (ANOVA) and Tukey's honest significance test were carried out using Minitab version 18 (Minitab Inc., State College, PA, USA) at 95% confidence interval.

3.3. Results and discussion

The proximate compositional analyses of barley and canola straws are reported in Table 3.1. Composition of the two straws varied, canola straw had lower quantities of total carbohydrates (68%) than barley straw (71%). The carbohydrate content obtained in this study for barley straw (71%) was similar to the 72% total carbohydrates of barley straw reported by Nabarlatz et al. (2007).

Also, the trend of lower content of carbohydrates in canola straw compared to barley straw agrees with data reported earlier (Pronyk & Mazza, 2012), where canola and barley straws had 72% and 82% of total carbohydrates, respectively. But, Pronyk & Mazza (2014) reported lower values for ash content (3-4%) than values obtained in this study (10-11%) or values (6%) reported by Nabarlatz et al. (2007) for agricultural straws. The differences in the values obtained in this study with the ones reported in the literature can be attributed to the different batches of straws used originating from different locations.

Table 3.1. Proximate compositional analysis of barley and canola straws.

Component	Barley straw	Canola straw
Moisture (%)	5.9	5.9
Ash (%)	10.1	11.3
Fat (%)	2.0	1.7
Protein (%)	10.7	12.8
Carbohydrates (%)	71.4	68.2

Contents are expressed as wt. % dry basis. Standard deviations were less than 0.01.

3.3.1. Subcritical water hydrolysis

Fig. 3.2 shows the effects of temperature (140-220 °C) and pressure (50-200 bar) at a constant flow rate (5 mL/min) for 40 min, for total phenolics and total carbohydrates removal from barley and canola straws. The total time of 40 min was chosen based on kinetics study of total phenolics and total carbohydrates removal from barley and canola straws as shown in Figs. A.2 and A.3 in the Appendix A.

Temperature was an important factor for the removal of bioactive compounds from the straws. Increasing temperature from 140 to 180 °C at 50 bar resulted in an increased carbohydrate removal from 91.7±11.7 to 325.0±13.3 mg GE/g barley straw (increase of 3.5 times), and from 51.5±8.7 to 298.5±13.6 mg GE/g canola straw (increase of 5.8 times) (Table A.1 in Appendix A). Canola straw yielded almost 9 mg GE/g straw less total carbohydrates than barley straw at 180 °C and 50 bar, due to the lower total carbohydrate content of canola straw (Table 3.1). These results are consistent with the findings reported by Sarkar et al. (2014) who used barley hull. They reported that increasing temperature from 140 to 180 °C within 15 min of static holding time at 150 bar, increased the carbohydrates removal from 70.3 to 250.3 mg GE/g barley hull, (an increase of 3.6 times).

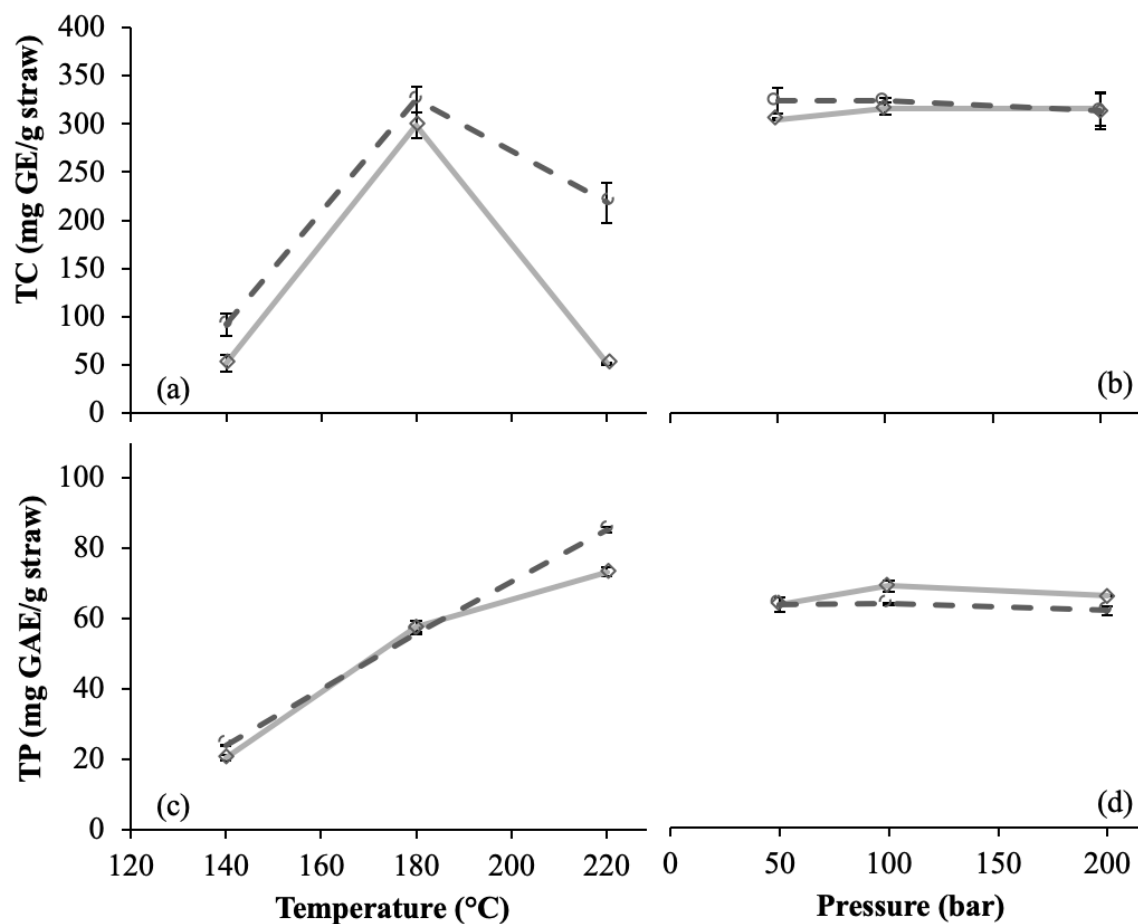


Fig. 3.2. Main effects diagram for total carbohydrates, TC (a, b) and total phenolics, TP (c, d) removal from barley (- -) and canola (—) straws using sCW at 5 mL/min for 40 min.

The total carbohydrate removal decreased for barley and canola straws when the temperature was increased from 180 to 220 °C at 50 bar due to hemicellulosic sugar depolymerization. Under sCW conditions, the water releases hydronium ions from its auto-ionization and releases acetic acid from acetyl groups found in the biomass structure, that catalyzes the hydrolysis of the hemicellulose polymeric structure. During this process, the hemicellulose is hydrolysed into sugar oligomers (mainly xylooligosaccharides) and its further monomer (xylose), which later dehydrate/degraded into furfural and organic acids such as formic and levulinic acids (see Fig. 2.4). The production of degradation products reduced the total carbohydrate content of hydrolysates at 220 °C. Therefore, the optimal

temperature in this study for the removal of total carbohydrates from both straws studied was 180 °C.

Pressure effect in the range of 50-200 bar at 180 °C on carbohydrate removal was not significant ($p > 0.05$) for barley and canola straws (Fig. 3.2b). Sarkar et al. (2014) also showed that a change in pressure from 50 to 250 bar at 150 °C was not significant ($p > 0.05$) on the extraction of total carbohydrates from barley hull mainly because the pressure applied is to keep the solvent in its subcritical state.

In Fig. 3.2c, increasing temperature from 140 °C to 220 °C at 50 bar, resulted in 3.5 times more total phenolic content in the extracts of barley and canola straws (from 23.9 ± 3.4 to 89.0 ± 6.7 mg GAE/g barley straw, and 20.5 ± 0.5 to 73.2 ± 1.3 mg GAE/g canola straw). Temperature is effective to extract phenolics because it facilitates the breakdown of lignin-carbohydrate complex (LCC). But pressure had no significant effect ($p > 0.05$) on phenolic extraction for barley or canola straws (Fig. 3.2d). These results agree with data reported by Ciftci & Saldaña (2015) for the removal of phenolics from lupin hull. The authors reported that increasing temperature from 160 to 200 °C at 200 bar resulted in ten times increased phenolic content from 0.07 to 0.72 mg gallic acid/g lupin hull, implying that high temperatures facilitated breaking interactions between carbohydrates and lignin.

3.3.2. Pressurized aqueous ethanol treatment

Based on the highest removal of carbohydrates and phenolics obtained with pressurized water at 180 °C (Fig. 3.2a), the effects of pressure (50-200 bar) and ethanol concentration (20-100%) to maximize the removal of total carbohydrates and phenolics were studied. Antioxidant activity (FRAP) and formation of brown color compounds (A_{420}) were also measured (Table 3.2 and Fig. 3.3).

Table 3.2. Influence of pressure and ethanol concentration on the removal of total carbohydrates and phenolics from barley and canola straws at 180 °C and 5 mL/min for 40 min.

Treatment condition		Liquid extracts			
EtOH (% v/v)	P (bar)	TC (mg GE/g straw)	TP (mg GAE/g straw)	FRAP (mM FeSO ₄ /g straw)	A ₄₂₀ (mL/g straw)
<i>Barley straw</i>					
0	50	325.0±13.3 ^{cde}	55.9±3.8 ^{ab}	51.9±9.2 ^{ab}	235.1±4.7 ^{ef}
0	100	325.0±2.6 ^{cde}	57.7±0.3 ^a	51.6±6.5 ^{ab}	202.9±16.9 ^f
0	200	313.8±18.6 ^{cde}	55.9±1.9 ^{ab}	50.9±1.4 ^{ab}	233.2±5.4 ^{ef}
20	50	527.6±0.5 ^a	45.4±1.8 ^{bcd}	63.8±1.9 ^a	579.3±52.1 ^a
20	100	351.0±36.5 ^{bcd}	41.0±3.4 ^{cde}	50.5±2.4 ^{ab}	417.2±7.8 ^{bcd}
20	200	446.5±66.5 ^{ab}	44.4±1.0 ^{cd}	53.1±1.4 ^{ab}	484.1±20.1 ^{ab}
60	50	413.4±24.5 ^{bc}	49.5±2.4 ^{abc}	42.3±4.0 ^{bcd}	433.2±41.1 ^{bc}
60	100	327.7±4.1 ^{cde}	46.8±5.2 ^{bcd}	34.9±2.0 ^{cde}	434.6±39.2 ^{bc}
60	200	349.9±17.4 ^{bcd}	47.2±0.2 ^{bcd}	43.0±0.5 ^{bc}	429.5±19.4 ^{bc}
100	50	237.5±15.8 ^{ef}	37.8±1.5 ^{de}	29.4±2.2 ^{cde}	306.8±24.6 ^{def}
100	100	177.5±14.1 ^f	32.6±5.8 ^e	27.3±2.5 ^{de}	305.0±20.5 ^{ef}
100	200	278.6±17.1 ^{def}	36.5±0.6 ^{de}	25.3±2.1 ^e	324.7±35.6 ^{cde}
<i>Canola straw</i>					
0	50	298.5±13.6 ^c	57.5±1.8 ^a	32.0±0.6 ^b	250.5±35.7 ^b
0	100	357.6±11.8 ^{abc}	57.7±0.3 ^a	37.6±2.7 ^b	224.2±35.4 ^b
0	200	315.9±17.2 ^{bc}	56.0±1.1 ^a	24.1±0.3 ^b	209.4±12.3 ^b
20	50	442.7±14.8 ^a	52.9±2.0 ^a	69.1±2.7 ^a	595.2±3.6 ^a
20	100	367.6±55.7 ^{abc}	54.7±3.9 ^a	55.7±3.5 ^{ab}	519.3±19.5 ^a
20	200	420.0±81.1 ^{ab}	49.2±0.6 ^a	58.9±3.1 ^{ab}	532.0±44.0 ^a
60	50	156.6±4.4 ^d	52.0± 2.1 ^a	32.9±3.5 ^c	206.7±6.2 ^b
60	100	140.4±3.7 ^{de}	54.6± 2.7 ^a	30.7±2.0 ^c	238.5±25.6 ^b
60	200	158.1±0.6 ^d	52.8± 1.4 ^a	29.8±1.6 ^c	204.8±15.1 ^b
100	50	92.3±2.0 ^{de}	27.1± 1.4 ^b	30.0±4.2 ^c	113.8±4.1 ^c
100	100	58.2±0.1 ^{de}	32.9± 2.5 ^b	16.9±0.7 ^c	105.7±3.9 ^c
100	200	38.7±0.1 ^e	32.3± 0.6 ^b	18.2±0.9 ^c	93.6±6.5 ^c

EtOH: ethanol; mg GE: mg glucose equivalent; mg GAE: mg gallic acid equivalent; TC: total carbohydrates; TP: total phenolics; FRAP: ferric reducing/antioxidant power and FeSO₄: ferrous sulphate. Contents are expressed as mean±standard deviation of at least duplicates. ^{a-f}For both straws values in the same column are different from each other at p < 0.05.

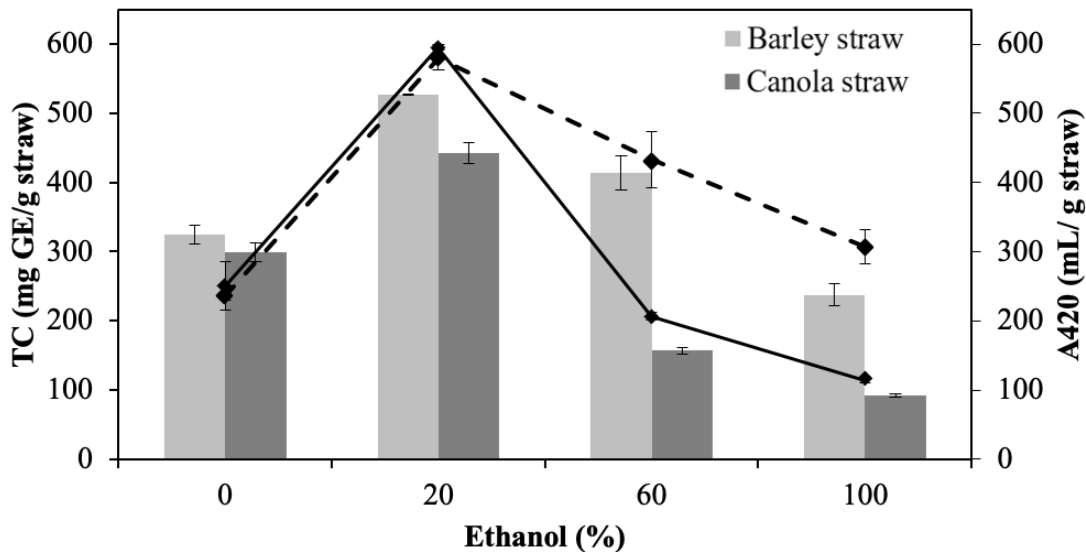


Fig. 3.3. Effect of ethanol concentration for total carbohydrate (TC) removal (bars) and A_{420} values (line) of barley straw (- -) and canola straw (-) at 180 °C, 50 bar and 5 mL/min for 40 min.

At 50-200 bar and 180 °C, the pressurized ethanol and pressurized aqueous ethanol (PAE) exerted a significant influence ($p < 0.05$) for carbohydrates removal from barley and canola straws (Table 3.2). Extracts with total carbohydrates content of 527.6 ± 0.5 mg GE/g barley straw and 442.7 ± 14.8 mg GE/g canola straw were obtained from both straws using 20% ethanol (PAE 20%) at 50 bar within 40 min. Total carbohydrates removal from barley and canola straws increased more than 1.4 times compared to sCW at 180 °C and 50 bar (Table 3.2). Consistently, the A_{420} values obtained for the pressurized extracts had similar trend as total carbohydrates removed as a function of ethanol concentration at 180 °C and 50 bar (Fig. 3.3). At 180 °C, 50 bar with 20% ethanol, the A_{420} values were 579.3 ± 52.1 mL/g barley straw and 595.2 ± 3.6 mL/g canola straw, representing an increase of 2.4 times in relation to treatments performed at the same conditions using sCW. Similar trends were reported by Haldar (2013) using lentil husks, where removal of total carbohydrates and phenolics were studied at ethanol concentrations of 0-80% (v/v), temperatures of 120-200 °C at 65 bar and 2 mL/min. Results at 183 °C showed that

increasing ethanol concentration from 16 to 64% increased 1.6 times the extraction of total carbohydrates in lentil husk.

The carbohydrate removal decreased more than twice for barley straw and more than 4 times for canola straw when ethanol concentration increased from 20 to 100% at 180 °C and 50 bar (Table 3.2). A similar trend was found for brown color formation at 180 °C, 50 bar and 100% ethanol, where A_{420} values decreased by about twice and 5 times for barley and canola straws, respectively. The decrease on total carbohydrate and brown color formation in pressurized ethanol solvent was due to the low solubility of sugar oligomers and monomers in 100% ethanol. Flood & Puagsa (2000) studied the solubility of glucose at 30 °C with ethanol concentrations of 40, 60, and 80% (v/v). The results showed a decrease in solubility as ethanol concentration increased. At 40% ethanol, 0.33 g glucose/g solution was dissolved. Increasing the ethanol concentration up to 60% and 80%, Flood & Puagsa (2000) reported solubilities of 0.15 and 0.05 g glucose/g solution, a reduction in solubility of 2.2 and 3 times, respectively.

Pressure showed no influence on the removal of phenolics from barley and canola straws ($p > 0.05$). Also, increasing ethanol concentration up to 20% at 180 °C and 50 bar did not change significantly ($p > 0.05$) the extraction of total phenolics for both straws (Table 3.2). However, the ethanol concentration had an impact on antioxidant activity ($p < 0.05$) of the hydrolysates. The highest antioxidant activity for barley straw (63.8 ± 1.9 mM FeSO_4/g straw) and canola straw (69.1 ± 2.7 mM FeSO_4/g straw) hydrolysates were obtained at 180 °C and 50 bar using 20% ethanol. Overall, using only pressurized ethanol, the amounts of total carbohydrates, phenolics and antioxidant activity decreased significantly ($p < 0.05$). Similarly, Chiou et al. (2012) used PAE (0-100%) at 120-237 °C

and ambient pressure for 5-60 min for extraction of protein, carbohydrates and phenolics from defatted rice bran. At 237 °C and 5 min of extraction, increasing the ethanol concentration from 30 to 100% resulted in a decrease of total phenolics from 53.3 to 31.9 mg GAE/g bran, and DPPH scavenging activity from 0.23 to 0.09 mmol ascorbic acid/g bran, respectively.

3.3.3. Solid residue after pressurized fluid treatment

Fig. 3.4 shows the lignin content of barley and canola straws solid residues after treatment with pressurized fluids at 180 °C and 50 bar. As known, lignin is a three-dimensional polymer of phenolic compounds linked by carbon-carbon (C-C), ether (C-O-C) and hydrophobic bonds. In the straws, lignin is also linked with cellulose and hemicellulose into a lignin-carbohydrate complex (LCC) structure via phenolic compounds. After sCW treatment the lignin content in barley straw increased from 22.4 (untreated) to 28.9 wt.%, and in canola straw it increased from 20.3 (untreated) to 27.5 wt.%. This behavior was mainly due the large amount of hemicellulose removed after sCW treatment. However, with the addition of ethanol in PAE treatment the lignin content of the solid residue decreased in both straws.

The PAE treatment with 20, 60 and 100% ethanol, led to a reduction in the lignin content of barley straw residue to 18.0, 14.4 and 16.6 wt.%, respectively, and a reduction in lignin content of canola straw residue to 16.1, 17.1, 19.9 wt.% respectively (Table A.2 in Appendix A). The decrease in lignin content of both straw solid residues using aqueous ethanol was due to the hydrolysis of the lignocellulosic straw and better solubility of lignin fragments under PAE conditions. Buranov et al. (2010) studied the solubility of three lignin samples, high molecular weight lignin from flax straw (HML), low molecular weight lignin

from flax straw (LML) and a commercially available Alcell® lignin (organosolv lignin, Sigma-Aldrich, ON, Canada) in water and ethanol concentrations of 0-100% at room temperature. The results indicated that all lignin samples exhibited higher solubility at ethanol concentrations of 60-80% at room temperature. The LML was highly soluble with 30-90% ethanol, and its maximum solubility (260 mg/L) was obtained at an ethanol concentration of 60%. The solubility of HML increased between 50 and 100% ethanol concentrations, reaching its maximum (56 mg/L) at an ethanol concentration of 70%.

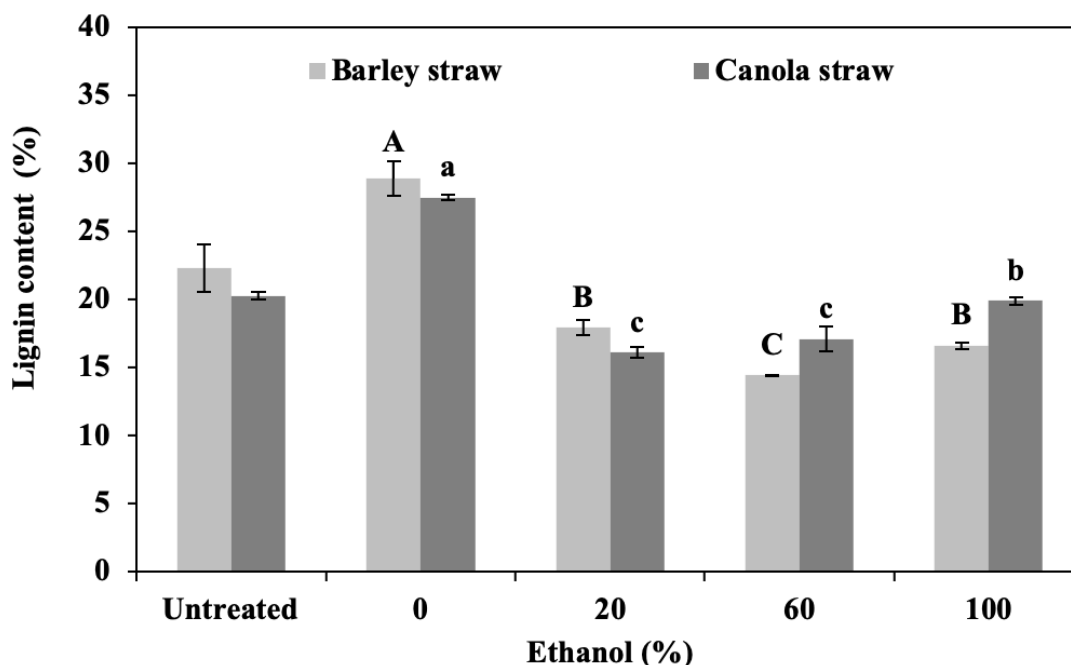


Fig. 3.4. Influence of pressurized fluid treatment (180 ° C, 50 bar and 5 mL/ min for 40 min) on lignin content of barley and canola straw residues. Means within the same group of straw with different letters are significantly different at $p < 0.05$.

Fourier Transform Infrared (FT-IR) spectra of untreated (raw), and sCW and PAE (20% ethanol) treated samples at 180 °C and 50 bar are shown in Fig. 3.5a and b, for barley straw and canola straw, respectively. The peak observed at 3000-3600 cm^{-1} band in the spectra of all samples are ascribed to the O-H stretching vibrations of hydrogen bonded hydroxyl groups, specifically intermolecular hydrogen bonds of cellulose (Yang et

al., 2007). The shoulder near the stretching vibrations of 2901 cm^{-1} was attributed to the C-H stretching vibrations and corresponded to the aliphatic moieties in polysaccharides (cellulose and any hemicellulose remaining) (Ibrahim, 2002). The peaks at 1374 cm^{-1} indicate the presence of bending vibration of C-H and C-O bonds in the polysaccharide aromatic rings (Fatah et al., 2014). As observed in Fig. 3.5, all the spectra have an intense peak at 1030 cm^{-1} , which is assigned to the C-C stretching and C-O stretching of hemicellulose and cellulose (Ibrahim et al., 2010). The increase on peak 1030 cm^{-1} of treated fibers in comparison to untreated straws are due to the increase of cellulose content on residual fibers. The peak at around 896 cm^{-1} corresponds to the β -glycosidic linkages of glucose in cellulose (Xiao et al., 2001). Its presence indicates that cellulose was preserved after the pressurized treatment.

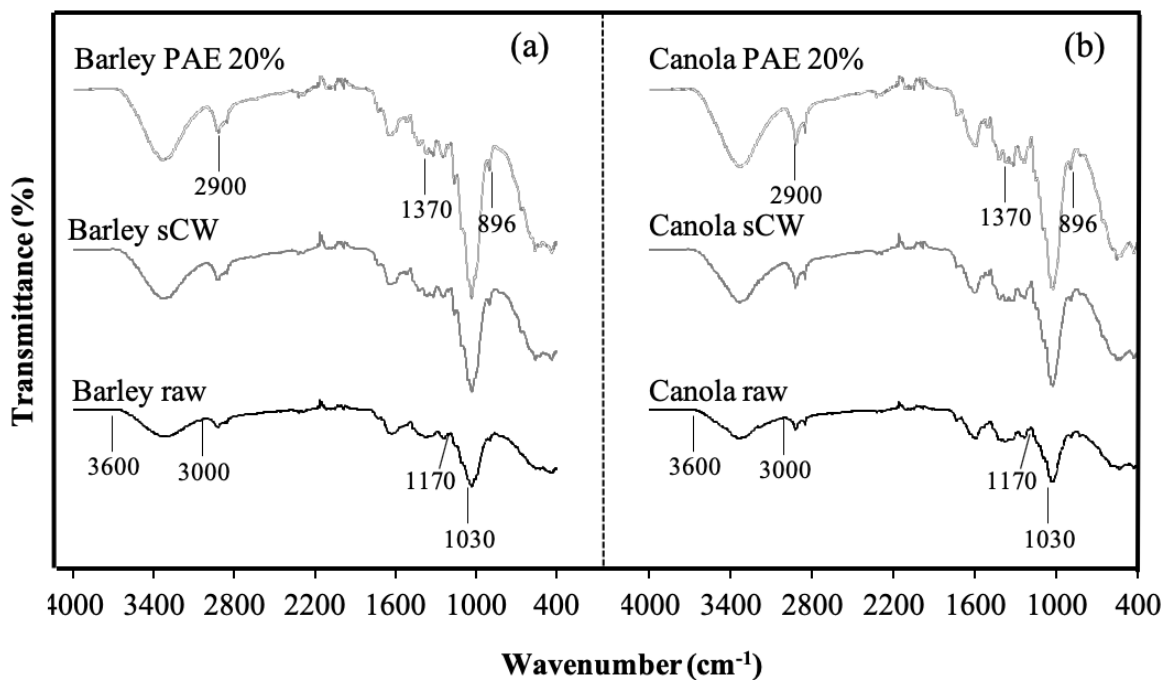


Fig. 3.5. FT-IR spectra of untreated, and sCW and PAE (20%) treated: (a) barley straw, and (b) canola straw.

Thermal behavior of untreated barley straw and canola straw, and sCW and PAE (20%) treated samples at 180 °C and 50 bar are shown as thermogravimetric (TG, weight %) and derivative thermogravimetric (DTG) curves in Fig. 3.6. The pyrolysis characteristics of the three main components in the straw (cellulose, hemicellulose and lignin) are divided into ranges according to the temperatures specified by individual components. Hemicellulose is substantially decomposed at 220-315 °C. The thermal stability of cellulose is higher than that of hemicellulose as its structure consists of a long polymer of glucose without branches and highly ordered, and its pyrolysis occurs at a temperature range of 315-400 °C. The thermal stability of lignin covers an extremely wide range due to its chemical bonds, which led to the degradation of lignin occurring at a temperature range of 100-900 °C (Yang et al., 2007).

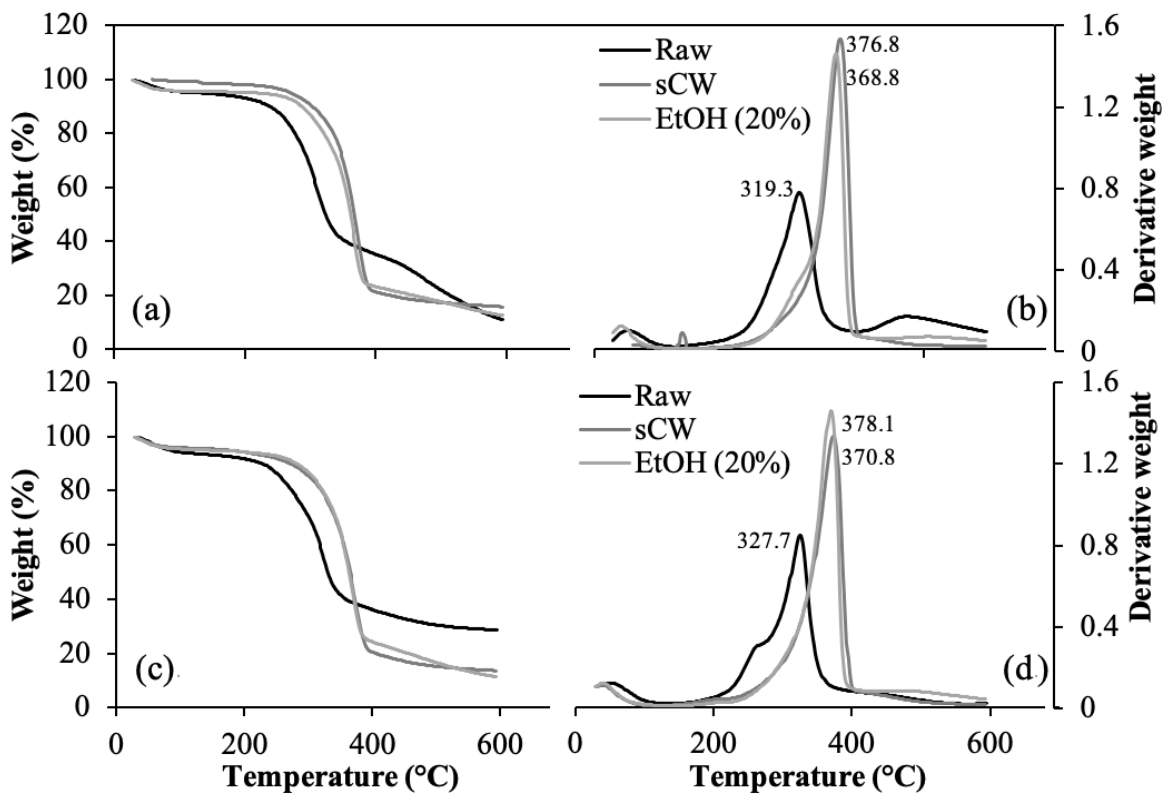


Fig. 3.6. TG thermograms of barley straw (a) and canola straws (c), and DTG curves for barley straw (b) and canola straw (d).

As the thermal degradation characteristics of straws are strongly affected by their chemical composition, the differences in the proportions of cellulose, hemicellulose and lignin strongly affect the thermal characteristics of the treated samples (Fig. 3.6). From the thermogravimetric curves, the degradation temperatures increased after pressurized treatments for both barley and canola straws (Fig. 3.6a and c) as more non-cellulosic material was removed and the material of high degree of structural order was retained. In addition, the DTG emphasizes the zone where various reactions occur over the entire temperature range tested. The DTG curves of pressurized samples had a slight shifting of the peak to a higher temperature compared to untreated straws (Fig. 3.6b and d) due to their high lignin content that requires higher temperature ranges for complete decomposition.

The decomposition characteristics of untreated barley and canola straws, and sCW and PAE (20%) treated straws are summarized in Table 3.3. The weight loss of untreated barley and canola straws between 220 and 315 °C were 36.5 and 28.1%, respectively. Less pronounced weight loss of 12.6% for barley straw, and 12.0% for canola straw at the same temperature range were obtained for the sCW treated samples. The least weight losses of 10.9% for barley straw, and 11.3% for canola straw at the same temperature range were obtained after PAE (20%) treatment which is attributed to the effective removal of hemicelluloses during pressurized fluid treatment. The weight losses between 315 and 400 °C increased for the sCW and PAE (20%) treated samples compared to the untreated barley and canola straws due to the increase of cellulose content on the treated samples. The residual weight was maximum for untreated barley and canola straws (27.2 and 28.5%, respectively), followed by the sCW treated barley and canola straws (15.8 and 13.6%,

respectively). The minimum residual weights were 12.6 and 11.3% for barley and canola straws, respectively, after the PAE (20%) treatment, due to the increased lignin removal compared to sCW.

Table 3.3. Decomposition characteristics of untreated barley and canola straws, and pressurized fluid treated straws at 180 °C, 50 bar and 5 mL/min for 40 min

Straw	Treatment	Weight loss between T_{220} and T_{315} (%)	Weight loss between T_{315} and T_{400} (%)	% Residue at T_{600} (%)
Barley	Raw	36.5	20.2	27.2
	sCW	12.6	65.9	15.8
	PAE (20%)	10.9	58.8	12.8
Canola	Raw	28.1	26.5	28.5
	sCW	12.0	61.3	13.6
	PAE (20%)	11.3	58.2	11.3

T_{220} : temperature at 220 °C; T_{315} : temperature at 315 °C; T_{600} : temperature at 600 °C; sCW: subcritical water; PAE: pressurized aqueous ethanol.

Morphology change of untreated and pressurized fluid treated barley and canola straws were observed by Scanning Electron Microscope (SEM). As shown in Fig. 3.7a and d, the untreated straws had compact rigid structures, with highly ordered fibers. Comparing the untreated straws images (Fig. 3.7a and d) with the straw residues obtained after the sCW and PAE (20%) treatments at 180 °C and 50 bar, clear cracks and large pores were observed on the surfaces of barley and canola straws (Fig. 3.7b-c and e-f, respectively). From the SEM analysis, partial removal of lignin and breaking of the cellulose-hemicellulose-lignin structure of resulted in smooth, more uniform and homogeneous treated fibers with increased surface area.

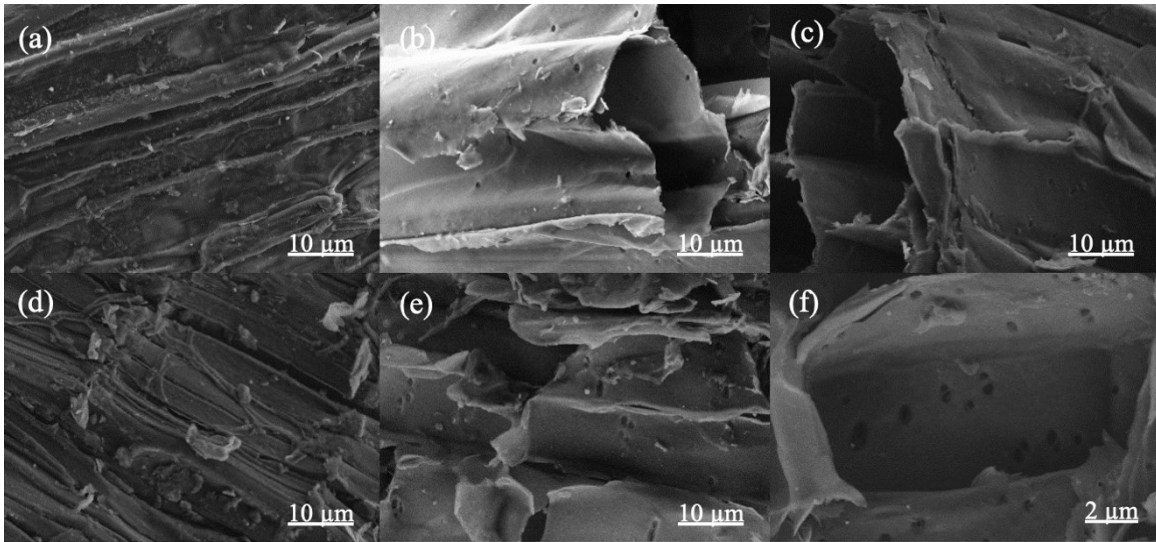


Fig. 3.7. Scanning electron microscopy (SEM) images of: (a) untreated barley straw, (b) sCW treated barley straw, (c) PAE (20%) treated barley straw, (d) untreated canola straw, (e) sCW treated canola straw, and (f) PAE (20%) treated canola straw at 180 °C, 50 bar and 5 mL/min for 40 min.

3.4. Conclusions

Bioactive compounds such as total carbohydrates and total phenolics were removed from barley and canola straws using pressurized fluids. Temperature and ethanol concentration were the most important process parameters for the removal of bioactive compounds from lignocellulosic straws. Total carbohydrates (527.6 ± 0.5 mg GE/g barley straw and 442.7 ± 14.8 mg GE/g canola straw) and total phenolics (45.4 ± 1.8 mg GAE/g barley straw and 52.9 ± 2.0 mg GAE/g canola straw) were successfully removed using the PAE (20% ethanol) treatment at optimal conditions of 180 °C, 50 bar and 5 mL/min for 40 min. Furthermore, the highest total antioxidant activity of each straw was obtained at optimized conditions using the PAE (20% ethanol) treatment. In addition, the use of PAE treatment improved delignification of barley and canola straws compared to the sCW treatment. Moreover, the thermal stability of straw residues was improved after pressurized fluid treatment.

Chapter 4. Sequential treatment with pressurized fluid processing and ultrasonication for biorefinery of canola straw towards lignocellulosic nanofiber production*

4.1. Introduction

The processing and conversion of agricultural and industrial residues into useful products such as fuels, energy, and value-added materials using the biorefinery concept is gaining increased interest. The biorefinery of lignocellulosic biomass such as stalk, straw, hull, peels and others, is a promising solution for the valorization of these types of residues. A lignocellulosic biomass biorefinery requires several steps to produce a portfolio of products; however, the primary refining step is the fractionation of biomass into its three main components: cellulose hemicellulose and lignin (Schröder et al., 2019). There are many methods available for this purpose, where the application of green technologies like pressurized fluid processing have gained increased attention due to the low-environmental impact and the use of non-toxic solvents.

Pressurized fluid fractionation is based on the principle of diluted acid technology, but it does not need to use hazardous chemicals, and neutralization steps, minimizing waste disposal. Pressurized fluid processing has been proven to be an efficient method for the removal of most non-cellulosic materials, producing a treated fiber mainly composed of cellulose and residual lignin (Fang et al., 2008; Pronyk and Mazza, 2011; Buranov & Mazza, 2012; Ciftci & Saldaña, 2015; Giummarella & Lawoko, 2017; Martinez-Abad et al., 2018).

*A version of this chapter was published as Huerta, R.R. and Saldaña, M.D.A. (2019). Sequential treatment with pressurized fluid processing and ultrasonication for biorefinery of canola straw towards lignocellulosic nanofiber production. *Industrial Crops and Products*, 139, 111521.

Nowadays, a fundamental part of the new biorefinery approach is the production of nanosized materials. The well-known long cellulose nanofibers (CNF) and short cellulose nanocrystals (CNC) have been produced from fully bleached biomass with low-lignin content. However, the production of lignocellulosic nanofibers (LCNF) from unbleached cellulose fibers has also attracted increased interest in the last few years (Delgado-Aguilar et al., 2016; Espinosa et al., 2017; Hassan et al., 2018; Jiang et al., 2018; 2019).

Espinosa et al. (2017) studied the production of LCNF from wheat, barley, corn and oats straw pulp using mechanical or enzymatic approaches followed by mechanical disintegration. The straw pulps were pre-treated with 7 wt.% sodium hydroxide (NaOH) solution at 100 °C for 2.5 h and disintegrated using high-pressure homogenization (4 times at 300 bar, 3 times at 600 bar and 3 times at 900 bar), producing LCNF with 62-71% cellulose and 9-13% lignin with an average diameter ranging from 14 to 116 nm. Furthermore, the obtained LCNF had greater resistance to thermal degradation in comparison with the TEMPO-oxidized CNF due to the presence of residual lignin. Similarly, Hassan et al. (2018) treated rice straw pulp with 10 wt.% NaOH solution at 160 °C for 2 h and with xylanase (0.05 g enzyme/g pulp) in pH 5.3 buffer at 50 °C for 4 h, followed by mechanical disintegration using grinding for approximately 2 h. The LCNF with 70% cellulose and 11% lignin had an average diameter of 11 nm that when incorporated into nanopaper sheets, it increased the maximum tensile stress from 66 to 82 MPa and elastic modulus from 4.9 to 7.3 GPa. However, the initial pulp treatment used is known to generate a black liquor that need further separation of the organic and inorganic chemicals in order to avoid environmental contamination. Therefore, the main objective of

this study was to develop an alternative process consisting of pressurized fluid technology and high-intensity ultrasound (HIUS) designed for LCNF production from canola straw. The effects of temperature (140-220 °C), pressure (50-200 bar) and ethanol co-solvent (0-100% v/v) on the composition of canola straw were first elucidated. Then, the disintegration of the treated fiber at 1 wt.% was induced by HIUS at theoretical specific energy (TSE) of 4-20 kJ/g. The untreated and treated materials were analyzed for morphology (SEM), crystallinity (XRD), functional groups (FT-IR) and thermal stability (TG and DTG). The LCNF were characterized for size (TEM), swelling capacity (WRV), surface charge density (ζ potential), fibrillation yield (nanofibril content) and optical transmittance (UV-vis).

4.2. Materials and methods

4.2.1. Materials

Canola straw was prepared according to Chapter 3 (Section 3.2). All chemicals used, including sodium carbonate anhydrous (99%, ACS reagent), sulfuric acid (72%, ACS reagent), and sugar standards ($\geq 96\%$ purity) were obtained from Sigma Aldrich (Oakville, ON, Canada).

4.2.2. Methods

4.2.2.1. Production of lignocellulosic nanofiber

For the pressurized fluid treatment, approximately 3 g of canola straw was loaded into the reactor with 27 g of glass beads (2.3 mm diameter) and the reactor was placed in a semi-continuous flow type subcritical fluid system as described in Chapter 3 (Section 3.2.2). A full factorial experimental design (3×3) was used to investigate the effects of temperature (140-220 °C) and pressure (50-200 bar) on the cellulose, hemicellulose and

lignin contents of the treated canola straw. All pressurized treatments were done at least in duplicate, with a constant flow rate of 5 mL/min and a liquid-to-solid ratio of 67 mL/g for 40 min. Then, pressurized aqueous ethanol (PAE) treatment with ethanol from 0 to 100% (v/v) was investigated at only 180 °C and 50 bar and the data were fitted with the third-order polynomial regression model as shown in Eq. (4.1):

$$Y = a_0 + \sum_{i=1}^k a_i X_i + \sum_{i=1}^k a_{ii} X_i^2 + \sum_{i=1}^k a_{iii} X_i^3 + \varepsilon \quad (4.1)$$

where, Y is the dependent variable (cellulose, hemicellulose or lignin); a_0 is the constant of the model; a_i , a_{ii} and a_{iii} are the model coefficients (linear, quadratic and cubic terms, respectively); X_i is the value of the independent variable (ethanol concentration); and ε is the experimental error.

The regression model and its goodness of fit were assessed by analysis of variance (ANOVA) and by the determination coefficient (R^2), adjusted determination coefficient (R_{adj}^2) and predicted determination coefficient ($R_{prediction}^2$).

The PAE treated fiber at optimal condition was ground and sieved to a particle size of $< 106 \mu\text{m}$ and dispersed in Type I water at a concentration of 1 wt.%. Then, the HIUS treatment was performed using a 20 kHz ultrasonic generator (Model FS-1200 N, Shanghai Sonxi Ultrasonic Instrument Co., Shanghai, ZJ, China) equipped with a cylindrical titanium alloy probe tip of 20 mm in diameter. The dispersion (30 g) was subjected to sonication at theoretical specific energy (TSE) of 4-20 kJ/g in a cold bath (4 °C) to prevent overheating during the process.

The TSE transferred from the ultrasound equipment to the dispersion was calculated according to Eq. (4.2) (Arruda et al., 2019) using nominal powers of 240-1200 W:

$$\text{TSE (kJ/g)} = \left(\frac{\text{Nominal power (W)} \times \text{Processing time (s)}}{\text{Sample mass (g)}} \right) \times 1000^{-1} \quad (4.2)$$

4.2.2.2. Characterization of canola straw

The cellulose, hemicellulose and lignin contents of untreated and treated samples were determined according to the NREL Chemical Analysis and Testing Standard Procedures (Sluiter et al., 2005). First, the samples were hydrolyzed using 72% sulfuric acid as described in Chapter 3 (Section 3.2.4). The acid insoluble lignin was determined from the solid fraction after hydrolysis and the acid soluble lignin from the acid hydrolysate according to Chapter 3 (Section 3.2.4). Then, the hydrolysate was neutralized and the theoretical hemicellulose (expressed as the sum of xylose, galactose, arabinose, and mannose contents) and cellulose (glucose and cellobiose contents) were determined using a Shimadzu HPLC system (Shimadzu Corp., Kyoto, Japan) with a refractive index detector and Aminex sugar HPX-87P column (300 mm x 7.8 mm) (Bio-Rad, Hercules, CA, USA). The system was operated at 85 °C and the mobile phase (HPLC grade water) was delivered at 0.6 mL/min.

Fourier transform infrared (FT-IR) spectra of the fibers were obtained using a spectroscopy (Nicolet 8700, Thermo Fisher Scientific Inc., Waltham, MA, USA) in absorbance mode from 4000 to 700 cm⁻¹.

The X-ray diffraction (XRD) spectra of untreated and PAE treated canola straw were obtained using a X-ray diffractometer (XRD Rigaku Ultima IV, Tokyo, Japan) equipped with a Cu X-ray tube operating at 40 kV and 40 mA. The samples were scanned at reflection angle (2θ) of 5-40° at a speed of 0.6°/min and a step size of 0.01°. The Segal crystallinity index (CI) of samples was calculated using Eq. (4.3) (Segal et al., 1959):

$$\text{Segal CI (\%)} = \frac{I_{200} - I_{am}}{I_{200}} \times 100 \quad (4.3)$$

where, I_{200} and I_{am} correspond to the diffraction intensity of the crystalline and amorphous regions of cellulose, respectively.

Thermogravimetric (TG) analysis and the derivative form of TG (DTG) were obtained using a TG analyzer (TGA Q50) following the procedure described in Chapter 3 (Section 3.2.4).

The morphology of untreated and PAE treated canola straw biomass was analyzed using Zeiss Sigma 300 VP-FESEM (Carl Zeiss AG, Oberkochen, BW, Germany), following the procedure described in Chapter 3 (Section 3.2.4).

4.2.2.3. Characterization of lignocellulosic nanofiber

The transmission electron microscope (TEM) (H7500 TEM, Hitachi, Tokyo, Japan) was used to analyze the LCNF dispersions for morphology and diameter size. A drop of the aqueous dispersion was deposited onto the surface of the TEM grid and coated with a thin layer of carbon. The sample was negatively stained in a solution of 1% uranyl acetate to bring contrast during the analysis. ImageJ software was calibrated using the scale bar on each TEM image and used to calculate the diameter of the nanofibers. A hundred measurements were made for each sample from 10 images selected to calculate the average diameter and size distribution.

The water retention value (WRV) of the LCNF (1 wt.%) was measured according to Gu et al. (2018), with slight modification. Briefly, the dispersion samples were placed in a 50 mL centrifuge filter tube and subjected to centrifugation (AccuSpin 400 Fisher Scientific, Hampton, NH, USA) at 900 g for 30 min at 25 °C. Then, the precipitated sample was dried at 105 °C until constant mass (W_{dry}), and the WRV was calculated using Eq. (4.4):

$$\text{WRV (g/g)} = \left(\frac{W_{\text{wet}} - W_{\text{dry}}}{W_{\text{dry}}} \right) \quad (4.4)$$

The surface charge density of the LCNF dispersions was measured via zeta (ζ) potential (Malvern 3000 Zetasizer Nano-ZS, Malvern Instruments, Worcestershire, WMD, UK). For the analysis, 1 mL of diluted (0.1 wt.%) LCNF dispersion was dispensed inside a Malvern folded capillary zeta cell and then a total of five scans were performed for each sample at 25 °C. The results are shown as an average of the scans.

The yield of fibrillation was determined via nanofibril content according to Bai et al. (2009). First, the diluted (0.2 wt.%) nanofiber dispersion was centrifuged at 1800 g for 20 min. Then, the supernatant was removed and the sediment was dried at 100 °C until constant mass. The nanofibril content was calculated according to Eq. (4.5):

$$\text{Nanofibril content (wt. \%)} = \left(1 - \left(\frac{\text{Mass of dried sediment (g)}}{\text{Mass of initial fiber before centrifugation (g)}} \right) \right) \times \text{cellulose content} \times 100 \quad (4.5)$$

The UV-vis transmittance measurements were performed on LCNF dispersions (1 mL) with 0.1 wt.% solid content according to the method of Delgado-Aguilar et al. (2016). The samples were introduced in quartz cuvettes and the optical transmittance readings were measured with a UV-vis spectrophotometer (UV-vis Shimadzu UV-160a, Shimadzu Corp., Kyoto, Japan) from 300 to 800 nm. Type I water was used as the reference.

4.2.2.4. Statistical analysis

One-way analysis of variance (ANOVA), two-way analysis of means (ANOM), and Tukey's honest significance test were used to evaluate the results and the differences between means, respectively (Minitab 18 software, Minitab Inc., State College, PA, USA)

at 95% confidence interval. All experiments were carried out at least in duplicate and the values were reported as mean±standard deviation.

4.3. Results and discussion

4.3.1. Pressurized fluid treatment of canola straw

In the first part of this study, the aim was to understand how temperature and pressure affect the simultaneous removal of non-cellulosic compounds from canola straw and at the same time use the biorefinery concept to achieve the highest possible recovery of hemicellulose and lignin. Therefore, the full factorial experimental design focused on the synergic effects among the variables was investigated. Table 4.1 shows the values of total cellulose, hemicellulose, and lignin contents of untreated and treated canola straw, and Fig. 4.1 shows the effects of pressurized hot water, also called sCW, treatment conditions on these responses. Untreated canola straw mainly consisted of 36.5±0.4% cellulose, 24.5±0.1% hemicellulose and 18.2±0.1% lignin. Other minor compounds are protein (10.8±0.1%), ash (5.3±0.5%), moisture (3.9±0.6%) and fat (1.7±0.1%).

The sCW treated canola straw had cellulose content ranging from 37.1 to 77.3 %, hemicellulose content from 2.1 to 22.0 % and total lignin content from 21.3 to 27.7 % (Table 4.1). The applied temperature (140-220 °C) significantly influenced the composition of treated canola straw ($p < 0.0001$), whereas the pressure (50-200 bar) was insignificant for total cellulose ($p = 0.846$), hemicellulose ($p = 0.315$) and lignin ($p = 0.696$) (Table B.1-3 in Appendix B). Therefore, the process temperature was the main factor for biomass fractionation. It is known that increasing the process temperature increases the thermal energy and the reaction rate due to water auto-ionization. An increased reaction

rate induces higher bond breakage, which allows the fractionation of biomass into a more diverse product spectrum.

Table 4.1. Influence of pressure and temperature on the treated fiber after sCW treatment of canola straw.

Treatment condition		Treated fiber				
T (°C)	P (bar)	Cellulose (%)	Hemicellulose (%)	Lignin (%)		
				Soluble	Insoluble	Total
<i>Untreated</i>		36.5±0.4	24.5±0.1	2.6±0.0	15.6±0.1	18.2±0.1
140	50	37.9±2.4 ^c	18.2±0.5 ^b	1.0±0.2 ^a	20.3±0.9 ^{bd}	21.4±0.8 ^b
	100	37.1±1.7 ^c	22.0±1.1 ^a	1.0±0.1 ^a	21.6±0.3 ^b	22.6±0.2 ^b
	200	38.1±0.1 ^c	20.4±2.0 ^a	0.9±0.0 ^a	20.4±0.1 ^d	21.3±0.5 ^b
180	50	59.4±2.2 ^b	10.4±0.9 ^c	0.7±0.0 ^b	26.8±0.2 ^a	27.5±0.2 ^a
	100	58.7±2.1 ^b	10.6±0.3 ^c	0.7±0.0 ^b	25.3±0.2 ^b	26.1±0.2 ^b
	200	59.5±1.3 ^b	11.4±0.5 ^c	0.6±0.0 ^b	27.1±0.8 ^a	27.7±0.8 ^a
220	50	77.3±1.9 ^a	2.6±0.1 ^d	0.4±0.0 ^c	22.0±1.2 ^b	22.5±1.2 ^b
	100	74.7±1.1 ^a	2.1±0.3 ^e	0.4±0.0 ^c	24.1±3.1 ^{ab}	24.5±3.1 ^{ab}
	200	74.7±0.6 ^a	2.2±0.1 ^e	0.4±0.0 ^c	23.7±2.3 ^b	24.1±2.3 ^b

Contents are expressed as mean±standard deviation of at least duplicates. T: temperature; P: pressure. ^{a-c}Different lowercase letters in the same column indicate significant differences ($p < 0.05$).

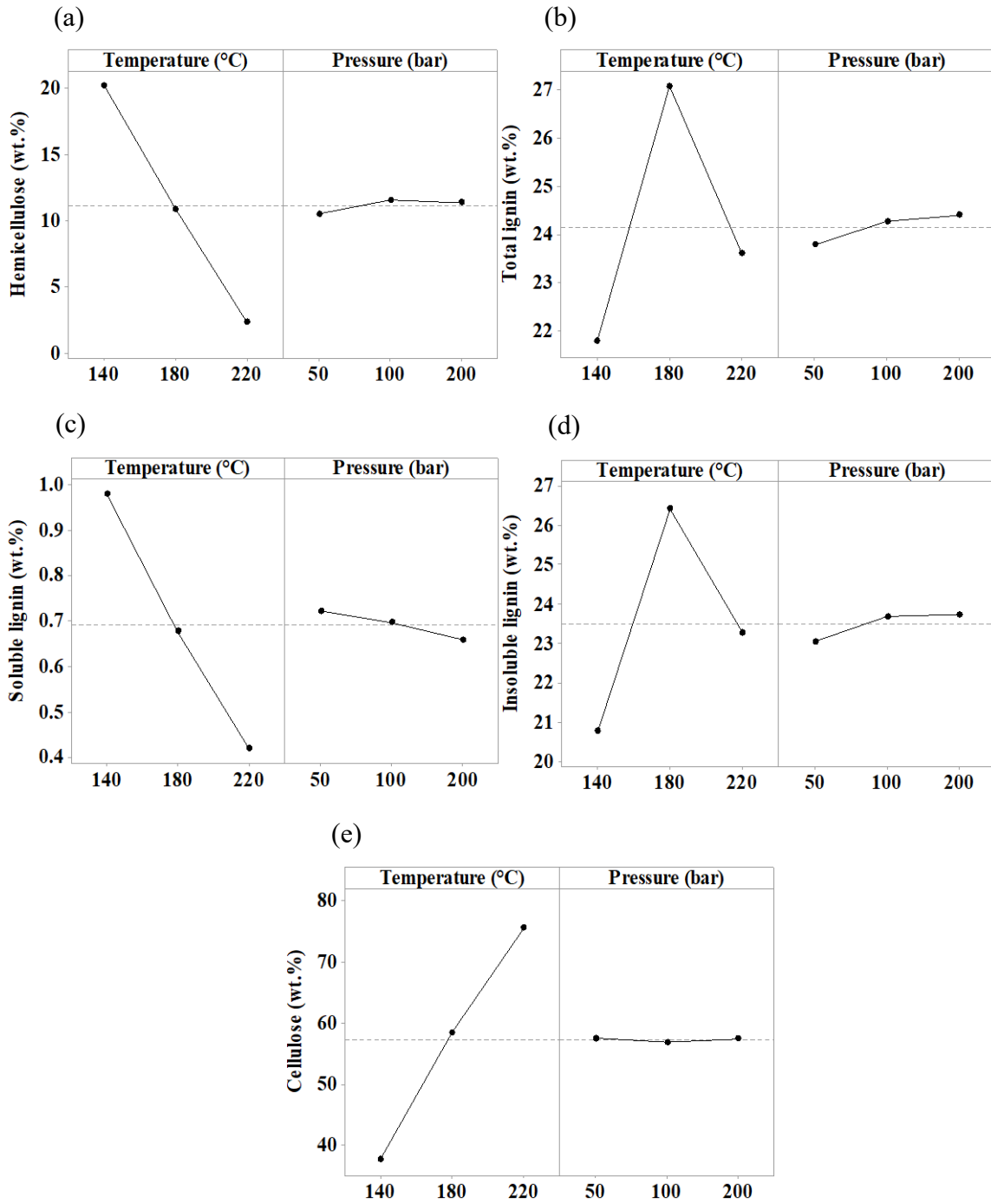


Fig. 4.1. Effects of the processing temperature (140-220 °C) and pressure (50-200 bar) on hemicellulose (a), total lignin (b), soluble lignin (c), insoluble lignin (d) and cellulose (e) contents on the sCW treated fiber. Dotted lines represent the mean values.

The increase in temperature from 140 to 220 °C had a positive effect on total hemicellulose removal for all isobars investigated (Fig. 4.1a), resulting in a reduced residual hemicellulose on the treated fibers. At 140 °C and 50 bar, the residual hemicellulose was 18.2 %, while after increasing the temperature to 180 and 220 °C, it drastically decreased to 10.4 and 2.6 %, respectively. Therefore, the analysis of the treated fiber indicated a theoretical removal of hemicellulose of more than 60% using sCW at 180 °C and 50 bar and almost 90% when the temperature was increased up to 220 °C at 50 bar. However, in Chapter 3 the actual yield of total carbohydrates (mainly hemicellulosic sugars) in the hydrolysate of canola straw decreased more than six times when sCW temperature was increased from 180 to 220 °C at 50 bar. This difference between the theoretical and actual yields of hemicellulosic sugars can be attributed to the production of degradation products.

The hemicellulose extraction using sCW process depends on the severity of the treatment conditions. According to Cocero et al. (2018), the hemicelluloses are cleaved into low molecular weight oligomers, followed by hemicellulose autohydrolysis and further production of sugar degradation products such as formic acid, furfural and HMF. Earlier, Pronyk & Mazza (2011) hydrolyzed triticale straw using a flow-through sCW system, where at 170 °C, 110 bar with a high flow rate of 200-100 mL/min and a liquid-to-solid ratio of 60 mL/g for 60 min, the accumulated yield of hemicellulose on the hydrolysate was 67-73%. However, the analysis of the residues showed that only 9-10% of the hemicellulose remained, indicating a conversion of removed hemicellulose into degradation products of almost 20%. Increasing the temperature above 180 °C, the difference between the theoretical and actual yields of hemicellulose obtained by Pronyk

& Mazza (2011) was 40%, confirming the correlation observed in the present study between the formation of degradation products and treatment temperature.

All treated fibers had increased total lignin content ($\geq 21.3\%$) compared to the untreated canola straw (18.2%) mainly due to the removal of hemicelluloses as shown in Fig. 4.1a and Table 4.1. However, the removal of soluble and insoluble lignin showed different trends depending on the temperature applied (Fig. 4.1c and d, and Table 4.1). At 50 bar, with increased temperature from 140 to 180 °C, an increase of total lignin content from 21.4 to 27.5% was observed. This increase in total lignin content between the treated fibers is mainly due to the increase in insoluble lignin from 20.3 to 26.8%, as the soluble lignin content slight decreased from 1.0 to 0.7% (Table 4.1). With a further increase in temperature to 220 °C, the dielectric constant of sCW decreased, which enhanced the solubility of some nonpolar compounds like insoluble lignin (Table 4.1). According to Fernández et al. (1997) the dielectric constant of water at 50 bar decreased from 39 to 30 when the temperature increased from 186 to 226 °C. However, even with some insoluble lignin-derived oligomers eluting in sCW at 220 °C, the treated fiber still had large amounts of insoluble and total lignin (22.0 and 22.5 %, respectively).

In the lignin-carbohydrate complex, the soluble lignin is mainly linked by phenyl glycosides (glycosidic bonds between C4 of lignin and C1-O of xylan and mannan), which are easily removed at hydrothermal treatments below 200 °C. While the lignin in the middle lamella (insoluble lignin) presents mainly gamma ester (ester linkage between 4-O-methyl glucuronic acid and gamma-C of lignin) and benzyl ether (linkage between lignin and C2, C3 or C6 hydroxyls of the sugar units) linkages, which can be depolymerized into reactive functional groups of monomers such as catechol, phenol,

syringols and guaiacols, promoting re-condensation reactions and increasing the hydrophobicity of the remaining lignin (Fang et al., 2008; Giummarella & Lawoko, 2017; Martinez-Abad et al., 2018; Takada et al., 2018). Besides the re-condensation reaction of insoluble lignin, the formation of pseudo-lignin could also take place during hydrothermal treatment at 220 °C. Few studies have proposed that treatments at high temperatures and low pH, such as sCW, steam explosion and diluted acid hydrolysis, may induce the formation of pseudo-lignin, which is indicated mainly by the high insoluble lignin content remaining after those treatments (Li et al., 2007; Sievers et al., 2009; Sannigrahi et al., 2011). However, the pseudo-lignin is not a native lignin. In fact, it is a carbon-enriched aromatic structure derived from the repolymerization of polysaccharide and lignin degradation products (Sannigrahi et al., 2011).

Increasing the temperature from 140 to 220 °C at 50 bar resulted in an increase in cellulose content from 37.9 to 77.3%, mainly due to the removal of more than 90% of the total hemicelluloses (Table 4.1). As expected, cellulose was not degraded at the range of temperature investigated. According to Bobleter (1994), cellulose I structure (the most abundant type in nature, including straw) is thermally stable due to the macromolecular structure, crystallinity, and formation of intramolecular hydrogen bonds, which elevates the temperature for its hydrolysis. Earlier, Sasaki et al. (2000) investigated the use of sCW at 190-400 °C for 30 min on the decomposition rate of microcrystalline cellulose. The results showed that at the lower temperature range of 190-250 °C, the cellulose particles gradually reduced in size as the reaction time increased. However, after increasing the temperature up to 320 °C, the cellulose decomposition rate was faster by more than two orders of magnitude compared to lower temperatures. The microcrystalline cellulose

completely disappeared at operational temperatures above 350 °C, mainly due to the cleavage of intra- and inter-molecular hydrogen bonds in the crystalline region, which increased the solubility of cellulose in sCW. Therefore, due to the depolymerization of hemicelluloses at 220 °C, the operational conditions further evaluated in this study were 180 °C and 50 bar, where canola straw treated fiber had mainly 59% cellulose, 10% hemicellulose and 28% lignin.

Table 4.2 shows the effect of ethanol concentration from 0 to 100% (v/v), at 180 °C and 50 bar, on the cellulose, hemicellulose, and lignin contents of treated canola straw. As aforementioned, a third-order polynomial model was used to evaluate the results as shown in Table 4.3. Also, the regression coefficients and the statistical significance of each coefficient were assessed and presented in Table 4.3, and their regression equation in Table B.4 in Appendix B. The statistical analysis indicated that the obtained polynomial model was significant for cellulose ($p = 0.009$) and hemicellulose ($p = 0.001$) and it was highly significant ($p < 0.0001$) for total lignin content, including soluble ($p = 0.029$) and insoluble ($p < 0.0001$) lignin (Table 4.3). Also, according to the lack-of-fit analysis, a non-significant value ($p = 0.129-0.147$) for the model equation was observed for total, soluble and insoluble lignin contents, which confirmed that the polynomial regression model and equation were a good fit to elucidate the responses of removal of lignin from canola straw using the PAE treatment. To further determine the accuracy between the experimental and predicted values, the determination coefficient (R^2), adjusted determination coefficient (R^2_{adj}) and predicted determination coefficient ($R^2_{prediction}$) were obtained (Table 4.3). For hemicellulose and total lignin contents, the regression models showed high values for R^2 (≥ 0.85), R^2_{adj} (≥ 0.80) and $R^2_{prediction}$ (≥ 0.70), indicating that the models adequately

represented the effect of ethanol addition as a co-solvent on hemicellulose and total lignin (non-cellulosic materials) removal.

Table 4.2. Cellulose, hemicellulose and lignin contents of canola straw treated fiber obtained using PAE at 180 °C, 50 bar and 5 mL/min for 40 min and addition of ethanol as a co-solvent from 0-100% (v/v).

Ethanol (v/v)	Cellulose (%)	Hemicellulose (%)	Lignin (%)		
			Soluble	Insoluble	Total
0%	59.4±2.2 ^a	10.4±0.9 ^b	0.7±0.0 ^a	26.8±0.2 ^a	27.5±0.2 ^a
20%	62.8±2.7 ^a	9.4±1.4 ^b	0.6±0.1 ^a	16.1±4.9 ^b	20.0±0.4 ^b
40%	56.0±2.5 ^{ab}	19.0±1.7 ^a	0.8±0.0 ^a	18.3±1.4 ^b	19.1±1.4 ^{bc}
60%	58.5±0.2 ^a	20.8±0.1 ^a	0.8±0.0 ^a	17.1±0.9 ^b	17.9±0.9 ^c
80%	52.6±0.9 ^b	21.2±0.4 ^a	0.8±0.0 ^a	18.0±0.1 ^b	18.8±0.1 ^c
100%	45.7±3.8 ^c	21.6±0.8 ^a	0.9±0.0 ^b	19.1±0.3 ^b	19.9±0.3 ^{bc}

Contents are expressed as mean±standard deviation of at least duplicates. ^{a-c}Different lowercase letters in the same column indicate significant differences (p < 0.05).

Table 4.3. Regression coefficients and evaluation of the mathematical models for cellulose, hemicellulose and lignin contents from PAE treated canola straw.

Model parameters	Cellulose (%)	Hemicellulose (%)	Lignin (%)		
			Soluble	Insoluble	Total
<i>Regression coefficients</i>					
a_0	60.11 [*]	9.59 [*]	0.68 [*]	26.55 [*]	27.22 [*]
a_1	0.029 ^{ns}	0.050 ^{ns}	-0.00271 ^{ns}	-0.4364 [*]	-0.4401 [*]
a_1^2	-0.00087 ^{ns}	0.00461 ^{ns}	0.00012 ^{ns}	0.00634 ^{**}	0.00649 ^{**}
a_1^3	-0.000008 ^{ns}	-0.00004 ^{ns}	-	-	-
			0.000001 ^{ns}	0.000027 ^{***}	0.000028 ^{***}
<i>Polynomial model</i>					
Regression (p-value)	0.009	0.001	0.029	<0.0001	<0.0001
Lack-of-fit	0.239	0.019	0.141	0.147	0.129
R^2	0.75	0.85	0.66	0.95	0.95
R_{adj}^2	0.65	0.80	0.53	0.94	0.93
$R_{prediction}^2$	0.37	0.70	0.32	0.91	0.90

ns: Not significant; *Significant at p < 0.001; **Significant at p < 0.01; ***Significant at p < 0.05.

The use of PAE (20% v/v ethanol) removed more than 60% of the initial hemicellulose, yielding a treated fiber mainly composed of 63% cellulose and 20% lignin (Table 4.2). Previously, PAE treatment at 0-95% ethanol (v/v) was used to simultaneously remove hemicellulose and lignin from flax straw (34% cellulose, 21% hemicellulose and 30% lignin) at 52 bar, 160-220 °C, 1.5-7 mL/min, sample sizes of 2.5-25 g and liquid-to-solid ratios of 27-100 mL/g (Buranov & Mazza, 2012). At 180 °C, 52 bar, 30% (v/v) ethanol, liquid-to-solid ratio of 45 mL/g, and flow rate of 3 mL/min for 10 g of flax straw, the PAE process reduced the hemicellulose to 11% and lignin to 20%, resulting in an cellulose enriched treated fiber (65%), which has similar composition to the PAE (20% v/v ethanol) treated fiber obtained for canola straw in this study.

Aqueous ethanol treatment, also known as organosolv treatment, has been recognized as an efficient delignification solvent in the pulp and paper industry. Organosolv processes rely on chemical breakdown of the lignin followed by its dissolution. According to McDonough (1993), the cleavages of α - and β -aryl ether linkage bonds are primarily responsible for lignin breakdown. Ni & Hu (1995) studied the dissolution process of commercial Alcell[®] lignin at ethanol concentrations of 0-100% (v/v) via solubility parameter (δ -value) analysis. The δ -values of pure water, pure ethanol and Alcell[®] lignin were calculated as 22.3, 12.1, and 13.7 cal/cm³, respectively. The maximum solubility of the Alcell[®] lignin was obtained at ethanol concentration of about 70% (δ -value of 14 cal/cm³) due to their δ -value similarities. However, in this study, the increased amounts of ethanol greatly decreased the hemicellulose removal (Table 4.2). Therefore, the fiber obtained after PAE treatment using 20% (v/v) ethanol was selected for further analysis, which is labelled as PAE (20%) treated fiber.

To further confirm the change in the composition of canola straw, the FT-IR spectra of untreated and PAE (20%) treated fibers were analyzed (Fig. 4.2). Both samples were characterized as a function of typical functional groups of lignin and carbohydrates, such as hydroxyl, carbonyl, methyl, carboxyl and aromatic and aliphatic C-H groups. A broad band at 3326 cm^{-1} corresponds to the O-H stretch of the hydroxyl groups of polysaccharides and lignin (Jiang et al., 2015), where the PAE treated fiber had a less pronounced band most likely due to the removal of hemicelluloses. The reduction of the FT-IR absorption peaks at 1734 and 1240 cm^{-1} in the PAE treated fiber compared to the untreated canola straw is also associated with the removal of hemicelluloses since those peaks are respectively assigned to carboxylic acid, and carbonyl groups of xylan (Sannigrahi et al., 2011; Jiang et al., 2015). Furthermore, according to Buranov & Mazza (2012), the reduction in the vibration bands between 1175 and 1000 cm^{-1} , with an intensive signal around 1049 cm^{-1} indicate that the hemicellulose rich in xylan was cleaved.

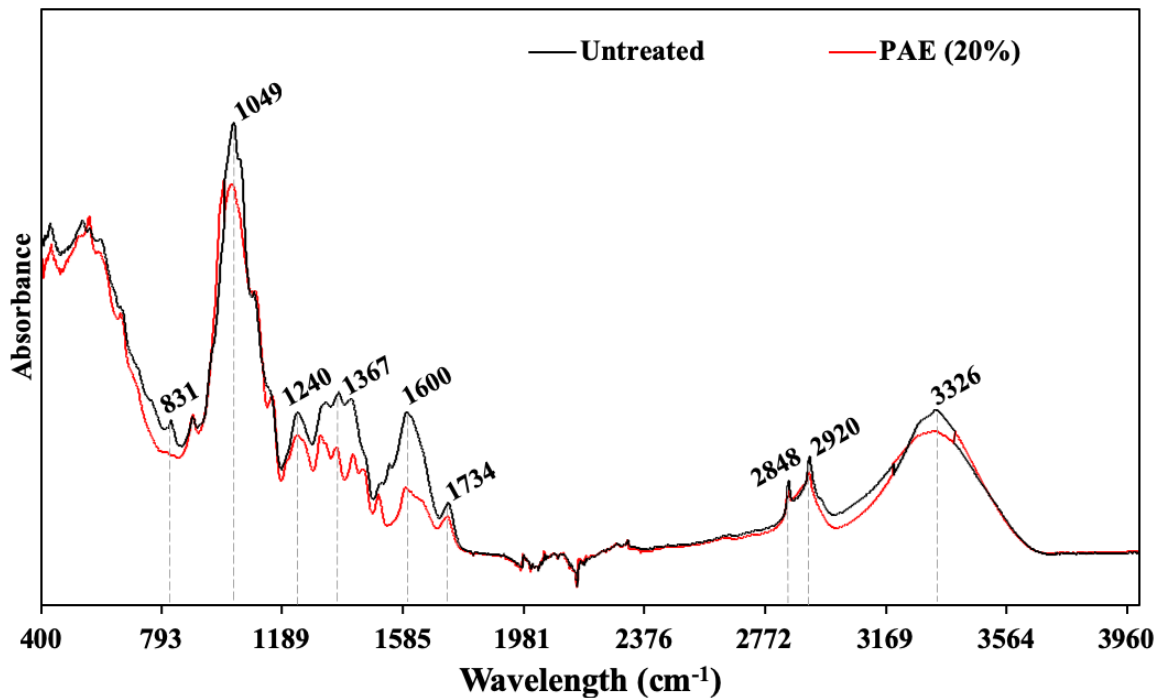


Fig. 4.2. FT-IR spectra of canola straw before and after PAE (20%) treatment at $180\text{ }^{\circ}\text{C}$, 50 bar and 5 mL/min for 40 min.

The FT-IR spectra of both samples had signals at 2920 and 2848 cm^{-1} , which were attributed to the C-H stretch in methyl and methylene groups, respectively, existing in the lignin aromatic structure (Yue et al., 2018; Jiang et al., 2015). The lower signals at 2920 and 2848 cm^{-1} of PAE treated fiber indicates a potential de-methoxylation of lignin after the PAE treatment (Sievers et al., 2009). The PAE treated fiber had a drastic reduction in the peak around 1600 cm^{-1} which is attributed to the cleavage of C-C aromatic skeletal vibration and C=O stretching in lignin (Sun et al., 2000; Yin et al., 2011). Since the aromatic skeletal vibration itself of lignin is assigned at 1508 cm^{-1} , where a minor change was observed, the loss of C=O group linked to the aromatic skeleton indicates the re-condensation reaction among aromatic units in the lignin (Yin et al., 2011). This could be the cause of the slight increase in insoluble lignin content of PAE treated fiber (16.1%) compared to untreated canola straw (15.6%) (Tables 4.1 and 4.2). The reduction of the peak at 1367 cm^{-1} in the PAE treated fiber represents a decrease in O-H of phenolic hydroxyl groups of lignin (Zhou et al., 2015). The formation of free phenolic hydroxyl groups was due to the cleavage of α - and β -aryl ether linkages (Nuopponen et al., 2005) during PAE treatment, which were eluted and removed with the hemicelluloses in the hydrolysate, as discussed in Chapter 3. A small peak at 831 cm^{-1} in the PAE treated fiber compared to untreated straw is also associated to the deformation of C-H out-of-plane in guaiacyl, and *p*-hydroxyphenyl units of lignin (Sannigrahi et al., 2011; Yue et al., 2018). Therefore, the FT-IR analysis confirmed the depolymerization and removal of hemicelluloses, and the cleavage of lignin aromatic units and its branching structure followed by re-condensation reactions.

Among the structural parameters of fibers isolated from lignocellulosic biomass, the determination of crystallinity, which is the ratio of the diffraction intensity of the crystalline region to the total intensity of the material, is meaningful since it can influence the physical and mechanical properties, which provide access for chemical reactions. Although different techniques, like solid-state ^{13}C NMR, have been proposed to calculate the crystallinity of cellulose, the Segal crystallinity index (CI) is a readily understood and useful method for comparing relative differences between samples (Park et al., 2010; French & Cintrón, 2013). The X-ray diffraction (XRD) patterns (Fig. 4.3) of canola straw changed significantly after most hemicelluloses were removed with the PAE treatment. The typical well-defined crystalline peaks of native cellulose I were present around $2\theta = 16^\circ$, 22.5° and 34.5° for untreated and treated samples. The calculated Segal CI values of untreated and PAE treated canola straw were 30.4% and 45.7%, respectively, representing an increase of 1.5 times after PAE treatment (Fig. 4.3). The results suggest that a significant portion of the amorphous material, such as hemicellulose and some lignin, were removed during the PAE treatment, increasing the relative amount of crystalline cellulose of the treated canola straw. Similar results were reported by Ciftci & Saldaña (2015) after subcritical water (180 °C and 50 bar) treatment, where the CI value of lupin hull increased 1.5 times from 38.2% to 58.6%. Such difference of CI values can be related to the type of lignocellulosic biomass used and the content of initial amorphous material. According to Alemdar & Sain (2008), an increased crystallinity of treated fibers is associated to high rigidity and stiffness, and can be a promising material for composites and packaging where high tensile strength is needed.

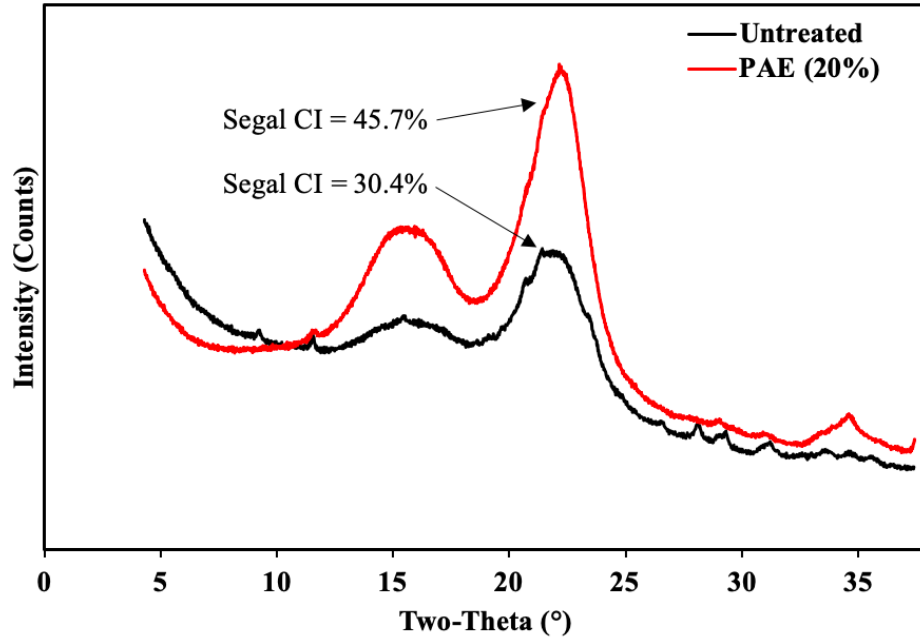


Fig. 4.3. XRD patterns of canola straw before and after PAE (20%) treatment at 180 °C, 50 bar and 5 mL/min for 40 min. Segal CI: Segal crystallinity index.

Another important property of isolated fibers is its stability at high temperatures. The TG and DTG curves for canola straw fibers before and after PAE treatment are shown in Fig. 4.4a and b, respectively. According to Yang et al. (2007), hemicelluloses are substantially decomposed at 220-315 °C, while the thermal stability of cellulose is high (315-400 °C) due to its structure that consists of highly ordered polymers of glucose without branches. The thermal decomposition of lignin covers an extremely wide range of temperatures between 100 and 900 °C (Yang et al., 2007).

In this study, the weight loss at 220-315 °C for the untreated canola straw was 28%, while for the PAE treated canola straw was 11% (Fig. 4.4a). The higher weight loss (%) obtained for untreated sample is simply attributed to the greater amount of hemicellulose present in the untreated canola straw. In contrast, the weight loss at 315-400 °C was 2.2 times higher for the PAE treated canola straw than the untreated sample due to the relative increase of its cellulose and lignin contents. The weight loss at 400-600 °C is mainly due

to the pyrolytic degradation of aromatic rings of lignin (Sun et al., 2000). At this temperature range, untreated canola straw had weight loss of 7%, while PAE treated fiber had weight loss of almost 13%. These results are in agreement with the FT-IR analysis, which indicated increased aromatic units in lignin after PAE treatment due to recondensation reactions. The char residue at 600 °C of PAE treated fiber (11%) was substantially lower than that of untreated canola straw (28%), due to the significant change in the inherent structure of aromatic rings, functional groups and degree of branching on the PAE treated fiber lignin. Also, the presence of free phenolic O-H groups in the untreated straw contributed greatly to the repolymerization and char formation at 600 °C (Zhou et al., 2015; Kim et al., 2017).

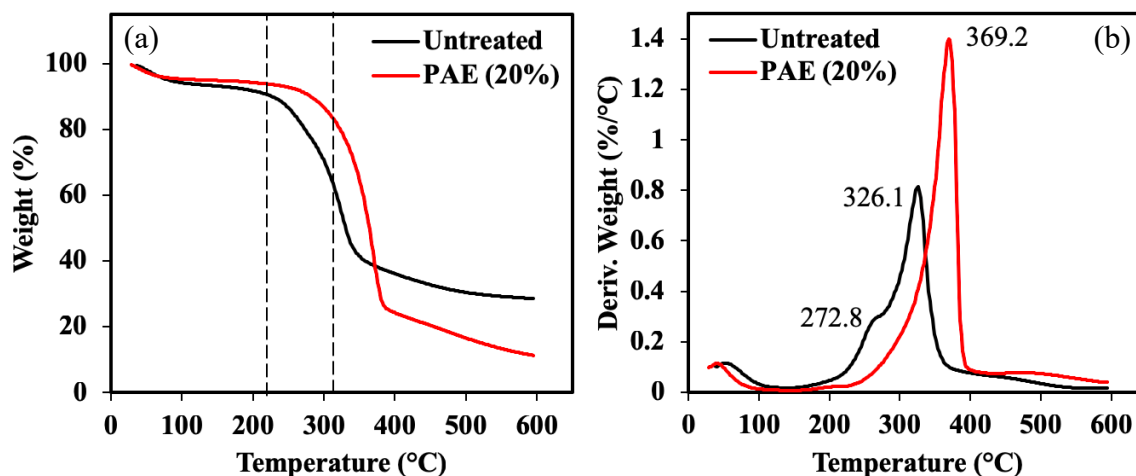


Fig. 4.4. TG (a) and DTG (b) thermograms of canola straw before and after PAE (20%) treatment at 180 °C, 50 bar and 5 mL/min for 40 min.

The DTG curves (Fig. 4.4b) show the maximum temperature at which the weight loss is most apparent. According to Fig. 4.4b, the DTG of untreated canola straw had a major weight loss peak at 326.1 °C, and a shoulder at approximately 272.8 °C, while the PAE treated straw had just one peak at 369.2 °C. The shoulder peak was absent from the curve of PAE treated canola straw because of the removal of most hemicelluloses during the PAE

treatment. These results clearly confirm a relationship between chemical structure and thermal degradation of canola straw fibers.

4.3.2. Production of lignocellulosic nanofibers

The micron-sized fibers obtained after PAE treatment were nanofibrillated using HIUS treatment to nano-sized fibers, herein called lignocellulosic nanofibers (LCNF). Mechanical disintegration using HIUS is highly dependent on the cavitation energy. First, the electrical energy from the power supply (ultrasound probe) is converted into mechanical energy, then into acoustical energy and consequently into cavitation energy and heat energy (Kobus & Kusinska, 2008). The mechanical vibration of ultrasound waves in a liquid medium allows production, growth and collapse of the dissolved gas nuclei existing within the medium. This phenomenon is known as acoustic cavitation, which promotes several physical effects such as shock waves, microjets, turbulence and shear forces (Ashokkumar, 2011). According to Kobus & Kusinska (2008), the physical effects of the cavitation phenomena can only be achieved by the cumulative effect, since the energy released into the liquid by each individual cavity is minimal. The cumulative effect can be observed as a consequence of increased electrical energy or long processing times. In this study, the cumulative effect was a result of increased electrical energy (nominal power) of 240 W (TSE = 4 kJ/g), to 480 W (TSE = 8 kJ/g), 720 W (TSE = 12 kJ/g), 960 W (TSE = 16 kJ/g), and 1200 W (TSE = 20 kJ/g).

Water retention value (WRV), surface charge density, and nanofibril content were determined to understand the nanofibrillation process of the PAE treated fiber (Table 4.4), where a two-way analysis of means (ANOM) was designed to evaluate the main effects of the ultrasonic TSE levels (4-20 kJ/g) on these properties (Fig. 4.5).

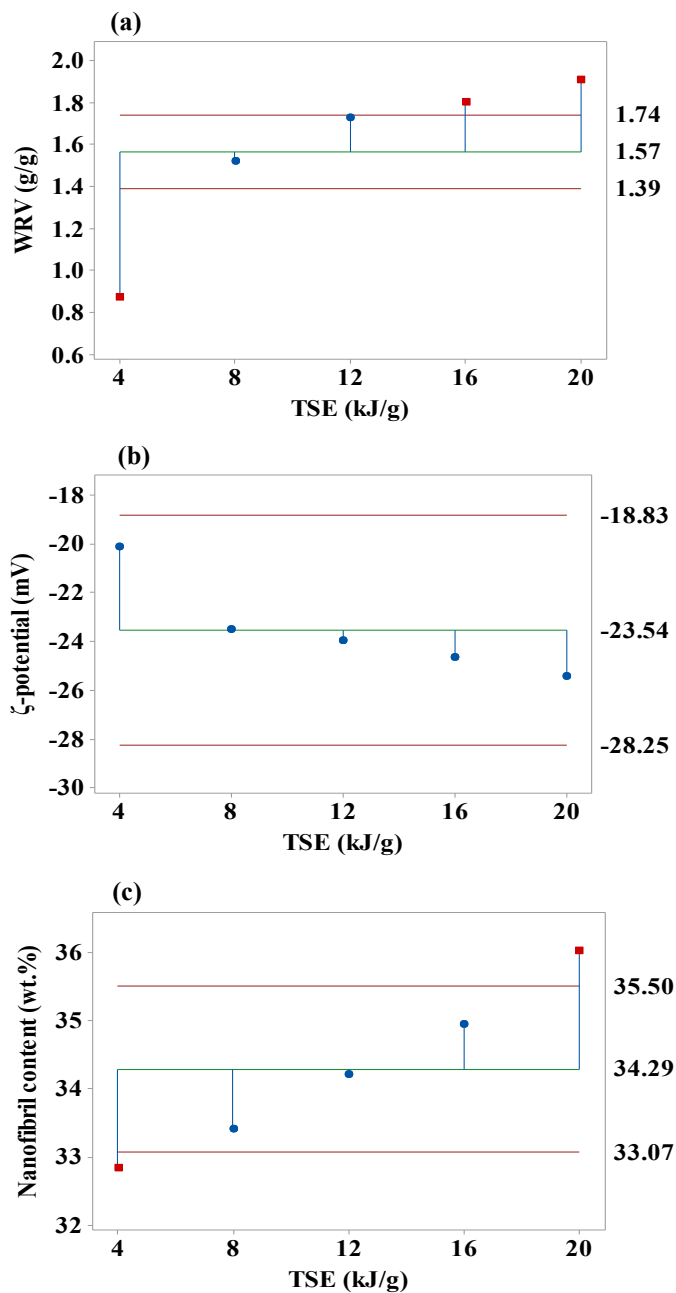


Fig. 4.5. Analysis of means for water retention value (WRV) (a), zeta (ζ) potential (b), and nanofibril content (c) of lignocellulosic nanofibers (1 wt. %) obtained using HIUS at theoretical specific energy (TSE) of 4-20 kJ/g.

Table 4.4. Water retention value, zeta (ζ) potential and nanofibril content of lignocellulosic nanofibers (1 wt.%) obtained using HIUS at theoretical specific energy of 4-20 kJ/g and its corresponded nominal power of 240-1200 W.

Theoretical specific energy (kJ/g)	Nominal power (W)	Water retention value (g/g)	ζ potential (mV)	Nanofibril content (wt.%)
4	240	0.9±0.0 ^c	-20.2±3.9 ^a	32.8±0.5 ^d
8	480	1.5±0.1 ^b	-23.5±1.6 ^a	33.4±0.8 ^{cd}
12	720	1.7±0.1 ^{ab}	-24.0±0.8 ^a	34.2±0.1 ^c
16	960	1.8±0.0 ^a	-24.6±1.2 ^a	34.9±0.1 ^b
20	1200	1.9±0.1 ^a	-25.5±0.6 ^a	36.0±0.6 ^a

Contents are expressed as mean±standard deviation of at least duplicates. ^{a-d}Different lowercase letters in the same column indicate significant differences ($p < 0.05$).

The ANOM plots have a centerline and decision limits. Points within the decision limits had no significant difference between them and the overall mean, but when the point is outside the decision limits it represent a significant difference between that point and the overall mean. In the main effect plot for WRV (g/g), the mean points that represent the factor level of TSE = 4 kJ/g and TSE \geq 16 kJ/g are outside of the decision limits, which indicates that the difference between each of these means and the overall mean is statistically significant (Fig. 4.5a). Similarly, the nanofibril content (wt.%) had the mean points of TSE = 4 kJ/g and TSE = 20 kJ/g outside of the decision limits, indicating a difference between these points and between these points and the overall mean (Fig. 4.5c). However, the main effect for surface charge density (ζ potential) is not statistically significant at any level of ultrasonic TSE studied (Fig. 4.5b).

The increased swelling capacity (WRV) of LCNF obtained using nominal power above 960W and ultrasound TSE \geq 16 kJ/g indicates a greater defibrillation process (Table 4.4 and Fig. 4.5). As previously explained, an increase on the nominal power promoted

greater acoustic cavitation, influencing the defibrillation/disintegration process of the PAE treated fiber. Because of the increased defibrillation process at ultrasound TSE ≥ 16 kJ/g, the LCNF had greater surface area, which increased the interaction between nanofibers hydroxyl group and water molecules via hydrogen bonds, increasing its swelling capacity. However, since the composition of the LCNF has not been changed by the mechanical process, all LCNF had negative charge due to the presence of negatively charged hydroxyl groups on the surface of cellulose, hemicellulose and lignin structures (Table 4.4). The zeta (ζ) potential measures the magnitude of surface charge of molecules and particles. Nanofibers with a higher surface charge density has enough repulsive forces to avoid aggregation or precipitation. Although, the difference on ζ potential was not statistically significant ($p = 0.223$), a slightly increase surface charge of LCNF from -20.2 ± 3.9 to -25.5 ± 0.6 mV was observed with the increase on ultrasound TSE from 4 to 20 kJ/g.

As expected, the nominal power and ultrasonic TSE significantly ($p = 0.009$) affected the nanofibril content (Table 4.4). HIUS treatment at TSE of 4 kJ/g (240 W) resulted in nanofibril content of 32.8 wt.%, while after mechanical treatment using ultrasonic at TSE of 20 kJ/g (1200 W) the nanofibril content increased up to 36.0 wt.%. The nanofibril content calculation is used to report the yield of fibrillation of LCNF (Jiang et al., 2018; 2019). Furthermore, since highly fibrillated LCNF scatter less light than those with lower fibrillation yield, the optical transmittance can also be used to indirectly assess the yield of fibrillation (Fig. 4.6a). As observed from the UV-vis spectra, the optical transmittance of the LCNF increased with the increased ultrasonic TSE and the nominal power used (Table B.5 in Appendix B). This indicates that the nanofibrils obtained at TSE of 20 kJ/g (1200 W) had smaller size than nanofibrils obtained at TSE of 4 kJ/g (240 W).

Furthermore, the results showed a strong correlation between ultrasonic TSE (kJ/g), nanofibril content (wt.%) and optical transmittance at 800 nm (%) (Fig. 4.6b and Table B.6 in Appendix B), which support the statement that a high nominal power and ultrasonic TSE applied caused a greater acoustic cavitation, increasing the nanofibrillation of the PAE treated fiber.

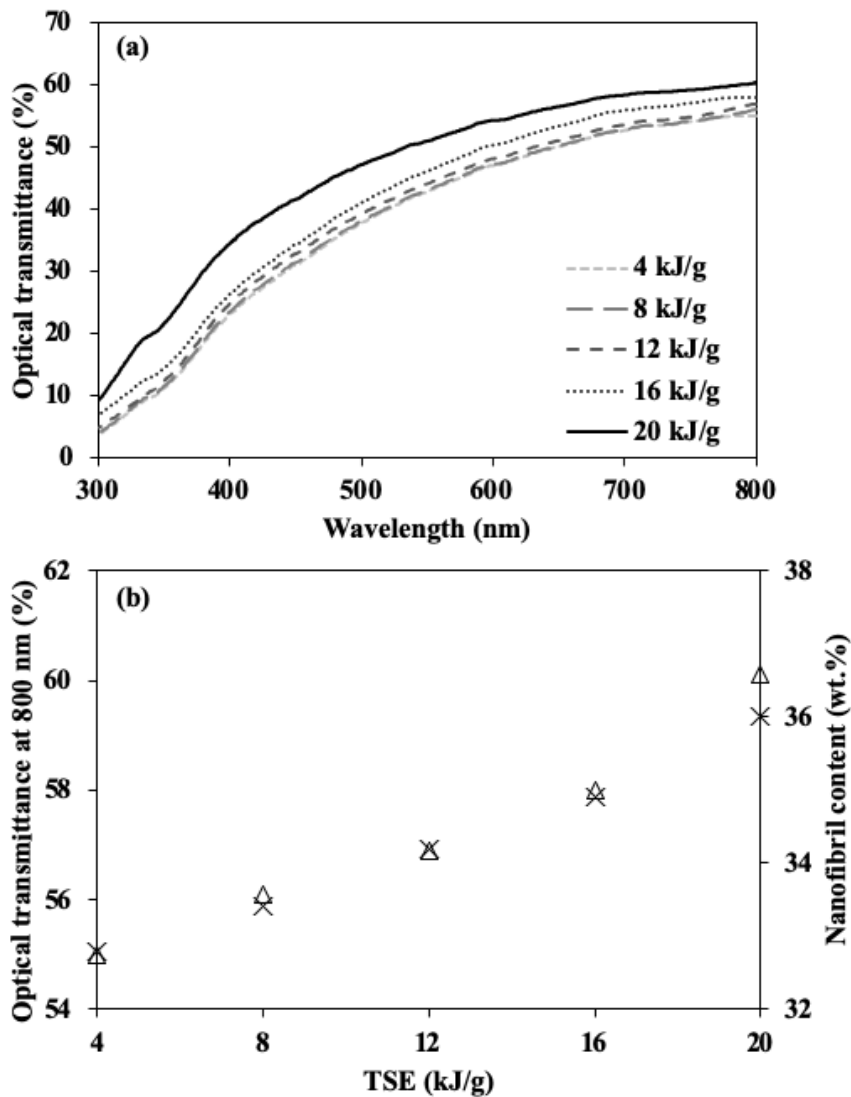


Fig. 4.6. Optical transmittance (%) of lignocellulosic nanofibers (1 wt. %) obtained using HIUS at theoretical specific energy (TSE) of 4-20 kJ/g (a), and correlation between optical transmittance at 800 nm (x), nanofibril content (Δ), and TSE (b).

Earlier, Espinosa et al. (2017) obtained LCNF from a variety of cereal straw pulps (wheat, barley, corn and oats) under different pre-treatment conditions (mechanical, enzymatic or TEMPO-oxidation). Specifically, the wheat and oat pulps with 62 and 69% cellulose, 23 and 16% hemicellulose and 9 and 13% lignin, respectively, were obtained using a beater at 20,000 revolutions per min followed by high-pressure homogenizer (4 times at 300 bar, 3 times at 600 bar and 3 times at 900 bar). The ζ potential of LCNF via mechanical pre-treatment ranged from -15 mV (wheat straw) and -29 mV (oat straw), which are in the range (between -20 and -26 mV) of the present study for LCNF obtained from canola straw (Table 4.4). However, the nanofibrillation yield of wheat straw LCNF was 56% higher than oat straw LCNF (30%, Espinosa et al., 2017) and canola straw LCNF (36%, Table 4.4). The differences in fibrillation yield can be due to the lower lignin content of wheat straw LCNF compared to oat and canola straw LCNF.

To further visualize the effect of the PAE and HIUS treatments on the structure of canola straw fibers, the scanning electron microscopy (SEM) (Fig. 4.7a and b) and transmission electron microscopy (TEM) (Fig. 4.7c and d) were used for the solid treated fiber and its aqueous nanofiber dispersion, respectively. The untreated canola straw showed intact morphology with material deposition on its surface structure (Fig. 4.7a). The significant change in fiber microscopic structure was clear after PAE treatment (Fig. 4.7b), where the cell walls of canola straw fiber were disintegrated, and the removal of non-cellulosic materials resulted in a rough surface with exposure of its internal structure.

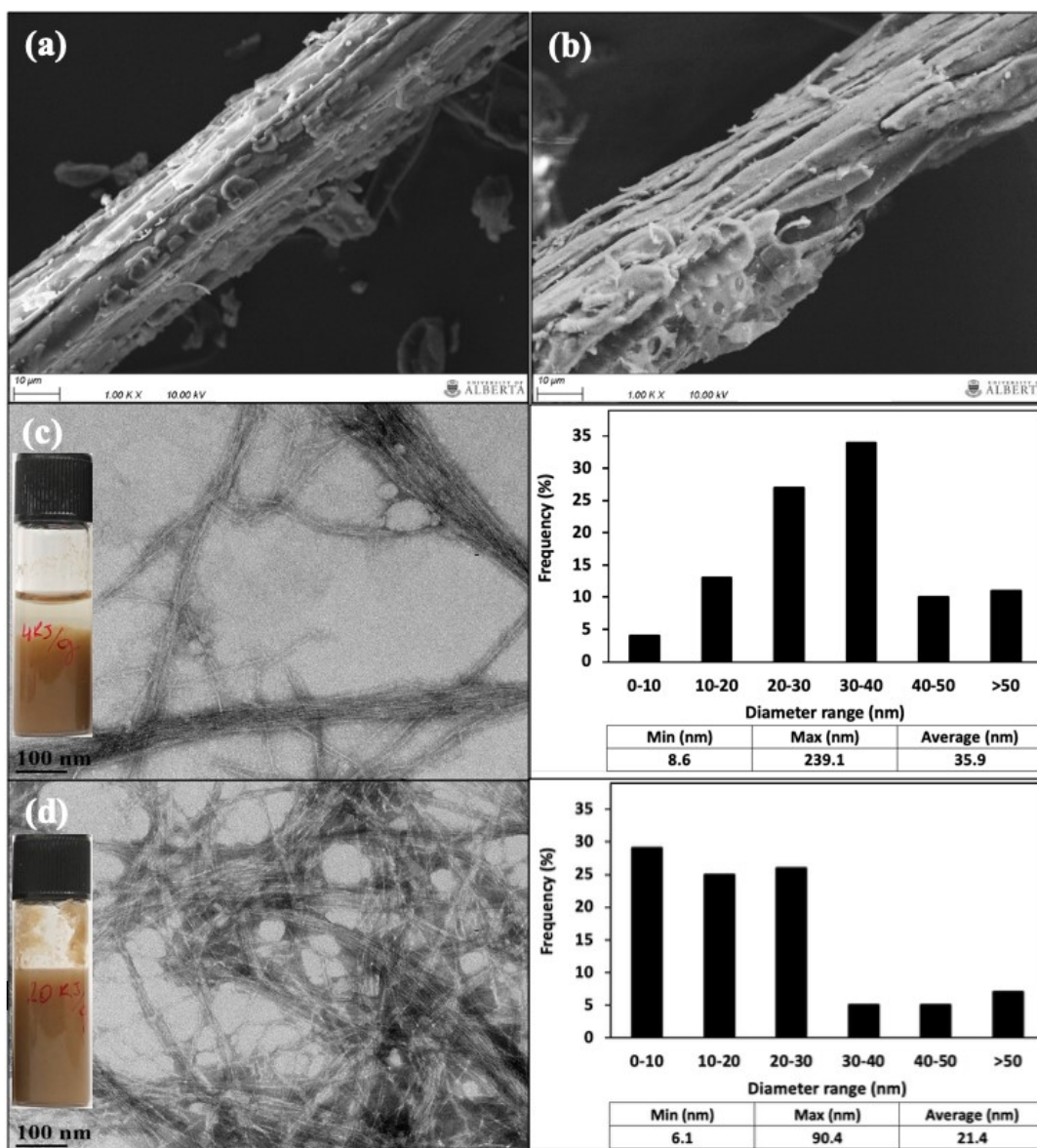


Fig. 4.7. Scanning electron microscopic analysis of untreated canola straw (a), PAE treated fiber (b). Transmission electron microscopic analysis and diameter distribution of lignocellulosic nanofibers obtained after HIUS at theoretical specific energy (TSE) of 4 kJ/g (c) and 20 kJ/g (d).

In the TEM analysis (Fig. 4.7c and d), the diameter distribution results confirm that the mechanical process using HIUS successfully nanofibrillated the PAE treated fiber into LCNF and different levels of nominal power and ultrasonic TSE significantly affected the defibrillation process. Although some fibril bundles and a small amount of aggregated bundles were obtained with all treatments, after HIUS treatment at TSE of 20 kJ/g

(1200 W), a more homogeneous web-like network and well dispersed LCNF was observed compared to the TSE of 4 kJ/g (240 W) (see diameter count distribution in Table B.7 in Appendix B). The average fiber diameter decreased from 35.9 nm to 21.4 nm when the ultrasonic TSE increased from 4 to 20 kJ/g, which supports the results where the higher fibrillation yield and optical transmittance of the LCNF obtained at the ultrasonic TSE of 20 kJ/g were due to the smaller (diameter) size of the nanofibrils. Therefore, the proposed sequential process using pressurized fluid technology and ultrasound offers a favorable alternative to the biorefinery of agricultural biomass towards LCNF production.

4.4. Conclusions

The biorefining of canola straw using environmentally friendly processes has been successfully studied to obtain lignocellulosic nanofibers (LCNF). Temperature and level of ethanol addition during pressurized fluid treatment significantly affected the chemical composition of canola straw, and the ultrasonic TSE significantly affected the swelling capacity, optical transmittance, nanofibril content and diameter size distribution of the LCNF. The PAE treated fiber, mainly composed of 62% cellulose and 20% lignin, was nanofibrillated using high-intensity ultrasound at a TSE of 20 kJ/g into LCNF with an average diameter of 21 nm and swelling capacity of 1.9 g water/g LCNF.

Chapter 5. The effect of residual lignin and ultrasound on the production of nanofibers from canola straw*

5.1. Introduction

Canola is one of the most important oilseed crops and the most profitable commodity for Canadian farmers. Lately, canola straw biomass has been utilized as a raw material for biofuel, bioactive compounds and bio-based nanomaterial production (Yuan et al., 2011; Yousefi et al., 2013; Zhao et al., 2019; Svärd et al., 2019). The production of engineered nanomaterials from canola straw biomass includes the well-known long cellulose nanofibers (CNF) and short, rod-like cellulose nanocrystals (CNC) from low-lignin bleached chemical biomass (Yousefi et al., 2013; Svärd et al., 2019). Because of the size reduction, nanomaterials from plant biomass possesses a high aspect ratio, large specific surface area, and vast number of hydroxyl groups, which allows its self-assembling or the interaction with other biopolymers. Although the most common techniques to obtain CNF are refining/grinding and high pressure homogenization, the use of high-intensity ultrasound (HIUS) processing is an emerging method that has also shown high performance to obtain nano-sized materials (Zhao et al., 2019).

The studies using HIUS process are predominantly focused to obtain nanofibers from fully bleached cellulosic material. However, only a few studies have reported the use of HIUS to obtain lignocellulosic nanofibers (LCNF) from unbleached biomass (Liu et al. 2019). Advantages to produce cellulose fibrils with residual lignin can include low aspect ratio, low production costs, low environmental impact, low hydrophilicity, increased dispersibility in non-polar solvents and increased thermal stability (Ferrer et al., 2012; Solala et

*A revised version of this chapter has been submitted to Cellulose as “Huerta, R.R. and Saldaña, M.D.A. (2019). The effect of residual lignin and ultrasound on the production of nanofibers from canola straw.”

al., 2012; Rojo et al., 2015; Bian et al., 2017; Espinosa et al., 2019; Jiang et al., 2019). However, at the same time, the residual lignin can result in lower fibrillation yield (Nair & Yan, 2015; Delgado-Aguilar et al., 2016, Jiang et al., 2018; 2019).

Rojo et al. (2015) nanofibrillated Norway spruce biomass with residual lignin contents of 2, 4, and 14% using a high-pressure microfluidizer for 6 passes (pressure not specified). Overall, the average nanofiber diameter was reduced with an increased lignin content from 2 to 4%, but there was no statistical difference was reported on the average nanofiber diameter when the residual lignin increased from 4 to 14% (nanofibers with 2, 4, and 14% lignin had an average diameter of 25 ± 1 , 20 ± 2 , and 16 ± 2 nm, respectively). Ferrer et al. (2012) also obtained finer nanofibers when the residual lignin of treated birch pulp increased from < 1 to 3%, using a high-pressure microfluidizer with 5 passes at 550 bar. Unbleached biomass (3% lignin) had an average nanofiber diameter of 8.1 ± 0.9 nm, whereas oxidized (2% lignin) and fully bleached biomass (< 1% lignin) had an average nanofiber diameter of 13.4 ± 1.8 and 17.1 ± 1.1 nm, respectively. However, in both studies the yield of fibrillation was not reported and only one processing condition for the mechanical approach was studied.

Recently, Jiang et al. (2018; 2019) reported that the interactive effect of residual lignin (2-15% lignin) and severity of mechanical treatment (3-7 h grinding) can highly influence the yield of fibrillation but not the diameter of the nanofibers obtained from sugarcane bagasse. According to Jiang et al. (2019), grinding time of up to 3 h induced a higher fibrillation yield of CNF (41 wt.%) compared to the LCNF (23 wt.%). However, increasing the grinding time up to 7 h, the fibrillation yield of LCNF (51 wt.%) had no statistical difference compared to the CNF (Jiang et al., 2019). Although the mechanical

approach influenced the fibrillation yield, it had no impact on the average nanofiber diameter, where the LCNF had lower average diameter (9-11 nm) compared to the CNF (23-28 nm). Rojo et al. (2015), Ferrer et al. (2012) and Jiang et al (2018; 2019) stated that the high lignin content could stabilize the cellulose mechano-radicals formed during nanofibrillation, which allowed a better deconstruction of the fibrils. However, this statement was an speculation because the authors have not measured the antioxidant capacity of the residual lignin.

Due to the controversy on the effect of residual lignin on the nanofibrillation of lignocellulosic biomass, the objective of this study was to evaluate the single effect of cellulosic material composition, ultrasound theoretical specific energy (TSE), and their interation, as an emerging method to produce LCNF and CNF from canola straw. First, the straw was treated using pressurized aqueous ethanol (PAE) at 180 °C, 50 bar, 20% (v/v) ethanol for 40 min, followed by bleaching with acidified sodium chlorite (ASC) at 75 °C for 2-6 h to reduce the lignin content of treated biomass. The obtained cellulosic fibers were characterized for morphology, crystallinity, chemical composition and thermal stability. Then, HIUS at TSE of 4-20 kJ/g was employed to produce the nanofibers. The LCNF and CNF were characterized by diameter size distribution, swelling capacity, fibrillation yield, and surface charge density.

5.2. Materials and Methods

5.2.1. Materials

Chemicals used such as sodium chlorite, acetic acid, sulfuric acid, calcium carbonate and sugar standards (arabinose, cellobiose, galactose, glucose, mannose and xylose) with

$\geq 96\%$ purity were ACS reagent grade (Sigma Aldrich, Oakville, ON, Canada) and used without further purification.

5.2.2. Cellulose fiber isolation

Pressurized aqueous ethanol treatment (180 °C, 50 bar, 5 mL/min, 20% v/v ethanol, 40 min) of canola straw was performed according to the methodology described in Chapter 3 (Section 3.2.2). To remove the residual lignin, a bleaching process using ASC was performed on the PAE treated fibers according to the modified method of Ahlgren (1970). Briefly, 10 g of fiber and 100 mL of 1.7 wt.% sodium chlorite, acidified with acetic acid to pH below 4 were placed in a conical flask and incubated at 75 °C for 2-6 h. For every interval of 2 h, the sample was filtered using a filter paper (pore size of 20-25 μm) and fresh ASC solution was added to the sample. After bleaching treatment, the fiber was separated and abundantly washed until the pH reached $\sim 6-7$, oven-dried at 35 °C and stored at 25 °C for further analysis.

5.2.3. Nanofiber production via high-intensity ultrasound

The nanofibers were obtained by mechanical disintegration using a high-intensity ultrasonicator (Model FS-1200N, Shanghai Sonxi Ultrasonic Instrument Co., Shanghai, ZJ, China) of 20 kHz equipped with a cylindrical titanium alloy probe tip of 20 mm in diameter. The theoretical specific energy (TSE) was calculated using Eq. (4.2) as described in Chapter 4 (Section 4.2.2.1). Unbleached nanofibers were referred as lignocellulosic nanofibers (LCNF) and bleached nanofibers for 2-6 h were referred as cellulose nanofibers (CNF).

5.2.4. Fibers characterization

The NREL standard analytical procedures (Sluiter et al., 2008) were used to obtain the chemical composition in terms of cellulose, hemicellulose and lignin contents of the untreated and treated canola straw, as described in Chapter 4 (Section 4.2.2.2).

The X-ray diffractograms (XRD) of untreated and treated fibers were obtained using X-ray diffractometer (Rigaku, Tokyo, Japan) at 40 kV and 40 mA, from 5 to 40° (2 θ) at 0.6°/min and 0.01° step size. The Segal crystallinity index (CI) was calculated according to Eq. (4.3) provided in Chapter 4 (Section 4.2.2.2).

Fourier transform infrared (FT-IR) spectra of the fibers were obtained using a spectrometer (Nicolet 8700, Thermo Fisher Scientific Inc., Waltham, MA, USA), as described in Chapter 4 (Section 4.2.2.2).

The thermogravimetric analyzer (TGA Q50, TA Instrument, New Castle, DE, USA) and the TA Universal software (Version 4.5A, TA Instruments, New Castle, DE, USA) were used to obtain the thermogravimetric (TG) values and the derivative form of the TG (DTG) of the samples, following the protocol described in Chapter 3 (Section 3.2.4). The morphology of the fibers was analyzed using a scanning electron microscope (SEM) (Zeiss Sigma SEM 300, Oberkochen, BW, Germany) as described in Chapter 3 (Section 3.2.4).

5.2.5. Nanofiber characterization

The water retention value (WRV) of nanofiber dispersions were measured according to the procedure of Gu et al. (2018), with slight modification, previously described in Chapter 4 (Section 4.2.2.3).

The diluted LCNF and CNF dispersions (0.1 wt.%) were analyzed for zeta (ζ) potential using a Malvern Zetasizer Nano-ZS apparatus (Malvern Instruments,

Worcestershire, WMD, UK). The same diluted samples were analyzed for nanofibril content according to the methodology reported by Bai et al. (2009) and described in Chapter 4 (Section 4.2.2.3).

The morphology of diluted LCNF and CNF dispersions (0.1 wt.%) were analyzed via transmission electron microscopy (TEM) (Morgagni 268, Field Electron and Ion Company, Hillsboro, OR, USA) following the protocol described in Chapter 4 (Section 4.2.2.3).

5.2.6. Statistical analysis

The results were reported as mean values \pm standard deviation of at least duplicate experiments. A general linear model in Minitab 18 Software (Minitab Inc., State College, PA, USA) was used to conduct the analysis of variance (ANOVA) and determine the differences between treatment means at 95% confidence interval using Tukey's honest significance test.

5.3. Results and discussion

5.3.1. Cellulose fiber isolation

Untreated canola straw consisted mainly of 36.5% cellulose, 24.5% hemicellulose and 18.2% lignin (Table 5.1). Other compounds were protein (10.8 \pm 0.1%), ash (5.3 \pm 0.5%), moisture (3.9 \pm 0.6%), and fat (1.7 \pm 0.1%). The PAE treatment at 180 °C, 50 bar and 20% (v/v) ethanol successfully removed more than 60% of the initial hemicellulose, yielding a treated fiber mainly composed of 62.0% cellulose and 20.0% lignin (other compounds were protein 2.3 \pm 0.4%, ash 3.0 \pm 0.7%, and moisture 2.6 \pm 0.1%). As the PAE solvent used was 20% ethanol and 80% water, the hemicelluloses were mainly solubilized due to the water ionization, which facilitated acid- or base-catalyzed reactions, such as ether and/or ester

bonds hydrolysis between hemicellulose and cellulose or lignin (Cocero et al., 2018). However, as observed in Table 5.1, the lignin was not removed using the PAE processing, due to its intermolecular re-condensation during the treatment. According to Chua & Wayman (1989), in most cases, lignin isolation using hydrothermal treatment led to more highly condensed and cross-linked materials, due to the high chemical reactivity of the lignin depolymerized fragments. Although a large portion of non-cellulosic material was eluted with the pressurized fluid, it accounted for less than 30% of the total mass of the starting material, indicating a solid recovery of almost 70%. However, the recovered solids after PAE treatment was only 46% due to the loss of PAE treated fibers during the post treatment (washing step) to separate the glass beads from the treated fiber.

Table 5.1. Chemical composition and recovered solid content of untreated, PAE treated and bleached PAE treated canola straw at different reaction times.

Fiber type	Recovered solid (%)[*]	Cellulose (%)	Hemicellulose (%)	Lignin (%)
Untreated	100	36.5±0.4	24.5±0.1	18.2±0.1
PAE	46.4±1.2	62.0±3.5 ^d	9.4±1.4 ^a	20.0±0.4 ^a
B (2 h)	78.5±0.6	70.7±1.0 ^c	4.9±1.0 ^b	18.2±0.2 ^b
B (4 h)	74.6±2.9	78.2±2.5 ^b	4.8±0.7 ^b	10.7±0.2 ^c
B (6 h)	68.3±2.4	81.9±1.0 ^a	3.7±0.1 ^c	8.0±0.2 ^d

^{*}Recovered solids for each bleached treatment were calculated based on the total dry weight of the PAE treatment. Contents are expressed as mean±standard deviation of at least duplicates. PAE: pressurized aqueous ethanol (180 °C, 50 bar, 20% ethanol, 5 mL/min for 40 min); B: bleached with acidified sodium chlorite for 2-6 h after PAE treatment. ^{a-d}Different lowercase letters in the same column indicate significant differences (p < 0.05).

To further remove the residual lignin, the PAE treated fiber was subjected to bleaching step using ASC at 75 °C for 2-6 h. The lignin content of bleached PAE treated fiber decreased from 20.0 to 18.2, 10.7 and 8.0%, while the cellulose content increased from 62.0 to 70.7, 78.2 and 81.9% after 2, 4 and 6 h of bleaching, respectively. Other minor

compounds of the bleached fibers were protein (2.4-2.5%), moisture (2.1-2.7%), and ash (1.2-1.8%). The ASC bleaching was selected because it is a common laboratory method for removal of lignin from lignocellulosic biomass. Also, compared to other bleaching agents like alkaline peroxide, which degrades polysaccharides by the peroxide radical, the ASC is more selective, as it primarily reacts with and solubilizes lignin, with only trace solubilization of glucan, depending on the processing times and sodium chlorite concentration (Ahlgren, 1970; Sun et al., 2004; Jiang et al., 2015). The sodium chlorite in acidified solution decomposes mainly to chlorous acid (HClO_2), which is unstable and further decomposes into chlorine dioxide (ClO_2), chlorite (ClO_2^-) and ultimately chloride (Cl^-) and oxygen (O_2) (Ahlgren, 1970). The HClO_2 and ClO_2 are strong oxidizing agents, and the main active components during the bleaching process. The main routes for lignin solubilization are the modification of its aromatic structure by hydrolytic cleavage, demethylation, quinone formation and electrophilic displacement (Gierer, 1985).

The FT-IR spectra shown in Fig. 5.1 was proposed to further understand the effects of hemicellulose removal and oxidation of lignin on functional groups of treated fibers. All samples had a broad band around the absorbance peak of 3326 cm^{-1} , which corresponds to the -OH stretching of the functional group on polysaccharides and lignin (Jiang et al., 2015). Longer bleaching times (4-6 h) reduced the intensity of the bands at 2920 cm^{-1} and 2848 cm^{-1} , which correspond to the asymmetric and symmetric C-H stretching in methoxy ($-\text{OCH}_3$) groups of aliphatic moieties in lignin (Agarwal & Atalla, 2010). The methoxy group loss, also known as demethylation, is commonly used as an indication of the degree of lignin oxidation during the bleaching process. Throughout the ClO_2 oxidation,

demethylation is a result of acid hydrolysis of phenolic lignin structures, with the formation of quinone, lactone ester, muconic acid derivative, and methanol (Ni et al., 1994).

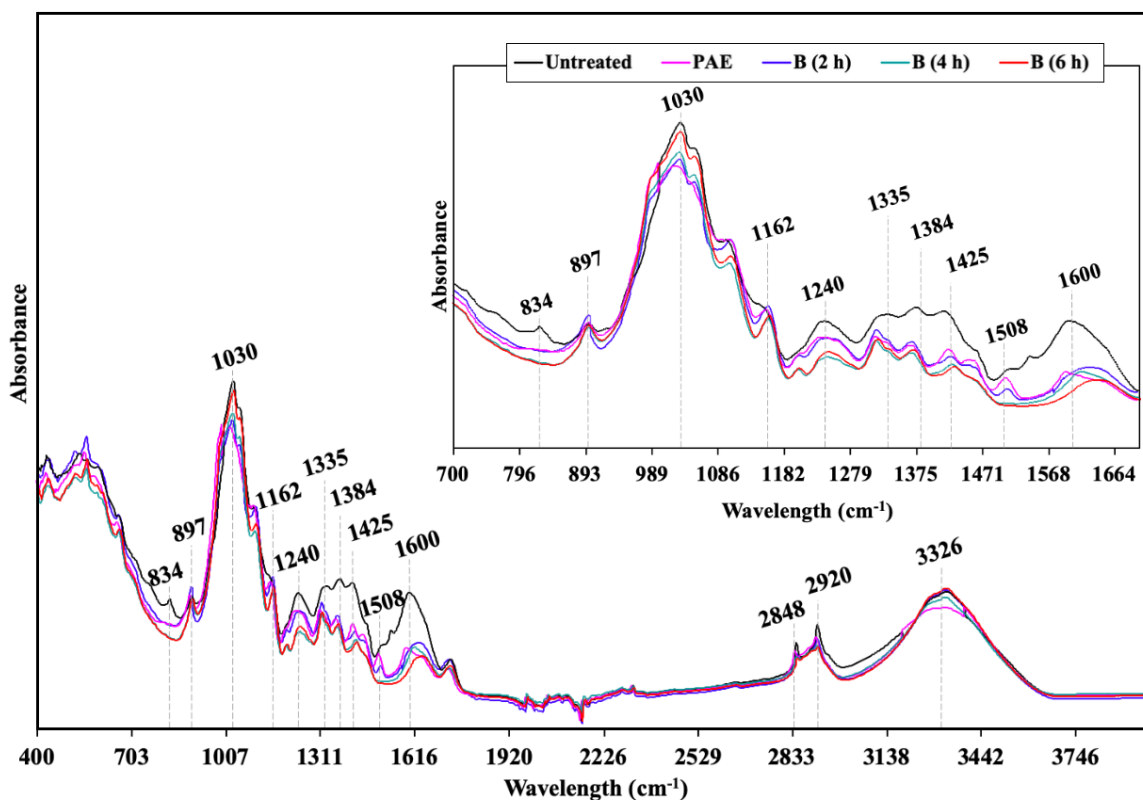


Fig. 5.1. FT-IR spectra of untreated canola straw, PAE treated fiber (180 °C, 50 bar, 20% (v/v) ethanol, 5 mL/min for 40 min) and bleached (2, 4 and 6 h) fibers.

All treated fibers also had a drastic reduction on the peak around 1600 cm^{-1} , which is attributed to the stretching of aryl aromatic rings, together with the C=O group linked to the aromatic skeleton of lignin (Agarwal & Atalla, 2010; Yin et al., 2011). These changes indicate depolymerization of lignin aromatic structure after PAE treatment. However, the peak assigned to 1508 cm^{-1} , which is attributed to the aromatic skeletal vibration of lignin itself and do not overlap with polysaccharide bands (Agarwal & Atalla, 2010), had a minor change in PAE treated fiber, indicating a re-condensation reaction among depolymerized lignin fragments (Yin et al., 2011). With a further increase in the bleaching time of up to 4

h, the peak at 1508 cm^{-1} was absent, due to the cleavage of lignin aromatic structure by the oxidation of β -aryl ether linkages by ClO_2 (Brage et al., 1991).

The reduction in the absorption peak at 1425 cm^{-1} for treated fibers compared to untreated canola straw is associated to the removal of guaiacyl and syringyl ring vibrations (Sun et al., 2000). A high deformation at 1240 cm^{-1} in bleached samples is due to the oxidation of coniferyl alcohol, which is bound to the guaiacyl in the lignin structure by the aryl-O (in aryl-OH and aryl-OCH₃) linkage (Troedec et al., 2008). In addition, all treated fibers presented a lower signal at 834 cm^{-1} compared to untreated canola straw, which indicated the cleavage of aromatic C–H out-of-plane in the guaiacyl units of lignin (Yue et al., 2018).

The bands at 1384 , 1335 , 1162 , 1030 , and 897 cm^{-1} are characteristics of polysaccharides (Sun et al., 2004; Liu et al., 2006; He et al., 2008; Troedec et al., 2008). For example, the band near 1384 cm^{-1} can be ascribed to C-H bending in cellulose and hemicellulose (He et al., 2008). Even after PAE and bleaching treatments the band close to 1335 cm^{-1} , a characteristic of C-O aromatic ring in cellulose, was maintained, which indicated that the cellulose structure was not degraded or oxidized by the treatments applied (Troedec et al., 2008). The two absorption bands at 1162 and 897 cm^{-1} indicate C-O-C stretching at β -glycosidic linkages between the sugar units (Liu et al., 2006). The strong peak at 1030 cm^{-1} indicate the C-C stretching and C-O stretching of the C6 of hemicellulose and cellulose (Sun et al., 2004; Liu et al., 2006). The PAE treated sample had the lowest peak at 1030 cm^{-1} due to the removal of $> 60\%$ of hemicellulose (Table 5.1). In the basic structure of hemicellulose, the C6 position is attached to side groups/chains. Therefore, due to the ionization of the pressurized solvent, hemicellulose side chains were cleaved into

low molecular weight oligomers and removed in the hydrolysate, as discussed in Chapter 3. As the untreated canola straw and bleached (6 h) fiber had the highest amount of hemicellulose and cellulose, respectively, both samples presented high absorption peak at 1030 cm^{-1} .

Overall, the FT-IR spectra confirmed the removal of hemicellulose from canola straw after the PAE treatment. Furthermore, due to the reduction of peaks characterized by lignin functional groups at 834 , 1240 , 1425 and 1508 cm^{-1} after the bleaching process, the FT-IR data also confirmed that most of the lignin was oxidized and removed during the ASC process. Besides the modification of functional groups, untreated and treated canola straw fibers were compared with respect to crystallinity, thermostability and morphology.

The XRD diffractograms and the Segal crystallinity index (CI) of untreated and treated samples are shown in Fig. 5.2. The Segal CI value of untreated canola straw was 30.4%, while after PAE and bleaching treatments, it increased up to 67.8% due to the removal of amorphous material. As the ASC bleaching dissolved the residual hemicellulose and lignin (both amorphous in nature), the bleached fibers had an increased percentage of highly crystalline cellulose. Furthermore, all the XRD patterns presented three peaks at around $2\theta = 16^\circ$, 22.5° and 34.5° , indicating that the crystalline structure of native cellulose (also known as cellulose I) was preserved. The crystalline transformation of cellulose I into cellulose II (two weaker peaks at $2\theta = 20^\circ$ and 22°) usually takes place when regeneration or mercerization alkaline process are used.

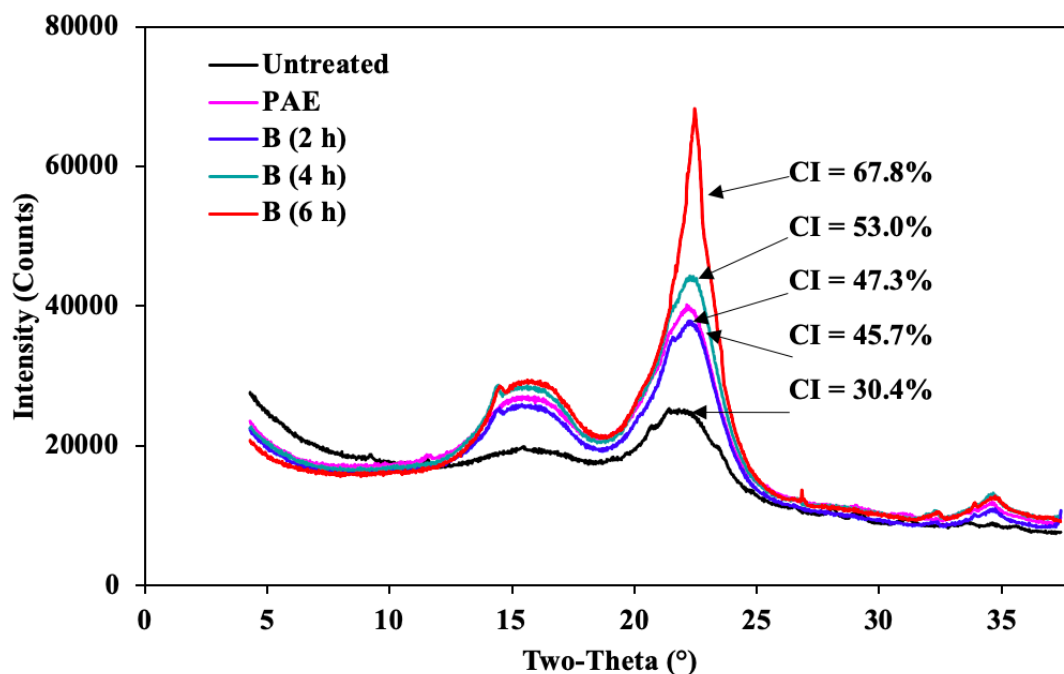


Fig. 5.2. X-ray diffractograms (XRD) of untreated canola straw and PAE treated fiber (180 °C, 50 bar, 20% (v/v) ethanol, 5 mL/min for 40 min) before and after bleaching (B2-6 h). CI: Segal crystallinity index.

As the chemical composition and crystallinity of the samples have an impact on their thermal degradation, the thermal stability (TG and DTG) of untreated and PAE treated fiber before and after bleaching (2-6 h) are shown in Fig. 5.3a and b, respectively. The hemicellulose is substantially decomposed at 220-315 °C, while cellulose and lignin require higher temperatures for decomposition, around 315-400 °C and up to 900 °C, respectively (Yang et al., 2007). As observed in Fig. 5.3a, at temperatures of 220-315 °C, the untreated canola straw showed a significantly higher weight loss (28%) compared to treated samples (11-14%). This behavior is associated with the high content of hemicellulose in the raw material (Table 5.1). Furthermore, on the DTG curves shown in Fig. 5.3b, two peaks were visualized only for untreated canola straw fiber a major peak at 326.1 °C, and a shoulder at approximately 272.8 °C, due to the presence of high hemicellulose content (Yang et al., 2007). In the second stage of degradation at 315-400

°C, the weight loss (%) of the samples increased constantly with the increase of cellulose content. In that region, the untreated straw and the PAE treated fiber before and after 2, 4 and 6 h of bleach treatment had weight losses of 26, 58, 59, 67 and 70%, respectively, which agreed with the results shown in Table 5.1.

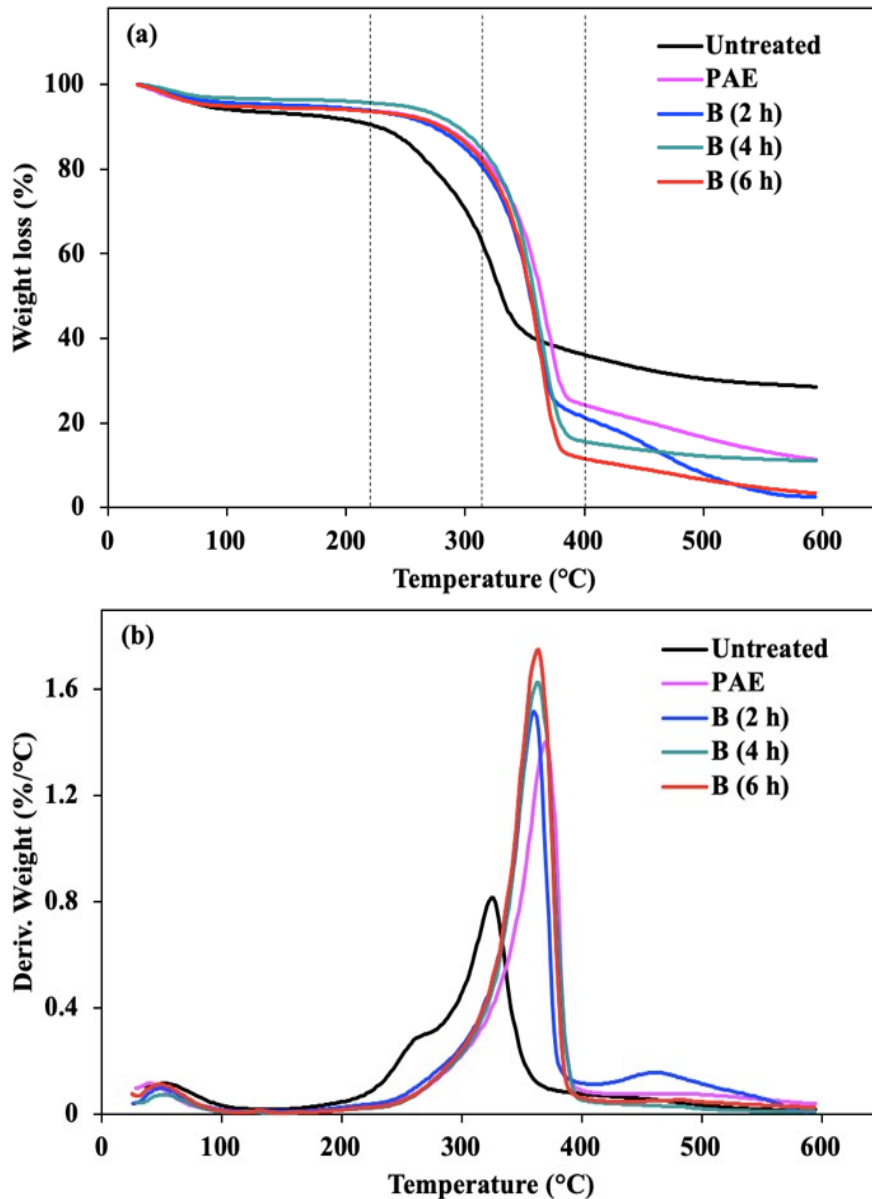


Fig. 5.3. TG (a) and DTG (b) thermograms of untreated canola straw and PAE treated fiber before and after bleaching treatments (B2-6 h).

Table 5.2 shows some thermal properties of the fibers. The onset value (T_{ON}) is defined as the temperature at which the sample weight loss becomes more apparent. The higher T_{ON} of all treated fibers compared to the raw canola straw reflected the removal of non-cellulosic materials and indicated the improved thermal stability of the samples. The parameter T_{MAX} showed the maximum decomposition temperature of the fibers and the residual weight at T_{MAX} was symbolized by MT_{MAX} . The T_{MAX} of canola straw increased from 326 °C to 369 °C after PAE treatment. However, after bleaching treatment for 6 h, the fiber had a reduction on the T_{MAX} to 362 °C. The higher temperature for maximum decomposition of the PAE treated fiber can be attributed to the large amount of residual lignin and the presence of covalent linkages between the cellulose and lignin, requiring more energy to initiate the thermal degradation. This behavior is in agreement with that of Bian et al. (2017), who also evaluated the effect of different lignin contents on the structure and physical performance of nanofibers isolated from a mix of hardwood pulp (mainly birch and maple). The unbleached fibers with 63% cellulose and 18% lignin had T_{MAX} of 393 °C, while bleached fibers with 75% cellulose and 5% lignin had a decrease in the T_{MAX} to 376 °C. Furthermore, according to Table 5.2 the MT_{MAX} of canola straw fiber decreased from 54% to 43% after PAE treatment and had the lowest value of 38% after 6 h of bleaching due to the high removal of lignin. As aforementioned, lignin has a broad range of temperature for its decomposition, and therefore, most of the residual weight at the maximum decomposition temperature reflects the amount of lignin present in the samples.

Table 5.2. Decomposition characteristics of untreated, PAE treated (180 °C, 50 bar, 20% ethanol, 5 mL/min for 40 min) and bleached (2, 4 and 6 h reaction time) fibers.

Fiber type	T_{ON} (°C)	T_{MAX} (°C)	MT_{MAX} (%)
Untreated	214	326	54
PAE	269	369	43
B (2 h)	270	364	42
B (4 h)	277	362	40
B (6 h)	279	362	38

T_{ON} = onset temperature, T_{MAX} = maximum decomposition temperature and MT_{MAX} = residual weight at T_{MAX} .

Fig. 5.4 shows the color and the morphology of untreated and treated canola straw fibers. During PAE treatment the lignin was not removed due to its re-condensation, which provided the brown color to the PAE treated fiber (Fig. 5.4). After bleaching treatments, the PAE fiber color significantly changed from dark brown to yellow/white. A single bleaching treatment (2 h) had a limited effect on the brightness of the PAE fiber, leaving a yellow colored treated fiber. The yellowing tendency of cellulose fibers upon heating is associated with the production of chromophores from monomeric sugar acids produced by the partial oxidation and degradation of unstable hemicelluloses (Beyer et al., 2005). However, with increased bleaching process time of up to 6 h, the brightness of cellulose fiber was improved (Fig. 5.4). According to Dence & Reeve (1996), the multi-stage application of bleaching chemicals associated with inter-stage washing can remove the dissolved impurities, extending the efficiency of bleaching and providing an increased brightness to the isolated cellulose fiber. Besides the difference in color, a significant change in the internal structure was also observed after bleaching treatments (Fig. 5.4).

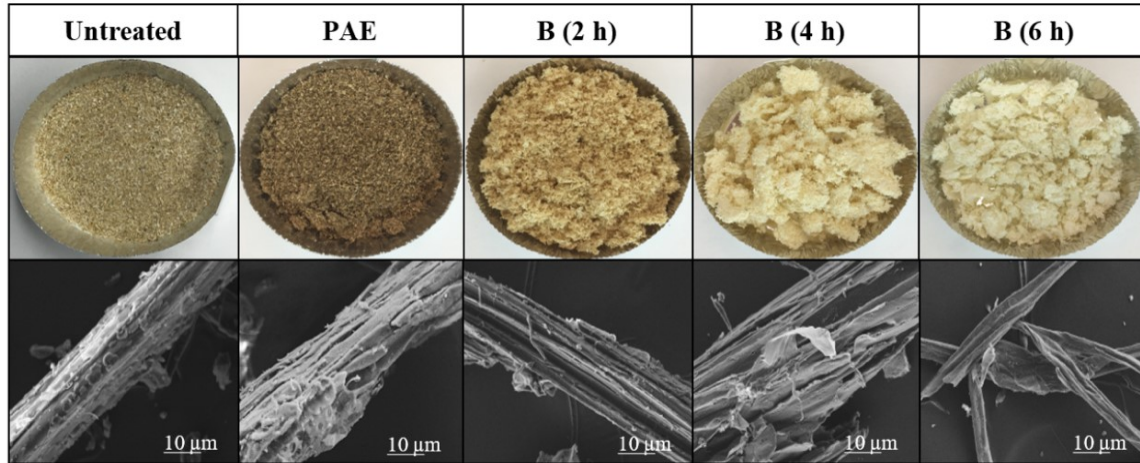


Fig. 5.4. Solid material, scanning electron microscopy (SEM) images of untreated canola straw fiber and PAE treated fiber (180 °C, 50 bar, 20% (v/v) ethanol, 5 mL/min for 40 min) before and after bleaching (2, 4 and 6 h reaction time) treatment.

Scanning electron microscope (SEM) was used to investigate the morphology of untreated and treated fibers (Fig. 5.4). Untreated canola straw had an intact fiber structure with no holes or cracks and a clear deposition of materials on its surface. After PAE treatment, the fiber diameter did not change but it had a rough surface, where the outer layer was partially stripped, probably due to the removal of the primary fiber wall and surrounding materials like hemicelluloses. Bleaching treatment reduced the remaining non-cellulosic compounds and uncover the structure of cellulose fibrils. Within 2 h of bleaching treatment, the cell walls of canola straw fiber were further disintegrated, exposing its internal structure. However, only after 4 h bleaching, the change in the size of the treated fibers was apparent. At the end of 6 h bleaching, the PAE fiber broke into smaller units with smoother surfaces. Cellulose fibers with significant lignin content are stiff and tend to retain their cylindrical shape; however, after the delignification process, cellulose fibers had lower degree of interfibrillar bonding and started to break apart from each other, increasing its surface area (Dence & Reeve, 1996).

5.3.2. Nanofiber production via high-intensity ultrasound

Single effect of the ultrasonic TSE (kJ/g) and residual lignin (%) and their interaction on the nanofibrillation process of cellulosic material were evaluated to understand the interactions between the ultrasonic TSE and lignin content on the swelling capacity (WRV), fibrillation yield (nanofibril content), and surface charge density (ζ potential) of the obtained nanofibers (Fig. 5.5 and Table 5.3). The ultrasonic TSE (4-20 kJ/g), residual lignin (8.0-20.0%), and their interaction significantly ($p < 0.0001$) affected the WRV of the nanofibers (Fig. 5.5a and d, and Table C.1 in Appendix C). When comparing unbleached and bleached nanofibers separately, the effect of ultrasonic TSE was statistically significant for both groups of samples. For LCNF, increasing ultrasonic TSE from 4 to 20 kJ/g, resulted in a significant ($p = 0.002$) increase of the WRV from 0.9 ± 0.1 to 1.9 ± 0.1 g/g (Table 5.3). For the bleached CNF samples, the single effect of ultrasonic TSE and residual lignin and their interaction were also significant ($p < 0.0001$) for the WRV response (Fig. 5.5c and Table 5.3). The decrease in residual lignin content from 18.2 to 8.0% of the bleached CNF obtained at ultrasonic TSE of 20 kJ/g, drastically increased the WRV from 33.8 ± 0.9 to 81.9 ± 1.1 g/g.

As lignin is a swelling restraining component, the bleaching treatment led to a reduction in the hydrophobicity of the fibers, which allowed an increased WRV of the CNF compared to LCNF. Also, during the bleaching treatment, the ClO_2 reacts with the aldehyde groups of reducing end units of lignin, oxidizing them to carboxyl groups, which led to a reduction in the hydrophobicity of any residual lignin remaining in the sample (Acharjee et al., 2017). Furthermore, since lignin fills the voids between carbohydrates during cell wall formation, removing the surrounding lignin provided a substantial increase

in the porosity and surface area of the fibers, which then induced higher percent ratio of water entrapped within the CNF network compared to LCNF. Therefore, the high WRV is intrinsically related to the fibrillation yield.

Table 5.3. Water retention value (WRV), nanofibril content and zeta (ζ) potential values of LCNF and CNF (1 wt.%) obtained using ultrasound at theoretical specific energy (TSE) of 4-20 kJ/g.

Nanofiber	TSE (kJ/g)	WRV (g/g)	Nanofibril content (wt.%)	ζ potential (mV)
LCNF (PAE)	4	0.9±0.1 ^l	32.8±0.5 ^l	-20.2±3.9 ^a
	8	1.5±0.1 ^l	33.4±0.8 ^{ij}	-23.5±1.6 ^{ab}
	12	1.7±0.1 ^l	34.2±0.1 ^{hij}	-24.0±0.8 ^{ab}
	16	1.8±0.1 ^l	34.9±0.1 ^{ghij}	-24.6±1.2 ^{abc}
	20	1.9±0.1 ^l	35.5±1.3 ^{ghij}	-25.5±0.6 ^{abcd}
CNF (B2 h)	4	17.1±1.2 ^k	36.5±2.0 ^{fghi}	-30.1±5.1 ^{bcde}
	8	22.2±1.2 ^j	37.0±0.1 ^{fgh}	-32.6±4.1 ^{bcde}
	12	29.0±1.1 ⁱ	37.6±0.3 ^{fgh}	-32.2±2.3 ^{bcde}
	16	28.6±0.8 ⁱ	38.2±0.8 ^{efg}	-32.1±0.5 ^{bcde}
	20	33.8±0.9 ^{gh}	39.6±0.1 ^{def}	-34.4±2.9 ^{de}
CNF (B4 h)	4	30.0±1.3 ^{hi}	37.6±1.1 ^{fgh}	-30.3±1.4 ^{bcde}
	8	37.0±1.2 ^{fg}	39.8±0.5 ^{cdef}	-31.6±2.7 ^{bcde}
	12	40.9±1.3 ^f	41.4±1.0 ^{bcde}	-33.6±0.2 ^{cde}
	16	48.0±1.1 ^e	43.3±0.7 ^{abc}	-32.8±0.7 ^{bcde}
	20	77.0±1.6 ^b	43.7±1.2 ^{ab}	-34.3±2.9 ^{de}
CNF (B6 h)	4	31.7±1.5 ^{hi}	43.1±1.5 ^{abc}	-30.6±0.1 ^{bbcde}
	8	39.0±1.2 ^f	42.0±0.1 ^{bcd}	-33.8±0.5 ^{cde}
	12	54.5±0.7 ^d	42.5±0.2 ^{bcd}	-32.8±4.0 ^{bcde}
	16	64.7±1.8 ^c	44.4±0.2 ^{ab}	-34.9±0.2 ^{de}
	20	81.9±1.1 ^a	46.1±0.7 ^a	-36.4±1.0 ^e

Contents are expressed as mean±standard deviation of at least duplicates. LCNF: lignocellulosic nanofibers obtained from pressurized aqueous ethanol treated fiber; CNF: cellulose nanofibers obtained from bleached (2-6 h) fibers. ^{a-l}Different lowercase letters in the same column indicate significant differences ($p < 0.05$).

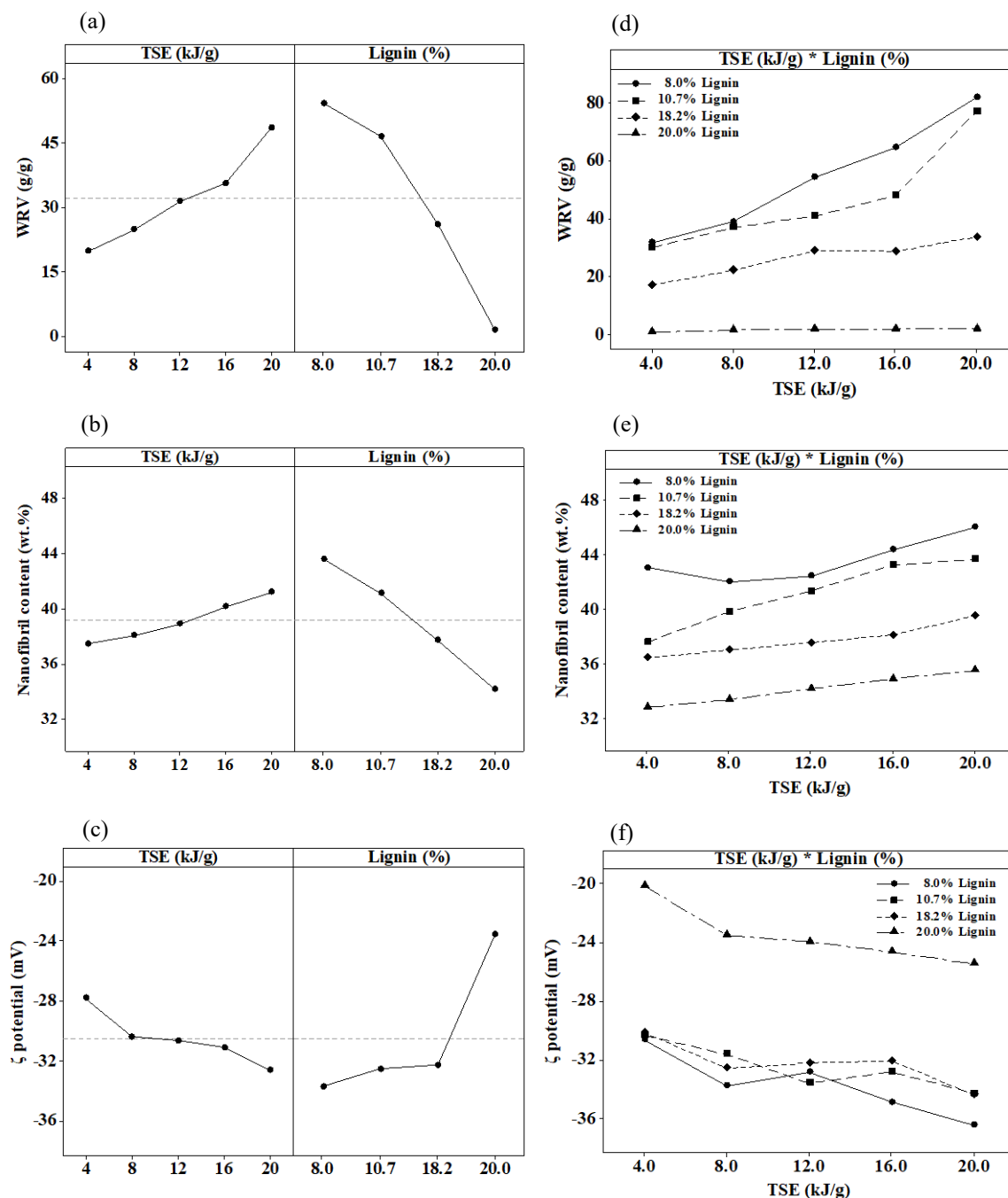


Fig. 5.5. Effect of the theoretical ultrasonic specific energy (TSE) and lignin on: (a) water retention value, WRV, (b) nanofibril content, and (c) zeta (ζ) potential, and the effect of interaction between ultrasonic TSE and lignin on: (d) WRV, (e) nanofibril content, and (f) ζ potential. Dotted lines represent the mean values.

To calculate the fibrillation yield, the centrifugation method reported by Bai et al. (2009) was used and the results are shown as nanofibril content in Table 5.3 and Fig. 5.5. The single effect of ultrasonic TSE (4-20 kJ/g) and residual lignin (8.0-20.0%) significantly influenced the nanofibril content ($p < 0.0001$), whereas their interaction did not affect the results ($p = 0.084$) (Table C.2 in Appendix C). With the intensification of ultrasonic TSE, the increased content of nanofibrils is expected since the phenomenon of acoustic cavitation is strengthened. However, at the same ultrasonic TSE, the LCNF resulted in less nanofibrils compared to all CNF, confirming that the high residual lignin delays the nanofibrillation process. In the study of Sánchez et al. (2016), the residual lignin from organosolv treated wheat straw (13% lignin) also reduced the fibrillation yield compared to Kraft pulped straw (6% lignin) using a high-pressure homogenizer with 4 passes at 300 bar, 3 passes at 600 bar and 3 passes at 900 bar. The organosolv and Kraft treated nanofibers had fibrillation yields of 11.2 and 20.0 wt.%, respectively, which were lower than those obtained in the present study (> 32 wt.%) (Sánchez et al., 2016).

Similarly, Jiang et al. (2019) recently compared the fibrillation yield of LCNF (16% lignin) obtained after organosolv treatment of sugarcane bagasse, and CNF (2% lignin) obtained after organosolv treatment, followed by bleaching process and grinding (gap of 100 μm for 1, 3 and 7 h). Up to 3 h of grinding, the fibrillation yield of LCNF and CNF reached a maximum of 22.6 wt.% and 41.1 wt.%, respectively, which were lower than those obtained in the present study (36.0 wt.% for LCNF and 46.1 wt.% for CNF 6 h), but higher than the values (11.2 and 20.2 wt.%) obtained by Sánchez et al. (2016). Longer grinding treatment of 7 h increased the fibrillation yield of LCNF up to 50.7 wt.%, which were higher than the present study for LCNF (36.0 wt.%) (Jiang et al., 2019). Although the

authors reported an increased fibrillation yield for LCNF, it was not significantly different from the fibrillation yield of CNF (45.7 wt.%) obtained at 7 h (Jiang et al., 2019). This long mechanical processing time required by Jiang et al. (2019) to increase the fibrillation yield of LCNF by only 9% remains a challenge that hinders the progress of nanocellulose field. In comparison, the HIUS treatment proposed herein successfully disintegrated LCNF and CNF within less than 9 min, but further scale up studies of the HIUS process is still needed. Since in the present study and on the studies of Sánchez et al. (2016) and Jiang et al. (2019) where a similar aqueous ethanol pre-treatment was used, the differences on the reported fibrillation yield were mainly due to the different mechanical processes applied (HIUS, high-pressure homogenizer, and grinding).

Recently, Espinosa et al. (2019) compared different mechanical approaches to disintegrate soda pulped wheat straw with 9% residual lignin. When the pulped straw was nanofibrillated using a high-pressure homogenizer (4 passes at 300 bar, 3 passes at 600 bar and 3 passes at 900 bar), it had a fibrillation yield of 56 wt.%; however, when it was nanofibrillated using a grinder (700 g for 2.5 h and a gap of -10 μm), it had a significantly lower fibrillation yield of 36 wt.%. However, the authors studied one variable of residual lignin at a time (same treated straw was fibrillated by different mechanical approaches). Further studies using different mechanical approaches such as HIUS, high-pressure homogenizer, grinding, and others, associated to different chemical composition of the initial fiber can bring more insights about the fibrillation yield of both LCNF and CNF.

To further characterize the nanofibril dispersions, the surface charge density of the nanoparticles was measured via ζ potential. The ζ potential values were significantly affected by the single effect of ultrasonic TSE (4-20 kJ/g) ($p = 0.014$) and residual lignin

(8.0-20.0%) ($p < 0.0001$), but the interaction of the variables did not have an effect ($p = 0.999$) (Table C.3 in Appendix C). As the delignification process increased the surface area of the nanofibers, an increased exposure of the -OH groups on the surface of bleached samples raised the ζ potential of CNF in comparison to LCNF. Furthermore, analyzing only the LCNF, the single effect of ultrasonic TSE (4-20 kJ/g) was not significant ($p = 0.223$) for the ζ potential values. For the CNF group, the model could not be adjusted ($p = 0.482$) to study the effects of ultrasonic TSE (4-20 kJ/g), residual lignin (8.0-18.2%), and their interactions on ζ potential responses, because the data do not fit a specific equation. The similarities on surface charge density of all CNF are due to the mild bleaching process used, whereas the added sodium chlorite was used only to oxidize of lignin, and not cellulose.

The ζ potential provided the magnitude of surface charge and described the stability of the colloidal dispersion. Nanofiber dispersion with a high ζ potential is electrically stable, whereas when the potential is low, the attraction of nanofibers exceeds repulsion and they tend to aggregate. This effect can be seen in Fig. 5.6, where the CNF with higher ζ potential had higher stability in comparison to LCNF and could self-assemble into a 3D matrix (hydrogel). Fig. 5.6 also shows the single effect of residual lignin on the nanofibrillation process and the diameter size distribution of the obtained nanofibers.

Using HIUS at a TSE of 20 kJ/g, the PAE treated fiber was nanofibrillated into LCNF with an average diameter of 21 nm, whereas the bleached (6 h) cellulose fiber was extensively nanofibrillated into CNF, having an average diameter of 14 nm. Although the LCNF had diameters in the nanoscale range, some fibril bundles were still present in relatively high amounts (Fig. 5.6 and Table C.7 in Appendix C). The recalcitrance, a

resistance to deconstruction, of the LCNF was due to the complex formed between cellulose and lignin, which created a stiff phase between cellulosic fibers, reducing the acoustic cavitation effects. A better nanofibrillation of bleached fibers compared to unbleached fibers was also observed by Nair and Yan (2015), who studied the effect of high (21%) and low (5%) lignin content on nanofibrillation of pine bark cellulose fibers using grinding at 252 g for 1-15 passes. Using a mechanical treatment with 5 passes, the high lignin cellulose fibers were reduced to sub-micron fibrils, ranging from 150 to 700 nm, whereas within 15 passes, the diameter was reduced to < 100 nm. In comparison, low lignin cellulose fibers were deconstructed within 5 passes into fibrils ranging from 80 to 150 nm, and after 15 passes the nanofibers were homogeneously distributed with diameters < 50 nm.

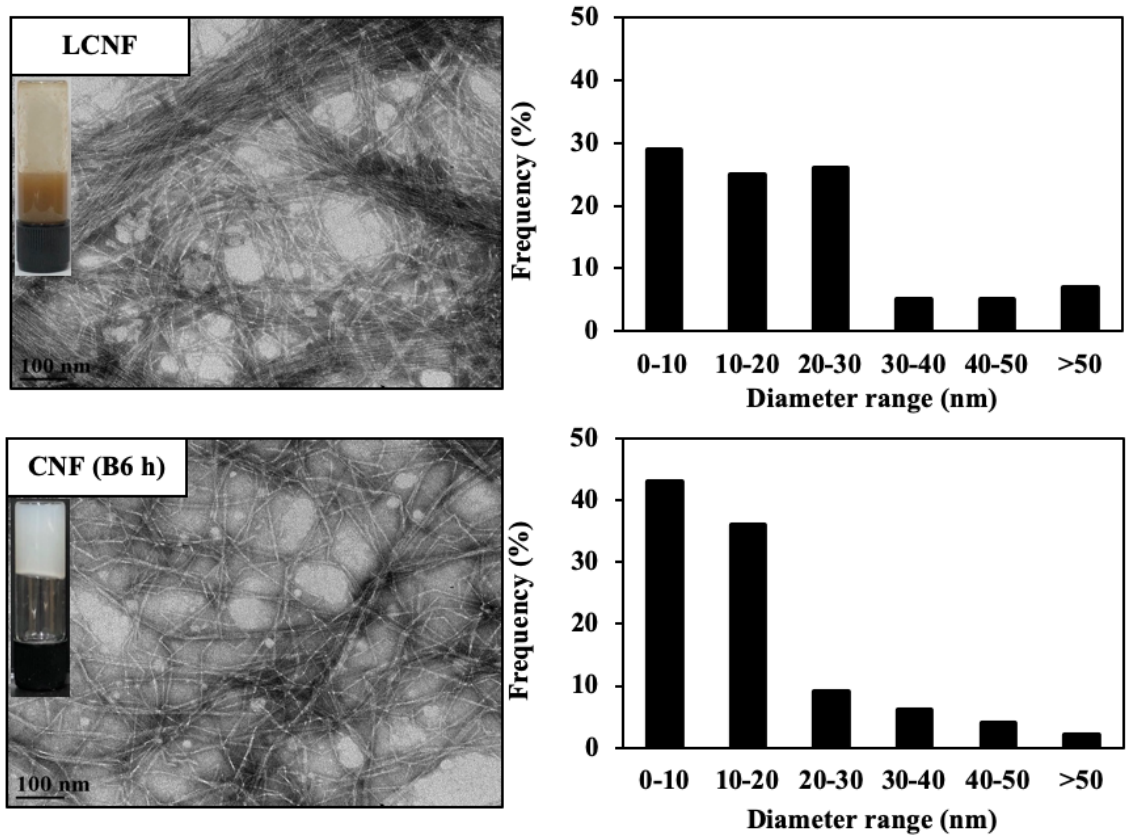


Fig. 5.6. Transmission electron microscopy (TEM) images and size distribution of 1 wt.% LCNF and CNF (B6 h) obtained using ultrasound at TSE of 20 kJ/g.

In a recent study, Liu et al. (2019) nanofibrillated treated reed straw with residual lignin contents from 7-15% using HIUS processing at 450 W for 2 h. First, the reed straw was treated using ball-milling assisted or not by NaOH (0-7 wt.%) for 2 h, followed by the HIUS nanofibrillation. The ball milled reed straw using 0, 1, 4, and 7 wt.% NaOH had lignin contents of 15, 14, 10, and 7%, respectively. The increase on lignin contents from 7 to 10, and to 14% resulted in a decrease on the average nanofiber diameter from 13 to 10, and to 6 nm, respectively. However, nanofibers with a slightly higher lignin content of 15% (0% NaOH during ball milling processing) had an average nanofiber diameter of 150 nm, which is bigger than the NaOH treated samples. Since the difference on lignin content was only 1% between ball milled reed straw with 0% NaOH (15% lignin) and ball milled reed straw with 1 wt.% NaOH (14% lignin), the impact on average nanofiber diameter is mainly attributed to the ball milling processing instead of lignin content. Besides the ball milling reduced the size of the reed straw, which facilitated the mechanical nanofibrillation, the mild alkaline solvent induced the breakage of ferulic acid linkages between the lignin and hemicellulose fractions, weakening the structural integrity of the lignocellulosic biomass (Buranov & Mazza, 2008). The weakening of the fiber structure associated with the swollen effect of an alkali treatment, led to an increased surface area, facilitating the HIUS nanofibrillation process.

Due to the controversies in the literature, further studies comparing pre-treated fibers with same lignin content but obtained by different pre-treatment approach followed by the same mechanical disintegration should be conducted for an in-depth discussion of the effects of lignin on the production of nanofibers. Furthermore, the nanofibrillation of a

pre-treated fiber using different mechanical approach can also help to understand the effects of a specific mechanical disintegration during the production of nanofibers.

5.4. Conclusions

The production of nanofibers from canola straw using combined technologies of pressurized fluids and ultrasound processing was investigated, where the impact of residual lignin during the production of nanofibers was elucidated. Within 40 min, more than 60% of the initial hemicellulose were removed from canola straw using PAE treatment. Besides the PAE treatment being effective, it is an environmentally friendly process as it only uses water and ethanol as solvent, without producing a chemical stream and the further need for neutralization steps. The use of a bleaching step prior to HIUS increased brightness of the sample, porosity, and surface area of the fiber, which facilitated the mechanical nanofibrillation process. HIUS as a mechanical treatment is an emerging method compared with traditional grinding and high pressure homogenization; however, it has not been fully studied for nanofibrillated cellulose materials with different chemical compositions. In this study, the ultrasonic TSE of 20 kJ/g was able to produce CNF with a fibrillation yield of 46 wt.% and swelling capacity to retain more than 80 g of water per g of sample, which is ideal for biomedical hydrogel and adsorbent product applications. Moreover, the obtained CNF had a homogeneous diameter size distribution with an average diameter of 14 nm, whereas LCNF had an average diameter of 21 nm with increased fiber bundles formation. Overall, the nanofibrillation process using HIUS was intrinsically dependent on the cellulose fiber composition and the severity of ultrasonic TSE.

Chapter 6. High-intensity ultrasound-assisted formation of cellulose nanofiber scaffold with low and high lignin content and their cytocompatibility with gingival fibroblast cells*

6.1. Introduction

Canola is one of the most important oilseed crops in Canada and worldwide. After harvesting the seeds, canola generates large quantities of straw that has been used as biorefinery feedstock to obtain fermentable sugars (López-Linares et al., 2013). The isolation of cellulose nanofibers (CNF) from agricultural biomass including straw is also gaining increased attention mainly due to their high availability and low cost (Tovar-Carillo et al., 2014; Nakasone & Kobayashi, 2016; Ciftci et al., 2017; Espinosa et al., 2017; Jiang et al., 2018). CNF is characterized by a three-dimensional (3D) network of fibrils with diameter in nanoscale (< 100 nm) and length of several microns that have unique properties such as biodegradability, high specific strength and stiffness, high aspect ratio and surface area and light weight.

Particularly, CNF hydrogels and aerogels create remarkable scaffolds for cell culture due to their outstanding mechanical stability, cytocompatibility, controllable nanomorphology and high porosity (Du et al., 2019). Overall, CNF scaffolds showed non-cytotoxicity *in vitro* and biocompatibility *in vivo* (Hickey et al., 2018; Rashad et al., 2019; Zhang et al., 2019). Furthermore, CNF scaffolds overcome the poor stability and mechanical properties of other natural polymers such as chitosan and alginate, and overcome the potential immunogenicity and disease transmission concerns by using

*A version of this chapter was published as Huerta, R.R., Silva E.K., Ekaette, I., El-Bialy, T., and Saldaña, M.D.A. (2019). High-intensity ultrasound-assisted formation of cellulose nanofiber scaffold with low and high lignin content and their cytocompatibility with gingival fibroblast cells. *Ultrasonics Sonochemistry*. <https://doi.org/10.1016/j.ultsonch.2019.104759>.

synthetic and animal derived polymeric matrices (Aamodt & Grainger, 2016; Turnbull et al., 2018).

CNF have been commonly prepared by mechanical nanofibrillation via grinding, high pressure homogenization and microfluidization, as discussed in Chapter 2. Meanwhile, the use of high-intensity ultrasound (HIUS) processing, a clean and emerging technology, has shown high performance on the nanofibrillation process of cellulosic materials such as lupin hull and wood, due to the acoustic cavitation phenomenon (Chen et al., 2011b; Ciftci et al., 2017). This phenomenon occurs due to the application of low-frequency (20-100 kHz) and high-power ultrasound in a liquid medium, promoting the formation and subsequent collapse of microbubbles associated with extreme levels of highly localized turbulence and shear stress (Chemat et al., 2017), which promotes the nanofibrillation.

Although the recent production of CNF from agricultural biomass containing residual non-cellulosic materials like lignin and without surface modification have attracted attention due to the low cost of the starting material and simple procedure (Tovar-Carillo et al., 2014; Nakasone & Kobayashi, 2016; Espinosa et al., 2017), only few researchers have studied the cytocompatibility of cellulose with residual lignin ad scaffold for cell culture (Tovar-Carillo et al., 2014; Nakasone & Kobayashi, 2016). Earlier, Nakasone and Kobayashi (2016) evaluated the cytocompatibility of cellulose hydrogel films with residual lignin of 0.6-1.6% obtained from sugarcane bagasse. After 3 days, mouse fibroblast cell density reached 4×10^4 cell/cm² for cellulose hydrogels with 0.6% lignin and 6×10^4 cell/cm² for cellulose hydrogels containing 1.6% lignin. However, the amount of lignin is still considerably low, and impartial to conclude its real cytocompatibility. In another study,

Quraishi et al. (2015) tested the cytocompatibility of lignin (isolated from wheat straw) in alginate-based aerogel composite as scaffold for mouse fibroblast cells. Aerogels with 2:1 (w/w) alginate-to-lignin ratio showed no cytotoxicity and promoted satisfactory cells adhesion and viability over 7 days compared to control (tissue culture polystyrene plate). However, the cellulose fiber was not used in this case.

Although lignin from agricultural biomass has been shown to be non-cytotoxic, there is scarce literature using CNF with high lignin content for *in vitro* tests. Therefore, the aim of this study was to evaluate the HIUS-assisted formation of CNF scaffolds containing low (8%) and high (18%) residual lignin contents and test their cytocompatibility with gingival fibroblast cells for periodontal therapy. In regenerative periodontal therapy, a major challenge is reconstruction of morphology and function of gingival tissues (Koopae et al., 2019). To obtain the CNF scaffold, bleached cellulose fibers with different lignin contents were first nanofibrillated using HIUS at 240, 720 and 1200 W to obtain hydrogels, and further freeze-dried to form aerogel scaffolds. The CNF suspensions and hydrogels were characterized for morphology, water retention value, surface charge density, fibrillation yield, and viscoelastic properties. The aerogels were characterized for porosity, swelling capacity, morphology, and cytocompatibility.

6.2. Materials and methods

All solvents and reagents used in this study were analytical grade. Sodium chlorite, acetic acid, and formaldehyde solution (36.5-38%) were purchased from Sigma Aldrich (Oakville, ON, Canada) and used without further purification. Dulbecco's Modified Eagle's Medium (DMEM), fetal bovine serum (FBS), penicillin-streptomycin, trypsin, and phosphate buffer solution (PBS, pH 7.4) were obtained from Fischer Scientific (Waltham, MA, USA).

AlamarBlue® cell proliferation assay was purchased from Bio-Rad (Bio-Rad, Hercules, CA, USA).

6.2.1. Cellulose fiber isolation

Bleached canola straw cellulose fibers were obtained according to the method previously described in Chapter 5 (Section 5.2.2). Low lignin (LL) cellulose fiber was obtained after 6 h of bleaching, while high lignin (HL) cellulose fiber was obtained after 2 h of bleaching treatment.

6.2.2. HIUS-assisted production of cellulose nanofiber scaffolds

The LL-CNF and HL-CNF suspensions/hydrogels were obtained by mechanical disintegration of cellulose fibers using the HIUS equipment (Model FS-1200N, Shanghai Sonxi Ultrasonic Instrument Co., Shanghai, ZJ, China) as described in Chapter 4 (Section 4.2.2.1). The sonication was performed at nominal power levels of 240, 720 and 1200 W for around 8 min, and the acoustical power was obtained according to the calorimetric assay using the Eq. (2.3) (Mason et al., 1994), described in Chapter 2 (Section 2.3.2.1.1).

The HIUS efficiency and intensity were calculated according to Eq. (6.1) and (6.2), respectively (Gogate et al., 2001), using the same nominal power as before (240, 720 and 1200 W).

$$\text{HIUS efficiency (\%)} = \left(\frac{\text{Acoustical power (W)}}{\text{Nominal power (W)}} \right) \times 100 \quad (6.1)$$

$$\text{HIUS intensity (W/cm}^2\text{)} = \left(\frac{4 \text{ Acoustical power (W)}}{\pi D^2} \right) \quad (6.2)$$

where, D (cm) is the probe diameter.

Then, the HL-CNF and LL-CNF (1-2 wt.%) hydrogels (10 g) were placed in cylindrical tubes (8 cm height and 1.6 cm diameter) to create the scaffold monoliths, frozen

overnight at -18 °C, and dried at -45 °C, 15 Pa for 3 days using a freeze dryer (FreeZone, Labco Corp., Kansas, MO, USA).

6.2.3. Cell culture and seeding

Gingival fibroblast cells were obtained from healthy donors. The protocol of obtaining these cells was approved by the University of Alberta Human Ethics Committee (protocol # MS6_Pro00056111) and used for the *in vitro* culture on HL-CNF and LL-CNF aerogel scaffolds. The cells at passage 3 were grown in culture flasks (T-75 cm²) containing Dulbecco's Modified Eagle Medium (DMEM) supplemented with 10% (v/v) fetal bovine serum (FBS), and 5% (v/v) penicillin-streptomycin, and incubated at 37 °C under 5% CO₂ and saturated water atmosphere. After the cells achieved approximately 90% of confluence, the cells were harvested via trypsinization. The number of viable cells in suspension was estimated by counting in the Bio-Rad TC20™ automated cell counter (Bio-Rad, Hercules, CA, USA).

The HL-CNF and LL-CNF scaffolds (10 mm height and 18 mm diameter) were placed in 24-well culture plates and sterilized using ethanol solutions from 10 to 70% (v/v) (Esparza, 2017). Briefly, the scaffolds were soaked with 1.5 mL of 10% (v/v) ethanol solution for 30 min, and gradually increased up to 70% (v/v) ethanol at a rate of 20% (v/v) ethanol concentration increase every 30 min. Then, the scaffolds were reverse washed from 70 to 10% (v/v) ethanol at the same rate and time described above. Finally, the sterile scaffolds were washed with sterile Hanks' Balanced Salt Solution (HBSS) at pH 7.4 for three times (30 min each). The control (glass cover slips) was sterilized with 70% (v/v) ethanol for 30 min (Esparza, 2017). Then, the scaffolds and control were soaked in 600 µL DMEM and incubated overnight at 37 °C under 5% CO₂ and water saturated atmosphere.

Quadruplicate of each scaffold and triplicate of the control were seeded with 50 μL gingival fibroblast cells suspension (1.6×10^6 cells/mL) with a micropipette on the center of the scaffolds and incubated for 24 h. The media was replaced every other day up to 11 days.

6.2.4. Cellulose nanofiber suspensions characterization

The water retention value (WRV), zeta (ζ) potential, fibrillation yield (nanofibril content determination) and morphology of HL-CNF and LL-CNF (1 wt.%) suspensions were determined according to methods described in Chapter 4 (Section 4.2.2.3).

The viscoelastic behaviors of HL-CNF and LL-CNF (1-2 wt.%) hydrogels were studied using a rotational rheometer (Physica MCR 302, Anton Paar, Ashland, VA, USA). Strain sweep test was performed to determine the linear viscoelastic region within a strain range from 0.01 to 1000% at an angular frequency of 6.28 rad/s (1 Hz). Angular frequency sweep measurements were conducted in a frequency range of 1-100 rad/s at 1.0% strain. Data were analyzed using the RheoPlus software, and the results are reported for storage modulus (G'), loss modulus (G''), and complex viscosity (η^*).

6.2.5. Cellulose nanofiber scaffolds characterization and cytocompatibility test

The mass of the HL-CNF and LL-CNF aerogels was determined using a sensitive electronic balance (ME104, Mettler-Toledo, Columbus, OH, USA) with a precision of 0.1 mg and the final dimensions were measured using a caliper with a precision of 0.05 mm. Then, the bulk density (d_a) values were obtained by calculating the ratio of the mass to the volume and the final internal porosity of the aerogels was calculated using to Eq. (6.3), where the density of CNF (d_n) is equal to 1.6 g/cm³ (Chen et al., 2011b):

$$\text{Porosity (\%)} = \left(1 - \frac{d_a}{d_n}\right) \times 100 \quad (6.3)$$

The swelling capacity of the HL-CNF and LL-CNF aerogels was determined by immersion in a phosphate buffer solution (PBS, pH 7.4) at 25 °C for 24 h (Esparza, 2017). After the immersion time, the excess of PBS was removed gently with filter paper and the swollen scaffold was weighed. The swelling capacity (g/g) was calculated by the mass difference of dry and swollen scaffold.

Cross sections of CNF aerogels were carbon coated using Nanotek SEMprep 2 sputter coater (Nanotech, Manchester, UK) for scanning electron microscopy (SEM) analysis. Samples were scanned at an accelerating voltage of 5 kV using a Zeiss Sigma 300 VP-FESEM equipment (Carl Zeiss AG, Oberkochen, BW, Germany).

The cell growth was quantified after 1, 3, 7 and 11 days of incubation using the alamarBlue® cell proliferation assay (Bio-Rad, Hercules, CA, USA). The assay incorporates a reduction-oxidation (REDOX) indicator that both fluoresces and undergoes colorimetric change in response to cellular metabolic reduction. The amount of fluorescence produced is proportional to the number of living cells. Briefly, the seeded scaffolds were cultured with 10% (v/v) alamarBlue reagent and incubated at 37 °C with 5% CO₂ for 4 h. Then, the fluorescence of the reduced media containing alamarBlue was measured at 560 nm excitation wavelength and 590 nm emission wavelength and the alamarBlue Fluorometric calculator (<https://www.bio-rad-antibodies.com/colorimetric-calculator-fluorometric-alarBlue.html#>) was used to measure cell respiration as an indicator for proliferation and cytotoxicity.

After 11 days of cell culture, the scaffolds were fixed with 4% (v/v) formaldehyde in PBS solution at 25 °C for 24 h for cell imaging. Briefly, the scaffolds were dehydrated gradually in ethanol/water and embedded in paraffin. A cross section (~7 µm) located at 1

mm depth from the surface was mounted on glass slides, stained with hematoxylin and eosin, and images were taken using a brightfield microscope (Zeiss Primo Vert, Carl Zeiss AG, Oberkochen, BW, Germany).

6.2.6. Statistical analysis



All experiments were carried out in duplicate and all values were reported as mean values \pm standard deviation. Analysis of variance (ANOVA) was performed using Minitab 18 Software (Minitab Inc., State College, PA, USA). The significant differences ($p < 0.05$) between the treatments were evaluated using Tukey's honest significance test.

6.3. Results and discussion

6.3.1. Characterization of cellulose nanofiber suspensions

Table 6.1 shows the compositional analysis of the cellulosic fibers used in this study. HL cellulosic fiber had mainly 71% cellulose, 5% hemicellulose and 18% lignin; whereas, the LL cellulosic fiber had mainly 82% cellulose, 4% hemicellulose and 8% lignin. Protein, ash and moisture contents were similar for both cellulosic fibers. Also, the visual appearance of the cellulosic fibers showed that a single bleaching application (2 h) had a limited effect on the fiber brightness, resulting in a yellow color of the HL fiber. However, with increased bleaching process time of up to 6 h and consecutive washings, large amounts of lignin were removed, improving the brightness of the LL fiber.

Table 6.1. Characterization and visual appearance of high lignin (HL) and low lignin (LL) cellulosic fibers obtained after 2 and 6 h of bleaching, respectively.

Fiber characterization (%)	High lignin (HL)	Low lignin (LL)
Cellulose	70.73±1.00	81.92±1.05
Hemicellulose	4.90±1.03	3.68±0.06
Total lignin	18.22±0.18	7.98±0.22
Soluble	1.23±0.08	0.85±0.01
Insoluble	17.00±0.08	7.12±0.22
Ash	1.80±0.07	1.24±0.03
Moisture	2.12±0.13	2.67±0.10
Protein	2.51±0.09	2.44±0.17
Visual appearance		

Contents are expressed as mean±standard deviation based on at least duplicates.

The HIUS treatment was then used to disintegrate the initial cellulosic fibers into LL-CNF and HL-CNF. Table 6.2 summarizes the nominal and acoustical power, HIUS efficiency and intensity, as well as the initial and final process temperatures recorded. The acoustical power dissipated into the system had slight variations upon different CNF used, mainly due to the different specific heat (C_p) of the nanofibers (Fig. D.1 and D.2 in Appendix D). The LL-CNF had C_p of 4.34 J/g°C and during HIUS treatment the acoustical power varied from 26 to 53 W. Meanwhile, HL-CNF had C_p of 4.06 J/g°C, and during HIUS treatment the acoustical power varied from 21 to 51 W (Table 6.2).

Increasing the nominal power from 240 to 1200 W resulted in a decrease in HIUS efficiency from 11 to 4% in the LL-CNF system, and from 9 to 4% in the HL-CNF system (Table 6.2). According to Gogate et al. (2001), the electric power energy (nominal power)

is first converted into mechanical energy, then acoustical energy (acoustical power), and finally into cavitation and heat energies. Therefore, as the HIUS efficiency (%) is the relation between acoustical power and nominal power (Eq. 6.1), the low HIUS efficiency was mainly due to the energy dissipation during the energy conversion stages in the ultrasound open system used.

Table 6.2. Nominal and acoustical power, HIUS efficiency and intensity, and the initial and final temperature recorded during HIUS processing of CNF (1 wt.%) suspensions.

CNF	Nominal power (W)	Temperature recorded (°C)	Acoustical power (W)	HIUS efficiency (%)	HIUS intensity (W/cm ²)
LL	240	21-55	25.86±0.04	10.78±0.03	8.24±0.00
	720	22-90	50.68±0.12	7.04±0.28	16.14±0.01
	1200	21-94	53.36±0.97	4.45±0.08	16.99±0.31
HL	240	20-51	21.35±0.79	8.90±0.60	6.80±0.03
	720	21-84	48.05±0.07	6.67±0.16	15.30±0.01
	1200	20-91	51.05±0.06	4.25±0.25	16.26±0.01

Contents are expressed as mean±standard deviation of duplicates.




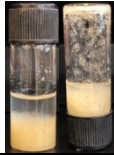


The low efficiency can also be attributed to the acoustic decoupling effect, which changed the acoustic impedance as the power increased, and the coalescence effect, which led to increased number of bubbles around the transducer surface absorbing/scattering the mechanical energy (Gogete et al., 2011). Also, by increasing the nominal power and, consequently, the acoustic streaming, a high turbulence inside the system lowered the cavitation effects (Pokhrel et al., 2016). The HIUS efficiency was also affected by the increased process temperature (Table 6.2). Increasing the nominal power from 240 to 1200 W, resulted in an increase in temperature from 55 to 94 °C on the LL-CNF system, and from 51 to 91 °C on the HL-CNF system, which led to an increased vapour pressure of the

system, reducing the gas content of the bubbles and minimizing the cavitation energy (Mason et al., 1994).

Recently, Mamvura et al. (2018) studied the energy change from electrical to acoustical, and to cavitation, and their efficiency of conversion from one form of energy to another during HIUS treatment. The acoustical energy was calculated as the acoustical power calculated herein, and the cavitation energy was calculated by the difference of calorimetric energy in both cavitating and non-cavitating systems. The conversion efficiency from electrical to acoustical energy decreased from 26 to 25% as the nominal power increased from 38 to 180 W. While, the conversion efficiency from acoustical to cavitation energy decreased from 11 to 7%, with the same nominal power rate increase (Mamvura et al., 2018). The conversion efficiency from electrical to acoustical energy was higher than those observed in the current study (7-17%), due to the lower nominal power used by Mamvura et al. (2018). Although several authors have used HIUS processing to obtain CNF (Chen et al., 2011b; Ciftci et al., 2017), to the best of the author's knowledge, there are no reports on the acoustical power dissipated in the system for an accurate cavitation/efficiency condition.

The effects of applied ultrasonic power on water retention value (WRV), surface charge density (ζ potential) and fibrillation yield of LL-CNF and HL-CNF are shown in Table 6.3.

Table 6.3. Water retention value (WRV), zeta (ζ) potential, fibrillation yield and visual appearance of LL-CNF and HL-CNF (1 wt.%) suspensions treated using HIUS at different nominal and acoustical powers.

	Nominal power (W)	Acoustical power (W)	WRV (g/g)	ζ potential (mV)	Fibrillation yield (wt.%)	Visual appearance
LL-CNF	240	26	31.72±1.51 ^{cd}	-30.6±0.14 ^a	42.36±0.45 ^b	
	720	51	54.45±0.72 ^b	-33.8±2.55 ^a	42.51±0.24 ^{ab}	
	1200	53	81.85±1.06 ^a	-36.40±0.99 ^a	46.07±0.67 ^a	
HL-CNF	240	21	17.08±1.23 ^c	-30.10±5.09 ^a	36.45±2.00 ^c	
	720	48	28.97±1.12 ^d	-32.2±2.26 ^a	37.60±0.35 ^c	
	1200	51	33.77±0.88 ^c	-34.0±0.35 ^a	39.56±0.15 ^{bc}	

HIUS: High-intensity ultrasound; LL-CNF: low lignin cellulose nanofiber; HL-CNF: high lignin cellulose nanofiber. Contents are expressed as mean±standard deviation of duplicates. ^{a-c}

Different lowercase letters in the same column indicate significant differences ($p < 0.05$).

Both the lignin content of CNF and power applied significantly ($p < 0.0001$) affected the WRV of the nanofibers. The maximum WRV obtained with the HL-CNF was 34 g water/g CNF, while the LL-CNF had a WRV of up to 82 g water/g CNF. Since the LL-CNF was bleached for a longer period of time, a major portion of the lignin material

could be oxidized, creating larger void volumes within the cellulose fibers, which increased the surface area and water absorption capacity of those nanofibers. Furthermore, when the cellulose fiber was fragmented into thinner fibrils as a consequence of the increased nominal/acoustical power its surface area was increased, which promoted a greater exposure of the hydroxyl (OH) groups, enhancing the hydrogen bonding with water molecules and improving the WRV capacity of the LL-CNF and HL-CNF.

Besides the WRV, the ζ potential and fibrillation yield were also assessed to evaluate the impact of applied ultrasonic power and lignin content of the CNF during the HIUS process. As the ζ potential measures the magnitude of surface charge of the nanofibers, it can describe the aggregation and dispersion stability of the suspension. However, in the present study, the ζ potential was not affected by the ultrasonic power used ($p = 0.136$) or the lignin content of CNF ($p = 0.386$). According to Sato et al. (2017), the aggregation and dispersion stability of CNF are mainly affected by the solution chemistry and surface modification. Because the use of any additional chemicals was avoided for surface modification and all CNF were dispersed in water in this study, they had similar ζ potential values, ranging between -30 and -36 mV.

The applied ultrasonic power ($p = 0.027$) and the lignin content of CNF ($p < 0.0001$) significantly affected the fibrillation yield. Increasing the ultrasonic acoustical power from 21-26 to 51-53 W increased the fibrillation yield of LL-CNF from 42 to 46 wt.% due to the increased cavitation phenomenon; but it had no statistical difference on the fibrillation yield of HL-CNF that ranged from 36 to 40 wt.%. Although the fibrillation yield showed only a small increase or no increase at all as the HIUS power increased from 21-26 to 51-53 W, the method used to calculate the fibrillation yield was based on the separation of small

fibrils to non-complete fibrillated fibers via the centrifugation approach, which presents some limitations. During the procedure, the centrifugation forces can induce an aggregation of the nanofibers into bundles, which will be further sedimented and not accounted as the nanofibril content on the supernatant fraction. Previous studies also reported a maximum fibrillation yield of CNF between 40-46 wt.% when similar centrifugation approach was used to calculate the fibrillation yield (Wang et al., 2012, Jiang et al., 2018).

Table 6.3 also shows the visual appearance of the CNF solution, which represents a qualitative analysis of the nanofibrillation process using the HIUS technology. Independent of the lignin content, the HIUS process at acoustical power of 21-26 W resulted in a heterogeneous solution due to the incomplete nanofibrillation achieved at this level of cavitation. A further increase on the acoustical power to 51-53 W resulted in well dispersed and highly nanofibrillated fibers that self-assembled as hydrogel structures.

Further, the TEM images confirm that independent of the lignin content, the HIUS treatment at acoustical power of 51-53 W successfully nanofibrillated the initial cellulosic material, producing an entangled micro/nanofibrillated network (Fig. 6.1). According to Wang et al. (2012), the nanofibrillation of cellulose starts by breaking down a “backbone” micron size structural fibril, which is highly compact and present a large diameter, into submicron and then nanoscale fibrils. The presence of “backbone” structural fibrils can still be observed in both samples, but more “backbone” fibrils were noticed in the HL-CNF hydrogels, indicating a lower nanofibrillation of this sample compared to LL-CNF. The recalcitrant property of the HL-CNF during nanofibrillation is due to the stiff complex formed between cellulose and lignin, which required a long mechanical treatment to be disintegrated.

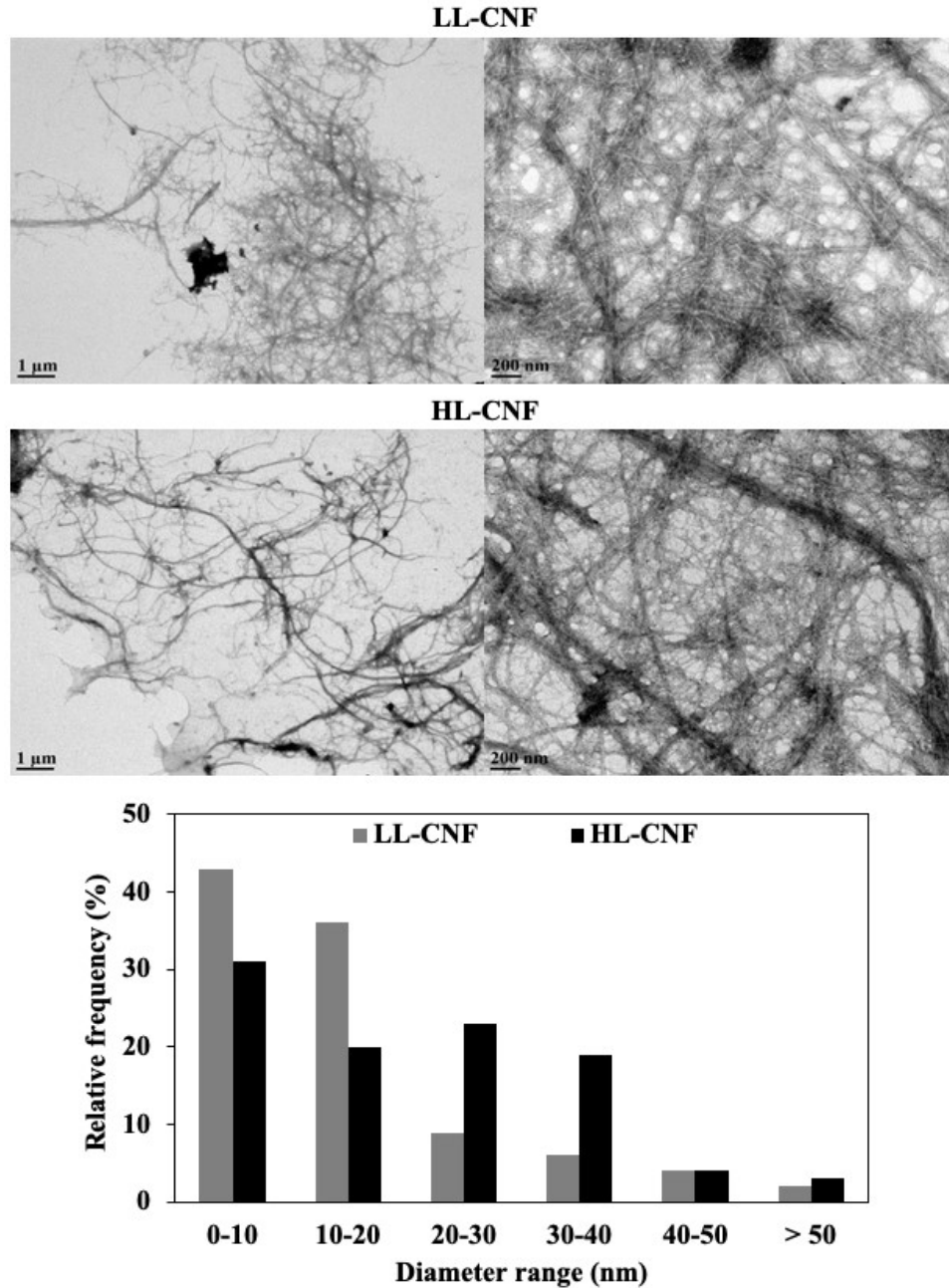


Fig. 6.1. Transmission electron microscopy (TEM) images and diameter size distribution of 1 wt.% LL-CNF and HL-CNF obtained using HIUS at acoustical powers of 53 and 51 W, respectively.

The higher level of nanofibrillation of LL-CNF was further confirmed by the size distribution calculated using the TEM images. For each type of CNF studied, the obtained nanofiber diameters were segregated into groups of diameter ranges between 0-10, 10-20, 20-30, 30-40 and > 50 nm, wherein their relative frequency is plotted in Fig. 6.1. The HL-CNF hydrogel had nanofibers with diameters of 20-30 nm in a relative frequency of 23% and nanofiber bundles (> 50 nm) in a low relative frequency of 3%, accounting for an average diameter of 18 nm. In comparison, the LL-CNF hydrogel had an average diameter of 14 nm, due to the small diameter of the nanofibers (43% of the nanofibers had diameter of < 10 nm) (Table D.1 in Appendix D). These results confirm that the higher WRV and fibrillation yield obtained by the LL-CNF compared to the HL-CNF was due to the higher aspect ratio and surface area of the LL-CNF.

The viscoelastic properties of the HL-CNF and LL-CNF hydrogels (1-2 wt.%) obtained using HIUS processing at acoustical power of 51 and 53 W, respectively, were first described by the elastic (storage) modulus G' , which is the reversible stored energy, and viscous (loss) modulus G'' , which is the irreversible energy loss of the gel system (Fig. 6.2). The strain sweep test is a rheological experiment where the variation of elastic modulus (G') and viscous modulus (G'') were monitored with the applied shear strain (γ) (0.01-1000%) at a constant angular frequency (ω) of 6.28 rad/s. The strain sweeps were executed to determine the linear viscoelastic region (LVR) and the onset of non-linearity, also known as critical strain % (γ_c). The LVR indicates the strain domains where the elastic structure of CNF hydrogels remains stable, and above the γ_c , the elastic CNF network is destroyed. According to Fig. 6.2a and c, for strain less than 1%, all the CNF hydrogels had G' basically independent of the applied strain (LVR).

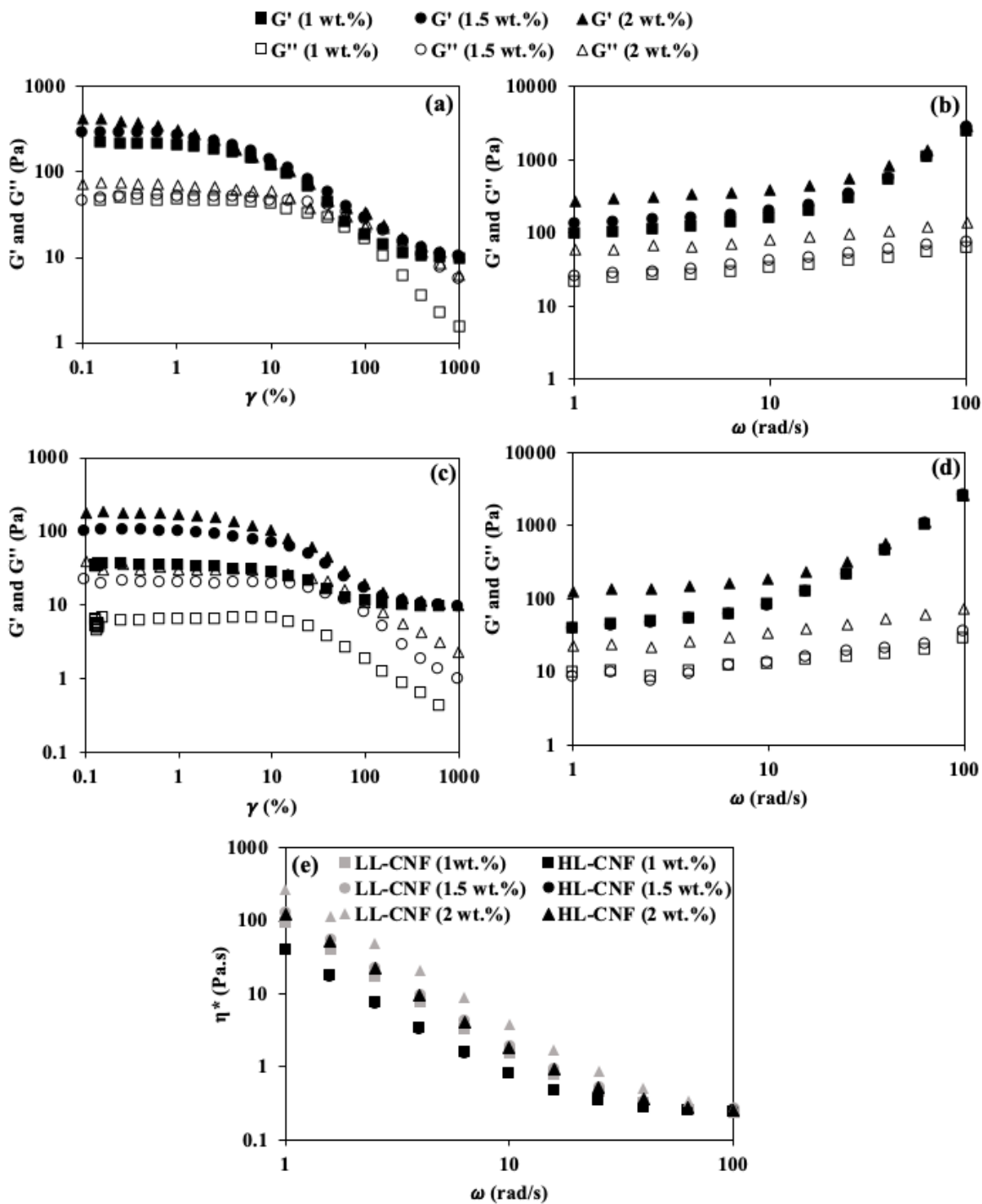


Fig. 6.2. Strain (γ) sweep and angular frequency (ω) sweep of modulus G' and G'' of LL-CNF hydrogels (a, b), and HL-CNF hydrogels (c, d) obtained using HIUS at acoustical powers of 53 and 51 W, respectively, and complex viscosity (η^*) of obtained CNF hydrogels (e).

The γ_c value of CNF hydrogels was defined by the CNF solid concentration and the residual lignin content. A decrease on the γ_c value of the hydrogels was observed when the CNF concentration was increased from 1 to 2 wt.% for both LL-CNF and HL-CNF hydrogels. The HL-CNF hydrogel at a lower solid concentration (1 wt.%) had the highest γ_c value of 4.0%, whereas the increase in CNF concentration to 1.5 and 2 wt.% resulted in a decrease in the γ_c values to 2.5 and 1.6%, respectively. Similar behavior was observed for LL-CNF hydrogel. The γ_c value of the 1-1.5 wt.% LL-CNF hydrogel was 1.6%, whereas when the concentration was increased up to 2 wt.%, the γ_c value of the LL-CNF hydrogel decreased to 1.0%. According to Yue et al. (2016), the lower the γ_c value, the shorter is the LVR, and increased is the rigidity of the hydrogel.

Fig. 6.2b and d show the rheological behaviour of the LL-CNF and HL-CNF hydrogels, respectively, obtained by angular frequency sweep test at 1% strain. Regardless of the lignin content and CNF solid concentration, all samples exhibited a typical elastic gel-like behavior, as the G' values were all higher than G'' values in the frequency range of 1-100 rad/s. The LL-CNF and HL-CNF hydrogels at 1 wt.% solid concentration had G' values of 93 and 38, respectively; whereas, the increase in solid concentration from 1 to 1.5 wt.% of the HL-CNF hydrogel did not result in any change of the G' value. However, the HL-CNF hydrogel at 2 wt.% had an increased G' value of 123 Pa. For the LL-CNF hydrogels, the G' value increased simultaneously with an increase in solid concentration, where the maximum G' value was 264 Pa at 2 wt.% solid concentration. Further, the power law model was applied to obtain better understanding of the interdependence of ω and dynamic modulus (Table 6.4).

Table 6.4. Power law parameters for elastic (G') and viscous (G'') modulus.

		$G' = a_1 \omega^{b_1}$			$G'' = a_2 \omega^{b_2}$		
		a_1	b_1	R^2	a_2	b_2	R^2
Angular frequency: 1-10 rad/s							
LL-CNF	1 wt.%	87.12±5.80	0.21±0.00	0.98	19.86±0.00	0.22±0.00	0.98
	1.5 wt.%	129.99±8.04	0.15±0.03	0.97	21.42±3.63	0.21±0.01	0.97
	2 wt.%	233.68±24.65	0.12±0.04	0.98	43.09±16.51	0.16±0.03	0.91
HL-CNF	1 wt.%	32.35±6.97	0.32±0.04	0.95	19.86±0.00	0.22±0.00	0.98
	1.5 wt.%	38.80±3.20	0.28±0.02	0.94	8.00±0.42	0.19±0.00	0.67
	2 wt.%	128.32±10.40	0.15±0.02	0.97	19.71±1.22	0.20±0.01	0.89
Angular frequency: 10-100 rad/s							
LL-CNF	1 wt.%	7.02±0.85	1.21±0.02	0.96	19.86±0.00	0.22±0.00	0.98
	1.5 wt.%	10.65±0.07	1.13±0.00	0.95	18.14±3.19	0.28±0.00	0.99
	2 wt.%	35.08±7.88	0.89±0.04	0.93	33.86±15.27	0.27±0.05	0.99
HL-CNF	1 wt.%	1.77±0.43	1.53±0.06	0.99	19.86±0.00	0.22±0.00	0.98
	1.5 wt.%	2.05±0.14	1.50±0.02	0.98	5.77±0.98	0.35±0.06	0.95
	2 wt.%	10.48±0.68	1.14±0.01	0.96	15.99±0.15	0.30±0.02	0.99

a_1 and a_2 : G' and G'' at an specific angular frequency; ω : angular frequency; b_1 and b_2 : degree of viscoelasticity; R^2 : goodness of fit.

The power law model is described by $G' = a_1 \omega^{b_1}$ and $G'' = a_2 \omega^{b_2}$, where a_1 and a_2 are the values of G' and G'' at a given angular frequency (ω), and b_1 and b_2 are the relative degrees of viscoelasticity of the gels (Richa et al., 2019). According to Table 6.4, the values of a_1 were greater than the values corresponding to a_2 at ω of 1-10 rad/s, indicating that the elastic responses were greater than the viscous for both CNF hydrogels.

Also, the values for b_1 were greater than those of b_2 at ω of 10-100 rad/s, indicating that even at high frequency the prepared CNF hydrogels had solid-like behaviour with a comparatively small dissipation in energy.

The results also indicated that the hydrogels had frequency dependence, as b_1 and b_2 increases towards higher ω . The b_1 values were between 0.12-1.21 for the LL-CNF hydrogels, and 0.15-1.53 for the HL-CNF hydrogels at ω of 1-100 rad/s. The lower b_1 values of the LL-CNF hydrogels compared to the HL-CNF hydrogels at all concentrations studied, indicated an intensive entanglement of the nanofiber, higher strength and stability of the hydrogel, and less deformation with increasing ω . The increased stability and mechanical strength of the LL-CNF hydrogel can be associated to the higher degree of nanofibrillation and WRV of the LL-CNF hydrogel compared to the HL-CNF hydrogel. As mentioned, the high degree of nanofibrillation obtained with the LL-CNF promoted greater aspect physical entanglements between nanofibers, and hydrogen bonding between nanofibers and water molecules, which promoting high stability and strength to the LL-CNF hydrogels.

The complex viscosity (η^*) plotted against the angular frequency is shown in Fig. 6.2e. According to Tanaka et al. (2015), as the aspect ratio of nanocelluloses increases, they become more flexible and their suspension network tends to have a higher viscosity. This agrees with the results obtained herein. The higher aspect ratio of the LL-CNF resulted in higher η^* at 1 rad/s (96-270 Pa.s) compared to HL-CNF (40-125 Pa.s). Furthermore, all CNF suspensions had a decline of the η^* as the ω increased. When the η^* of a suspension decreased in response to increased deformation, the material has a typical shear-thinning behavior (Nazari et al., 2016). According to Moberg et al. (2017), the shear-thinning

behavior of elastic CNF suspensions is expected since the nanofibrils tend to orient themselves in a network when no forces are applied, but under external deformation, their physical interactions are disassembled, increasing flow of the suspensions and decreasing the viscosity.

6.3.2. Cellulose nanofiber scaffolds characterization and cytocompatibility

The aerogel scaffold porosity, swelling capacity and structural stability can certainly affect their practical use in biomedical applications. For instance, controllable swelling capacity and porosity > 90% are desirable to induce adequate diffusion of metabolites and vascularization, avoiding a necrotic core in the scaffold due to hypoxia (Hickey et al., 2018; Zhang et al., 2019). Table 6.5 shows the properties of the LL-CNF and HL-CNF aerogels prepared with different initial CNF concentrations ranging from 1 to 2 wt.% via freeze-drying (Fig. 6.3).

Table 6.5. Comparison of LL-CNF and HL-CNF aerogel properties obtained by freeze drying.

		Aerogel properties			
		Diameter (cm)	Bulk density (g/cm ³)	Porosity (%)	Swelling capacity (g/g)
LL-CNF	1 wt.%	1.21±0.06 ^a	0.009±0.001 ^c	99.44±0.06 ^a	23.06±2.38 ^d
	1.5 wt.%	1.14±0.01 ^{ab}	0.021±0.000 ^b	98.67±0.01 ^a	29.11±2.15 ^b
	2 wt.%	1.30±0.05 ^a	0.025±0.003 ^b	98.44±0.12 ^{ab}	42.14±0.59 ^a
HL-CNF	1 wt.%	1.11±0.02 ^{ab}	0.029±0.005 ^b	98.21±0.34 ^{ab}	20.08±3.70 ^d
	1.5 wt.%	0.95±0.09 ^{bc}	0.031±0.010 ^{ab}	98.04±0.62 ^{ab}	24.64±1.51 ^d
	2 wt.%	0.89±0.04 ^c	0.051±0.012 ^a	96.81±0.76 ^b	26.25±0.66 ^c

Contents are expressed as mean±standard deviation duplicates. ^{a-d}Different lowercase letters in the same column indicate significant differences (p < 0.05).

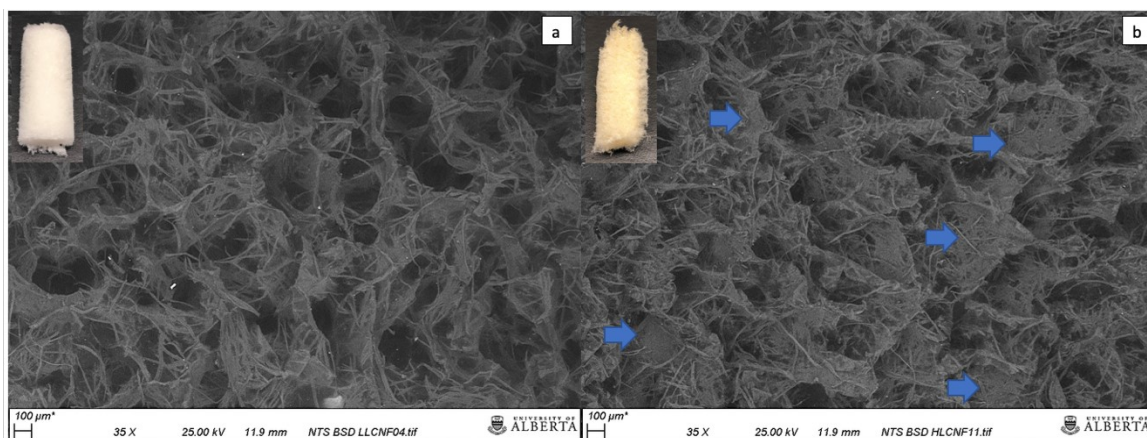


Fig. 6.3. Scanning electron microscopy (SEM) images of 1 wt.% LL-CNF aerogel (a) and HL-CNF aerogel (b) obtained using HIUS at acoustical powers of 53 and 51 W, respectively. Blue arrows show the nanofibers aggregation after freezing step.

The lignin content of the initial CNF solids greatly affected the bulk density of the aerogels. The lowest densities of the LL-CNF and HL-CNF aerogels were 0.009 and 0.029 g/cm³, respectively, achieved at 1 wt.% initial CNF concentration. As the bulk density is calculated based on the mass and volume of the aerogel (Eq. 6.3), increasing the initial solid concentration increased the mass of the aerogel, resulting in increased bulk density. At 2 wt.% concentration, the LL-CNF and HL-CNF aerogels had bulk densities of 0.025 and 0.051 g/cm³, respectively. Furthermore, the difference in the density values of the LL-CNF and HL-CNF aerogels at the same initial solid concentration is attributed to the diameter shrinkage during the freezing step prior to drying (Table 6.5).

During the freezing step, the HL-CNF dispersed in water were segregated by the ice crystal growth and moved together, triggering large fiber walls as shown in the blue arrows in Fig. 6.3b. These nanofiber aggregations led to shrinkage of the aerogel after sublimation (Table 6.5). Since the LL-CNF were more homogeneously distributed in the hydrogel complex (Fig. 6.1), they were also more homogeneously distributed during the ice crystal growth (Fig. 6.3a). This fact assisted the structural integrity and wall diameter of LL-CNF aerogel after sublimation. Earlier, Martoia et al. (2016) used TEMPO-oxidized and

enzymatic processed CNF to obtain aerogels. The CNF aerogels from the TEMPO-oxidized process exhibited pores with more regular geometry and size than those of the enzymatic process due to the smallest dimension and the highest aspect ratio of the TEMPO-oxidized nanofibers, which were more homogeneously redistributed during the ice crystal growth step (Martoia et al., 2016).

As the density of the aerogel is inversely correlated to the porosity (Eq. 6.3), the highest porosity was calculated as 99.4% for the LL-CNF aerogel at 1 wt.% concentration with a density of 0.009 g/cm³. With the increase of initial CNF concentration to 1.5 wt.%, and the increase of density to 0.019 g/cm³, the LL-CNF aerogel had a porosity of 98.7%. The trend and values herein obtained were compatible with those reported by Ciftci et al. (2017), who obtained highly purified CNF aerogels (1-2 wt.%) from treated lupin hull (~97%) via HIUS at 560 W and supercritical CO₂ (SCCO₂) drying at 40 °C, 100 bar and CO₂ flow rate of 0.5 L/min (measured at ambient conditions) for 4 h. The aerogels at a concentration of 1 wt.% had density of 0.009 g/cm³ and porosity of 99.4%, whereas CNF aerogels at a concentration of 1.5 wt.% had increased density of 0.019 g/cm³ and lower porosity of 98.8%. It is worth mentioning that Ciftci et al. (2017) also dried the obtained CNF hydrogels using freeze drying, the same method used in the present study. Using freeze drying, the CNF aerogels at 1 wt.% and 1.5 wt.% had porosities of 98.6% and 98.1%, respectively, which were lower than those of the LL-CNF aerogels herein obtained (99.4% and 98.4%, respectively). This can be attributed to the lower nominal power applied by Ciftci et al. (2017) (560 W) compared to that used in this study (1200 W).

Table 6.5 also shows the swelling capacity of the LL-CNF and HL-CNF aerogels in PBS (pH 7.4) at 25 °C after 24 h immersion time. The LL-CNF aerogels had maximum

swelling capacity of 42.1 g PBS/g aerogel, whereas the HL-CNF had maximum swelling capacity of 26.2 g PBS/g aerogel. This trend was similar to the WRV responses of the HL-CNF and LL-CNF hydrogels (Table 6.3), whereas the high lignin content reduced the absorption capacity of the hydrogels. As lignin is hydrophobic in nature, HL-CNF aerogels/hydrogels are expected to have lower swelling capacity and WRV than LL-CNF samples. Furthermore, it can be inferred that a high porosity structure of the LL-CNF aerogels induced a fast and increased PBS uptake ability than the HL-CNF aerogels. Rashad et al. (2019) obtained similar swelling capacity of 25 g PBS/g aerogel for TEMPO-oxidized and carboxymethylated CNF aerogels (1 wt.%) after 24 h immersion time. However, bacterial CNF aerogel showed lower swelling capacity of 12 g PBS/g aerogel within 2 h of immersion time (Chiaoprakobkij et al., 2011). Higher swelling capacity of CNF aerogel obtained herein and by Rashad et al. (2019) shows potential for its application as wound healing scaffold.

To further explore the use of these LL-CNF and HL-CNF aerogels for biomedical applications, the first step was to test the material cytocompatibility, which must be as high as possible to eliminate any adverse effect within the living tissue or microbial contamination. In this study, gingival fibroblast cells were used for the evaluation of cell adhesion and proliferation of the LL-CNF and HL-CNF scaffolds (1-2 wt.%) obtained using ultrasound at acoustical powers of 51-53 W (Fig. 6.4).

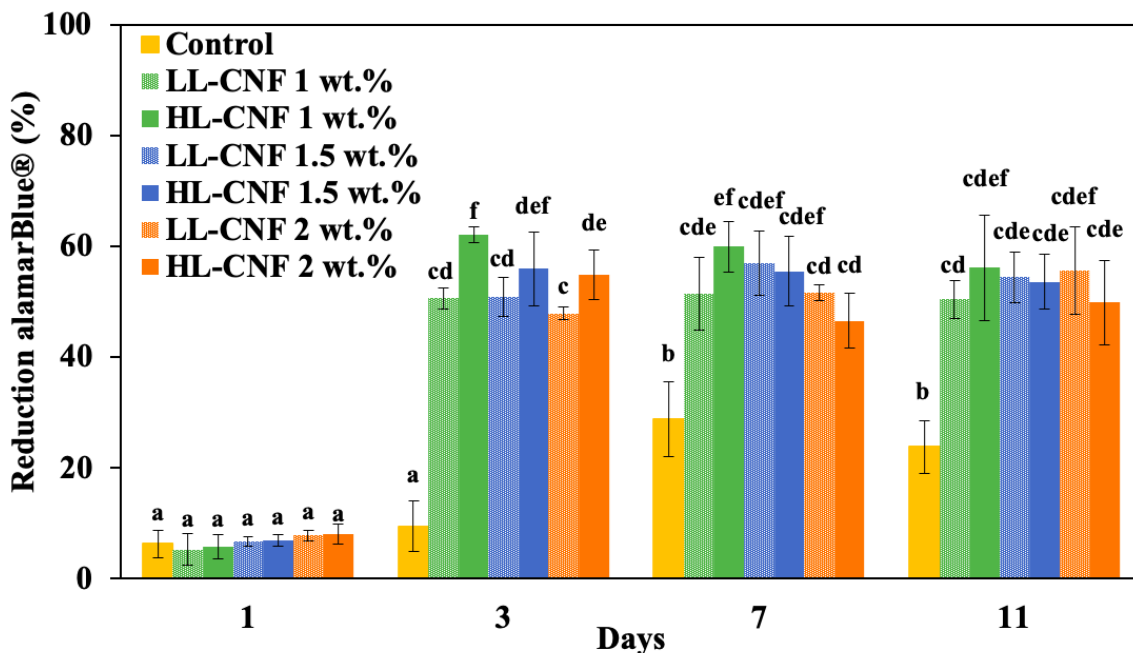


Fig. 6.4. Biocompatibility test of control (glass slip), LL-CNF and HL-CNF aerogels (1-2 wt.%) on gingival fibroblast cells cultured for 11 days. ^{a-f}Different lowercase letters indicate significant differences ($p < 0.05$).

Within day 1, the LL-CNF and HL-CNF scaffolds demonstrated similar cell adhesion as the control (glass slip) (see Table D.2 in Appendix D). This suggests that both of these surfaces can further stimulate human gingival fibroblast cell proliferation with no cytotoxicity. However, throughout the 11 days, the LL-CNF and HL-CNF scaffolds significantly increased the cell proliferation rate of the fibroblast cells compared to the control (Fig. 6.4). This increased cell viability and proliferation of prepared CNF scaffolds are probably due to the 3D morphology, which allowed the cells to proliferate not only along the surface but also inside its internal structure. In case of the control (a 2D glass slip), the cells grew only on the surface of the glass, which reduced the cell proliferation rate. Furthermore, according to the protocol used for scaffold preparation (Esparza, 2017), the control sample (glass slip) was sterilized for only 30 min compared to 3.5 h of sterilization for the CNF scaffolds. This short sterilization time of the control may not be enough to provide a sterile glass slip, which may have reduced the cell proliferation in the

control sample. Earlier, Chiaoprakobkij et al. (2011) reported a different behavior when using a 3D scaffold from bacterial CNF. The proliferation test of gingival fibroblast cells showed that on day 2 (the longest day analysed), the percentage of relative cell viability on bacterial CNF scaffolds were lower than those of control (2D tissue culture polystyrene plate). Therefore, besides the fact that the CNF scaffold obtained in this study showed outstanding ability to support cell growth over the control, it also showed better results compared to the scaffold from bacterial CNF.

On day 3, no statistical difference ($p = 0.653$) of cell proliferation within the LL-CNF scaffolds was observed. However, the HL-CNF scaffold at 1 wt.% had higher cell population compared to the HL-CNF scaffold at 2 wt.%. It is possible that the higher cell growth observed on the HL-CNF scaffold at a lower concentration may be related to the higher porosity compared to the same scaffold at 2 wt.% (Table 6.4). Furthermore, the statistical difference between LL-CNF and HL-CNF scaffolds at 1 wt.% be related to the induced segregation of the HL-CNF scaffold walls compared to the LL-CNF, which provided stiffer and larger substrate area for the cell proliferation (Fig. 6.3). From day 3 to day 11, no statistical difference on cell population was observed for each group of CNF scaffold at any specific concentration ($p = 0.460$). However, according to Fig. 6.5b, the HL-CNF scaffold preserved most of its porosity and showed less rupture of its walls compared to the LL-CNF scaffolds (Fig. 6.5a). It is likely that in a long term, the HL-CNF scaffolds can induce favorable cell-scaffold interaction due to its morphology and possible higher mechanical properties. But, further studies need to be performed to confirm this statement.

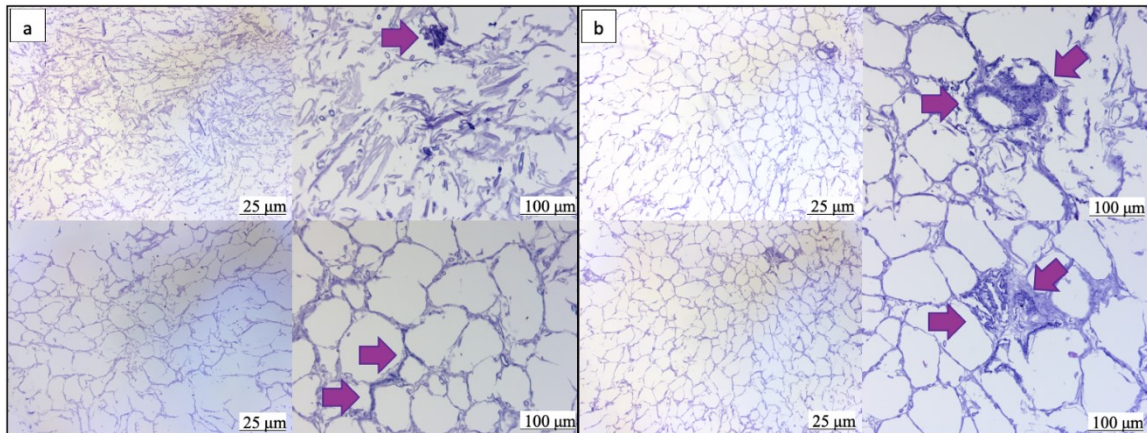


Fig. 6.5. Stained scaffold sections of LL-CNF aerogel (a) and HL-CNF aerogel (b) after incubation for 11 days. The pink arrows and the dark purple stain indicate the cell nuclei.

6.4. Conclusions

The HIUS processing was demonstrated to be an effective approach for successful production of CNF scaffolds with low (8%) and high (18%) residual lignin contents. The HIUS treatment induced the self-assembling process of CNF into hydrogels (1-2 wt.%) without the need for surface modification or cross-linkers. When freeze dried, the CNF aerogels with 18% lignin content had thicker cell walls and lower swelling capacity than the CNF scaffolds with 8% lignin content, mainly due to the hydrophobicity of the nanofibers. However, the cytocompatibility assay indicated that the residual lignin in CNF scaffolds is nontoxic and the prepared scaffolds induced higher human gingival cell viability and proliferation than the control sample. For the first time, CNF scaffolds with residual lignin content up to 18%, and without surface modification were reported as a promising material for biomedical applications, which opens new opportunities for nanocelluloses in the biomedical field.

Chapter 7. Clove essential oil emulsion-filled cellulose nanofiber hydrogel produced by high-intensity ultrasound technology for tissue engineering applications*

7.1. Introduction

Essential oils are widely used in Ayurvedic medicine as therapeutic compounds, promoters of health and well-being, and have become an important product in many fields, including pharmaceutical, medicinal, and food industries. Several encapsulating systems have been developed aiming for stabilization, solubilization, and delivery of these valuable compounds, such as oil-in-water emulsions, spray-dried microparticles, liposomes, lipidic nanoparticles, biopolymer-based films, emulsion-filled gels, and others (Fernandes et al., 2016; Torres et al., 2016; Feng et al., 2018; Zhao et al., 2018b; Cao et al., 2019; Wu et al., 2019).

Emulsion-filled gels or gels containing oil droplets are potential matrices for essential oil encapsulation due to their good stability and high applicability in the development of new products, as previously discussed in Chapter 2. High-energy based homogenization techniques have been used to form emulsions and immobilize large amounts of water within a biopolymer network as performed in a gel structure. In this sense, mechanical energy provided by a high-speed blender, high-pressure homogenizer and high-intensity ultrasound (HIUS) are recognized as effective approaches to produce colloidal and gel systems (Oliver et al., 2015; Feng et al., 2019; Perdih et al., 2019). The HIUS processing has been shown to be effective to produce emulsion-filled gels due to the homogenization mechanism based on

*A version of this chapter was published as Huerta, R.R., Silva E.K., El-Bialy, T., and Saldaña, M.D.A. (2019). Clove essential oil emulsion-filled cellulose nanofiber hydrogel produced by high-intensity ultrasound technology for tissue engineering applications. *Ultrasonics Sonochemistry*. <https://doi.org/10.1016/j.ultsonch.2019.104845>.

micro-shear generated by the collapse of microbubbles formed during the cavitation phenomenon (Oliver et al., 2015).

Biopolymers such as pectin, soy and whey protein, inulin and cellulose, have been used as gel phase in emulsion-filled gel systems, and their applications vary from food formulations to scaffolds in tissue engineering (Laikos et al., 2015; Oliver et al., 2015; 2016; Paradiso et al., 2015; Nourbehesht et al., 2018; Feng et al., 2019). Laikos et al. (2015) prepared wound dressing scaffolds using cellulose acetate with encapsulated essential oils (cinnamon, lemongrass and peppermint) via the electrospinning process. First, the cellulose acetate suspension (15 wt.%) was mixed with 1 or 5 wt.% essential oil, and then the suspensions were electrospun at 3-5 mL/h and 15-25 kV. The electrospun mats (0.2 mm thickness) were able to inhibit the growth of *Escherichia coli*, and the mats had non-cytotoxicity (75-90% viability) for human keratinocyte cells.

In the tissue engineering field, the use of essential oils within the scaffold matrix is a promising strategy to develop novel therapeutic multifunctional biomaterials. In a recent study, *Zataria multiflora*, a thyme-type essential oil, at concentrations of 0, 2, 5 and 10% (v/v) was incorporated into chitosan/poly(vinyl alcohol)/gelatin nanofiber mats using glutaraldehyde chemical crosslinking and tested as wound dressing scaffold (Ardekani et al., 2019). The nanofiber mat loaded with 10% (v/v) essential oil inhibited the growth of *Staphylococcus aureus*, *Pseudomonas aeruginosa* and *Candida albicans* after 24 h of incubation, while it also showed non-cytotoxicity (91% viability) for dermal fibroblast cells. Also, Han & Parker (2017) have shown that the essential oil extracted from the dried flower buds of clove, *Eugenia caryophyllata* L., besides its anesthetic, antioxidant, anti-inflammatory, antimicrobial and antifungal properties, also induced immune-modulating and tissue

remodelling activities in human dermal fibroblast cells. Although essential oils may be used in the tissue engineering field, an increased database on *in vitro* analysis is still needed (Raut, 2014).

Particularly, hydrogels of nanocellulose, like cellulose nanofibers (CNF), create a remarkable three-dimensional (3D) scaffold for cell culture due to their outstanding mechanical stability, cytocompatibility, controllable nanomorphology and high porosity (Du et al., 2019). The use of CNF alone or in combination with other natural or synthetic polymers have been widely studied; however, there is a lack of information about the use of CNF hydrogels to prepare emulsion-filled gels for possible tissue engineering applications. Therefore, the objective of the present study is to use HIUS processing to assist the formation of emulsion-filled gels using clove essential oil (0.1, 0.5 and 1.0 wt.%) as a dispersed agent, and CNF hydrogel obtained in Chapter 6 as a gelling agent, and evaluated their cytocompatibility with human gingival fibroblast cells for periodontal therapy. The HIUS specific energy effects on the structure of emulsion-filled CNF hydrogels were evaluated at 0.10, 0.17, and 0.24 kJ/g. The encapsulating systems were characterized for oil entrapment efficiency, microstructure, water retention value, color parameters and viscoelastic properties. The freeze-dried emulsion-filled CNF hydrogels were characterized for porosity, and swelling capacity prior to the cytocompatibility test using human gingival fibroblast cells.

7.2. Materials and methods

Saponin was purchased from Sigma Aldrich (Oakville, ON, Canada). The clove essential oil was obtained from a local store (Calia, Elite Energy Enterprises Inc, Vancouver, BC, Canada).

7.2.1. Preparation of cellulose nanofiber and emulsion-filled hydrogels by HIUS technology

First, the bleached cellulose fiber obtained in Chapter 5 (Section 5.2.2) for 6 h, was nanofibrillated according to the method described in Chapter 4 (Section 4.2.2.1) using ultrasound at 20 kJ/g to obtain CNF hydrogel (1 wt.%). Then, the emulsion-filled CNF hydrogels were prepared using 0.1, 0.5 and 1.0 wt.% clove essential oil, and the total amount of saponin (emulsifier) was kept constant at 0.25 wt.% of the mass of essential oil (Table 7.1). For the material loading, 10 g of CNF hydrogel were weighed (bottom layer), then the clove essential oil and emulsifier were added on top (middle layer), and the remaining mass of hydrogel was added as the uppermost layer. This system was used to avoid a loss of clove essential oil during the beginning of the mechanical turbulence of HIUS equipment.

Table 7.1. Clove essential oil emulsion-filled CNF hydrogel composition.

Clove essential oil (wt.%)	Emulsion-filled gel composition		
	CNF hydrogel (g)	Clove essential oil (g)	Saponin (g)
0.1	19.975	0.02	0.005
0.5	19.875	0.10	0.025
1.0	19.750	0.20	0.050

CNF: cellulose nanofibers (1 wt.%).

The mixture was treated using the same high-intensity ultrasonicator previously described in Chapter 4 (Section 4.2.2.1) with a probe of 10 mm in diameter, at a nominal power of 600 W, and without cold bath. The theoretical specific energy (SE) was calculated according to Eq. (4.1) using theoretical power of 600 W, and the real SE was calculated

using the acoustical power obtained using the calorimetric assay of Mason et al. (1994) and using the Eq. (2.3), described in Chapter 2 (Section 2.3.2.1.1). The HIUS efficiency and intensity were calculated according to Eqs. (6.1) and (6.2), previously described in Chapter 6 (Section 6.2.2).

A full factorial experimental design (3×3) was performed in duplicate, with a total of 18 experiments to investigate the effects of the real SE (0.10, 0.17, and 0.24 kJ/g) and clove essential oil content (0.1, 0.5, and 1.0 wt.%) on the properties of the emulsion-filled CNF hydrogels. Then, the samples were placed in 24-well culture plates, frozen overnight at -18°C , and dried at -45°C , 15 Pa for 2 days using a freeze dryer (FreeZone, Labco Corp., Kansas, MO, USA), and used as scaffolds for the cytocompatibility analysis.

7.2.2. Cell culture and seeding

The cell culture and seeding protocol was carried out following the method described in Chapter 6 (Section 6.2.3). Control (glass slip) was sterilized using the same protocol as the CNF scaffold for 3.5 h. Cells at passage 4, were seeded with 50 μL gingival fibroblast cells suspension (1.9×10^6 cells/mL) and cultivated for 24 h.

7.2.3. Characterization

7.2.3.1. Emulsion-filled CNF hydrogel

7.2.3.1.1. Oil entrapment efficiency

The oil entrapment efficiency was determined by the total oil entrapped by the CNF hydrogel relative to the oil added into the matrix using the centrifugation approach described earlier by Zobot et al. (2016), with slight modification. Approximately 0.1 mL of each sample was mixed with 4 mL of Type 1 water, manually agitated and maintained static overnight. Then, 4 mL of ethyl acetate was added to the diluted sample, manually

agitated and maintained overnight. The mixtures were centrifuged at 2800 g for 20 min and 11200 g for 5 min to capture the oil extracted from the matrix. After centrifugation, the supernatant was removed and the amount of eugenol (4-allyl-2-methoxyphenol), the main constituent of clove essential oil, was determined by measuring absorbance at 282 nm with a SpectraMax M3 Multi-Mode Microplate Reader (Molecular Devices LLC, San Jose, CA, USA) and its concentration was calculated using a calibration curve (see Fig. E.1 in Appendix E). The oil entrapment efficiency of clove essential oil (based on eugenol retention) in the encapsulating matrix was determined using Eq. (7.1):

$$\text{Oil entrapment efficiency (\%)} = \left(\frac{W_e}{W_i} \right) \times 100 \quad (7.1)$$

where, W_e is the total oil entrapped by the CNF hydrogel, and W_i is the initial oil added to the system.

7.2.3.1.2. Water retention value

The water retention value (WRV) of emulsion-filled CNF hydrogels was performed using the methodology described by Gu et al. (2018), previously detailed in Chapter 4 (Section 4.2.2.3).

7.2.3.1.3. Color

The emulsion-filled CNF hydrogel color was determined by a Hunter Lab colorimeter (CR-400/CR-410, Konica Minolta, Ramsey, NJ, USA) that uses a D65 illuminant with an opening of 14 mm and a 10° standard observer according to the ASTM D2244 method. Measurements were performed by transferring 1 mL of the sample over a watch glass plate (60 mm diameter) placed on top of the standard white plate ($L^* = 93.49$, $a^* = -0.25$ and $b^* = -0.09$). Specifically, the L (lightness), a (red to green) and b (blue to

yellow) values were used to calculate the total color difference (ΔE), yellowness index (YI) and whiteness index (WI) according to Eqs. (7.2-4) (Zhao et al., 2019):

$$\Delta E = \left(\sqrt{(L^* - L)^2 + (a^* - a)^2 + (b^* - b)^2} \right) \quad (7.2)$$

$$YI = 142.86 \times \left(\frac{b}{L} \right) \quad (7.3)$$

$$WI = 100 - [(100 - L)^2 + a^2 + b^2]^{0.5} \quad (7.4)$$

7.2.3.1.4. Optical microscopy

The microstructure of the emulsion-filled CNF hydrogels was analysed in an optical microscope (Carl Zeiss AG, Oberkochen, BW, Germany), with magnification of 100x using immersion oil technique.

7.2.3.1.5. Viscoelastic behavior

The viscoelastic behavior of the samples was studied using a rotational rheometer (Physica MCR 302, Anton Paar, Ashland, VA, USA), following the method described in Chapter 6 (Section 6.2.4). The results are shown as storage modulus (G'), loss modulus (G''), and the relative importance of G' and G'' given by $\tan \delta$ and calculated using Eq. (7.5):

$$\tan \delta = \left(\frac{G''}{G'} \right) \quad (7.5)$$

7.2.3.2. Dried emulsion-filled CNF hydrogel

The porosity and swelling capacity of the freeze-dried emulsion-filled CNF hydrogels were determined following the method described in Chapter 6, Section 6.2.5.

The cytocompatibility test was quantified using the alamarBlue® cell proliferation assay described in Chapter 6 (Section 6.2.5).

7.2.4. Statistical analysis

All experiments were performed in duplicate and the results were reported as mean values \pm standard deviation. The Minitab 18 Statistical Software (Minitab Inc., State College, PA, USA) was used to determine the difference between measurements using the analysis of variance (ANOVA) at 95% confidence interval determined by Tukey's honest significance test.

7.3. Results and discussion

7.3.1. HIUS processing parameters

The theoretical specific energy (TSE) levels (3, 5, and 7 kJ/g) used to produce emulsion-filled CNF hydrogels were calculated from the nominal power of 600 W. Then, the real SE levels (0.10, 0.17, and 0.24 kJ/g) were calculated by first determining the acoustical power applied to the encapsulating system. This was achieved by performing the calorimetric assay as shown in Fig. E.2 and E.3 in Appendix E. The acoustical power applied to the system was 20.55 W, which corresponded to a HIUS intensity of 26.18 W/cm², and an efficiency of 3.43% (Table 7.2). Using the same nominal power of 600 W, Encalada et al. (2019a and b) reported acoustical powers of 49.48 and 69.15 W, which are higher than that in the present study (20.55 W) (Table 7.2). This difference in the acoustical powers is mainly due to the different sample mass used, since Encalada et al. (2019a and b) used the specific heat of water (4.18 J/g°C), which is similar to the specific heat of CNF hydrogel (4.34 J/g°C) herein used.

Table 7.2. Nominal and acoustical power, theoretical and real specific energy, time, temperature, efficiency and intensity of the HIUS process.

HIUS processing parameter	This study	Encalada et al. (2019a)	Encalada et al. (2019b)
Nominal power (W)	600	600	600
Time (min)	1 3 4	20	20
Sample mass (g)	20	205	505
Theoretical SE (kJ/g)	3 5 7	3.51	1.43
Temperature (°C)	32 63 81	83	61
Acoustical power (W)	20.55	49.48	65.15
Real SE (kJ/g)	0.10 0.17 0.24	0.29	0.15
HIUS intensity (W/cm²)	26.18	37.30	49.11
HIUS efficiency (%)	3.43	8.25	10.86

HIUS: high-intensity ultrasound; SE: specific energy.

The differences in the acoustical power of the present study compared to the literature also led to different calculated HIUS intensity and efficiency (Table 7.2). Since the nominal power used in the present study and by Encalada et al. (2019a and b) was the same (600 W), and treatments with higher acoustical power had higher process efficiency according to Eq. (6.1). As observed in Table 7.2, a HIUS efficiency of 3.43% was obtained herein, while Encalada et al. (2019a and b) reported an efficiency of up to 10.86%. According to Gogate et al. (2001), most of the ultrasound devices equipped with a probe have energy efficiency less than 10% due to the high-energy dissipation through a small area (tip of the probe). In contrast, due to the wide surface area of the ultrasound bath, it can usually reach

an efficiency of around 40% (Gogete et al., 2001). Although Encalada et al. (2019a and b) obtained higher HIUS intensity and efficiency than herein, the real SE (amount of energy per mass) applied during the process was similar to this study (Table 7.2). Therefore, we highlight the importance to calculate the real SE when different systems are compared. Even though Encalada et al. (2019a and b) used the HIUS process for extraction and not emulsification, a further comparison of HIUS using real SE for emulsion purposes can be done with the present study even when different nominal powers, mass and/or times were used.

7.3.2. Characterization of emulsion-filled CNF hydrogels

The optical microscopy analysis of the emulsion-filled CNF hydrogels with different amounts of clove essential oil entrapped (0.1, 0.5 and 1.0 wt.%) obtained using ultrasonic SE of 0.10, 0.17, and 0.24 kJ/g is shown in Fig. 7.1. Increasing the ultrasonic SE from 0.17 to 0.24 kJ/g of emulsion-filled hydrogel with 0.5-1.0 wt.% clove essential oil resulted in small size and more homogeneous distribution of the clove essential oil droplets in the CNF hydrogel matrix. The fine dispersion of the smallest droplets was more evident when high amounts of clove essential oil (1.0 wt.%) was used at 0.24 kJ/g, which indicated that the phenomenon of coalescence and over-processing did not happen in this system.

The proposed mechanism for the emulsion-filled CNF hydrogel system assisted by HIUS technology can be divided into two sequential phases. First, the acoustical waves disrupt the interface of the essential oil and emulsifier-added water, resulting in the separation of the oil phase into the CNF aqueous phase in the form of large droplets. Then, the acoustic cavitation phenomenon induces the micro-shearing of the oil droplets into small ones. This process is assisted by the emulsifier that adsorbs onto the oil-water

interface reducing the interfacial tension and increasing the dispersibility of the clove essential oil in the matrix. Furthermore, in the present study, the oil droplets suspended in the hydrogel matrix, were classified as inactive fillers, since low chemical interaction between the clove essential oil and CNF matrix is expected (Farjami & Madadlou, 2019). After the HIUS treatment, the gelation was induced during storage of the samples at 4 °C. It is worth mentioning that emulsion-filled gels have exclusive advantages over ordinary oil-in-water emulsions due to the high stability against sedimentation and creaming, high bioavailability, lower demand of emulsifier agent, low turbidity, and scale-up potential (Farjami & Madadlou, 2019; Koshani & Jafari, 2019).

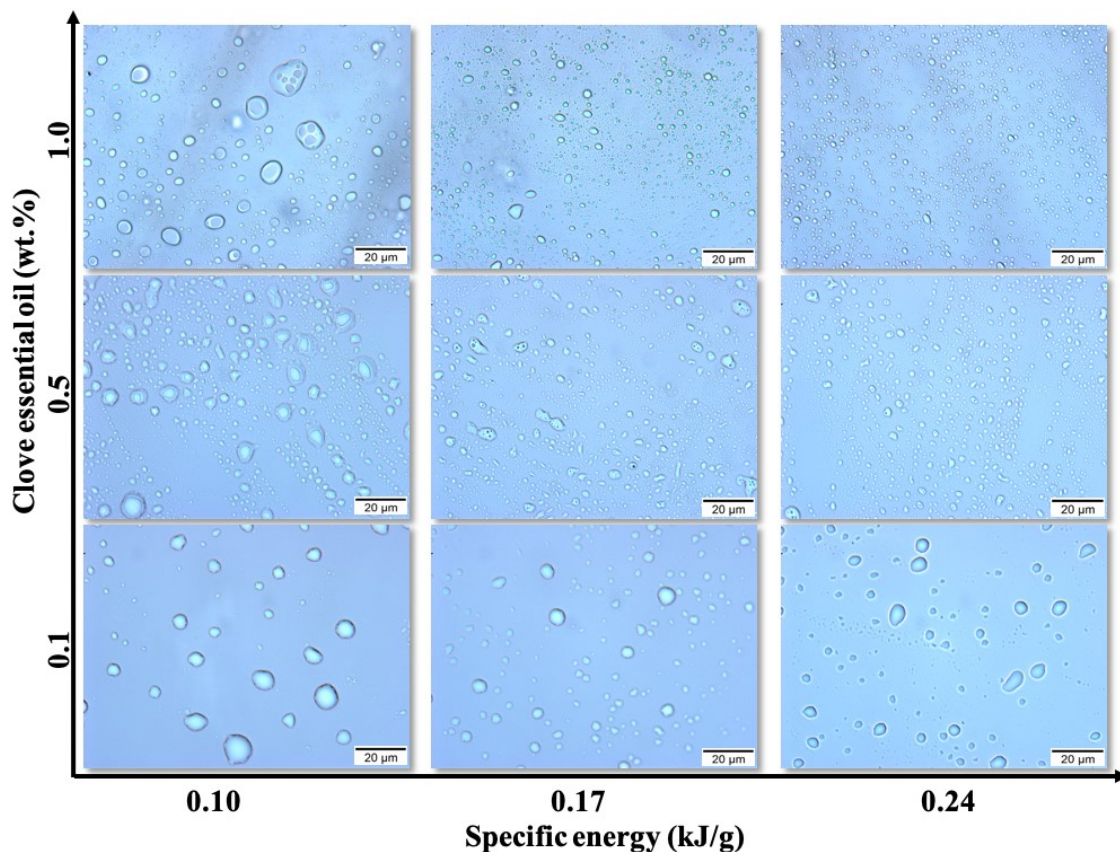


Fig. 7.1. Optical microscopy of the fresh clove essential oil emulsion-filled CNF hydrogels.

The prepared emulsion-filled CNF hydrogels were characterized for oil entrapment efficiency, water retention value (WRV), and color (Table 7.3). The clove essential oil entrapment efficiency was assessed based on eugenol retention to verify the ability of saponin to create a suitable interfacial film, and the ability of CNF hydrogel to act as a protective continuous phase in the emulsion-filled gel system. Results showed that entrapment efficiency of clove essential oil was not influenced by the HIUS process ($p = 0.918$), but highly affected by the oil content ($p < 0.001$) (Table 7.3). At an ultrasonic SE of 0.10 kJ/g, increasing the clove essential oil content from 0.1 to 0.5 wt.%, led almost doubling of the oil entrapped into the emulsion-filled CNF hydrogel system. However, a further increase in clove essential oil content from 0.5 to 1.0 wt.% resulted in a reduction of the oil entrapped from 34.09 to 26.93%. Under high ultrasonic SE of ≥ 0.17 kJ/g, there was no statistical difference on the oil entrapment when the clove essential oil in the system increased from 0.5 to 1.0 wt.%. Therefore, we assume that the prepared emulsion-filled CNF hydrogel with 1.0 wt.% clove essential oil obtained at an ultrasonic SE of 0.10 kJ/g induced coalescence of oil droplets, which led to a reduction on oil entrapment efficiency compared to other samples.

To date, there are no reports in the literature to compare our findings on essential oil entrapment efficiency using CNF as a continuous phase. Earlier, Zabet et al. (2016) reported thymol retention values as low as 16% using HIUS at a theoretical SE of 8 kJ/g, where inulin was used as the continuous phase, and oregano essential oil was the dispersed phase. However, higher values of thymol retention (84%) were reported when modified starch was used together with inulin as the continuous phase (Zabet et al., 2016).

Table 7.3. Clove essential oil emulsion-filled CNF hydrogels (0.1-1.0 wt.% clove essential oil) obtained at ultrasonic SE of 0.10, 0.17 and 0.24 kJ/g.

Clove essential oil (wt.%)	SE (kJ/g)	Oil entrapment (%)	WRV (g/g)	Color		
				ΔE	YI	WI
0.1	0.10	18.37±1.95 ^c	65.35±4.03 ^a	7.15±0.01 ^{ab}	3.60±0.00 ^c	96.80±0.00 ^a
	0.17	18.24±2.37 ^c	63.25±0.49 ^a	7.30±0.00 ^a	3.65±0.07 ^c	96.65±0.07 ^{ab}
	0.24	18.52±1.13 ^c	68.05±0.78 ^a	7.00±0.00 ^{ab}	3.75±0.07 ^c	96.75±0.07 ^{ab}
0.5	0.10	34.09±0.63 ^a	55.00±2.38 ^b	6.85±0.07 ^{ab}	4.35±0.07 ^a	96.40±0.00 ^{ab}
	0.17	32.55±2.83 ^{ab}	54.70±7.35 ^b	6.70±0.00 ^{ab}	4.25±0.07 ^{ab}	96.35±0.07 ^{ab}
	0.24	32.74±1.22 ^{ab}	52.30±1.56 ^b	6.55±0.21 ^b	4.40±0.28 ^a	96.20±0.28 ^b
1.0	0.10	26.93±1.94 ^b	46.25±1.20 ^c	6.45±0.21 ^b	4.30±0.14 ^a	96.40±0.14 ^{ab}
	0.17	27.46±0.84 ^{ab}	42.00±2.40 ^c	6.45±0.07 ^b	4.55±0.21 ^a	96.25±0.21 ^{ab}
	0.24	28.06±1.94 ^{ab}	44.20±4.10 ^c	6.70±0.42 ^{ab}	4.40±0.00 ^a	96.40±0.14 ^{ab}

SE: specific energy; WRV: water retention value; ΔE : color difference; YI: yellowness index; WI: whiteness index. Contents are expressed as mean±standard deviation of duplicates. ^{a-c}Different lowercase letters in the same column indicate significant differences ($p < 0.05$).

Overall the low entrapment efficiency values obtained herein (maximum of 34%) can also be associated with the intense conditions on the hydrogel system during the HIUS process, where the acoustic cavitation induces the formation and subsequent collapse of microbubbles. According to Chemat et al. (2017), around these microbubbles extreme local conditions of temperatures of up to 4000 °C and estimated pressures of around 50-1000 bar with high shear rates can be observed. Those “hotspots” created by the cavitation phenomenon reduced the viscosity of the CNF hydrogel and subsequent the oil entrapment efficiency, since essential oils are extremely volatile and labile compounds composed mainly of alcohols, ethers, esters, and others (Turek & Stintzing, 2013).

The WRV of the emulsion-filled CNF hydrogels was also highly influenced ($p < 0.001$) by the amount of oil added into the system but not to the HIUS treatment used ($p = 0.541$). The WRV value of the emulsion-filled CNF hydrogel prepared at 0.24 kJ/g decreased from 68.05 to 44.20 g/g as the clove essential oil content increased from 0.1 to 1.0 wt.% (Table 7.3). The ability of the CNF hydrogel to absorb water is based on the high aspect ratio of the nanofibers and its complex networking morphology, which have various hydroxyl groups on its surface, promoting the stability of surrounding water molecules into the network via hydrogen bonding. However, when the clove essential oil was introduced into the CNF hydrogel, besides its natural hydrophobicity, the oil droplets occupied the pores of the nanofibers network, resulting in less hydrogen bonding between CNF and water, which reduced the WRV of the prepared emulsion-filled CNF hydrogels.

Color difference (ΔE) parameter was also strongly affected by the clove essential oil content ($p < 0.001$), but not affected by the ultrasonic SE used ($p = 0.762$). As seen in Table 7.3, the main difference in color between emulsion-filled CNF hydrogels was when the oil

content increased from 0.1 to 1.0 wt.% in samples treated at an ultrasonic SE of 0.17 kJ/g, where the ΔE was reduced from 7.30 to 6.45. Also, between emulsion-filled CNF hydrogels, the amount of clove essential oil significantly influenced ($p = 0.007$) the whiteness index (WI) of the samples, whereas the ultrasonic SE had no effect ($p = 0.072$) over the WI responses. Emulsion-filled CNF hydrogel with 0.1 wt.% clove essential oil treated at an ultrasonic SE of 0.10 kJ/g had WI of 96.80, being reduced to 96.20, when higher amounts of clove essential oil was added (0.5 wt.%) and the ultrasonic SE increased to 0.24 kJ/g. However, the yellowness index (YI) was strongly affected by both clove essential oil content ($p < 0.001$) and ultrasonic SE used ($p = 0.023$). The lowest YI value of 3.60-3.75 was obtained with emulsion-filled CNF hydrogels with the lowest amount of oil added (0.1 wt.% clove essential oil) at all ultrasonic SE levels tested. The YI increased up to 4.55 when increased amounts (≥ 0.5 wt.%) of clove essential oil were added to the CNF hydrogel matrix at all ultrasonic SE levels tested. In general, the emulsion is a complex system and its color is affected by several factors such as concentration and absorbance of the existing oil chromophores, and oil droplet characteristics (e.g. radius, concentration) (McClements, 2002). The full color analysis is shown in Table E.1 in Appendix E.

The viscoelastic properties of emulsion-filled CNF hydrogels are shown in Figs. 7.2 and 7.3. The analysis was based on the elastic (storage) modulus G' , which is the reversible stored energy, and viscous (loss) modulus G'' , which is the irreversible energy loss of the system.

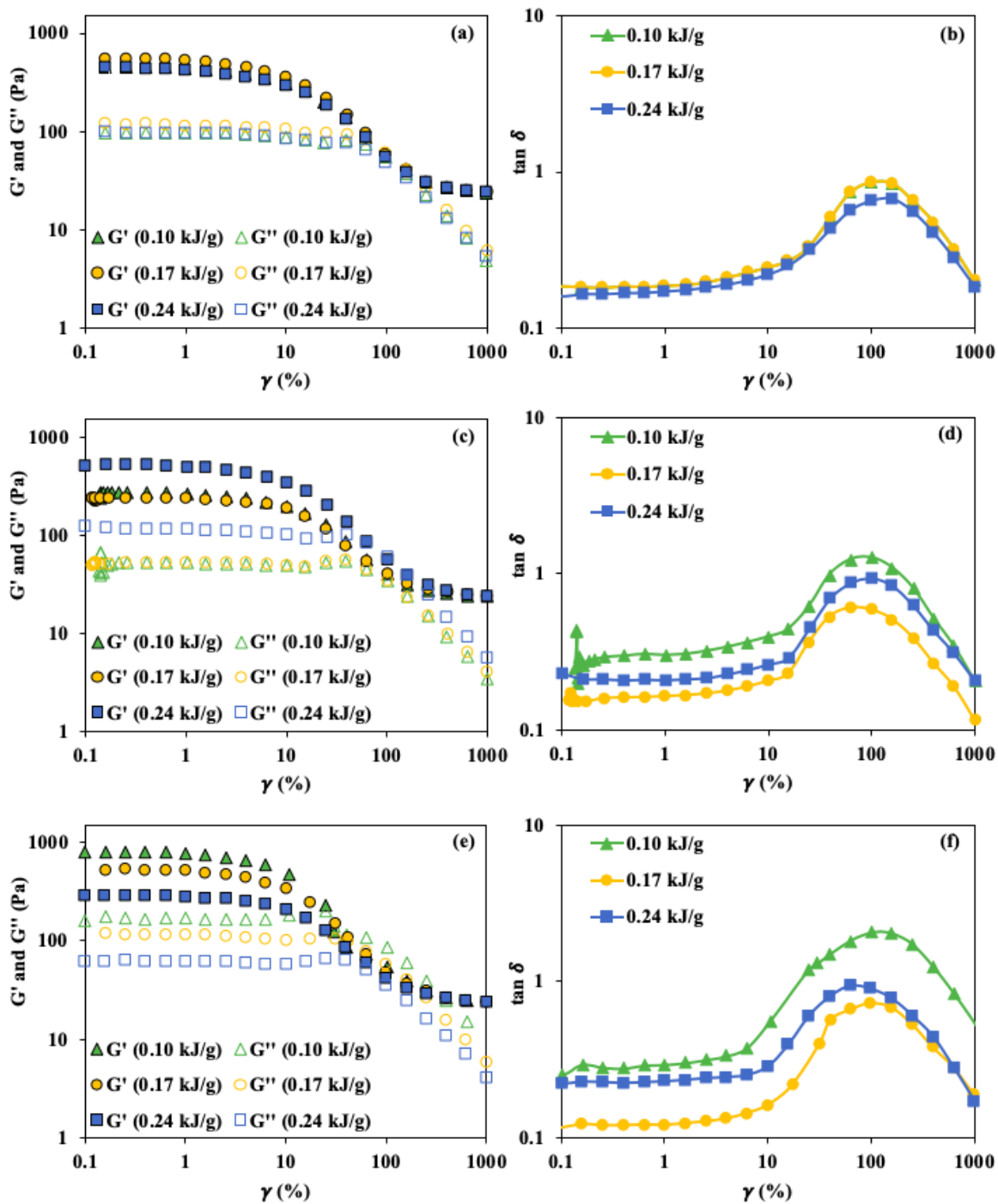


Fig. 7.2. Strain (γ) sweep of modulus G' and G'' and $\tan \delta$ of clove essential oil emulsion-filled CNF hydrogels with 0.1 wt.% (a, b), 0.5 wt.% (c, d), and 1.0 wt.% (e, f) clove essential oil.

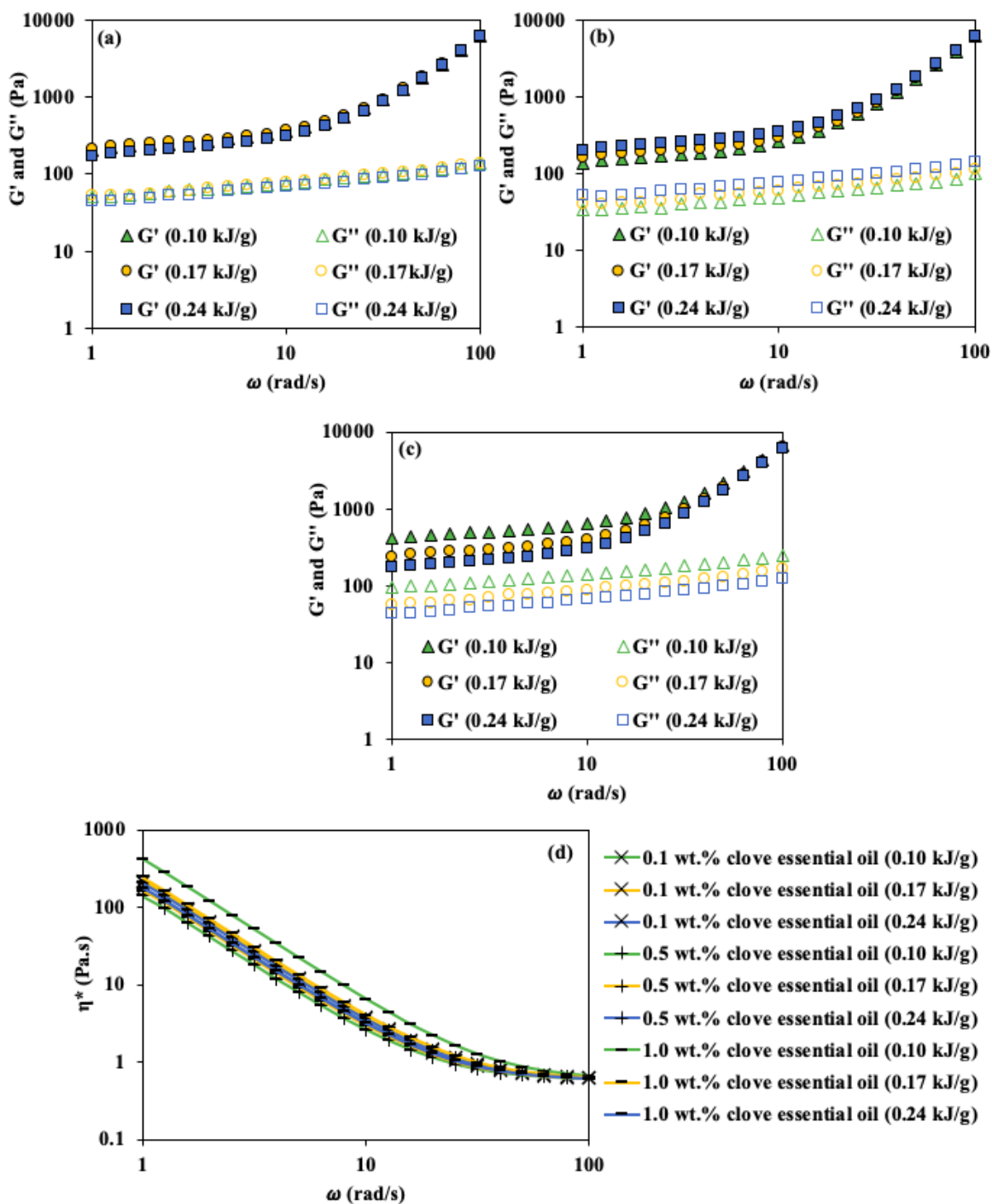


Fig. 7.3. Angular frequency (ω) sweep of modulus G' and G'' of clove essential oil emulsion-filled CNF hydrogels with 0.1 wt.% (a), 0.5 wt.% (b), and 1.0 wt.% (c) clove essential oil. Complex viscosity η^* against ω at 1-100 rad/s (d) for all prepared emulsion-filled CNF hydrogels.

The strain (γ) sweep test was performed at applied shear strains of 0.01-1000% and a constant angular frequency (ω) of 6.28 rad/s to determine the linear viscoelastic region (LVR). The LVR is a region where the elastic structure of emulsion-filled CNF hydrogels remains stable, whereas the strain point where the LVR ends is known as the critical strain % (γ_c). According to Fig. 7.2a, c and e, for strain less than 2.5% (γ_c), all the emulsion-filled CNF hydrogels had G' basically independent of the applied strain (LVR). Since the $\tan \delta$ is the ratio of loss modulus to storage modulus (Eq. 7.5), it can describe if the sample is more elastic ($\tan \delta < 1$) or more viscous ($\tan \delta > 1$) in the specific shear γ applied. Independent of the amount of clove essential oil added, all emulsion-filled CNF hydrogels treated at ultrasonic SE of 0.17 and 0.24 kJ/g showed elastic behavior ($\tan \delta < 1$) over the shear γ range tested (0.01-1000%) (Fig. 7.2b, d and f). This means that although few individual bonds in the emulsion-filled CNF hydrogel have ruptured, the entire surrounding matrix still held together the elastic structure of the initial material. This behavior can be due to the small oil droplets observed in those systems (Fig. 7.1) that did not interfere with the 3D CNF network stability. However, the emulsion-filled CNF hydrogels treated at 0.10 kJ/g with 0.1 and 0.5 wt.% clove essential oil had its 3D network structure yielded ($\tan \delta > 1$) at γ of $\geq 24\%$, behaving as more viscous fluid than elastic.

The angular frequency (ω) sweep test was performed at 1% strain (within the LVR), and ω of 1-100 rad/s (Fig. 7.3). Overall, the G' of emulsion-filled CNF hydrogels were higher than the G'' values at the range of ω tested, indicating that they had predominantly gel-like property. The emulsion-filled CNF hydrogels treated at 0.10 kJ/g with 0.1 wt.% clove essential oil had a G' of 204.84 ± 15.30 Pa, which decreased to 134.97 ± 49.19 Pa when the amount of clove essential oil increased to 0.5 wt.%. However, when the amount of

clove essential oil in the system was 1.0 wt.%, the G' drastically increased up to 411.42 ± 66.80 Pa. Similar behavior was observed for the samples treated at 0.17 kJ/g, whereas the G' of the emulsion-filled CNF hydrogels decreased from 211.29 ± 60.07 to 159.21 ± 16.30 Pa when the clove essential oil increased from 0.1 to 0.5 wt.%, and when the clove essential oil increased from 0.5 to 1.0% the G' of the emulsion-filled CNF hydrogel increased from 159.21 ± 16.30 to 237 ± 51.20 Pa. However, samples treated at higher ultrasonic SE (0.24 kJ/g) had no effect ($p = 0.797$) on the G' of the emulsion-filled CNF hydrogels at any concentration of the clove essential oil used. Furthermore, the complex viscosity (η^*) against the ω (1-100 rad/s) indicated that for all emulsion-filled CNF hydrogels, the η^* decreased in response to increased deformation (Fig. 7.3d), which is typical behavior of a shear-thinning material (Nazari et al., 2016). The similar shear-thinning behavior of the samples is mainly due to the 3D network of the CNF hydrogel, which under external deformation, the nanofibers align along shear direction and lose its entanglements, decreasing the system viscosity (Moberg et al., 2017).

The power law model was applied to better understand the interdependence of ω and dynamic modulus (Table 7.4). The power law model is described by $G' = a_1 \omega^{b_1}$ and $G'' = a_2 \omega^{b_2}$, where a_1 and a_2 are the values of G' and G'' at a given angular frequency (ω), and b_1 and b_2 are the relative degrees of viscoelasticity of the gels (Richa et al., 2019).

Table 7.4. Power law parameters for elastic (G') and viscous (G'') modulus.

Clove essential oil (wt.%)	SE (kJ/g)	$G' = a_1 \omega^{b_1}$			$G'' = a_2 \omega^{b_2}$		
		a_1	b_1	R^2	a_2	b_2	R^2
Angular frequency: 1-10 rad/s							
	0.10	203.56±14.67	0.22±0.01	0.98	49.85±2.94	0.18±0.01	0.98
0.1	0.17	235.52±31.79	0.21±0.01	0.99	55.87±7.83	0.18±0.01	0.98
	0.24	190.92±23.67	0.23±0.01	0.98	47.68±5.88	0.19±0.01	0.98
0.5	0.10	154.94±27.10	0.24±0.02	0.97	36.74±5.70	0.17±0.01	0.94
	0.17	165.35±6.63	0.23±0.00	0.97	38.84±0.57	0.20±0.01	0.94
	0.24	212.51±14.23	0.22±0.01	0.98	50.68±2.44	0.20±0.00	0.98
1.0	0.10	487.86±105.30	0.17±0.00	0.99	19.86±0.00	0.22±0.00	0.98
	0.17	237.92±51.20	0.20±0.01	0.99	19.86±0.00	0.22±0.00	0.98
	0.24	189.06±15.42	0.22±0.01	0.98	19.86±0.00	0.22±0.00	0.98
Angular frequency: 10-100 rad/s							
0.1	0.10	14.86±1.45	1.25±0.02	0.97	43.77±1.74	0.25±0.00	0.99
	0.17	18.69±4.10	1.21±0.05	0.96	48.19±6.19	0.24±0.01	0.99
	0.24	15.25±0.00	1.31±0.08	0.97	41.47±4.64	0.25±0.00	0.99
0.5	0.10	9.60±2.46	1.35±0.06	0.97	29.42±1.96	0.25±0.00	0.99
	0.17	10.02±1.21	1.34±0.03	0.97	32.37±2.67	0.26±0.00	0.99
	0.24	16.01±1.62	1.25±0.05	0.97	44.92±2.82	0.25±0.00	0.99
1.0	0.10	97.36±22.12	1.03±0.20	0.91	19.86±0.00	0.22±0.00	0.98
	0.17	23.44±7.12	1.16±0.07	0.96	19.86±0.00	0.22±0.00	0.98
	0.24	12.88±2.42	1.32±0.09	0.97	19.86±0.00	0.22±0.00	0.98

a_1 and a_2 : G' and G'' at a specific angular frequency; ω : angular frequency; b_1 and b_2 : degree of viscoelasticity; R^2 : goodness of fit.

According to Table 7.4, at lower ω of 1-10 rad/s, the values of a_1 were greater than the values corresponding to a_2 , indicating that the 3D emulsion-filled CNF hydrogels maintained its elastic gel-like behavior. However, at higher ω of 10-100 rad/s, most of the emulsion-filled CNF hydrogels lost its structural integrity and had a_2 values greater than

the a_1 values, with the exception of the emulsion-filled CNF hydrogel with 1.0% clove essential oil obtained at an ultrasonic SE of 0.10 kJ/g that presented a_1 value of 97.36 greater than a_2 value of 19.86. This behavior indicates that this sample had higher strength and stability with the clove essential oil droplets intensively entangled into the 3D CNF network, that even at high deformation energy, it did not lose its elastic structure. This result could also be seen in Fig. 7.3c, as the emulsion-filled CNF hydrogel with 1.0% clove essential oil obtained at ultrasonic SE of 0.10 kJ/g had the highest G' of 411.42 ± 105.30 Pa. Also, both b_1 and b_2 at ω of 10-100 rad/s had higher values compared to lower ω of 1-10 rad/s for all samples. This result indicates that the elastic and viscous modulus of the filled-emulsion CNF hydrogels depend on the frequency with a comparatively small dissipation in energy. Particularly, the lower b_1 value of 1.03 of the emulsion-filled CNF hydrogel with 1.0% clove essential oil obtained at an ultrasonic SE of 0.10 kJ/ compared with the other samples (b_1 values of ≥ 1.16) indicate less frequency dependency of the elastic modulus in this sample and increased stability towards higher deformation energy.

7.3.3. Characterization of freeze-dried emulsion-filled CNF hydrogels and its cytocompatibility

Table 7.5 shows the properties of the dried emulsion-filled CNF hydrogels obtained via freeze drying technique. The diameter, bulk density and porosity of the dried samples were not affected by the ultrasonic SE used ($p \geq 0.105$) or clove essential oil added ($p \geq 0.072$). Since the main structure of the emulsion-filled gel was the 3D CNF hydrogel, and this was not different between treatments, the diameter and bulk density of the samples remained similar between 1.45-1.49 cm and 0.01-0.04 g/cm³, respectively. The porosity of

the dried emulsion-filled CNF hydrogels was as high as 99.19%, envisioning its application as tissue engineering scaffold.

Table 7.5. Diameter, bulk density, porosity and swelling capacity properties of freeze-dried clove essential oil emulsion-filled CNF hydrogels.

Clove essential oil (wt.%)	SE (kJ/g)	Freeze-dried emulsion-filled CNF hydrogel			
		Diameter (cm)	Bulk density (g/cm ³)	Porosity (%)	Swelling capacity (g/g)
0.1	0.10	1.45±0.02 ^a	0.04±0.01 ^a	97.43±0.87 ^a	22.80±0.57 ^{ab}
	0.17	1.45±0.00 ^a	0.01±0.00 ^a	99.19±0.00 ^a	24.55±0.91 ^a
	0.24	1.45±0.04 ^a	0.04±0.02 ^a	97.41±0.85 ^a	22.20±0.71 ^{abc}
0.5	0.10	1.47±0.01 ^a	0.02±0.00 ^a	99.07±0.01 ^a	21.10±1.27 ^{abcd}
	0.17	1.48±0.03 ^a	0.02±0.00 ^a	98.73±0.04 ^a	20.10±1.41 ^{bcd}
	0.24	1.49±0.06 ^a	0.02±0.00 ^a	98.94±0.28 ^a	19.05±0.64 ^{bcd}
1.0	0.10	1.48±0.05 ^a	0.01±0.00 ^a	98.62±0.57 ^a	20.10±1.31 ^{bcd}
	0.17	1.48±0.00 ^a	0.02±0.00 ^a	98.86±0.12 ^a	18.55±0.50 ^{cd}
	0.24	1.47±0.00 ^a	0.02±0.01 ^a	98.48±0.62 ^a	17.76±1.20 ^d

Contents are expressed as mean±standard deviation duplicates. ^{a-d}Different lowercase letters in the same column indicate significant differences ($p < 0.05$).

Table 7.5 also shows the swelling capacity of the dried samples in PBS (pH 7.4) at 25 °C after 24 h immersion time. The swelling capacity was strongly affected by the clove essential oil content ($p < 0.001$) and ultrasonic SE used ($p = 0.035$). Increasing the clove essential oil content from 0.1 to 1.0 wt.% at ultrasonic SE of 0.17 and 0.24 kJ/g decreased the swelling capacity of the dried emulsion-filled hydrogels from 24.55 to 18.55 g PBS/g emulsion-filled CNF hydrogel, and from 22.20 to 17.76 g PBS/g emulsion-filled CNF hydrogel, respectively. However, increasing the clove essential oil content from 0.1 to 1.0 wt.% at the lowest ultrasonic SE tested (0.10 kJ/g) did not show any effect on swelling capacity responses, which ranged from 20.10 to 22.80 g PBS/g emulsion-filled CNF

hydrogel. This behavior can be due to their non-homogeneous distribution of the oil droplets (Fig 7.1), which allowed the entangled CNF network to swell. The chitosan/poly(vinyl alcohol)/gelatin nanofiber dried mats incorporated with *Zataria multiflora*, a thyme-type essential oil, also had reduction on swelling capacity as the essential oil content increased from 0 to 10% (v/v) (Ardekani et al., 2019). The composite mat without oil had a maximum swelling capacity of 10 g PBS/g mat, whereas the composite mat with 10% (v/v) thyme-type essential oil had maximum swelling capacity of 7 g PBS/g mat. As less essential oil was incorporated, the swelling capacity of the dried emulsion-filled CNF hydrogel herein prepared was more than 3.5 times higher than the values obtained by Ardekani et al. (2019). Also, this behavior can be attributed to the higher aspect ratio of the nanofibers herein obtained via HIUS processing (average nanofiber diameter of 14 nm) compared to the nanofibers obtained via electrospinning (range of nanofiber diameters of 95-321 nm) by Ardekani et al. (2019).

The cytocompatibility of the dried emulsion-filled CNF hydrogels (0.1-1 wt.% clove oil) with human gingival fibroblast cells was investigated using the alamarBlue® assay. In this assay, the resazurin (blue dye) is reduced to resorufin, a highly fluorescent pink compound, in response to cellular metabolic reduction. The intensity of the fluorescence produced is proportional to population of living cells and used as direct indicator of cell viability and cytotoxicity. According to Fig. 7.4, the emulsion-filled hydrogels with clove essential oil concentration up to 0.5 wt.% were non-toxic to the cells, represented by cell viability in the range of 74-101% (Table E.2 in Appendix E). No significant ($p = 0.059$) difference in cell viability was found between samples with 0.1 and 0.5 wt.% clove essential oil treated using the same ultrasonic SE. However, independent of the ultrasonic

SE applied, the emulsion-filled CNF hydrogels with 1 wt.% clove oil showed high cytotoxicity, which reduced the cell viability to a minimum of 18% at an ultrasonic SE of 0.17 kJ/g. Furthermore, measuring the cell proliferation over 11 days was attempted; however, since day 3 the non-seeded emulsion-filled CNF hydrogel scaffolds had increased fluorescence, which indicates that the clove essential oil may have a direct reducing effect on resazurin.

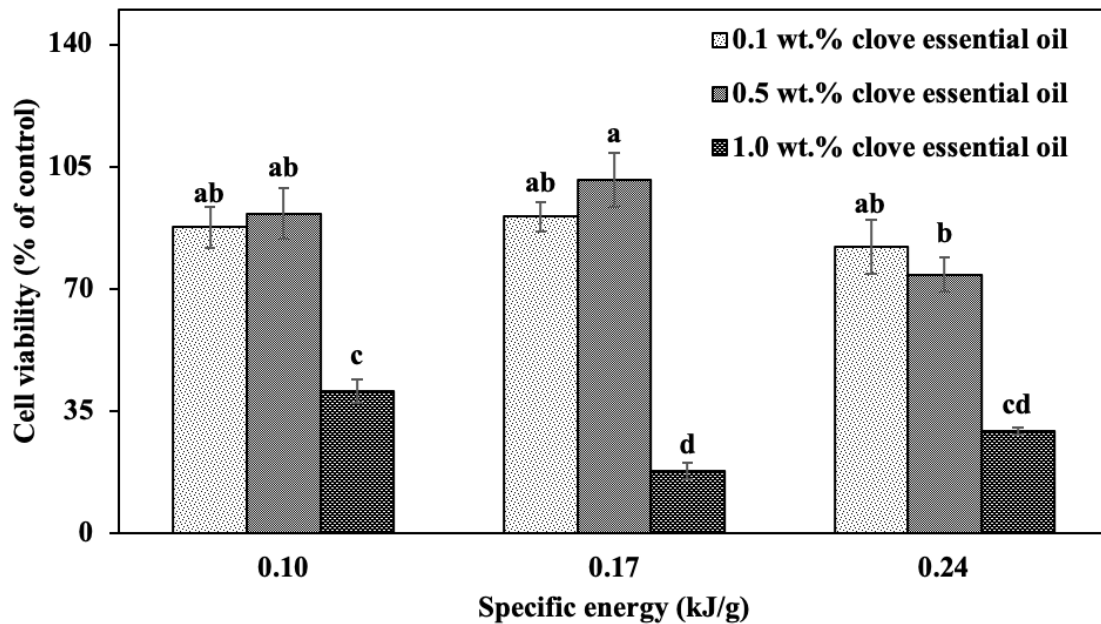


Fig. 7.4. Cell viability of the freeze-dried clove essential oil emulsion-filled CNF hydrogels after 24 h.

7.4. Conclusions

For the first time, clove essential oil emulsion-filled hydrogel using CNF as a gelling agent was developed as a scaffold for tissue engineering applications. The use of HIUS processing with CNF hydrogel and clove essential oil yielded highly efficient emulsion-filled CNF hydrogels. The CNF hydrogel had the greatest oil entrapment efficiency of 33-34% with 0.5 wt.% clove essential oil independent of the HIUS energy used. All emulsion-filled CNF hydrogels showed decreased water retention value as well as swelling capacity

as the oil content increased, mainly due to the hydrophobicity of the clove essential oil. Overall, the emulsion-filled CNF hydrogels had typical shear-thinning behavior, as under increased deformation energy, the physical interaction between the nanofibrils were dissembled and the gels had lower viscosity. Furthermore, according to the cell viability assay, the incorporation of clove essential oil up to 0.5 wt.% did not show cytotoxicity against human gingival fibroblast cells, being a promising scaffold material for tissue engineering applications.

Chapter 8. Conclusions and recommendations

8.1. Conclusions

In this thesis, straw biomass of two important Canadian crops, barley and canola, were processed via emerging and green technologies to obtain value-added products such as phenolic compounds and hemicellulosic sugars. Due to the higher volume of production of canola compared to barley in Canada, canola straw was chosen for further processing. For the first time a biorefinery approach for canola straw was studied towards nanofiber production and application. Pressurized fluid processing was used as a fractionation technique mainly because it uses solvents that are generally recognized as safe (GRAS), avoid the neutralization step, and do not produce hazardous waste. After pressurized fluid processing, the enriched cellulose fiber from canola straw was further converted into nanofibers including lignocellulosic nanofiber and cellulose nanofiber via high-intensity ultrasound technology. In depth understanding of the nanofibrillation process towards hydrogel formation and further aerogel production allowed the investigation of tissue engineering scaffolds. The prepared scaffolds showed promising applications in the biomedical field.

The fractionation of barley and canola straws was performed using pressurized fluids, including subcritical water and pressurized aqueous ethanol, targeting the maximum removal of total carbohydrates (Chapter 3). The fractionation mechanism is mainly attributed to the increased ionization of the pressurized fluid that catalyses the breakdown of hemicellulosic polysaccharides into soluble oligomers. Also, the decrease in the dielectric constant of pressurized fluids induce lignin depolymerization and release phenolic compounds of the linkages between carbohydrates and lignin in the straw cell

wall. The effects of process parameters, such as temperature (140-220 °C), pressure (50-200 bar), and ethanol concentration (0-100% v/v), at a constant flow rate of 5 mL/min for 40 min were investigated for the simultaneous recovery of hemicellulosic sugars and phenolic compounds from straws. Subcritical water treatment at 180 °C removed large amounts of carbohydrates, mainly hemicellulosic sugars, without inducing further depolymerization of sugars. Then, pressurized aqueous ethanol (20% v/v) at 180 °C and 50 bar induced the maximum simultaneous extraction of carbohydrates (528 mg GE/g barley straw and 443 mg GE/g canola straw) and phenolics (45 mg GAE/g barley straw and 53 mg GAE/g canola straw) from the straws. The morphology analysis of the treated straw residues showed partial disruption of the outer layer and increased surface area of the treated fibers. Furthermore, increased thermal stability of the treated straw residues confirm the removal of hemicellulosic sugars and their increased cellulose content.

In depth understanding of the effects of pressurized fluid fractionation (temperatures of 140-220 °C, pressures of 50-200 bar, and ethanol concentrations of up to 100% (v/v) on the cellulose, hemicellulose and lignin contents, as well as the crystallinity, and functional groups of the pre-treated canola straw fiber were investigated using a biorefinery approach (Chapter 4). Even though treatments at high temperature of 220 °C resulted in a maximum removal of hemicelluloses, the increase in sugar degradation products such as HMF and furfural at this temperature can impact its further conversion into biofuel. Therefore, pressurized aqueous ethanol (20% v/v ethanol) at 180 °C and 50 bar was used to hydrolyze more than 60% of the initial hemicellulose mainly into soluble oligomers and monomers, and yielded a treated fiber mostly composed of 63% cellulose, 20% lignin, and others. The hydrolysis of hemicellulose led to a reduction on the xylan backbone functional groups

such as carboxylic acid, and carbonyl groups, and induced the depolymerization of lignin into soluble compounds, which further re-condensed into the enriched cellulose fiber. The improvement of crystallinity from 30 to 46% of the pre-treated straw fiber compared to untreated straw confirmed the successful fractionation process and increased cellulose content of the fiber. Then, high-intensity ultrasound was studied to disintegrate the enriched cellulose fiber into lignocellulosic nanofiber, a high-value product of biomass biorefinery. The nanofibrillation process relies on the acoustic cavitation phenomenon and the physical effects associated with it such as shear forces, shock waves, microjets and turbulence. Therefore, increasing the ultrasound theoretical specific energy from 4 to 20 kJ/g resulted in a fibrillation yield of 36 wt.% and nanofibers with an average diameter of 21 nm. The fibrillation yield value is not as high as the one reported for wheat straw nanofibrillated using a high-pressure homogenizer (56 wt.%), but higher than the reported fibrillation yield for barley, corn and oat straws (14, 26 and 31 wt.%, respectively) nanofibrillated using a high-pressure homogenizer. Furthermore, a similar value of 36 wt.% was obtained for wheat straw nanofibrillated using a grinder.

The use of high-intensity ultrasound in the nanofibrillation process has been commonly investigated in bleached cellulose fibers. Although some studies have shown that the residual lignin can be beneficial for the nanofibrillation process using other mechanical approaches, there is a lack of information in the literature on how the residual lignin of a cellulose fiber can impact the nanofibrillation process using high-intensity ultrasound. Therefore, in Chapter 5, the impact of lignin content of the enriched cellulose fiber during the nanofibrillation via high-intensity ultrasound was elucidated. The enriched cellulose fiber with 63% cellulose, 9% hemicellulose, 20% lignin, and others obtained after

pressurized fluid fractionation of canola straw, was bleached using acidified sodium chlorite at 75 °C for 2-6 h to induce oxidation of residual lignin and maximum recovery of cellulose. This bleaching process was chosen because it is a commonly applied method in laboratory and uses low chemical input (< 2 wt.%). The bleaching step induced the demethylation of lignin, and modified its aromatic structure by hydrolytic cleavage of mainly β -aryl ether linkages. This process led to a reduction of lignin content from 20 to 8%, while the cellulose content increased from 62 to 82% after 6 h bleaching. The crystallinity of the bleached fiber also increased from 46 to 68% after the removal of amorphous lignin. Furthermore, a significant improvement of the brightness, porosity, and surface area of the bleached fiber was observed mainly due to its structural change and reduced recalcitrance. Those aforementioned features of bleached fiber facilitated the mechanical nanofibrillation process using high-intensity ultrasound compared to unbleached pre-treated canola straw fiber. At an ultrasound theoretical specific energy of 20 kJ/g, unbleached fiber was nanofibrillated into lignocellulosic nanofiber with an average diameter of 21 nm, whereas the bleached fiber was nanofibrillated into cellulose nanofiber with an average diameter of 14 nm. The small diameter of cellulose nanofiber compared to lignocellulosic nanofiber indicates a higher nanofibrillation (fibrillation yield of 46 wt.%), and an increased physical entanglement between the nanofibers. The reduction of lignin content, a natural hydrophobic polymer, coupled with the small diameter of the bleached cellulose nanofiber, also increased the capacity of the nanofiber to retain water up to 80 g of water per g of sample, making it an ideal hydrogel towards biomedical applications.

The production and characterization of cellulose nanofiber hydrogels with low and high lignin contents (8 and 18%, respectively) were then investigated in Chapter 6, and

tested as scaffolds for human gingival cell culture. The high-intensity ultrasound treatment induced the self-assembling of cellulose nanofibers into hydrogels (1-2 wt.%) without the need for surface modification or cross-linkers. The hydrogels exhibited non-Newtonian properties like shear-thinning behaviour, where under deformation forces, the 3D entanglement of the nanofibers were disrupted and the hydrogel had decreased viscosity. Increasing concentration from 1 to 2 wt.% led to an increase in the dynamic moduli, favoring the formation of hydrogels with stronger network using both low and high lignin cellulose fibers. Furthermore, the *in vitro* cytocompatibility assay indicated that the residual lignin on cellulose nanofiber is nontoxic and the prepared scaffolds induced higher human gingival cell viability and proliferation than the control (2D glass slip). For the first time, cellulose nanofiber scaffolds with residual lignin content up to 18%, and without surface modification were reported as a promising material for biomedical applications. However, a challenge of the application of such a scaffold *in vivo* is its risk of microbial contamination due to blood-contacting surface of implanted scaffold, which can prevent tissue regeneration. Therefore, considerable attention has been provided to develop scaffolds with increased antimicrobial properties. In this context, a novel biomedical material using clove essential oil and cellulose nanofiber was developed via high-intensity ultrasound technology (Chapter 7).

Emulsion-filled gel with cellulose nanofiber as a continuous phase and clove essential oil (0.1, 0.5 and 1.0 wt.%) as a dispersed phase were obtained using ultrasound specific energies of 0.10, 0.17, and 0.24 kJ/g (Chapter 7). The cellulose nanofiber induced a maximum oil entrapment efficiency of 34% when 0.5 wt.% clove essential oil was added to the system. The encapsulated system had predominantly gel-like property with

maximum elastic modulus of 411 Pa. Furthermore, the emulsion-filled cellulose nanofiber hydrogels with the addition of clove essential oil up to 0.5 wt.% indicated non-cytotoxicity to human gingival fibroblast cells, and achieved cell viability of 74-101%. The newly developed clove essential oil emulsion-filled cellulose nanofiber hydrogel showed desirable cytocompatibility characteristics and can be considered as an alternative scaffold for tissue engineering applications.

Overall, throughout the research presented in this PhD thesis, canola straw biomass was refined towards value-added materials using green and emerging technologies, reducing the use of hazardous chemicals and providing a promising approach to biomass biorefinery. The high-intensity ultrasound showed to be a promising technology for nanofibrillation of either unbleached or bleached fibers that can be further explored in biomedical applications. The renewability, biodegradability and cytocompatibility of cellulose nanofibers with residual lignin content make it a promising alternative scaffold in tissue engineering. Also, the use of clove essential oil with cellulose nanofiber suggested the possible antimicrobial properties of the scaffolds towards regenerative medicine applications.

8.2. Recommendations

Further HPLC characterization of hydrolysates after pressurized fluid treatment with respect to the type of free phenolic compounds (vanillin, benzoic acid, and *trans-p*-coumaric, cinnamic and ferrulic acids) can provide a better understanding of which phenolics are predominantly present in the linkages of lignin-carbohydrate complex (LCC) in canola and barley straw biomass, and how the process parameters affect the release of those phenolic compounds (Chapter 3). The HPLC characterization of oligomers (mainly

xylooligosaccharides) and sugar monomers (glucose, xylose, arabinose, mannose and galactose) from the hemicellulose fractionation process, as well as the characterization of degradation products (HMF, furfural and organic acids) should be further quantified to design an end use of the hydrolysates after pressurized fluids processing (Chapters 3 and 4).

The separation of hemicellulose and lignin in the hydrolysate after pressurized aqueous ethanol via cold centrifugation at 4 °C or diluted acid precipitation using acetic acid or H₂SO₄ (pH ~3 at 4 °C for 12 h) can recover both components for further refinery applications (Chapter 4). Depending on the purity of the lignin that can reach up to 93%, it can be further explored as a natural antioxidant for food and pharmaceutical uses, or in biocomposite applications.

Elemental chlorine free bleaching using chlorine dioxide (0.6-2%, at 80 °C for 2 h) and/or hydrogen peroxide (1-2%, at 80 °C for 2 h) can be introduced as a more environmentally friendly approach for the bleaching step of pre-treated canola straw instead of acidified sodium chlorite (Chapter 5). Furthermore, the bleaching step could be coupled with the high-intensity ultrasound, reducing the time and the chemical intake due to the simultaneous fractionation of the fiber and increased surface area, facilitating lignin oxidation.

The use of SCCO₂ drying can be explored instead of the freeze-drying to reduce the drying time (Chapter 6). In this context, ethanol can be used as a medium during the nanofibrillation process where a straightforward drying can reduce the time of common solvent exchange steps up to 4 days prior to SCCO₂ drying. Furthermore, since the

cellulose nanofibers can be immersed in ethanol prior to drying, the sample might be technically sterile, and might be directly used for scaffolding after SCCO₂ drying.

Further studies in Chapters 6 and 7 should evaluate Brunauer-Emmett-Teller (BET) surface area, Barrett-Joyner-Halenda (BJH) pore size, and mechanical properties (e.g., tensile test, compressibility) of the aerogels used as scaffolds. Also, for the cytocompatibility test, the commercially available 3D scaffold (e.g. Matrigel™, Extracel™, Bioglass®) should be used instead of a 2D glass slip for comparison.

The antimicrobial activity of the emulsion-filled CNF hydrogel against *Porphyromonas gingivalis* and *Enterococcus faecalis* biofilms *in vitro* should be carried out to evaluate its ability to inhibit the growth of microorganisms (Chapter 7).

References

- Aamodt, J.M., & Grainger, D.W. (2016). Extracellular matrix-based biomaterial scaffolds and the host response. *Biomaterials*, *86*, 68-82.
- Aarstad, O., Heggset, E., Pedersen, I., Bjørnøy, S., Syverud, K., & Strand, B. (2017). Mechanical properties of composite hydrogels of alginate and cellulose nanofibrils. *Polymers*, *9*, 378.
- Abaide, E.R., Dotto, G.L., Tres, M.V., Zabet, G.L., & Mazutti, M.A. (2019a). Adsorption of 2-nitrophenol using rice straw and rice husks hydrolyzed by subcritical water. *Bioresource Technology*, *284*, 25-35.
- Abaide, E.R., Mortari, S.R., Ugalde, G., Valério, A., Amorim, S.M., Di Luccio, M., Moreira, R.F.P.M., Kuhn, R.C., Priamo, W.L., Tres, M.V., & Zabet, G.L. (2019b). Subcritical water hydrolysis of rice straw in a semi-continuous mode. *Journal of Cleaner Production*, *209*, 386-397.
- Abbasian, M., Massoumi, B., Mohammad-Rezaei, R., Samadian, H., & Jaymand, M. (2019). Scaffolding polymeric biomaterials: are naturally occurring biological macromolecules more appropriate for tissue engineering?. *International Journal of Biological Macromolecules*, *134*, 673-694.
- Abraham, A., Mathew, A. K., Sindhu, R., Pandey, A., & Binod, P. (2016). Potential of rice straw for bio-refining: an overview. *Bioresource Technology*, *215*, 29-36.
- Abudula, T., Saeed, U., Memic, A., Gauthaman, K., Hussain, M.A., & Al-Turaif, H. (2019). Electrospun cellulose nano fibril reinforced PLA/PBS composite scaffold for vascular tissue engineering. *Journal of Polymer Research*, *26*, 110.
- Acharjee, T.C., Jiang, Z., Haynes, R.D., & Lee, Y.Y. (2017). Evaluation of chlorine dioxide as a supplementary pretreatment reagent for lignocellulosic biomass. *Bioresource Technology*, *244*, 1049-1054.
- Ahlgren, P.A. (1970). Chlorite delignification of spruce wood. McGill University, PhD thesis, Montreal, QC, Canada, pp. 244.
- Ahlgren, P.A., & Goring, D.A.I. (1971). Removal of wood components during chlorite delignification of black spruce. *Canadian Journal of Chemistry*, *49*(8), 1272-1275.
- Ahmed, I.N., Sutanto, S., Huynh, L.H., Ismadji, S., & Ju, Y.H. (2013). Subcritical water and dilute acid pretreatments for bioethanol production from *Melaleuca leucadendron* shedding bark. *Biochemical Engineering Journal*, *78*, 44-52.
- Ajandouz, E.H., & Puigserver, A. (1999). Nonenzymatic browning reaction of essential amino acids: effect of pH on caramelization and Maillard reaction kinetics. *Journal of Agricultural and Food Chemistry*, *47*, 1786-1793.
- Akerlof, G. (1932). Dielectric constants of some organic solvent-water mixtures at various temperatures. *Journal of the American Chemical Society*, *54*, 4125-4139.
- Akpınar, O., Erdogan, K., & Bostancı, S. (2009). Production of xylooligosaccharides by controlled acid hydrolysis of lignocellulosic materials. *Carbohydrate Research*, *344*, 660-666.

- Alemdar, A., & Sain, M. (2008). Biocomposites from wheat straw nanofibers: morphology, thermal and mechanical properties. *Composites Science and Technology*, *68*, 557-565.
- Alexander, B. W., Gordon, A. H., Lomax, J. A., & Chesson, A. (1987). Composition and rumen degradability of straw from three varieties of oilseed rape before and after alkali, hydrothermal and oxidative treatment. *Journal of the Science of Food and Agriculture*, *41*, 1-15.
- Alvarez, V.H., Cahyadi, J., Xu, D., & Saldaña, M.D.A. (2014). Optimization of phytochemicals production from potato peel using subcritical water: experimental and dynamic modeling. *The Journal of Supercritical Fluids*, *90*, 8-17.
- Ardekani, N. T., Khorram, M., Zomorodian, K., Yazdanpanah, S., Veisi, H., & Veisi, H. (2019). Evaluation of electrospun poly (vinyl alcohol)-based nanofiber mats incorporated with zataria multiflora essential oil as potential wound dressing. *International Journal of Biological Macromolecules*, *125*, 743-750.
- Arruda, H.S., Silva, E.K., Pereira, G.A., Angolini, C.F.F., Eberlin, M.N., Meireles, M.A.A., & Pastore, G.M. (2019). Effects of high-intensity ultrasound process parameters on the phenolic compounds recovery from araticum peel. *Ultrasonics Sonochemistry*, *50*, 82-95.
- Ashokkumar, M. (2011). The characterization of acoustic cavitation bubbles-an overview. *Ultrasonics Sonochemistry*, *18*, 864-872.
- Bai, W., Holbery, J., & Li, K. (2009). A technique for production of nanocrystalline cellulose with a narrow size distribution. *Cellulose*, *16*, 455-465.
- Barakat, A., Monlau, F., Steyer, J.P., & Carrere, H. (2012). Effect of lignin-derived and furan compounds found in lignocellulosic hydrolysates on biomethane production. *Bioresource Technology*, *104*, 90-99.
- Batista, G., Souza, R.B., Pratto, B., dos Santos-Rocha, M.S., & Cruz, A.J. (2019). Effect of severity factor on the hydrothermal pretreatment of sugarcane straw. *Bioresource Technology*, *275*, 321-327.
- Benito-Román, Ó., Alvarez, V.H., Alonso, E., Cocero, M.J., & Saldaña, M.D.A. (2015). Pressurized aqueous ethanol extraction of β -glucans and phenolic compounds from waxy barley. *Food Research International*, *75*, 252-259.
- Benzie, I.F., & Strain, J.J. (1996). The ferric reducing ability of plasma (FRAP) as a measure of "antioxidant power": the FRAP assay. *Analytical Biochemistry*, *239*, 70-76.
- Beyer, M., Koch, H., & Fischer, K. (2005). Role of hemicelluloses in the formation of chromophores during heat treatment of bleached chemical pulps. *Macromolecular Symposia*, *232*, 98-106
- Bian, H., Chen, L., Dai, H., & Zhu, J.Y. (2017). Integrated production of lignin containing cellulose nanocrystals (LCNC) and nanofibrils (LCNF) using an easily recyclable dicarboxylic acid. *Carbohydrate Polymers*, *167*, 167-176.

- Bian, H., Wei, L., Lin, C., Ma, Q., Dai, H., & Zhu, J.Y. (2018). Lignin-containing cellulose nanofibril-reinforced polyvinyl alcohol hydrogels. *ACS Sustainable Chemistry & Engineering*, 6, 4821-4828.
- Biswas, R., Uellendahl, H., & Ahring, B.K. (2015). Wet explosion: a universal and efficient pretreatment process for lignocellulosic biorefineries. *BioEnergy Research*, 8, 1101-1116.
- Blanco, A., Monte, M. C., Campano, C., Balea, A., Merayo, N., & Negro, C. (2018). Nanocellulose for industrial use: cellulose nanofibers (CNF), cellulose nanocrystals (CNC), and bacterial cellulose (BC). In Hussain C. M. (Ed.), *Handbook of Nanomaterials for Industrial Applications* (pp. 74-126). Elsevier, New York, USA.
- Bobleter, O. (1994). Hydrothermal degradation of polymers derived from plants. *Progress in Polymer Science*, 19, 797-841.
- Boufi, S., & Chaker, A. (2016). Easy production of cellulose nanofibrils from corn stalk by a conventional high speed blender. *Industrial Crops and Products*, 93, 39-47.
- Brage, C., Eriksson, T., & Gierer, J. (1991). Reactions of chlorine dioxide with lignins in unbleached pulps, part II. *Holzforschung-International Journal of the Biology, Chemistry, Physics and Technology of Wood*, 45, 147-152.
- Brahim, M., Boussetta, N., Grimi, N., Vorobiev, E., Zieger-Devin, I., & Brosse, N. (2017). Pretreatment optimization from rapeseed straw and lignin characterization. *Industrial Crops and Products*, 95, 643-650.
- Brandt, T.A., Gschwend, F.J., Fennell, P.S., Lammens, T.M., Tan, B., Weale, J., & Hallett, J.P. (2017). An economically viable ionic liquid for the fractionation of lignocellulosic biomass. *Green Chemistry*, 19, 3078-3102.
- Buranov, A.U., & Mazza, G. (2007). Fractionation of flax shives by water and aqueous ammonia treatment in a pressurized low-polarity water extractor. *Journal of Agricultural and Food Chemistry*, 55, 8548-8555.
- Buranov, A.U., & Mazza, G. (2008). Lignin in straw of herbaceous crops. *Industrial Crops and Products*, 28, 237-259.
- Buranov, A.U., & Mazza, G. (2010). Extraction and characterization of hemicelluloses from flax shives by different methods. *Carbohydrate Polymers*, 79, 17-25.
- Buranov, A.U., Ross, K.A., & Mazza, G. (2010). Isolation and characterization of lignins extracted from flax shives using pressurized aqueous ethanol. *Bioresource Technology*, 101, 7446-7455.
- Buranov, A.U., & Mazza, G. (2012). Fractionation of flax shives with pressurized aqueous ethanol. *Industrial Crops and Products*, 35, 77-87.
- Cabeza, A., Piqueras, C.M., Sobrón, F., & García-Serna, J. (2016). Modeling of biomass fractionation in a lab-scale biorefinery: solubilization of hemicellulose and cellulose from holm oak wood using subcritical water. *Bioresource Technology*, 200, 90-102.

- Candido, R.G., & Gonçalves, A.R. (2016). Synthesis of cellulose acetate and carboxymethylcellulose from sugarcane straw. *Carbohydrate Polymers*, *152*, 679-686.
- Cao, T.L., & Song, K.B. (2019). Effects of gum karaya addition on the characteristics of loquat seed starch films containing oregano essential oil. *Food Hydrocolloids*, *97*, 105198.
- Chandrapala, J., Oliver, C., Kentish, S., & Ashokkumar, M. (2012). Ultrasonics in food processing. *Ultrasonics Sonochemistry*, *19*, 975-983.
- Chang, C., & Zhang, L. (2011). Cellulose-based hydrogels: present status and application prospects. *Carbohydrate Polymers*, *84*, 40-53.
- Chemat, F., Rombaut, N., Sicaire, A. G., Meullemiestre, A., Fabiano-Tixier, A.S., & Abert-Vian, M. (2017). Ultrasound assisted extraction of food and natural products. mechanisms, techniques, combinations, protocols and applications. a review. *Ultrasonics Sonochemistry*, *34*, 540-560.
- Chen, W., Yu, H., Liu, Y., Hai, Y., Zhang, M., & Chen, P. (2011a). Isolation and characterization of cellulose nanofibers from four plant cellulose fibers using a chemical-ultrasonic process. *Cellulose*, *18*, 433-442.
- Chen, W., Yu, H., Li, Q., Liu, Y., & Li, J. (2011b). Ultralight and highly flexible aerogels with long cellulose I nanofibers. *Soft Matter*, *7*, 10360-10368.
- Chen Z, & Wan C. (2018). Ultrafast fractionation of lignocellulosic biomass by microwave-assisted deep eutectic solvent pretreatment. *Bioresource Technology*, *250*, 532-537.
- Cheng, K.C., Huang, C.F., Wei, Y., & Hsu, S.H. (2019). Novel chitosan-cellulose nanofiber self-healing hydrogels to correlate self-healing properties of hydrogels with neural regeneration effects. *NPG Asia Materials*, *11*, 25.
- Chiaoprakobkij, N., Sanchavanakit, N., Subbalekha, K., Pavasant, P., & Phisalaphong, M. (2011). Characterization and biocompatibility of bacterial cellulose/alginate composite sponges with human keratinocytes and gingival fibroblasts. *Carbohydrate Polymers*, *85*, 548-553.
- Chiou, T.Y., Neoh, T.L., Kobayashi, T., & Adachi, S. (2012). Properties of extract obtained from defatted rice bran by extraction with aqueous ethanol under subcritical conditions. *Food Science and Technology Research*, *18*, 37-45.
- Choudhury, A.R. (2019). Synthesis and rheological characterization of a novel thermostable quick setting composite hydrogel of gellan and pullulan. *International Journal of Biological Macromolecules*, *125*, 979-988.
- Chua, M.G., & Wayman, M. (1979). Characterization of autohydrolysis aspen (*P. tremuloides*) lignins. part 1. composition and molecular weight distribution of extracted autohydrolysis lignin. *Canadian Journal of Chemistry*, *57*, 1141-1149.
- Chua, M.G., & Wayman, M. (1979). Characterization of autohydrolysis aspen (*P. tremuloides*) lignins. part 3. infrared and ultraviolet studies of extracted autohydrolysis lignin. *Canadian Journal of Chemistry*, *57*, 2603-2611.

- Ciftci, D., & Saldaña, M.D.A. (2015). Hydrolysis of sweet blue lupin hull using subcritical water technology. *Bioresource Technology*, *194*, 75-82.
- Ciftci, D., Ubeyitogullari, A., Huerta, R.R., Ciftci, O.N., Flores, R.A., & Saldaña, M.D.A. (2017). Lupin hull cellulose nanofiber aerogel preparation by supercritical CO₂ and freeze drying. *The Journal of Supercritical Fluids*, *127*, 137-145.
- Ciftci, D., Flores, R.A., & Saldaña, M.D.A. (2018). Cellulose fiber isolation and characterization from sweet blue lupin hull and canola straw. *Journal of Polymers and the Environment*, *26*, 2773-2781.
- Ciolacu, D., Rudaz, C., Vasilescu, M., & Budtova, T. (2016). Physically and chemically cross-linked cellulose cryogels: Structure, properties and application for controlled release. *Carbohydrate Polymers*, *151*, 392-400.
- Cocero, M.J., Cabeza, A., Abad, N., Adamovic, T., Vaquerizo, L., Martinez, C.M., & Pazo-Cepeda, M.V. (2018). Understanding biomass fractionation in subcritical & supercritical water. *The Journal of Supercritical Fluids*, *133*, 550-565.
- Cornejo, A., Alegria-Dallo, I., García-Yoldi, Í., Sarobe, Í., Sánchez, D., Otazu, E., Funcia, I., Gil, M.J., & Martínez-Merino, V. (2019). Pretreatment and enzymatic hydrolysis for the efficient production of glucose and furfural from wheat straw, pine and poplar chips. *Bioresource Technology*, 121583.
- Costa, A.L.R., Gomes, A., Tibolla, H., Menegalli, F.C., & Cunha, R.L. (2018). Cellulose nanofibers from banana peels as a Pickering emulsifier: high-energy emulsification processes. *Carbohydrate Polymers*, *194*, 122-131.
- Costa, S.M., Mazzola, P. G., Silva, J.C., Pahl, R., Pessoa, A., & Costa, S.A. (2013). Use of sugar cane straw as a source of cellulose for textile fiber production. *Industrial Crops and Products*, *42*, 189-194.
- Dai, L., Cheng, T., Duan, C., Zhao, W., Zhang, W., Zou, X., Aspler, J., & Ni, Y. (2018). 3D printing using plant-derived cellulose and its derivatives: a review. *Carbohydrate Polymers*, *203*, 71-86.
- Davoudpour, Y., Hossain, S., Khalil, H. A., Haafiz, M.M., Ishak, Z.M., Hassan, A., & Sarker, Z.I. (2015). Optimization of high pressure homogenization parameters for the isolation of cellulosic nanofibers using response surface methodology. *Industrial Crops and Products*, *74*, 381-387.
- Delgado-Aguilar, M., González Tovar, I., Tarrés Farrés, Q., Alcalà, M., Pèlach Serra, M. À., & Mutjé Pujol, P. (2015). Approaching a low-cost production of cellulose nanofibers for papermaking applications. *Bioresources*, *10*, 5435-5355.
- Delgado-Aguilar, M., González, I., Tarrés, Q., Pèlach, M. À., Alcalà, M., & Mutjé, P. (2016). The key role of lignin in the production of low-cost lignocellulosic nanofibres for papermaking applications. *Industrial Crops and Products*, *86*, 295-300.
- Dence, C. W. (1996). Pulp bleaching principles and practice. *TAPPI*, 812-815.
- Doench, I., Tran, T.A., David, L., Montembault, A., Viguier, E., Gorzelanny, C., Sudre, G., Cachon, T., Louback-Mohamed, M., Horbelt, N., & Peniche-Covas, C. (2019).

Cellulose nanofiber-reinforced chitosan hydrogel composites for intervertebral disc tissue repair. *Biomimetics*, 4, 19.

- Dong, H., Snyder, J.F., Williams, K.S., & Andzelm, J.W. (2013). Cation-induced hydrogels of cellulose nanofibrils with tunable moduli. *Biomacromolecules*, 14, 3338-3345.
- Du, H., Liu, W., Zhang, M., Si, C., Zhang, X., & Li, B. (2019). Cellulose nanocrystals and cellulose nanofibrils based hydrogels for biomedical applications. *Carbohydrate Polymers*, 209, 130-144.
- Dubois, M., Gilles, K.A., Hamilton, J.K., Rebers, P.T., & Smith, F. (1956). Colorimetric method for determination of sugars and related substances. *Analytical Chemistry*, 28, 350-356.
- Duque, A., Manzanares, P., Ballesteros, I., & Ballesteros, M. (2016). Steam explosion as lignocellulosic biomass pretreatment. In Mussatto, S. I. (Ed.), *Biomass Fractionation Technologies for a Lignocellulosic Feedstock Based Biorefinery* (pp. 349-368). Elsevier, New York, USA.
- Ebringerová, A., Hromádková, Z., & Heinze, T. (2005). Hemicellulose. In Heinze, T. (Ed.), *Polysaccharides i* (pp. 1-67). Springer, Berlin, Heidelberg.
- Encalada, A.M.I., Pérez, C.D., Calderón, P.A., Zukowski, E., Gerschenson, L.N., Rojas, A.M., & Fissore, E.N. (2019a). High-power ultrasound pretreatment for efficient extraction of fractions enriched in pectins and antioxidants from discarded carrots (*Daucus carota* L.). *Journal of Food Engineering*, 256, 28-36.
- Encalada, A.M.I., Pérez, C.D., Gerschenson, L.N., Rojas, A.M., & Fissore, E.N. (2019b). Gelling pectins from carrot leftovers extracted by industrial-enzymes with ultrasound pretreatment. *LWT*, 111, 640-646.
- Esparza, Y.O. (2017). Fabrication of feather keratin bio-based materials: thermoplastics and tissue engineered scaffolds. University of Alberta, PhD thesis, Edmonton, AB, Canada, pp. 275.
- Espinosa, E., Tarrés, Q., Delgado-Aguilar, M., González, I., Mutjé, P., & Rodríguez, A. (2016). Suitability of wheat straw semichemical pulp for the fabrication of lignocellulosic nanofibres and their application to papermaking slurries. *Cellulose*, 23, 837-852.
- Espinosa, E., Sánchez, R., Otero, R., Domínguez-Robles, J., & Rodríguez, A. (2017). A comparative study of the suitability of different cereal straws for lignocellulose nanofibers isolation. *International Journal of Biological Macromolecules*, 103, 990-999.
- Espinosa, E., Rol, F., Bras, J., & Rodríguez, A. (2019). Production of lignocellulose nanofibers from wheat straw by different fibrillation methods. Comparison of its viability in cardboard recycling process. *Journal of Cleaner Production*, *In press*.
- Ewulonu, C. M., Liu, X., Wu, M., & Huang, Y. (2019). Ultrasound-assisted mild sulphuric acid ball milling preparation of lignocellulose nanofibers (LCNFs) from sunflower stalks (SFS). *Cellulose*, 26, 4371-4389.

- Fakhree, M.A.A., Delgado, D.R., Martínez, F., & Jouyban, A. (2010). The importance of dielectric constant for drug solubility prediction in binary solvent mixtures: electrolytes and zwitterions in water+ ethanol. *Aaps Pharmscitech*, *11*, 1726-1729.
- Fang, Z., Sato, T., Smith Jr, R. L., Inomata, H., Arai, K., & Kozinski, J.A. (2008). Reaction chemistry and phase behavior of lignin in high-temperature and supercritical water. *Bioresource Technology*, *99*, 3424-3430.
- Farjami, T., & Madadlou, A. (2019). An overview on preparation of emulsion-filled gels and emulsion particulate gels. *Trends in Food Science & Technology*, *86*, 85-94.
- Fatah, I., Khalil, H.P.S.A., Hossain, M., Aziz, A., Davoudpour, Y., Dungani, R., & Bhat, A. (2014). Exploration of a chemo-mechanical technique for the isolation of nanofibrillated cellulosic fiber from oil palm empty fruit bunch as a reinforcing agent in composites materials. *Polymers*, *6*, 2611-2624.
- Feng, L., Jia, X., Zhu, Q., Liu, Y., Li, J., & Yin, L. (2019). Investigation of the mechanical, rheological and microstructural properties of sugar beet pectin/soy protein isolate-based emulsion-filled gels. *Food Hydrocolloids*, *89*, 813-820.
- Feng, W., Yue, C., Ni, Y. & Liang, L. (2018). Preparation and characterization of emulsion-filled gel beads for the encapsulation and protection of resveratrol and α -tocopherol. *Food Research International*, *108*, 161-171.
- Fernandes, R.V.B., Botrel, D.A., Silva, E.K., Borges, S.V., Oliveira, C.R., Yoshida, M.I., Feitosa, J.P.a., & Paula, R.C.M. (2016). Cashew gum and inulin: new alternative for ginger essential oil microencapsulation. *Carbohydrate Polymers*, *153*, 133-142.
- Fernández, D.P., Goodwin, A.R.H., Lemmon, E.W., Levelt Sengers, J.M.H., & Williams, R.C. (1997). A formulation for the static permittivity of water and steam at temperatures from 238 K to 873 K at pressures up to 1200 MPa, including derivatives and Debye-Hückel coefficients. *Journal of Physical and Chemical Reference Data*, *26*, 1125-1166.
- Flax Council of Canada. (2016). Growing flax production management & diagnostic guide 5th ed. Saskatoon: Saskatchewan Flax Development Commission.
- Flood, A.E., & Puagsa, S. (2000). Refractive index, viscosity, and solubility at 30 °C, and density at 25 °C for the system fructose+ glucose+ ethanol+ water. *Journal of Chemical & Engineering Data*, *45*, 902-907.
- France, K. J., Hoare, T., & Cranston, E. D. (2017). Review of hydrogels and aerogels containing nanocellulose. *Chemistry of Materials*, *29*, 4609-4631.
- French, A.D., & Cintrón, M.S. (2013). Cellulose polymorphy, crystallite size, and the Segal crystallinity index. *Cellulose*, *20*, 583-588.
- Fu, D., Mazza, G., & Tamaki, Y. (2010). Lignin extraction from straw by ionic liquids and enzymatic hydrolysis of the cellulosic residues. *Journal of Agricultural and Food Chemistry*, *58*, 2915-2922.
- Fu, D., & Mazza, G. (2011). Optimization of processing conditions for the pretreatment of wheat straw using aqueous ionic liquid. *Bioresource Technology*, *102*, 8003-8010.

- Gao, J., Xin, S., Wang, L., Lei, Y., Ji, H., & Liu, S. (2019). Effect of ionic liquid/inorganic salt/water pretreatment on the composition, structure and enzymatic hydrolysis of rice straw. *Bioresource Technology Reports*, 5, 355-358.
- Garrote, G., Domínguez, H., & Parajó, J.C. (2002). Interpretation of deacetylation and hemicellulose hydrolysis during hydrothermal treatments on the basis of the severity factor. *Process Biochemistry*, 37, 1067-1073.
- Garrote, G., Cruz, J.M., Domínguez, H., & Parajó, J.C. (2008). Non-isothermal autohydrolysis of barley husks: product distribution and antioxidant activity of ethyl acetate soluble fractions. *Journal of Food Engineering*, 84, 544-552.
- Gaur, R., Semwal, S., Raj, T., Lamba, B.Y., Ramu, E., Gupta, R.P., Kumar, R., & Puri, S.K. (2017). Intensification of steam explosion and structural intricacies impacting sugar recovery. *Bioresource Technology*, 241, 692-700.
- Ghaffar, S. H., Fan, M., & McVicar, B. (2015). Bioengineering for utilisation and bioconversion of straw biomass into bio-products. *Industrial Crops and Products*, 77, 262-274.
- Gierer, J. (1985). Chemistry of delignification. *Wood Science and technology*, 19, 289-312.
- Giummarella, N., & Lawoko, M. (2017). Structural insights on recalcitrance during hydrothermal hemicellulose extraction from wood. *ACS Sustainable Chemistry & Engineering*, 5, 5156-5165.
- Gogate, P. R., Shirgaonkar, I. Z., Sivakumar, M., Senthilkumar, P., Vichare, N.P., & Pandit, A.B. (2001). Cavitation reactors: efficiency assessment using a model reaction. *AIChE Journal*, 47, 2526-2538.
- Gogate, P.R., Sutkar, V.S., & Pandit, A.B. (2011). Sonochemical reactors: important design and scale up considerations with a special emphasis on heterogeneous systems. *Chemical Engineering Journal*, 166, 1066-1082.
- Gregorio, G. F., Weber, C. C., Gräsvik, J., Welton, T., Brandt, A., & Hallett, J. P. (2016). Mechanistic insights into lignin depolymerisation in acidic ionic liquids. *Green Chemistry*, 18, 5456-5465.
- Gu, F., Wang, W., Cai, Z., Xue, F., Jin, Y., & Zhu, J.Y. (2018). Water retention value for characterizing fibrillation degree of cellulosic fibers at micro and nanometer scales. *Cellulose*, 25, 2861-2871.
- Haldar, A. (2013). Subcritical water extraction of bio-molecules from lentil biomass. University of Alberta, MSc thesis, Edmonton, AB, Canada, pp. 179.
- Halder, P., Kundu, S., Patel, S., Setiawan, A., Atkin, R., Parthasarthy, R., Paz-Ferreiro, J., Surapaneni, A., & Shah, K. (2019). Progress on the pre-treatment of lignocellulosic biomass employing ionic liquids. *Renewable and Sustainable Energy Reviews*, 105, 268-292.
- Han, X., & Parker, T.L. (2017). Anti-inflammatory activity of clove (*Eugenia caryophyllata*). essential oil in human dermal fibroblasts. *Pharmaceutical Biology*, 55, 1619-1622.

- Hans, M., Kumar, S., Chandel, A. K., & Polikarpov, I. (2019). A review on bioprocessing of paddy straw to ethanol using simultaneous saccharification and fermentation. *Process Biochemistry, In press*.
- Hasanzadeh, H., Hedjazi, S., Ashori, A., Mahdavi, S., & Yousefi, H. (2014). Effects of hemicellulose pre-extraction and cellulose nanofiber on the properties of rice straw pulp. *International Journal of Biological Macromolecules*, 68, 198-204.
- Hassan, M.L., Fadel, S.M., El-Wakil, N.A., & Oksman, K. (2012). Chitosan/rice straw nanofibers nanocomposites: Preparation, mechanical, and dynamic thermomechanical properties. *Journal of Applied Polymer Science*, 125, 216-222.
- Hassan, E.A., & Hassan, M.L. (2016). Rice straw nanofibrillated cellulose films with antimicrobial properties via supramolecular route. *Industrial Crops and Products*, 93, 142-151.
- Hassan, M., Berglund, L., Hassan, E., Abou-Zeid, R., & Oksman, K. (2018). Effect of xylanase pretreatment of rice straw unbleached soda and neutral sulfite pulps on isolation of nanofibers and their properties. *Cellulose*, 25, 2939-2953.
- He, Y., Pang, Y., Liu, Y., Li, X., & Wang, K. (2008). Physicochemical characterization of rice straw pretreated with sodium hydroxide in the solid state for enhancing biogas production. *Energy & Fuels*, 22, 2775-2781.
- Heitner, C., Dimmel, D., & Schmidt, J. (2016). *Lignin and lignans: advances in chemistry*. CRC press, Florida, pp 103-136.
- Hickey, R.J., Modulevsky, D.J., Cuerrier, C.M., & Pelling, A.E. (2018). Customizing the shape and microenvironment biochemistry of biocompatible macroscopic plant-derived cellulose scaffolds. *ACS Biomaterials Science & Engineering*, 4, 3726-3736.
- Hou, X.D., Smith, T.J., Li, N., & Zong, M.H. (2012). Novel renewable ionic liquids as highly effective solvents for pretreatment of rice straw biomass by selective removal of lignin. *Biotechnology and Bioengineering*, 109, 2484-2493.
- Hou, X.D., Lin, K.P., Li, A.L., Yang, L.M., & Fu, M.H. (2018). Effect of constituents molar ratios of deep eutectic solvents on rice straw fractionation efficiency and the micro-mechanism investigation. *Industrial Crops and Products*, 120, 322-329.
- Huijgen, W.J.J., Smit, A.T., Wild, P.J., & Den Uil, H. (2012). Fractionation of wheat straw by prehydrolysis, organosolv delignification and enzymatic hydrolysis for production of sugars and lignin. *Bioresource Technology*, 114, 389-398.
- Ibrahim, M.M. (2002). Preparation of cellulose and cellulose derivative azo compounds. *Cellulose*, 9, 337-349.
- Ibrahim, M.M., Agblevor, F.A., & El-Zawawy, W.K. (2010). Isolation and characterization of cellulose and lignin from steam-exploded lignocellulosic biomass. *BioResources*, 5, 397-418.
- Immonen, K., Lahtinen, P., Isokangas, P., & Torvinen, K. (2018). Potential of hemp in thermoplastic biocomposites—the effect of fibre structure. In Fangueiro, R., Rana,

- S. (Eds.), *Advances in Natural Fibre Composites* (pp. 1-11). Springer, Basel, Switzerland.
- Isogai, A., Saito, T., & Fukuzumi, H. (2011). TEMPO-oxidized cellulose nanofibers. *Nanoscale*, *3*, 71-85.
- Jack, A.A., Nordli, H.R., Powell, L.C., Farnell, D.J., Pukstad, B., Rye, P.D., Thomas, D.W., Chinga-Carrasco, G., & Hill, K.E. (2019). Cellulose nanofibril formulations incorporating a low-molecular-weight alginate oligosaccharide modify bacterial biofilm development. *Biomacromolecules*, *20*, 2953-2961.
- Jeong, T.S., Um, B.H., Kim, J.S., & Oh, K.K. (2010). Optimizing dilute-acid pretreatment of rapeseed straw for extraction of hemicellulose. *Applied Biochemistry and Biotechnology*, *161*, 22-33.
- Jiang, F., & Hsieh, Y.L. (2013). Chemically and mechanically isolated nanocellulose and their self-assembled structures. *Carbohydrate Polymers*, *95*, 32-40.
- Jiang, Y., Liu, X., Yang, Q., Song, X., Qin, C., Wang, S., & Li, K. (2018). Effects of residual lignin on mechanical defibrillation process of cellulosic fiber for producing lignocellulose nanofibrils. *Cellulose*, *25*, 6479-6494.
- Jiang, Y., Liu, X., Yang, Q., Song, X., Qin, C., Wang, S., & Li, K. (2019). Effects of residual lignin on composition, structure and properties of mechanically defibrillated cellulose fibrils and films. *Cellulose*, *26*, 1577-1593.
- Jiang, Z., Yi, J., Li, J., He, T., & Hu, C. (2015). Promoting effect of sodium chloride on the solubilization and depolymerization of cellulose from raw biomass materials in water. *ChemSusChem*, *8*, 1901-1907.
- Jin, A.X., Ren, J.L., Peng, F., Xu, F., Zhou, G. Y., Sun, R.C, & Kennedy, J.F. (2009). Comparative characterization of degraded and non-degradative hemicelluloses from barley straw and maize stems: composition, structure, and thermal properties. *Carbohydrate Polymers*, *78*, 609-619.
- Joelsson, E., Erdei, B., Galbe, M., & Wallberg, O. (2016). Techno-economic evaluation of integrated first-and second-generation ethanol production from grain and straw. *Biotechnology for Biofuels*, *9*, 1.
- Jonoobi, M., Harun, J., Tahir, P. M., Shakeri, A., SaifulAzry, S., & Makinejad, M.D. (2011). Physicochemical characterization of pulp and nanofibers from kenaf stem. *Materials Letters*, *65*, 1098-1100.
- Kabirian, F., Milan, P.B., Zamanian, A., Heying, R., & Mozafari, M. (2019). Nitric oxide-releasing vascular grafts: a therapeutic strategy to promote angiogenic activity and endothelium regeneration. *Acta Biomaterialia*, *92*, 82-91.
- Kargarzadeh, H., Ioelovich, M., Ahmad, I., Thomas, S., & Dufresne, A. (2017). Methods for extraction of nanocellulose from various sources. *Handbook of Nanocellulose and Cellulose Nanocomposites* (pp. 1-49). Wiley-VCH, Weinheim, Germany.
- Karimi, K., Kheradmandinia, S., & Taherzadeh, M.J. (2006). Conversion of rice straw to sugars by dilute-acid hydrolysis. *Biomass and Bioenergy*, *30*, 247-253.

- Kaushik, A., Singh, M., & Verma, G. (2010). Green nanocomposites based on thermoplastic starch and steam exploded cellulose nanofibrils from wheat straw. *Carbohydrate Polymers*, 82, 337-345.
- Kentish, S., & Ashokkumar, M. (2011). The physical and chemical effects of ultrasound. In Feng, H., Barbosa-Canovas, G., Weiss, J. (Eds.), *Ultrasound Technologies for Food and Bioprocessing* (pp. 1-12). Springer, New York, USA.
- Khalid, A., Khan, R., Ul-Islam, M., Khan, T., & Wahid, F. (2017). Bacterial cellulose-zinc oxide nanocomposites as a novel dressing system for burn wounds. *Carbohydrate Polymers*, 164, 214-221.
- Khalil, H.A., Davoudpour, Y., Islam, M.N., Mustapha, A., Sudesh, K., Dungani, R., & Jawaid, M. (2014). Production and modification of nanofibrillated cellulose using various mechanical processes: a review. *Carbohydrate Polymers*, 99, 649-665.
- Kim, H.J., Oh, D.X., Choy, S., Nguyen, H.L., Cha, H.J., & Hwang, D.S. (2018). 3D cellulose nanofiber scaffold with homogeneous cell population and long-term proliferation. *Cellulose*, 25, 7299-7314.
- Kim, I., Lee, B., Park, J. Y., Choi, S.A., & Han, J.I. (2014). Effect of nitric acid on pretreatment and fermentation for enhancing ethanol production of rice straw. *Carbohydrate Polymers*, 99, 563-567.
- Kim, K.H., Dutta, T., Walter, E.D., Isern, N.G., Cort, J.R., Simmons, B.A., & Singh, S. (2017). Chemoselective methylation of phenolic hydroxyl group prevents quinone methide formation and repolymerization during lignin depolymerization. *ACS Sustainable Chemistry & Engineering*, 5, 3913-3919.
- Kim, S.B., Lee, J.H., Oh, K.K., Lee, S.J., Lee, J.Y., Kim, J.S., & Kim, S.W. (2011). Dilute acid pretreatment of barley straw and its saccharification and fermentation. *Biotechnology and Bioprocess Engineering*, 16, 725.
- Kim, T.H., & Lee, Y.Y. (2006). Fractionation of corn stover by hot-water and aqueous ammonia treatment. *Bioresource Technology*, 97, 224-232.
- Kobus, Z., & Kusinska, E. (2008). Influence of physical properties of liquid on acoustic power of ultrasonic processor. *TEKA Kom Mot Energy Roln*, 8, 71-78.
- Koopaie, M. (2019). Scaffolds for gingival tissues. In Mozafari, M., Sefat, F., Atala, A. (Eds.), *Handbook of Tissue Engineering Scaffolds* (pp. 521-543). Elsevier, New York, USA.
- Koshani, R., & Jafari, S.M. (2019). Ultrasound-assisted preparation of different nanocarriers loaded with food bioactive ingredients. *Advances in Colloid and Interface Science*, 270, 123-146.
- Kruse, A., & Dinjus, E. (2007). Hot compressed water as reaction medium and reactant: properties and synthesis reactions. *The Journal of Supercritical Fluids*, 39, 362-380.
- Laurén, P., Somersalo, P., Pitkänen, I., Lou, Y.R., Urtti, A., Partanen, J., Seppälä, J., Madetoja, M., Laaksonen, T., Mäkitie, A., & Yliperttula, M. (2017). Nanofibrillar cellulose-alginate hydrogel coated surgical sutures as cell-carrier systems. *PLoS One*, 12.

- Lavoine, N., Desloges, I., Dufresne, A., & Bras, J. (2012). Microfibrillated cellulose-its barrier properties and applications in cellulosic materials: a review. *Carbohydrate Polymers*, *90*, 735-764.
- Leonelli, C., & Mason, T. J. (2010). Microwave and ultrasonic processing: now a realistic option for industry. *Chemical Engineering and Processing: Process Intensification*, *49*, 885-900.
- Troedec, M.L., Sedan, D., Peyratout, C., Bonnet, J.P., Smith, A., Guinebretiere, R., Gloaguen, V., & Krausz, P. (2008). Influence of various chemical treatments on the composition and structure of hemp fibres. *Composites Part A: Applied Science and Manufacturing*, *39*, 514-522.
- Li, J., Henriksson, G., & Gellerstedt, G. (2007). Lignin depolymerization/repolymerization and its critical role for delignification of aspen wood by steam explosion. *Bioresource Technology*, *98*, 3061-3068.
- Li, M.K., & Fogler, H.S. (1978). Acoustic emulsification. Part 2. Breakup of the large primary oil droplets in a water medium. *Journal of Fluid Mechanics*, *88*, 513-528.
- Li, Q., Xie, B., Wang, Y., Wang, Y., Peng, L., Li, Y., Li, B., & Liu, S. (2019). Cellulose nanofibrils from miscanthus floridulus straw as green particle emulsifier for O/W pickering emulsion. *Food Hydrocolloids*, *97*, 105214.
- Li, Z., Lv, X., Chen, S., Wang, B., Feng, C., Xu, Y., & Wang, H. (2016). Improved cell infiltration and vascularization of three-dimensional bacterial cellulose nanofibrous scaffolds by template biosynthesis. *RSC Advances*, *6*, 42229-42239.
- Liakos, I., Rizzello, L., Hajiali, H., Brunetti, V., Carzino, R., Pompa, P.P., Athanassiou, A., & Mele, E. (2015). Fibrous wound dressings encapsulating essential oils as natural antimicrobial agents. *Journal of Materials Chemistry B*, *3*, 1583-1589.
- Lin, N., & Dufresne, A. (2014). Nanocellulose in biomedicine: current status and future prospect. *European Polymer Journal*, *59*, 302-325.
- Liu, C.F., Xu, F., Sun, J.X., Ren, J.L., Curling, S., Sun, R.C., Fowler, P., & Baird, M.S., (2006). Physicochemical characterization of cellulose from perennial ryegrass leaves (*lolium perenne*). *Carbohydrate Research*, *341*, 2677-2687.
- Liu, Q., Lu, Y., Aguedo, M., Jacquet, N., Ouyang, C., He, W., Yan, C., Bai, W., Guo, R., Goffin, D., & Song, J., (2017). Isolation of high-purity cellulose nanofibers from wheat straw through the combined environmentally friendly methods of steam explosion, microwave-assisted hydrolysis, and microfluidization. *ACS Sustainable Chemistry & Engineering*, *5*, 6183-6191.
- Liu, R., Yu, H., & Huang, Y. (2005). Structure and morphology of cellulose in wheat straw. *Cellulose*, *12*, 25-34.
- Liu, X., Li, Y., Ewulonu, C.M., Ralph, J., Xu, F., Zhang, Q., Wu, M., & Huang, Y. (2019). Mild alkaline pretreatment for isolation of native-like lignin and lignin-containing cellulose nanofibers (LCNF) from crop waste. *ACS Sustainable Chemistry & Engineering*, *7*, 14135-14142.

- López-Linares, J. C., Cara, C., Moya, M., Ruiz, E., Castro, E., & Romero, I. (2013). Fermentable sugar production from rapeseed straw by dilute phosphoric acid pretreatment. *Industrial Crops and Products*, *50*, 525-531.
- López-Linares, J. C., Ballesteros, I., Tourán, J., Cara, C., Castro, E., Ballesteros, M., & Romero, I. (2015). Optimization of uncatalyzed steam explosion pretreatment of rapeseed straw for biofuel production. *Bioresource Technology*, *190*, 97-105.
- Lu, X., Zhang, Y., & Angelidaki, I. (2009). Optimization of H₂SO₄-catalyzed hydrothermal pretreatment of rapeseed straw for bioconversion to ethanol: focusing on pretreatment at high solids content. *Bioresource Technology*, *100*, 3048-3053.
- Luo, H., Cha, R., Li, J., Hao, W., Zhang, Y., & Zhou, F. (2019). Advances in tissue engineering of nanocellulose-based scaffolds: a review. *Carbohydrate Polymers*, 115144.
- Mamvura, T.A., Iyuke, S.E., & Paterson, A.E. (2018). Energy changes during use of high-power ultrasound on food grade surfaces. *South African Journal of Chemical Engineering*, *25*, 62-73.
- Markstedt, K., Mantas, A., Tournier, I., Martínez Ávila, H., Hägg, D., & Gatenholm, P. (2015). 3D bioprinting human chondrocytes with nanocellulose-alginate bioink for cartilage tissue engineering applications. *Biomacromolecules*, *16*, 1489-1496.
- Marshall, W.L., & Franck, E.U. (1981). Ion product of water substance, 0-1000 C, 1-10,000 bars new international formulation and its background. *Journal of Physical and Chemical Reference Data*, *10*, 295-304.
- Martelli-Tosi, M., Masson, M.M., Silva, N.C., Esposto, B.S., Barros, T.T., Assis, O.B., & Tapia-Blácido, D.R. (2018). Soybean straw nanocellulose produced by enzymatic or acid treatment as a reinforcing filler in soy protein isolate films. *Carbohydrate Polymers*, *198*, 61-68.
- Martinez-Abad, A., Giummarella, N., Lawoko, M., & Vilaplana, F. (2018). Differences in extractability under subcritical water reveal interconnected hemicellulose and lignin recalcitrance in birch hardwoods. *Green Chemistry*, *20*, 2534-2546.
- Martoia F., Cochereau T., Dumont P.J.J., Orgéas L., Terrien M., & Belgacem M.N. (2016). Cellulose nanofibril foams: links between ice-templating conditions, microstructures and mechanical properties. *Materials & Design*, *104*, 376-391.
- Mason, T.J., Lorimer, J.P., Bates, D.M., & Zhao, Y. (1994). Dosimetry in sonochemistry: the use of aqueous terephthalate ion as a fluorescence monitor. *Ultrasonics Sonochemistry*, *1*, S91-S95.
- McClements, D.J. (2002). Theoretical prediction of emulsion color. *Advances in Colloid and Interface Science*, *97*, 63-89.
- McDonough, T.J. (1993). The chemistry of organosolv delignification. *TAPPI* *76*, 186-193.
- Meier, H. (1962). Chemical and morphological aspects of the fine structure of wood. *Pure and Applied Chemistry*, *5*, 37-52.

- Mertaniemi, H., Escobedo-Lucea, C., Sanz-Garcia, A., Gandía, C., Mäkitie, A., Partanen, J., Ikkala, O., & Yliperttula, M. (2016). Human stem cell decorated nanocellulose threads for biomedical applications. *Biomaterials*, *82*, 208-220.
- Mesa, L., Albornas, Y., Morales, M., Corsano, G., & González, E. (2016). Integration of organosolv process for biomass pretreatment in a biorefinery. In Mussatto, S. I. (Ed.), *Biomass Fractionation Technologies for a Lignocellulosic Feedstock Based Biorefinery* (pp. 229-254). Elsevier, New York, USA.
- Moberg T., Sahlin K., Yao K., Geng S., Westman G., Zhou Q., Oksman K., & Rigdahl M. (2017). Rheological properties of nanocellulose suspensions: effects of fibril/particle dimensions and surface characteristics. *Cellulose*, *24*, 2499-2510.
- Monschein, M., & Nidetzky, B. (2016). Effect of pretreatment severity in continuous steam explosion on enzymatic conversion of wheat straw: evidence from kinetic analysis of hydrolysis time courses. *Bioresource Technology*, *200*, 287-296.
- Morone, A., Chakrabarti, T., & Pandey, R.A. (2017). Assessment of alkaline peroxide-assisted wet air oxidation pretreatment for rice straw and its effect on enzymatic hydrolysis. *Cellulose*, *24*, 4885-4898.
- Morone, A., Chakrabarti, T., & Pandey, R.A. (2018). Effect of chemical input during wet air oxidation pretreatment of rice straw in reducing biomass recalcitrance and enhancing cellulose accessibility. *Korean Journal of Chemical Engineering*, *35*, 2403-2412.
- Motasemi, F., & Afzal, M.T. (2013). A review on the microwave-assisted pyrolysis technique. *Renewable and Sustainable Energy Reviews*, *28*, 317-330.
- Mueller-Harvey, I., Hartley, R.D., Harris, P.J., & Curzon, E.H. (1986). Linkage of p-coumaroyl and feruloyl groups to cell-wall polysaccharides of barley straw. *Carbohydrate Research*, *148*, 71-85.
- Nabarlantz, D., Farriol, X., & Montané, D. (2004). Kinetic modeling of the autohydrolysis of lignocellulosic biomass for the production of hemicellulose-derived oligosaccharides. *Industrial & Engineering Chemistry Research*, *43*, 4124-4131.
- Nabarlantz, D., Ebringerová, A., & Montané, D. (2007). Autohydrolysis of agricultural by-products for the production of xylo-oligosaccharides. *Carbohydrate Polymers*, *69*, 20-28.
- Nair, S.S., & Yan, N. (2015). Effect of high residual lignin on the thermal stability of nanofibrils and its enhanced mechanical performance in aqueous environments. *Cellulose*, *22*, 3137-3150.
- Nakasone, K., & Kobayashi, T. (2016). Cytocompatible cellulose hydrogels containing trace lignin. *Materials Science and Engineering: C*, *64*, 269-277.
- Nam, S., French, A. D., Condon, B. D., & Concha, M. (2016). Segal crystallinity index revisited by the simulation of X-ray diffraction patterns of cotton cellulose I β and cellulose II. *Carbohydrate Polymers*, *135*, 1-9.
- Naseri, N., Poirier, J.M., Girandon, L., Fröhlich, M., Oksman, K., & Mathew, A.P. (2016). 3-Dimensional porous nanocomposite scaffolds based on cellulose nanofibers for

- cartilage tissue engineering: tailoring of porosity and mechanical performance. *Rsc Advances*, 6, 5999-6007.
- Nazari, B., Kumar, V., Bousfield, D.W., & Toivakka, M. (2016). Rheology of cellulose nanofibers suspensions: boundary driven flow. *Journal of Rheology*, 60, 1151-1159.
- Nechyporchuk, O., Belgacem, M.N., & Bras, J. (2016). Production of cellulose nanofibrils: a review of recent advances. *Industrial Crops and Products*, 93, 2-25.
- Ni, Y., Shen, X., & Van Heiningen, A.R.P. (1994). Studies on the reactions of phenolic and non-phenolic lignin model compounds with chlorine dioxide. *Journal of Wood Chemistry and Technology*, 14, 243-262.
- Ni, Y., & Hu, Q. (1995). Alcell® lignin solubility in ethanol-water mixtures. *Journal of Applied Polymer Science*, 57, 1441-1446.
- Nishino, T., Takano, K., & Nakamae, K. (1995). Elastic modulus of the crystalline regions of cellulose polymorphs. *Journal of Polymer Science Part B: Polymer Physics*, 33, 1647-1651.
- Nishiyama, Y., Langan, P., & Chanzy, H. (2002). Crystal structure and hydrogen-bonding system in cellulose I β from synchrotron X-ray and neutron fiber diffraction. *Journal of the American Chemical Society*, 124, 9074-9082.
- Nishiyama, Y., Sugiyama, J., Chanzy, H., & Langan, P. (2003). Crystal structure and hydrogen bonding system in cellulose I α from synchrotron X-ray and neutron fiber diffraction. *Journal of the American Chemical Society*, 125, 14300-14306.
- Nourbehesht, N., Shekarchizadeh, H., & Soltanzadeh, N. (2018). Investigation of stability, consistency, and oil oxidation of emulsion filled gel prepared by inulin and rice bran oil using ultrasonic radiation. *Ultrasonics Sonochemistry*, 42, 585-593.
- Nuopponen, M., Vuorinen, T., Jämsä, S., & Viitaniemi, P. (2005). Thermal modifications in softwood studied by FT-IR and UV resonance Raman spectroscopies. *Journal of Wood Chemistry and Technology*, 24, 13-26.
- Nuruddin, M., Hosur, M., Uddin, M. J., Baah, D., & Jeelani, S. (2016). A novel approach for extracting cellulose nanofibers from lignocellulosic biomass by ball milling combined with chemical treatment. *Journal of Applied Polymer Science*, 133.
- Okano, T., & Sarko, A. (1985). Mercerization of cellulose. II. Alkali-cellulose intermediates and a possible mercerization mechanism. *Journal of Applied Polymer Science*, 30, 325-332.
- Oliver, L., Berndsen, L., van Aken, G.A., & Scholten, E. (2015). Influence of droplet clustering on the rheological properties of emulsion-filled gels. *Food Hydrocolloids*, 50, 74-83.
- Oliver, L., Wieck, L., & Scholten, E. (2016). Influence of matrix inhomogeneity on the rheological properties of emulsion-filled gels. *Food Hydrocolloids*, 52, 116-125.
- Pääkkö, M., Ankerfors, M., Kosonen, H., Nykänen, A., Ahola, S., Österberg, M., Ruokolainen, J., Laine, J., Larsson, P.T., Ikkala, O., & Lindström, T. (2007). Enzymatic hydrolysis combined with mechanical shearing and high-pressure

homogenization for nanoscale cellulose fibrils and strong gels. *Biomacromolecules*, 8, 1934-1941.

- Pacaphol, K., & Aht-Ong, D. (2017). Preparation of hemp nanofibers from agricultural waste by mechanical defibrillation in water. *Journal of Cleaner Production*, 142, 1283-1295.
- Pant, J., Sundaram, J., Goudie, M.J., Nguyen, D.T., & Handa, H. (2019). Antibacterial 3D bone scaffolds for tissue engineering application. *Journal of Biomedical Materials Research Part B: Applied Biomaterials*, 107, 1068-1078.
- Paradiso, V. M., Giarnetti, M., Summo, C., Pasqualone, A., Minervini, F., & Caponio, F. (2015). Production and characterization of emulsion filled gels based on inulin and extra virgin olive oil. *Food Hydrocolloids*, 45, 30-40.
- Park, S., Baker, J.O., Himmel, M.E., Parilla, P.A., & Johnson, D.K. (2010). Cellulose crystallinity index: measurement techniques and their impact on interpreting cellulase performance. *Biotechnology for Biofuels*, 3, 10.
- Perdih, T.S., Zupanc, M., & Dular, M. (2019). Revision of the mechanisms behind oil-water (O/W) emulsion preparation by ultrasound and cavitation. *Ultrasonics Sonochemistry*, 51, 298-304.
- Petroudy, S.R.D., Ranjbar, J., & Garmaroody, E.R. (2018). Eco-friendly superabsorbent polymers based on carboxymethyl cellulose strengthened by TEMPO-mediated oxidation wheat straw cellulose nanofiber. *Carbohydrate Polymers*, 197, 565-575.
- Pokhrel, N., Vabbina, P.K., & Pala, N. (2016). Sonochemistry: science and engineering. *Ultrasonics Sonochemistry*, 29, 104-128.
- Prakobna, K., Kisonen, V., Xu, C., & Berglund, L.A. (2015). Strong reinforcing effects from galactoglucomannan hemicellulose on mechanical behavior of wet cellulose nanofiber gels. *Journal of Materials Science*, 50, 7413-7423.
- Pronyk, C., & Mazza, G. (2012). Fractionation of triticale, wheat, barley, oats, canola, and mustard straws for the production of carbohydrates and lignins. *Bioresource Technology*, 106, 117-124.
- Qiang, Z., & Thomsen, A.B. (2012). Effect of different wet oxidation pretreatment conditions on ethanol fermentation from corn stover. In Zhu, E. & Sambath, S. (Eds.), *Information Technology and Agricultural Engineering* (pp. 953-958). Springer, Berlin, Heidelberg.
- Quraishi, S., Martins, M., Barros, A.A., Gurikov, P., Raman, S.P., Smirnova, I., Duarte, A.R.C., & Reis, R.L. (2015). Novel non-cytotoxic alginate-lignin hybrid aerogels as scaffolds for tissue engineering. *The Journal of Supercritical Fluids*, 105, 1-8.
- Rashad, A., Suliman, S., Mustafa, M., Pedersen, T.Ø., Campodoni, E., Sandri, M., Syverud, K., & Mustafa, K. (2019). Inflammatory responses and tissue reactions to wood-based nanocellulose scaffolds. *Materials Science and Engineering: C*, 97, 208-221.
- Raut, J.S., & Karuppayil, S.M. (2014). A status review on the medicinal properties of essential oils. *Industrial Crops and Products*, 62, 250-264.

- Ren, H., Zong, M.H., Wu, H., & Li, N. (2016). Utilization of seawater for the biorefinery of lignocellulosic biomass: ionic liquid pretreatment, enzymatic hydrolysis, and microbial lipid production. *ACS Sustainable Chemistry & Engineering*, 4, 5659-5666.
- Ren, J. L., & Sun, R. C. (2010). Hemicelluloses. In Sun, R.C. (Ed.), *Cereal Straw as a Resource for Sustainable Biomaterials and Biofuels* (pp. 73-130). Elsevier, New York, USA.
- Richa, Choudhury, A.R. (2019). Synthesis and rheological characterization of a novel thermostable quick setting composite hydrogel of gellan and pullulan. *International Journal of Biological Macromolecules*, 125, 979-988.
- Rodrigues, R.C.L.B., Rocha, G.J., Rodrigues, D., Filho, H.J.I., Graças, M.A.F., & Pessoa, A. (2010). Scale-up of diluted sulfuric acid hydrolysis for producing sugarcane bagasse hemicellulosic hydrolysate (SBHH). *Bioresource Technology*, 101, 1247-1253.
- Royo, E., Peresin, M. S., Sampson, W.W., Hoeger, I.C., Vartiainen, J., Laine, J., & Rojas, O.J. (2015). Comprehensive elucidation of the effect of residual lignin on the physical, barrier, mechanical and surface properties of nanocellulose films. *Green Chemistry*, 17, 1853-1866.
- Rol, F., Belgacem, M.N., Gandini, A., & Bras, J. (2018). Recent advances in surface-modified cellulose nanofibrils. *Progress in Polymer Science*, 88, 241-264.
- Rosatella, A.A., Simeonov, S.P., Frade, R.F., & Afonso, C.A. (2011). 5-Hydroxymethylfurfural (HMF) as a building block platform: biological properties, synthesis and synthetic applications. *Green Chemistry*, 13, 754-793.
- Saito, T., & Isogai, A. (2004). TEMPO-mediated oxidation of native cellulose. The effect of oxidation conditions on chemical and crystal structures of the water-insoluble fractions. *Biomacromolecules*, 5, 1983-1989.
- Saito, T., Nishiyama, Y., Putaux, J.L., Vignon, M., & Isogai, A. (2006). Homogeneous suspensions of individualized microfibrils from TEMPO-catalyzed oxidation of native cellulose. *Biomacromolecules*, 7, 1687-1691.
- Saito, T., Hirota, M., Tamura, N., Kimura, S., Fukuzumi, H., Heux, L., & Isogai, A. (2009). Individualization of nano-sized plant cellulose fibrils by direct surface carboxylation using TEMPO catalyst under neutral conditions. *Biomacromolecules*, 10, 1992-1996.
- Sanandiyaa, N.D., Vasudevan, J., Das, R., Lim, C.T., & Fernandez, J.G. (2019). Stimuli-responsive injectable cellulose thixogel for cell encapsulation. *International Journal of Biological Macromolecules*, 130, 1009-1017.
- Sánchez, R., Espinosa, E., Domínguez-Robles, J., Loaiza, J.M., & Rodríguez, A. (2016). Isolation and characterization of lignocellulose nanofibers from different wheat straw pulps. *International Journal of Biological Macromolecules*, 92, 1025-1033.
- Sannigrahi, P., Kim, D.H., Jung, S., & Ragauskas, A. (2011). Pseudo-lignin and pretreatment chemistry. *Energy & Environmental Science*, 4, 1306-1310.

- Sarkar, S., Alvarez, V.H., & Saldaña, M.D.A. (2014). Relevance of ions in pressurized fluid extraction of carbohydrates and phenolics from barley hull. *The Journal of Supercritical Fluids*, 93, 27-37.
- Sasaki, M., Fang, Z., Fukushima, Y., Adschiri, T., & Arai, K. (2000). Dissolution and hydrolysis of cellulose in subcritical and supercritical water. *Industrial & Engineering Chemistry Research*, 39, 2883-2890.
- Satlewal, A., Agrawal, R., Bhagia, S., Sangoro, J., & Ragauskas, A.J. (2018). Natural deep eutectic solvents for lignocellulosic biomass pretreatment: recent developments, challenges and novel opportunities. *Biotechnology Advances*, 36, 2032-2050.
- Sato, Y., Kusaka, Y., & Kobayashi, M. (2017). Charging and aggregation behavior of cellulose nanofibers in aqueous solution. *Langmuir*, 33, 12660-12669.
- Schröder, T., Lauven, L.P., Sowlati, T., & Geldermann, J. (2019). Strategic planning of a multi-product wood-biorefinery production system. *Journal of Cleaner Production*, 211, 1502-1516.
- Segal, L. Creely, J.J., Martin Jr, A.E., & Conrad, C.M. (1959). An empirical method for estimating the degree of crystallinity of native cellulose using the X-ray diffractometer. *Textile Research Journal*, 29, 786-794.
- Sharma, S., Kumar, R., Gaur, R., Agrawal, R., Gupta, R.P., Tuli, D.K., & Das, B. (2015). Pilot scale study on steam explosion and mass balance for higher sugar recovery from rice straw. *Bioresource Technology*, 175, 350-357.
- Shin, S., Park, S., Park, M., Jeong, E., Na, K., Youn, H.J., & Hyun, J. (2017). Cellulose nanofibers for the enhancement of printability of low viscosity gelatin derivatives. *BioResources*, 12, 2941-2954.
- Sievers, C., Marzalletti, T., Hoskins, T.J., Olarte, M.B.V., Agrawal, P.K., & Jones, C.W. (2009). Quantitative solid state NMR analysis of residues from acid hydrolysis of loblolly pine wood. *Bioresource Technology*, 100, 4758-4765.
- Zabot, G.L., Silva, E.K., Azevedo, V. M., & Meireles, M.A.A. (2016). Replacing modified starch by inulin as prebiotic encapsulant matrix of lipophilic bioactive compounds. *Food Research International*, 85, 26-35.
- Singleton, V.L., & Rossi, J.A. (1965). Colorimetry of total phenolics with phosphomolybdic-phosphotungstic acid reagents. *American journal of Enology and Viticulture*, 16, 144-158.
- Siqueira, P., Siqueira, É., Lima, A.E., Siqueira, G., Pinzón-Garcia, A.D., Lopes, A.P., Segura, M.E.C., Isaac, A., Pereira, F.V., & Botaro, V.R. (2019). Three-dimensional stable alginate-nanocellulose gels for biomedical applications: towards tunable mechanical properties and cell growing. *Nanomaterials*, 9, 78.
- Sluiter, A., Hames, B., Ruiz, R., Scarlata, C., Sluiter, J., Templeton, D., & Crocker, D. (2008). Determination of structural carbohydrates and lignin in biomass. *Laboratory Analytical Procedure*, 1617, 1-16.
- Soni, B., & Mahmoud, B. (2015). Chemical isolation and characterization of different cellulose nanofibers from cotton stalks. *Carbohydrate Polymers*, 134, 581-589.

- Spence, K.L., Venditti, R.A., Rojas, O.J., Habibi, Y., & Pawlak, J.J. (2011). A comparative study of energy consumption and physical properties of microfibrillated cellulose produced by different processing methods. *Cellulose*, *18*, 1097-1111.
- Suenaga, S., & Osada, M. (2018). Self-sustaining cellulose nanofiber hydrogel produced by hydrothermal gelation without additives. *ACS Biomaterials Science & Engineering*, *4*, 1536-1545.
- Sun, R.C., Lawther, J.M., & Banks, W.B. (1996). Fractional and structural characterization of wheat straw hemicelluloses. *Carbohydrate Polymers*, *29*, 325-331.
- Sun, R.C., Lawther, J.M., & Banks, W.B. (1998). Isolation and characterization of hemicellulose B and cellulose from pressure refined wheat straw. *Industrial Crops and Products*, *7*, 121-128.
- Sun, R.C., & Tomkinson, J. (2000). Essential guides for isolation/purification of polysaccharides. *Encyclopedia of Separation Science*, 4568-4574.
- Sun, R.C., Tomkinson, J., & Jones, G.L. (2000). Fractional characterization of ash-AQ lignin by successive extraction with organic solvents from oil palm EFB fibre. *Polymer Degradation and Stability*, *68*, 111-119.
- Sun, R.C., Sun, X. F., Wang, S. Q., Zhu, W., & Wang, X.Y. (2002). Ester and ether linkages between hydroxycinnamic acids and lignins from wheat, rice, rye, and barley straws, maize stems, and fast-growing poplar wood. *Industrial Crops and Products*, *15*, 179-188.
- Sun, J.X., Sun, X.F., Sun, R.C., & Su, Y.Q. (2004). Fractional extraction and structural characterization of sugarcane bagasse hemicelluloses. *Carbohydrate Polymers*, *56*, 195-204.
- Sun, Y., & Cheng, J. (2002). Hydrolysis of lignocellulosic materials for ethanol production: a review. *Bioresource technology*, *83*, 1-11.
- Sun, Y., Liu, D., Chen, J., Ye, X., & Yu, D. (2011). Effects of different factors of ultrasound treatment on the extraction yield of the all-trans- β -carotene from citrus peels. *Ultrasonics Sonochemistry*, *18*, 243-249.
- Suslick, K.S., Eddingsaas, N.C., Flannigan, D.J., Hopkins, S.D., & Xu, H. (2011). Extreme conditions during multibubble cavitation: sonoluminescence as a spectroscopic probe. *Ultrasonics Sonochemistry*, *18*, 842-846.
- Svärd, A., Moriana, R., Brännvall, E., & Edlund, U. (2018). Rapeseed straw biorefinery process. *ACS Sustainable Chemistry & Engineering*, *7*, 790-801.
- Takada, M., Minami, E., & Saka, S. (2018). Decomposition behaviors of the lignocellulosics as treated by semi-flow hot-compressed water. *The Journal of Supercritical Fluids*, *133*, 566-572.
- Tanaka, R., Saito, T., Hondo, H., & Isogai, A. (2015). Influence of flexibility and dimensions of nanocelluloses on the flow properties of their aqueous dispersions. *Biomacromolecules*, *16*, 2127-2131.

- Tarrés, Q., Ehman, N.V., Vallejos, M.E., Area, M.C., Delgado-Aguilar, M., & Mutjé, P. (2017). Lignocellulosic nanofibers from triticale straw: the influence of hemicelluloses and lignin in their production and properties. *Carbohydrate Polymers*, *163*, 20-27.
- Toivonen, M.S., Kurki-Suonio, S., Schacher, F.H., Hietala, S., Rojas, O.J., & Ikkala, O. (2015). Water-resistant, transparent hybrid nanopaper by physical cross-linking with chitosan. *Biomacromolecules*, *16*, 1062-1071.
- Torres, O., Murray, B., & Sarkar, A. (2016). Emulsion microgel particles: novel encapsulation strategy for lipophilic molecules. *Trends in Food Science & Technology*, *55*, 98-108.
- Tovar-Carrillo, K.L., Nakasone, K., Sugita, S., Tagaya, M., & Kobayashi, T. (2014). Effects of sodium hypochlorite on agave tequilana weber bagasse fibers used to elaborate cyto and biocompatible hydrogel films. *Materials Science and Engineering: C*, *42*, 808-815.
- Turek, C., & Stintzing, F.C. (2013). Stability of essential oils: a review. *Comprehensive Reviews in Food Science and Food Safety*, *12*, 40-53.
- Turnbull, G., Clarke, J., Picard, F., Riches, P., Jia, L., Han, F., Li, B. & Shu, W. (2018). 3D bioactive composite scaffolds for bone tissue engineering. *Bioactive Materials*, *3*, 278-314.
- Vanda, H., Dai, Y., Wilson, E.G., Verpoorte, R., & Choi, Y.H. (2018). Green solvents from ionic liquids and deep eutectic solvents to natural deep eutectic solvents. *Comptes Rendus Chimie*, *21*, 628-638.
- Vázquez, M., Oliva, M., Tellez-Luis, S. J., & Ramírez, J.A. (2007). Hydrolysis of sorghum straw using phosphoric acid: evaluation of furfural production. *Bioresource Technology*, *98*, 3053-3060.
- Verdia, P., Brandt, A., Hallett, J.P., Ray, M.J., & Welton, T. (2014). Fractionation of lignocellulosic biomass with the ionic liquid 1-butylimidazolium hydrogen sulfate. *Green Chemistry*, *16*, 1617-1627.
- Vernès, L., Abert-Vian, M., El Maâtaoui, M., Tao, Y., Bornard, I., & Chemat, F. (2019). Application of ultrasound for green extraction of proteins from spirulina. mechanism, optimization, modeling, and industrial prospects. *Ultrasonics Sonochemistry*, *54*, 48-60.
- Wang, H., Li, D., Yano, H., & Abe, K. (2014). Preparation of tough cellulose II nanofibers with high thermal stability from wood. *Cellulose*, *21*, 1505-1515.
- Wang, P., Liu, C., Chang, J., Yin, Q., Huang, W., Liu, Y., Dang, X., Gao, T., & Lu, F. (2019). Effect of physicochemical pretreatments plus enzymatic hydrolysis on the composition and morphologic structure of corn straw. *Renewable Energy*, *138*, 502-508.
- Wang, Q., Hu, J., Shen, F., Mei, Z., Yang, G., Zhang, Y., Hu, Y., Zhang, J., & Deng, S. (2016b). Pretreating wheat straw by the concentrated phosphoric acid plus hydrogen

- peroxide (PHP): investigations on pretreatment conditions and structure changes. *Bioresource Technology*, 199, 245-257.
- Wang, Q.Q., Zhu, J.Y., Gleisner, R., Kuster, T.A., Baxa, U., & McNeil, S.E. (2012). Morphological development of cellulose fibrils of a bleached eucalyptus pulp by mechanical fibrillation. *Cellulose*, 19, 1631-1643.
- Wang, S., & Cheng, Q. (2009). A novel process to isolate fibrils from cellulose fibers by high-intensity ultrasonication, part 1: process optimization. *Journal of Applied Polymer Science*, 113, 1270-1275.
- Wang, Z.W., Zhu, M.Q., Li, M.F., Wang, J.Q., Wei, Q., & Sun, R.C. (2016a). Comprehensive evaluation of the liquid fraction during the hydrothermal treatment of rapeseed straw. *Biotechnology for Biofuels*, 9, 142.
- Wei, L., Li, K., Ma, Y., & Hou, X. (2012). Dissolving lignocellulosic biomass in a 1-butyl-3-methylimidazolium chloride-water mixture. *Industrial Crops and Products*, 37, 227-234.
- Weinwurm, F., Turk, T., Denner, J., Whitmore, K., & Friedl, A. (2017). Combined liquid hot water and ethanol organosolv treatment of wheat straw for extraction and reaction modeling. *Journal of Cleaner Production*, 165, 1473-1484.
- Wörmeyer, K., Ingram, T., Saake, B., Brunner, G., & Smirnova, I. (2011). Comparison of different pretreatment methods for lignocellulosic materials. Part II: Influence of pretreatment on the properties of rye straw lignin. *Bioresource Technology*, 102, 4157-4164.
- Wu, Z., Zhou, W., Pang, C., Deng, W., Xu, C., & Wang, X. (2019). Multifunctional chitosan-based coating with liposomes containing laurel essential oils and nanosilver for pork preservation. *Food Chemistry*, 295, 16-25.
- Xiao, B., Sun, X., & Sun, R.C. (2001). Chemical, structural, and thermal characterizations of alkali-soluble lignins and hemicelluloses, and cellulose from maize stems, rye straw, and rice straw. *Polymer Degradation and Stability*, 74, 307-319.
- Xu, F., Sun, J.X., Sun, R.C., Fowler, P., & Baird, M.S. (2006). Comparative study of organosolv lignins from wheat straw. *Industrial Crops and Products*, 23, 180-193.
- Xu, J., Krietemeyer, E.F., Boddu, V.M., Liu, S.X., & Liu, W.C. (2018). Production and characterization of cellulose nanofibril (CNF) from agricultural waste corn stover. *Carbohydrate Polymers*, 192, 202-207.
- Yang, H., Yan, R., Chen, H., Lee, D.H., & Zheng, C. (2007). Characteristics of hemicellulose, cellulose and lignin pyrolysis. *Fuel*, 86, 1781-1788.
- Yang, H., Yan, R., Chen, H., Zheng, C., Lee, D.H., & Liang, D.T. (2006). In-depth investigation of biomass pyrolysis based on three major components: hemicellulose, cellulose and lignin. *Energy & Fuels*, 20, 388-393.
- Yang, Y., Belghazi, M., Lagadec, A., Miller, D.J., & Hawthorne, S.B. (1998). Elution of organic solutes from different polarity sorbents using subcritical water. *Journal of Chromatography A*, 810, 149-159.

- Yin, Y., Berglund, L., & Salmén, L. (2011). Effect of steam treatment on the properties of wood cell walls. *Biomacromolecules*, *12*, 194-202.
- Yousefi, H., Azari, V., & Khazaeian, A. (2018). Direct mechanical production of wood nanofibers from raw wood microparticles with no chemical treatment. *Industrial Crops and Products*, *115*, 26-31.
- Yousefi, H., Faezipour, M., Hedjazi, S., Mousavi, M.M., Azusa, Y., & Heidari, A.H. (2013). Comparative study of paper and nanopaper properties prepared from bacterial cellulose nanofibers and fibers/ground cellulose nanofibers of canola straw. *Industrial Crops and Products*, *43*, 732-737.
- Yu, H., Guo, J., Chen, Y., Fu, G., Li, B., Guo, X., & Xiao, D. (2017). Efficient utilization of hemicellulose and cellulose in alkali liquor-pretreated corncob for bioethanol production at high solid loading by *Spathaspora passalidarum* U1-58. *Bioresource Technology*, *232*, 168-175.
- Yuan, J.H., Xu, R.K., & Zhang, H. (2011). The forms of alkalis in the biochar produced from crop residues at different temperatures. *Bioresource Technology*, *102*, 3488-3497.
- Yuan, T., & Sun, R.C. (2010). Introduction. In Sun, R.C. (Ed.), *Cereal Straw as a Resource for Sustainable Biomaterials and Biofuels* (pp. 1-7). Elsevier, New York, USA.
- Yue, P.P., Hu, Y.J., Fu, G.Q., Sun, C.X., Li, M.F., Peng, F., & Sun, R.C. (2018). Structural differences between the lignin-carbohydrate complexes (LCCs) from 2- and 24-month-old bamboo (*Neosinocalamus affinis*). *International Journal of Molecular Sciences*, *19*, 1.
- Yue, Y., Han, J., Han, G., French, A.D., Qi, Y., & Wu, Q. (2016). Cellulose nanofibers reinforced sodium alginate-polyvinyl alcohol hydrogels: core-shell structure formation and property characterization. *Carbohydrate Polymers*, *147*, 155-164.
- Zander, N.E., Dong, H., Steele, J., & Grant, J.T. (2014). Metal cation cross-linked nanocellulose hydrogels as tissue engineering substrates. *ACS Applied Materials & Interfaces*, *6*, 18502-18510.
- Zdanowicz, M., Wilpiszewska, K., & Szychaj, T. (2018). Deep eutectic solvents for polysaccharides processing: a review. *Carbohydrate Polymers*, *200*, 361-380.
- Zhang, X., Wang, C., Liao, M., Dai, L., Tang, Y., Zhang, H., Coates, P., Sefat, F., Zheng, L., Song, J., & Zheng, Z. (2019). Aligned electrospun cellulose scaffolds coated with rhBMP-2 for both *in vitro* and *in vivo* bone tissue engineering. *Carbohydrate Polymers*, *213*, 27-38.
- Zhao, Y., Sun, W., & Saldaña, M.D.A. (2018b). Nanogels of poly-N-isopropylacrylamide, poly-N, N-diethylacrylamide and acrylic acid for controlled release of thymol. *Journal of Polymer Research*, *25*, 253.
- Zhao, Y., Huerta, R.R., & Saldaña, M.D.A. (2019). Use of subcritical water technology to develop cassava starch/chitosan/gallic acid bioactive films reinforced with cellulose nanofibers from canola straw. *The Journal of Supercritical Fluids*, *148*, 55-65.

- Zhao, Z., Chen, X., Ali, M. F., Abdeltawab, A.A., Yakout, S.M., & Yu, G. (2018a). Pretreatment of wheat straw using basic ethanalamine-based deep eutectic solvents for improving enzymatic hydrolysis. *Bioresource Technology*, *263*, 325-333.
- Zhou, S., Brown, R.C., & Bai, X. (2015). The use of calcium hydroxide pretreatment to overcome agglomeration of technical lignin during fast pyrolysis. *Green Chemistry*, *17*, 4748-4759.
- Zhu, S., Wu, Y., Yu, Z., Chen, Q., Wu, G., Yu, F., Wang, C., & Jin, S. (2006). Microwave-assisted alkali pre-treatment of wheat straw and its enzymatic hydrolysis. *Biosystems Engineering*, *94*, 437-442.

Appendix A: Pressurized fluid fractionation of barley and canola straws

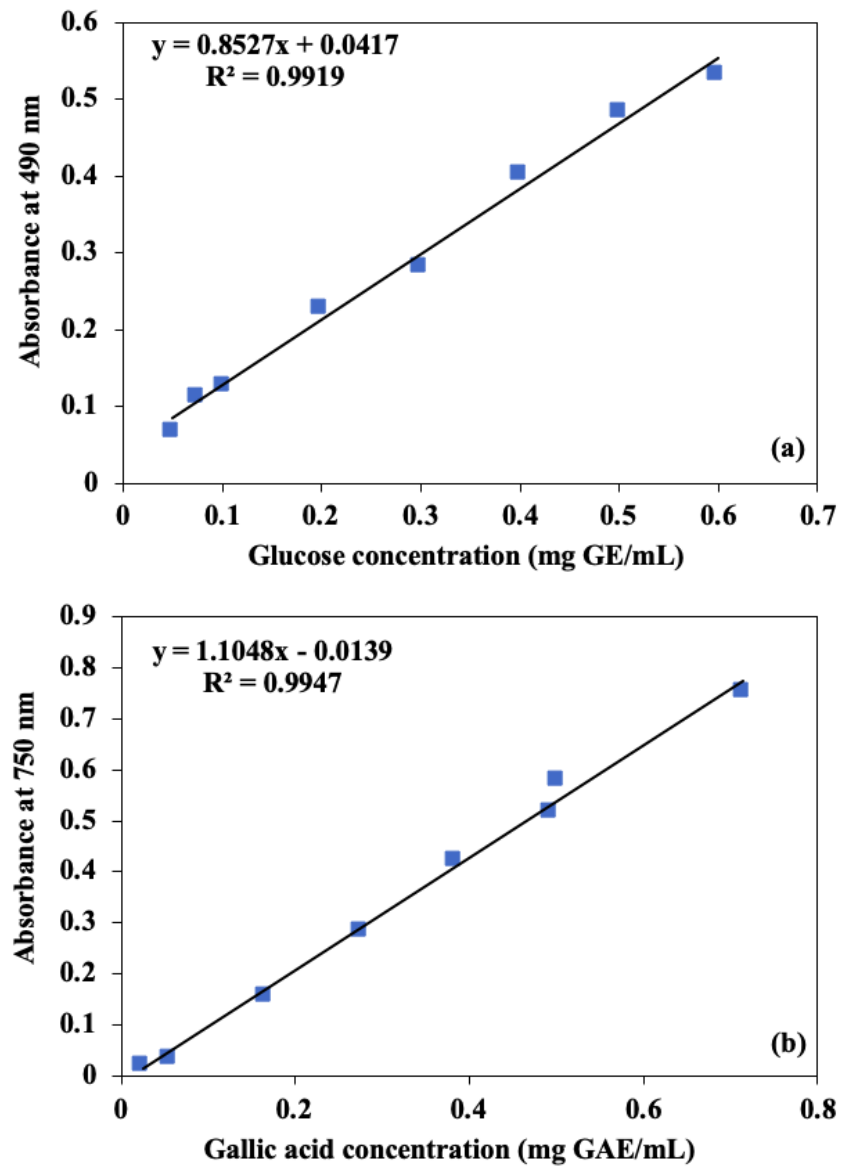


Fig. A.1. Standard curves for: (a) total carbohydrates and (b) total phenolics. GE: glucose equivalent; GAE: gallic acid equivalent.

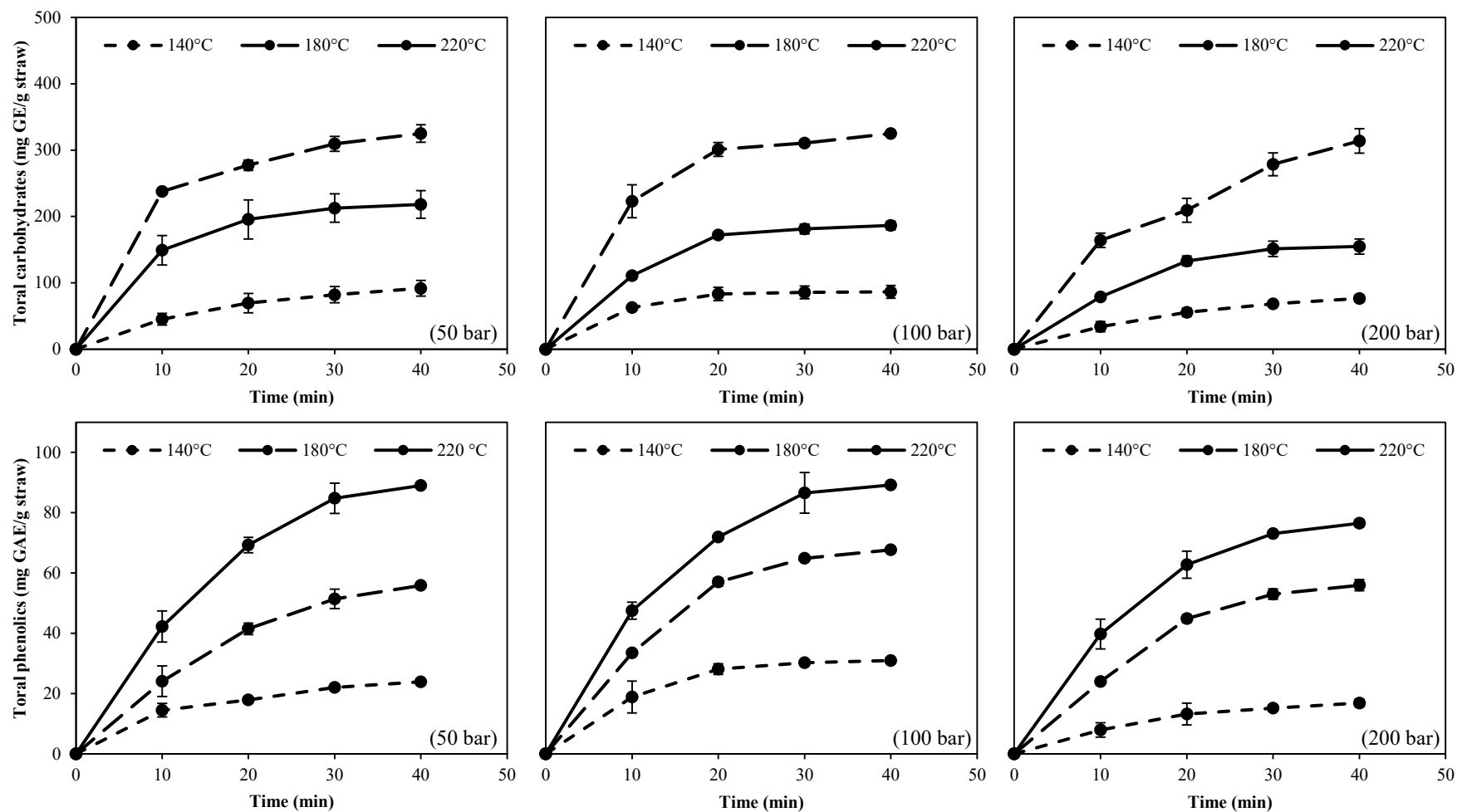


Fig. A2. Kinetics of total carbohydrates extracted from barley straw using sCW at 140-220 °C, 50-200 bar and 5 mL/min for 40 min. GE: glucose equivalent; GAE: gallic acid equivalent.

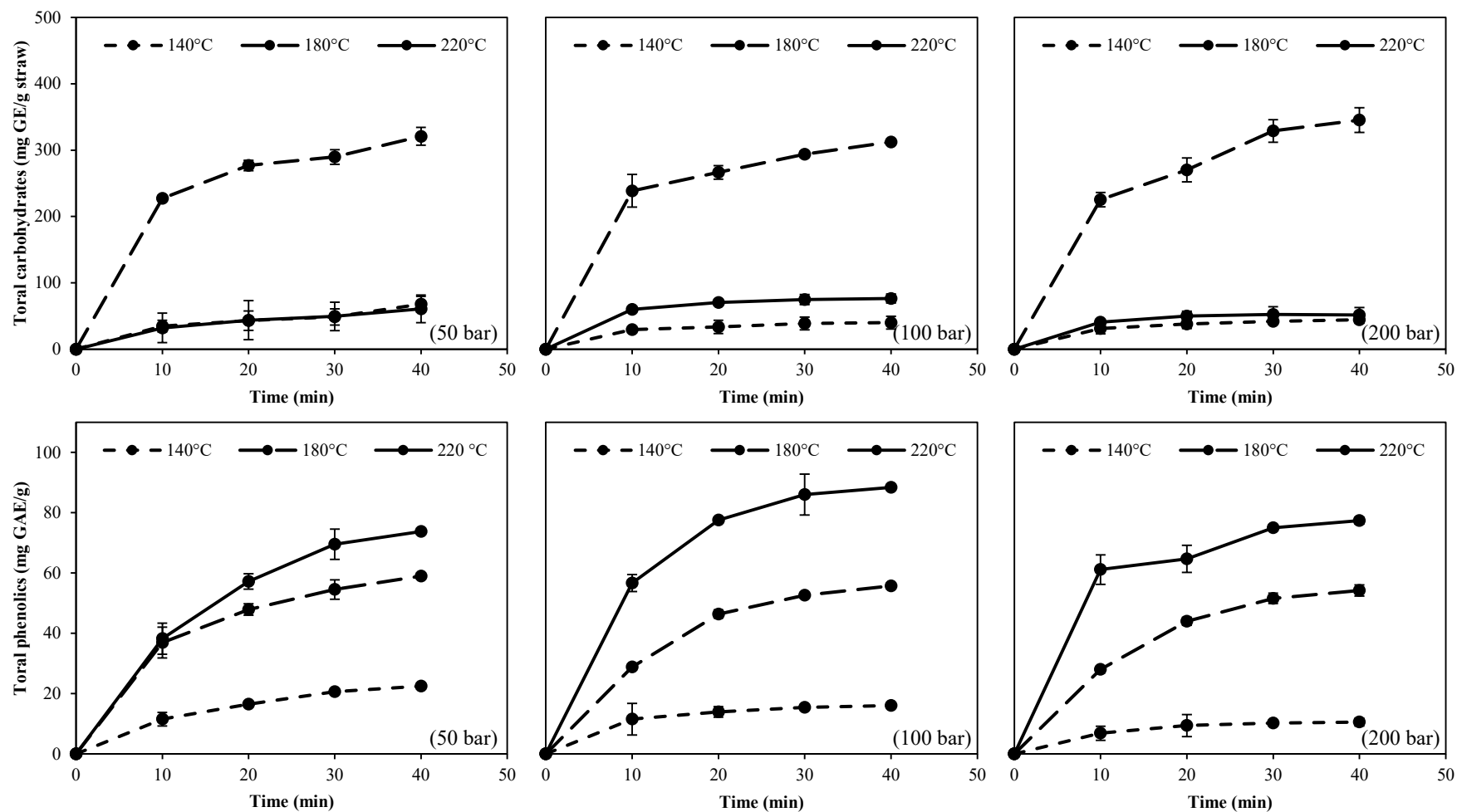


Fig. A3. Kinetics of total carbohydrates extracted from canola straw using sCW at 140-220 °C, 50-200 bar and 5 mL/min for 40 min. GE: glucose equivalent; GAE: gallic acid equivalent.

Table A.1. Total carbohydrates and total phenolics from liquid extracts obtained after subcritical water treatment at 140-220 °C, 50-200 bar, and 5 mL/min for 40 min.

Treatment condition		Liquid extracts	
Temperature (°C)	Pressure (bar)	Total carbohydrates (mg GE/g straw)	Total phenolics (mg GAE/g straw)
<i>Barley straw</i>			
140	50	91.7 ± 11.7	23.9 ± 3.4
	100	120.5 ± 53.0	31.0 ± 7.0
	200	148.2 ± 28.3	16.9 ± 2.7
180	50	325.0 ± 13.3	55.9 ± 3.8
	100	325.0 ± 2.6	57.7 ± 0.3
	200	313.8 ± 18.6	55.9 ± 1.9
220	50	218.2 ± 20.8	89.0 ± 6.7
	100	186.4 ± 6.7	89.2 ± 3.7
	200	133.9 ± 40.7	76.5 ± 9.2
<i>Canola straw</i>			
140	50	51.5 ± 8.7	20.5 ± 0.5
	100	39.1 ± 4.0	16.1 ± 1.4
	200	44.3 ± 6.3	10.56 ± 1.5
180	50	298.5 ± 13.6	57.5 ± 1.8
	100	357.6 ± 11.8	57.7 ± 0.3
	200	315.9 ± 17.2	56.0 ± 1.1
220	50	50.8 ± 0.2	73.2 ± 1.3
	100	51.0 ± 6.2	86.7 ± 1.2
	200	51.3 ± 3.7	76.1 ± 11.3

Table A.2. Lignin content of barley and canola straw residues treated at 180 °C, 50 bar and 5 mL/ min for 40 min.

Sample	Ethanol (%)	Lignin content (wt.%)
Barley straw	0	28.9 ± 0.9
	20	18.0 ± 0.4
	60	14.4 ± 0.3
	100	16.6 ± 0.2
Canola straw	0	27.5 ± 0.2
	20	16.1 ± 0.4
	60	17.1 ± 0.9
	100	19.9 ± 0.3

Appendix B: Biorefinery of canola straw towards lignocellulosic nanofiber production

Table B.1. General factorial regression of cellulose.

Factor	Levels	Values		
Temperature (°C)	3	140	180	220
Pressure (bar)	3	50	100	200

Source	DF	Adj SS	Adj MS	F-Value	P-Value
Model	8	4325.46	540.68	122.31	0.000
Linear	4	4311.77	1077.94	243.85	0.000
Temperature (°C)	2	4310.26	2155.13	487.53	0.000
Pressure (bar)	2	1.50	0.75	0.17	0.846
2-Way Interactions	4	13.69	3.42	0.77	0.569
Temperature (°C)*Pressure (bar)	4	13.69	3.42	0.77	0.569
Error	9	39.78	4.42		
Total	17	4365.24			
Summary	S	R-sq	R-sq(adj)	R-sq(pred)	
	2.10250	99.09%	98.28%	96.35%	

Table B.2. General factorial regression of hemicellulose.

Factor	Levels	Values		
Temperature (°C)	3	140	180	220
Pressure (bar)	3	50	100	200

Source	DF	Adj SS	Adj MS	F-Value	P-Value
Model	8	976.94	122.12	84.39	0.000
Linear	4	965.66	241.42	166.84	0.000
Temperature (°C)	2	961.85	480.93	332.36	0.000
Pressure (bar)	2	3.81	1.90	1.32	0.315
2-Way Interactions	4	11.28	2.82	1.95	0.187
Temperature (°C)*Pressure (bar)	4	11.28	2.82	1.95	0.187
Error	9	13.02	1.45		
Total	17	989.960			
Summary	S	R-sq	R-sq(adj)	R-sq(pred)	
	1.20292	98.68%	97.52%	94.74%	

Table B.3. General factorial regression of total lignin.

Factor	Levels	Values		
Temperature (°C)	3	140	180	220
Pressure (bar)	3	50	100	200

Source	DF	Adj SS	Adj MS	F-Value	P-Value
Model	8	96.30	12.038	7.18	0.004
Linear	4	88.79	22.197	13.24	0.001
Temperature (°C)	2	87.52	43.762	26.11	0.000
Pressure (bar)	2	1.26	0.632	0.38	0.696
2-Way Interactions	4	7.51	1.88	1.12	0.405
Temperature (°C)*Pressure (bar)	4	7.51	1.88	1.12	0.405
Error	9	15.09	1.68		
Total	17	111.39			
Summary	S	R-sq	R-sq(adj)	R-sq(pred)	
	1.29465	86.46%	74.42%	45.83%	

Table B.4. Regression equation obtained via third-order polynomial regression analysis of cellulose, hemicellulose and lignin (total, soluble and insoluble lignin).

Regression Equation	
Cellulose (%)	$= 60.11 + 0.029 \text{ Ethanol } (\%) - 0.00086 \text{ Ethanol } (\%)*\text{Ethanol } (\%)$ $- 0.000009 \text{ Ethanol } (\%)*\text{Ethanol } (\%)*\text{Ethanol } (\%)$
Hemicellulose (%)	$= 9.59 + 0.050 \text{ Ethanol } (\%) + 0.00461 \text{ Ethanol } (\%)*\text{Ethanol } (\%)$ $- 0.000040 \text{ Ethanol } (\%)*\text{Ethanol } (\%)*\text{Ethanol } (\%)$
Total lignin (%)	$= 27.224 - 0.4401 \text{ Ethanol } (\%) + 0.00649 \text{ Ethanol } (\%)*\text{Ethanol } (\%)$ $- 0.000028 \text{ Ethanol } (\%)*\text{Ethanol } (\%)*\text{Ethanol } (\%)$
Soluble lignin (%)	$= 0.6788 - 0.00271 \text{ Ethanol } (\%) + 0.000119 \text{ Ethanol } (\%)*\text{Ethanol } (\%)$ $- 0.000001 \text{ Ethanol } (\%)*\text{Ethanol } (\%)*\text{Ethanol } (\%)$
Insoluble lignin (%)	$= 26.553 - 0.4364 \text{ Ethanol } (\%) + 0.00634 \text{ Ethanol } (\%)*\text{Ethanol } (\%)$ $- 0.000027 \text{ Ethanol } (\%)*\text{Ethanol } (\%)*\text{Ethanol } (\%)$

Table B.5. Optical transmittance of lignocellulosic nanofiber at 300-800 nm.

Optical transmittance (%)	Theoretical specific energy (kJ/g)				
	4	8	12	16	20
300	3.5	4.0	4.7	6.8	9.0
400	22.9	23.5	24.7	26.2	34.3
500	37.7	38.1	39.2	41.0	47.1
600	47.0	47.2	48.1	50.3	54.2
700	52.7	52.7	53.6	56.0	58.3
800	55.0	56.1	56.9	58.0	60.1

Table B.6. Optical transmittance at 800 nm and nanofibril content of lignocellulosic nanofibers (1 wt.%) obtained using high-intensity ultrasound at theoretical specific energy of 4-20 kJ/g.

Theoretical specific energy (kJ/g)	Optical transmittance (%)	Nanofibril content (wt.%)
4	55.0	32.8
8	56.1	33.4
12	56.9	34.2
16	58.0	34.9
20	60.1	36.0

Table B.7. Diameter frequency count of lignocellulosic nanofibers obtained using high-intensity ultrasound at 4 kJ/g and 20 kJ/g.

Diameter range (nm)	Frequency count (%)	
	HIUS at 4 kJ/g	HIUS at 20 kJ/g
0-10	4	29
10-20	13	26
20-30	27	27
30-40	34	5
40-50	10	5
> 50	12	8

Appendix C: Nanofibers production with different residual lignin content

Table C.1. General factorial regression of water retention value.

Factor	Levels	Values				
Theoretical specific energy (kJ/g)	5	4	8	12	16	20
Lignin (wt.%)	4	8.0	10.7	18.2	20.0	-

Source	DF	Adj SS	Adj MS	F-Value	P-Value
Model	8	96.3	12.0	7.2	0.004
Linear	7	20623.0	2946.1	8502.6	0.000
Theoretical specific energy (kJ/g)	4	3899.2	974.8	2813.3	0.000
Lignin (wt.%)	3	16723.7	5574.6	16088.4	0.000
2-Way Interactions	12	2323.2	193.6	558.7	0.000
Theoretical specific energy (kJ/g)*Lignin (wt.%)	12	2323.2	193.6	558.7	0.000
Error	19	6.6	0.4		
Total	39	22968.9			
Summary	S	R-sq	R-sq(adj)	R-sq(pred)	
	0.588640	99.97%	99.94%	99.87%	

Table C.2. General factorial regression of nanofibril content.

Factor	Levels	Values				
Theoretical specific energy (kJ/g)	5	4	8	12	16	20
Lignin (wt.%)	4	8.0	10.7	18.2	20.0	

Source	DF	Adj SS	Adj MS	F-Value	P-Value
Model	20	599.7	30.0	39.0	0.000
Linear	7	580.9	83.0	107.8	0.000
Theoretical specific energy (kJ/g)	4	73.8	18.5	24.0	0.000
Lignin (wt.%)	3	507.1	169.0	219.6	0.000
2-Way Interactions	12	18.6	1.6	2.0	0.084
Theoretical specific energy (kJ/g)*Lignin (wt.%)	12	18.6	1.6	2.0	0.084
Error	19	14.6	0.8		
Total	39	614.3			
Summary	S	R-sq	R-sq(adj)	R-sq(pred)	
	0.87734	97.62%	95.11%	89.45%	

Table C.3. General factorial regression of zeta potential.

Factor	Levels	Values				
Theoretical specific energy (kJ/g)	5	4	8	12	16	20
Lignin (wt.%)	4	8.0	10.7	18.2	20.0	-

Source	DF	Adj SS	Adj MS	F-Value	P-Value
Model	20	766.3	38.3	6.5	0.000
Linear	7	753.8	107.7	18.4	0.000
Theoretical specific energy (kJ/g)	4	97.6	24.4	4.2	0.014
Lignin (wt.%)	3	656.2	218.7	37.3	0.000
2-Way Interactions	12	11.7	1.0	0.2	0.999
Theoretical specific energy (kJ/g)*Lignin (wt.%)	12	11.7	1.0	0.2	0.999
Error	19	111.4	5.9		
Total	39	877.7			
Summary	S	R-sq	R-sq(adj)	R-sq(pred)	
	2.42101	87.31%	73.96%	43.76%	

Table C.4. General factorial regression of water retention value of cellulose nanofiber only.

Factor	Levels	Values				
		Theoretical specific energy (kJ/g)	5	4	8	12
Lignin (wt.%)	3	8.0	10.7	18.2	-	

Source	DF	Adj SS	Adj MS	F-Value	P-Value
Model	14	10468.8	747.8	494.2	0.000
Linear	6	9366.1	1561.0	1031.7	0.000
Theoretical specific energy (kJ/g)	4	5118.3	1279.6	845.7	0.000
Lignin (wt.%)	2	4247.7	2123.9	1403.6	0.000
2-Way Interactions	8	1102.7	137.8	91.1	0.000
Theoretical specific energy (kJ/g)*Lignin (wt.%)	8	1102.7	137.8	91.1	0.000
Error	15	22.7	1.5		
Total	29	10491.5			
Summary	S	R-sq	R-sq(adj)	R-sq(pred)	
	1.23009	99.78%	99.58%	99.13%	

Table C.5. General factorial regression of zeta potential of cellulose nanofiber only.

Factor	Levels	Values				
Theoretical specific energy (kJ/g)	5	4	8	12	16	20
Lignin (wt.%)	3	8.0	10.7	18.2	-	

Source	DF	Adj SS	Adj MS	F-Value	P-Value
Model	14	87.9	6.3	1.0	0.482
Linear	6	78.5	13.1	2.1	0.110
Theoretical specific energy (kJ/g)	4	66.9	16.7	2.7	0.070
Lignin (wt.%)	2	11.7	5.8	1.0	0.409
2-Way Interactions	8	9.4	1.2	0.2	0.988
Theoretical specific energy (kJ/g)*Lignin (wt.%)	8	9.4	1.2	0.2	0.988
Error	15	92.2	6.2		
Total	29	180.1			
Summary	S	R-sq	R-sq(adj)	R-sq(pred)	
	2.47972	48.79%	0.99%	0.00%	

Table C.6. General factorial regression of nanofibril content of cellulose nanofiber only.

Factor	Levels	Values				
Theoretical specific energy (kJ/g)	5	4	8	12	16	20
Lignin (wt.%)	3	8.0	10.7	18.2	-	

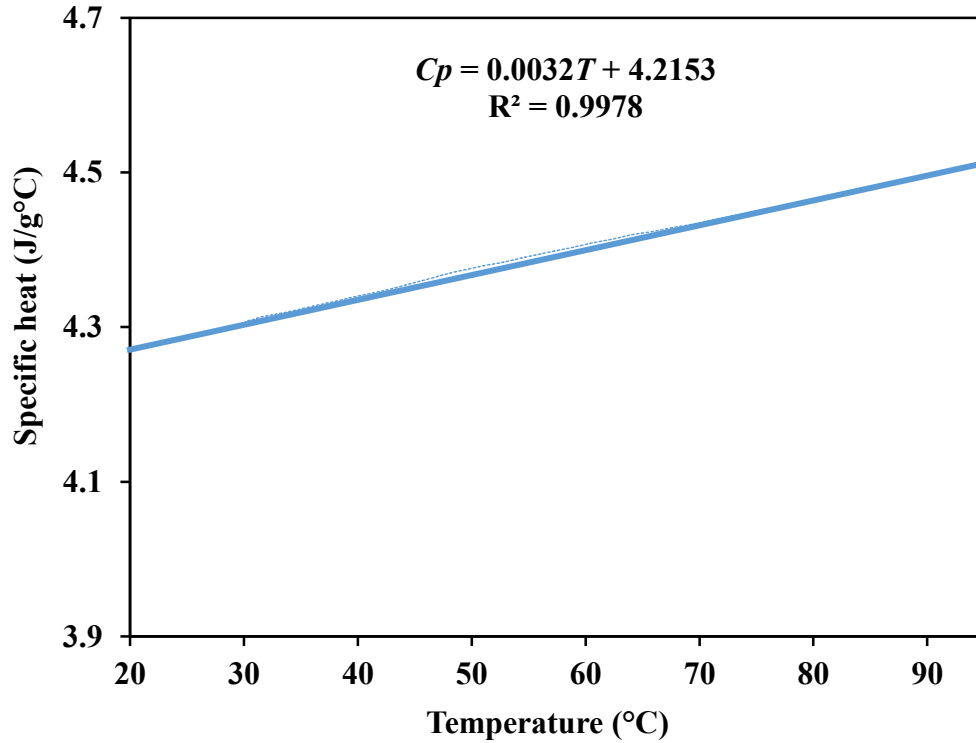
Source	DF	Adj SS	Adj MS	F-Value	P-Value
Model	14	251.7	17.9	27.0	0.000
Linear	6	237.9	39.7	59.7	0.000
Theoretical specific energy (kJ/g)	4	72.1	18.0	27.1	0.000
Lignin (wt.%)	2	165.8	82.9	124.8	0.000
2-Way Interactions	8	13.1	1.6	2.5	0.084
Theoretical specific energy (kJ/g)*Lignin (wt.%)	8	13.1	1.6	2.5	0.084
Error	15	9.9	0.7		
Total	29	261.0			
Summary	S	R-sq	R-sq(adj)	R-sq(pred)	
	0.81513	96.18%	92.62%	84.73%	

Table C.7. Diameter frequency count of lignocellulosic nanofibers (LCNF) and cellulose nanofibers (CNF) obtained using high-intensity ultrasound at 20 kJ/g.

Diameter range (nm)	Frequency count (%)	
	LCNF	CNF (B6 h)
0-10	29	43
10-20	26	36
20-30	27	9
30-40	5	6
40-50	5	4
> 50	8	2

B6 h: bleached for 6 hours.

Appendix D: Production of cellulose nanofiber scaffolds using high-intensity ultrasound

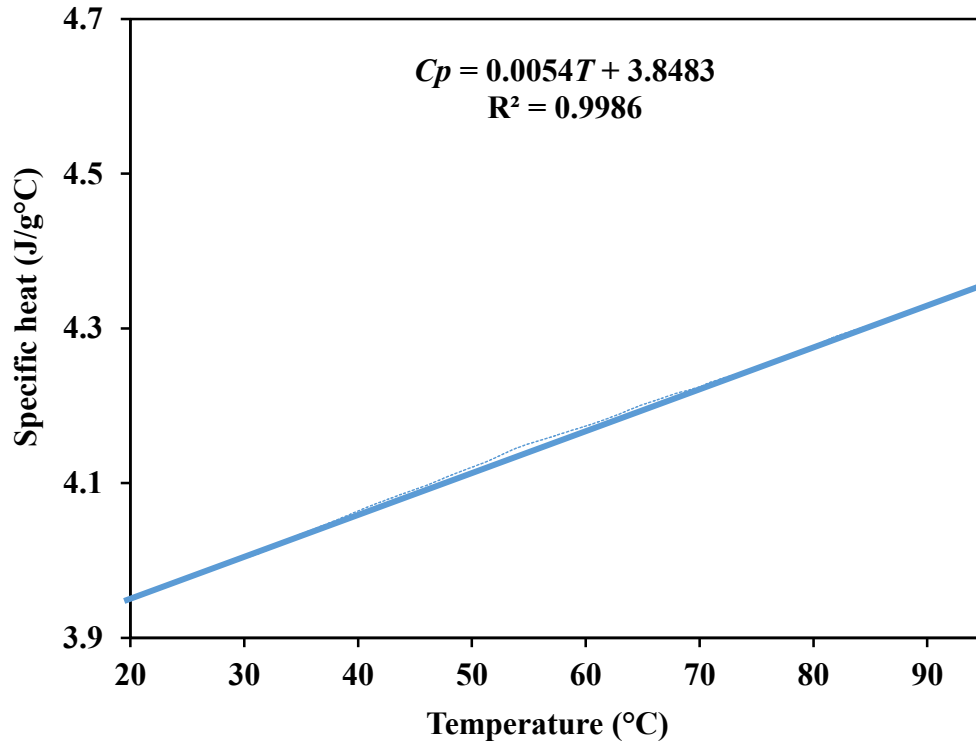


$$C_P = \frac{\int_{T_1}^{T_2} (0.0032T + 4.2153) dT}{\Delta T} = \frac{\int_{20^\circ\text{C}}^{95^\circ\text{C}} (0.0032T + 4.2153) dT}{(95 - 20)}$$

$$C_P = \frac{\left| \frac{0.0032T^2}{2} + 4.2153T \right|_{20^\circ\text{C}}^{95^\circ\text{C}}}{75} = \frac{0.0016(95 - 20)^2 + 4.2153(95 - 20)}{75}$$

$$C_P = 4.34 \frac{J}{g^\circ\text{C}}$$

Fig. D.1. Specific heat and heat capacity calculation of low lignin cellulose nanofiber obtained by differential scanning calorimetry analysis.



$$C_p = \frac{\int_{T_1}^{T_2} (0.0054T + 3.8483) dT}{\Delta T} = \frac{\int_{20^\circ\text{C}}^{95^\circ\text{C}} (0.0054T + 3.8483) dT}{(95 - 20)}$$

$$C_p = \frac{\left| \frac{0.0054T^2}{2} + 3.8483T \right|_{20^\circ\text{C}}^{95^\circ\text{C}}}{75} = \frac{0.0027(95 - 20)^2 + 3.8483(95 - 20)}{75}$$

$$C_p = 4.06 \frac{J}{g^\circ\text{C}}$$

Fig. D.2. Specific heat and heat capacity calculation of high lignin cellulose nanofiber obtained by differential scanning calorimetry analysis.

Table D.1. Diameter frequency count of low lignin cellulose nanofibers (LL-CNF) and high lignin cellulose nanofiber (HL-CNF) obtained using high-intensity ultrasound at acoustical powers of 53 and 51 W, respectively.

Diameter range (nm)	Frequency count (%)	
	LL-CNF	HL-CNF
0-10	43	31
10-20	36	20
20-30	9	23
30-40	6	19
40-50	4	4
> 50	2	3

Table D.2. Reduction alamarBlue® of control (glass slip), LL-CNF and HL-CNF scaffolds (1-2 wt.%) seeded with gingival fibroblast cells cultured up to 11 days.

Day	Reduction alamarBlue® (%)						
	Control	LL-CNF			HL-CNF		
		1 wt.%	1.5 wt.%	2 wt.%	1 wt.%	1.5 wt.%	2 wt.%
1	6.3 ± 2.5	5.2 ± 2.8	6.7 ± 0.8	7.7 ± 1.0	5.8 ± 2.2	6.9 ± 1.1	8.0 ± 1.8
3	9.4 ± 4.5	50.6 ± 1.9	50.9 ± 3.5	47.9 ± 1.1	62.0 ± 1.4	55.9 ± 6.7	54.8 ± 4.5
7	28.8 ± 6.8	51.4 ± 6.6	56.9 ± 5.8	51.6 ± 1.4	59.9 ± 4.5	55.5 ± 6.3	46.5 ± 5.0
11	23.7 ± 4.8	50.4 ± 3.4	54.4 ± 4.6	55.6 ± 7.9	56.1 ± 9.6	53.6 ± 5.0	49.8 ± 7.6

**Appendix E: Production of emulsion-filled cellulose nanofibers hydrogel
via high-intensity ultrasound**

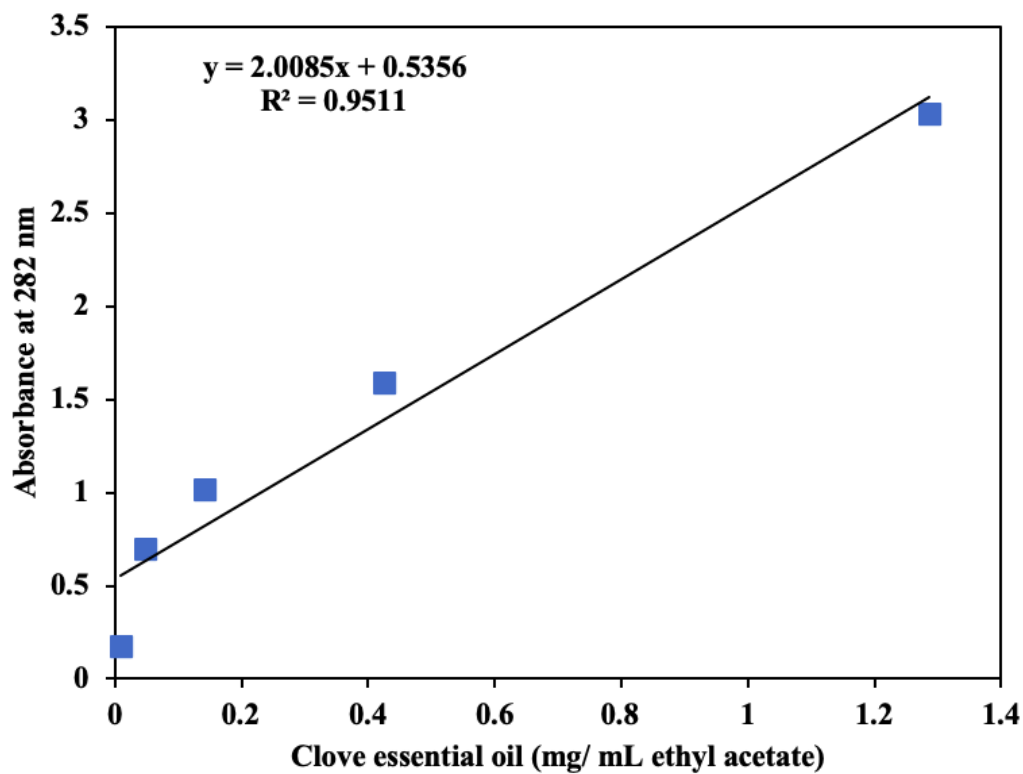
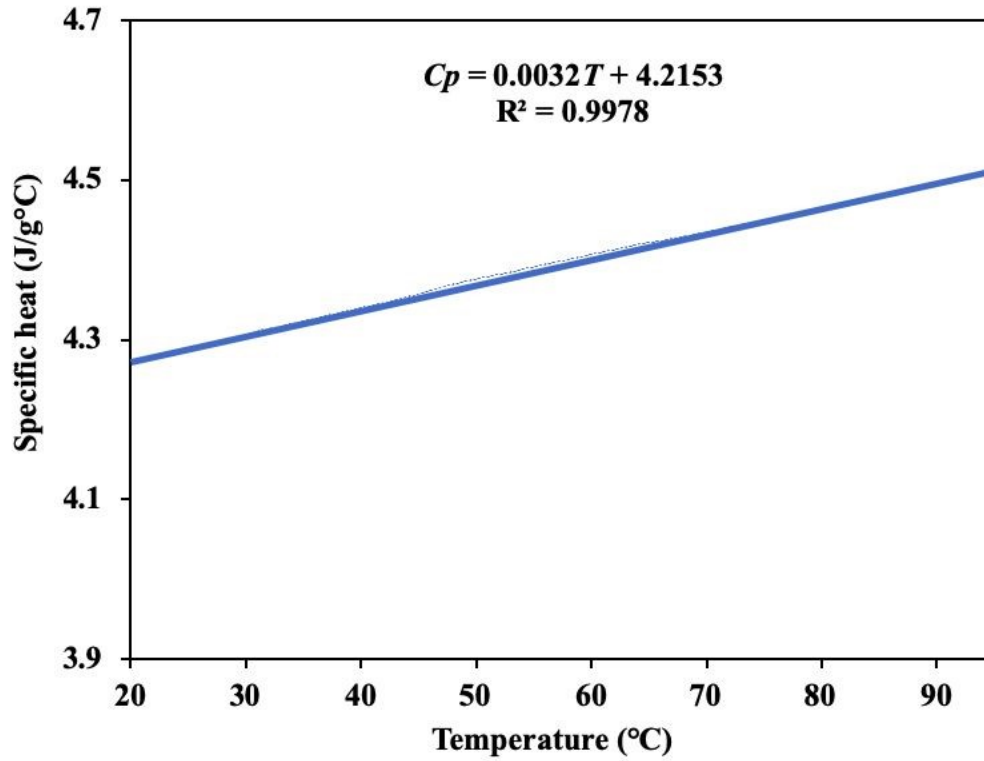


Fig. E.1. Standard curve for clove essential oil (based on eugenol absorbance).

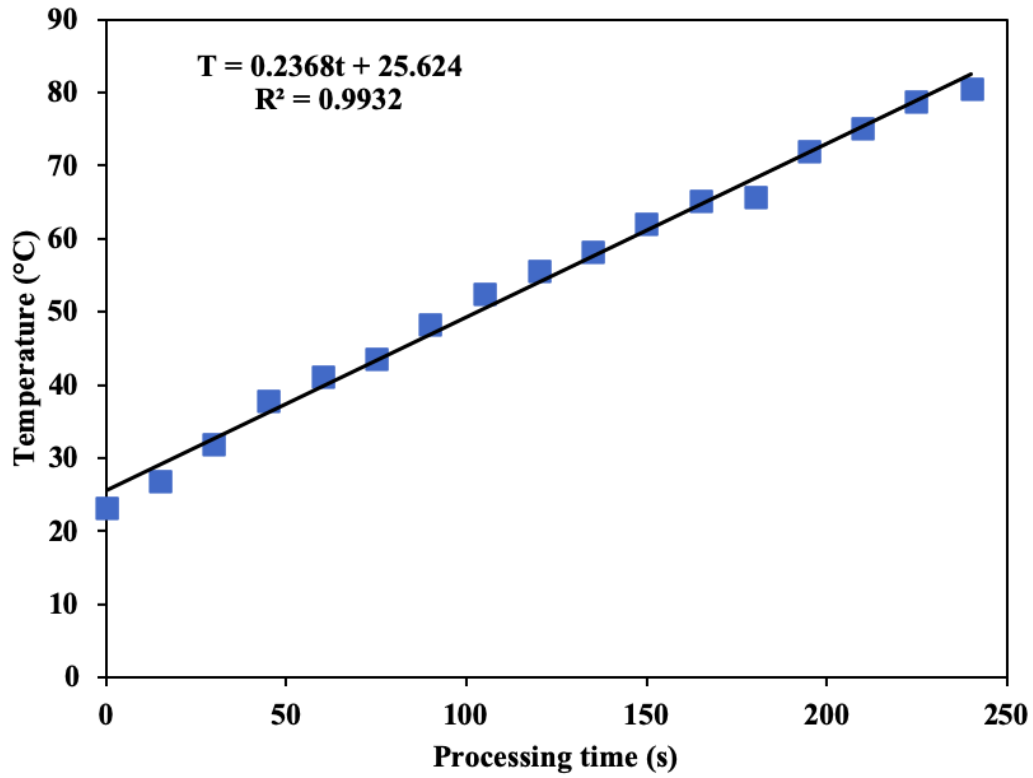


$$C_p = \frac{\int_{T_1}^{T_2} (0.0032T + 4.2153) dT}{\Delta T} = \frac{\int_{20^{\circ}\text{C}}^{95^{\circ}\text{C}} (0.0032T + 4.2153) dT}{(95 - 20)}$$

$$C_p = \frac{\left| \frac{0.0032T^2}{2} + 4.2153T \right|_{20^{\circ}\text{C}}^{95^{\circ}\text{C}}}{75} = \frac{0.0016(95 - 20)^2 + 4.2153(95 - 20)}{75}$$

$$C_p = 4.34 \frac{J}{g^{\circ}\text{C}}$$

Fig. E.2. Specific heat and heat capacity calculation of cellulose nanofiber obtained by differential scanning calorimetry analysis.



$$\text{Acoustical power (W)} = m C_p \left(\frac{\Delta T}{\Delta t} \right)$$

$$T = 0.2368t + 25.624$$

$$\frac{\Delta T}{\Delta t} = 0.2368 \frac{^{\circ}\text{C}}{\text{s}}$$

$$\text{Acoustical power} = (20 \text{ g}) \times \left(4.34 \frac{\text{J}}{\text{g}^{\circ}\text{C}} \right) \left(0.2368 \frac{^{\circ}\text{C}}{\text{s}} \right)$$

$$\text{Acoustical power} = 20.55 \text{ W}$$

Fig. E.3. Acoustical power calculation of emulsion-filled CNF hydrogel system.

Table E.1. Color analysis of emulsion-filled cellulose nanofiber hydrogel obtained using high-intensity ultrasound at specific energies of 0.10, 0.17 and 0.24 kJ/g.

Sample		Color		
		<i>L</i> *	<i>a</i> *	<i>b</i> *
Control		93.49	-0.25	-0.09
0.1 wt.% clove essential oil	0.10 kJ/g	99.95 ± 0.04	-1.88 ± 0.01	3.07 ± 0.00
	0.17 kJ/g	100.05 ± 0.05	-1.89 ± 0.01	3.04 ± 0.00
	0.24 kJ/g	99.71 ± 0.01	-1.87 ± 0.02	2.86 ± 0.21
0.5 wt.% clove essential oil	0.10 kJ/g	99.39 ± 0.05	-1.91 ± 0.01	3.05 ± 0.17
	0.17 kJ/g	99.19 ± 0.05	-1.95 ± 0.04	2.96 ± 0.02
	0.24 kJ/g	99.97 ± 0.38	-1.94 ± 0.07	3.00 ± 0.05
1.0 wt.% clove essential oil	0.10 kJ/g	99.40 ± 0.86	-1.85 ± 0.05	2.64 ± 0.06
	0.17 kJ/g	99.20 ± 0.32	-1.78 ± 0.18	2.68 ± 0.05
	0.24 kJ/g	99.19 ± 0.49	-1.69 ± 0.02	2.55 ± 0.00

Table E.2. Cell viability of the freeze-dried clove essential oil emulsion-filled cellulose nanofiber hydrogels obtained using high-intensity ultrasound at specific energies of 0.10, 0.17 and 0.24 kJ/g.

CNF scaffold		Cell viability (% of control)
0.1 wt.% clove essential oil	0.10 kJ/g	87.6 ± 6.0
	0.17 kJ/g	90.6 ± 4.1
	0.24 kJ/g	82.0 ± 7.8
0.5 wt.% clove essential oil	0.10 kJ/g	91.5 ± 7.2
	0.17 kJ/g	101.2 ± 7.8
	0.24 kJ/g	74.1 ± 4.8
1.0 wt.% clove essential oil	0.10 kJ/g	40.6 ± 3.4
	0.17 kJ/g	17.8 ± 2.5
	0.24 kJ/g	29.3 ± 1.1